University of Augsburg
Faculty of Applied Computer Science
Institute of Geography
Alter Postweg 118
D - 86159 Augsburg


# Particulate Matter and Climate Change in Bavaria (Germany)

DISSERTATION
FOR THE DOCTORAL DEGREE IN NATURAL SCIENCES
AT THE FACULTY OF APPLIED COMPUTER SCIENCE
OF THE UNIVERSITY OF AUGSBURG

SUBMITTED BY
CLAUDIA MARIA WEITNAUER

AUGSBURG 2016

Advisor: Prof. Dr. Jucundus Jacobeit
Reviewer: Prof. Dr. Jucundus Jacobeit
Prof. Dr. Karl-Friedrich Wetzel
Thesis Defence: 27.07.2016

# Contents

# List of Figures

# List of Tables

# Glossary

**AIR** air temperature

**AR5** Fifth Assessment Report

**AOGCM** Atmosphere-Ocean Coupled General Circulation Models

**BSS** Brier Skill Score

**BSS50** Brier Skill Score for the number of days exceeding $PM_{10}$ concentrations of 50 $\mu g/m^3$

**CC** cloud cover

**CMIP5** Fifth Phase of the Coupled Model Intercomparison Project

**CTC** Circulation Type Classifications

**CTs** Circulation Types

**DKM** K-means cluster analysis with most differing start partitions

**DWD** German Weather Service/Deutscher Wetterdienst

**ECHAM6** Atmospheric Component of the MPI-M Earth System Model

**ECMWF** European Centre for Medium-Range Weather Forecasts

**EV** Explained Variance

**GCM** General Circulation Model

**GLM** Generalized Linear Model

**GWT** Großwetter-Type or prototype classification

**HGT** geopotential height

**HR** Hit Rate

**HSS** Heidke Skill Score

**IPCC** Intergovernmental Panel on Climate Change

**LfU** Bavarian Environment Agency/Landesamt für Umwelt

**LÜB** Bavarian Air Quality monitoring network/Lufthygienisches Landesüberwachungssystem Bayern

**MPI-ESM-LR** Max-Planck-Institute Earth System Model Low Resolution

**MLR** Multiple Linear Regression Analysis

**MSSS** Mean Squared Skill Score

**NWP** Numerical Weather Prediction Model

**OMEGA** vertical velocity

**PC** Principal Component

**PCA** Principal Component Analysis

**PM** Particulate Matter

**PM$_{10}$** particulate matter with aerodynamic diameter < 10 $\mu$m

**PM$_{daily}$** daily mean PM$_{10}$ concentrations

**PM$_{mean}$** monthly mean PM$_{10}$ concentrations

**PM$_{50}$** monthly exceedances of a daily mean PM$_{10}$ value of 50 $\mu$g/m$^3$

**PREC** precipitation

**PRES** pressure

**RCP** Representative Concentration Pathway

**RHUM** relative humidity

**RF** Random Forests

**RVORT** relative vorticity

**SANDRA** Simulated annealing and diversified randomization

**SD** Synoptic Downscaling

**SHUM** specific humidity

**SLP** mean sea level pressure

**SRES** Special Report on Emission Scenarios

**SUN** sunshine duration

**$T_{max}$** maximum temperature

**$T_{mean}$** mean temperature

**$T_{min}$** minimum temperature

**UBA** German Federal Environment Agency/Umweltbundesamt

**UWND** zonal wind component

**VWND** meridional wind component

**VP** vapour pressure

**WS** wind speed

# Abstract

In the last decades, the critical increase of the emissions of particulate matter with aerodynamic diameter < 10 $\mu$m ($PM_{10}$), especially in urban areas, has become a problem for the environment and human health. High concentration episodes of fine particles increase the risk of cardiovascular or respiratory tract diseases, as several studies confirm. Local concentrations of $PM_{10}$ are influenced by meteorological parameters on different scales, e.g. local meteorological conditions and large-scale circulation dynamics. With climate changing rapidly, these connections need to be better understood in order to be able to estimate climate-change-related consequences for air quality management purposes.

To detect critical periods of high $PM_{10}$ concentrations, one focus in recent studies is set on the improvement of accurate short-term deterministic, statistical prediction models or reliable approaches for long-term air quality prediction. The general relationship between local particle concentrations and large-scale circulation dynamics, as for example reflected by weather or circulation types, has been proven in several studies. Thus far, only a few systematic attempts have been made to optimize objective classifications concerning their relationship to local $PM_{10}$ concentrations. Against this background, the aim of this study is to evaluate various approaches for the optimization of circulation type classifications with respect to their relevance for $PM_{10}$ levels in Bavarian cities (Germany) to detect those classifications, that are best suited for the use in statistical downscaling models.

The used data set of daily mean $PM_{10}$ concentrations has been provided by the Bavarian Environmental Agency (Landesamt für Umwelt) from their air quality monitoring network. For the analysed period 1980-2011, measurements from 16 urban stations with over 90 % data availability, spread over the target region, are available. (Initial characteristics of this data set concerning basic quality aspects, long-term trends and correspondence between locations are presented in this thesis. To characterize the correspondence between the $PM_{10}$ measurements of the different stations by spatial patterns, a regionalization by a s-mode Principal Component Analysis is realized on the data set.

Objective circulation type classifications are optimized with respect to their synoptic skill for the target variable $PM_{10}$ in a stepwise procedure. Seasonal patterns emerging from this optimization are varying weighted combinations of three large-scale atmospheric variables in several pressure levels. Their performance is evaluated by using a range of skill scores for varying calibration and validation periods. Results from these analyses have revealed highest synoptic skill for classifications based on a mid-size domain (7.5°-27.5° E and 40°-60° N), 18 number of classes, seasonal

classifications, a weighted combination of three large-scale atmospheric input variables and the conditioning by the target variable. Depending on the season and the considered $PM_{10}$ station, the combinations of classified atmospheric parameters vary. Air temperature (1000 hPa level), relative (850 hPa level) and specific humidity (1000 hPa level), mean sea level pressure, geopotential height at the 500 hPa level as well as zonal wind (500 hPa level) are detected to be the most relevant parameters throughout the seasons. Best performing classifications, in terms of maximum skill from evaluation, have been ascertained for each station and each season.

Monthly occurrence frequencies of circulation types (predictors), resulting from the previous optimization of classifications, are related to daily and monthly $PM_{10}$ indices (predictands) by using different statistical downscaling techniques. The comprehensive set of downscaling tools comprise variants of Synoptic Downscaling and regression-based methods (Multiple Linear Regression, Generalized Linear Models, Random Forests). $PM_{daily}$, $PM_{mean}$ and $PM_{50}$ are used as $PM_{10}$ indices. The generated transfer models are evaluated via cross-validation using different subintervals of the 1980-2011 period as calibration and validation periods, respectively. Highest model skill in cross-validation is detected for $PM_{mean}$ in winter, using the Random Forest approach, at all stations. Model results for $PM_{daily}$ have revealed positive but less pronounced skill for variants of the synoptic downscaling. Hence, the synoptic downscaling models are used for estimating $PM_{mean}$ as well.

Most suitable downscaling procedures, in terms of model skill determined from cross-validation, are finally applied to CMIP5 climate model data (ECHAM6, EC-Earth) to derive estimates of possible future climate-change-related variations in $PM_{10}$ concentrations. Projections are used for two time periods (2021-2050, 2071-2100) and two different scenarios (RCP 4.5, RCP 8.5). Possible model biases evoking from the climate models and the downscaling approaches are assessed by numerical and statistical ensembles. A bias correction is applied on the modelled $PM_{10}$ time series in the observational period as well as on the estimated future particle levels.

On the one hand, climate-change-induced variations of particle levels have yielded out a decrease in winter at nearly all stations in Bavaria. An increase of particle levels is estimated for summer months, independent from considered scenario and time step, on the other hand. Detected changes in winter and summer correspond with variations in the frequencies of occurrence of $PM_{10}$-relevant large-scale atmospheric dynamics. An increase of zonal, cyclonic weather and circulation types for example is estimated in winter and a decrease in summer until the end of this century. In the transitional seasons, variations of estimated $PM_{10}$ levels are less pronounced, more variable and remain insignificant in most of the cases.

Finally, the model skill of the circulation-type-based downscaling models in cross-validation and estimated future climate-change-induced variations of particle levels are compared to results from statistical downscaling models based on local meteorological parameters as predictors. In a two-step process, the local transfer models have been developed in the framework of the research project "Particulate matter and climate change in Bavaria", funded by the German Research Foundation. First of all, local $PM_{10}$-relevant meteorological variables are downscaled from large-scale atmospheric fields and are applied as predictors in statistical downscaling models for estimating $PM_{10}$ concentrations afterwards. Circulation-type-based downscaling models and local transfer models use objective circulation type classifications, that are optimized with respect to their synoptic skill for the target variable $PM_{10}$. All downscaling approaches are evaluated via the aforementioned cross-validation procedure. Detected changes in future $PM_{10}$ concentrations have revealed similar tendencies of decreasing levels in winter and increasing ones in summer for all downscaling approaches. Nevertheless, estimations from circulation-type-based models have shown partly pronounced differences concerning climate models, numerical and statistical ensembles and downscaling approaches compared to results from local transfer models.

# Zusammenfassung

Ein bedenklicher Anstieg von Emissionen feiner Partikel mit einem mittleren Durchmesser < 10 $\mu$m ($PM_{10}$) konnte in den vergangenen Jahrzehnten beobachtet werden, der zu einer zunehmenden Belastung für die Umwelt und die menschliche Gesundheit geworden ist. Urbane Räume sind von der Luftverschmutzung besonders betroffen. Einige Studien belegen die Gesundheitsgefährdung des Menschen durch hohe Feinstaubbelastungen, inbesondere für die Atemwege und das Herz-Kreislauf-System. Raumzeitliche Variationen der $PM_{10}$-Konzentrationen sind auf entsprechende Schwankungen der lokalen Emissionen, aber auch auf den Einfluß der lokalen meteorologischen sowie der großräumigen zirkulationsdynamischen Rahmenbedingungen zurückzuführen. Dementsprechend werden mögliche zukünftige, von der globalen Klimawandeldynamik verursachte Veränderungen der oben genannten meteorologisch-witterungsklimatologischen Einflussgrößen zu korrespondierenden klimawandelbedingten Variationen der lokalen $PM_{10}$-Konzentrationen führen.

Die hier vorgestellten Untersuchungen verfolgen das Ziel der Optimierung von objektiven Zirkulations- und Wetterlagenklassifkationen hinsichtlich ihrer Aussagekraft für $PM_{10}$-Konzentrationen an 16 bayerischen Messstationen (Messnetz des Bayerischen Landesamtes für Umwelt) im Zeitraum 1980-2011. Der Feinstaubdatensatz wird zunächst anhand statistischer Maßzahlen charakterisiert sowie eine Trendanalyse durchgeführt. Mittels einer s-modalen Hauptkomponentenanalyse wird zudem eine Regionalisierung der Feinstaubdaten realisiert. Jeweils eine repräsentative Messstation der resultierenden Regionen wird, je nach Fragestellung und Analysemethode, für die in dieser Arbeit präsentierten Untersuchungen herangezogen.

Die Erstellung von Zirkulations- und Wetterlagenklassifikationen erfolgt auf der Grundlage täglicher, gegitterter atmosphärischer Felder (2,5 x 2,5 horizontale Auflösung) des NCEP/NCAR Reanalysedatensatzes für verschiedene meteorologische Parameter. Die Optimierung der Klassifikationsansätze bezüglich ihrer Trennschärfe für tägliche $PM_{10}$-Konzentrationen beruht auf Variationen der zugrundeliegenden Klassifikationsmethode, der Klassenanzahl, des räumlichen und zeitlichen Betrachtungsausschnitts sowie der Auswahl und variabel gewichteten Kombination der klassifizierten Variablen. Alle Klassifikationsvarianten werden schließlich mittels objektiver Gütemaße evaluiert und verglichen, um auf diese Weise die geeignetsten Ansätze für weiterführende Analysen zu ermitteln. Dabei zeigt sich eine höhere Güte des Zusammenhangs bei Berücksichtigung eines mittleren räumlichen Betrachtungsausschnitts (7,5°-27,5° O und 40°-60° N), 18 Klassen, einer saisonalen Klassifizierung sowie einer gewichteten Kombination mehrerer Einflussvariablen, besonders Lufttemperatur, Bodenluftdruck, spezifische und relative Feuchte, zonaler Wind, Vertikalgeschwindigkeit sowie die geopotentielle Höhe der 500 hPa-Fläche. Die höchste Güte wird

insbesondere in den Wintermonaten (Dezember, Januar, Februar) erzielt. Für jede Station und jede Jahreszeit werden so die geeignetsten Klassifikationen ermittelt.

Für den Zeitraum 1980-2011 werden anschließend verschiedene Ansätze zum statistischen Downscaling lokaler Partikelkonzentrationen entwickelt. Diese umfassen das synoptische Downscaling täglicher $PM_{10}$-Werte sowie unterschiedliche multivariate statistische Modellansätze (Multiple Lineare Regression, Random Forests, Generalisierte Lineare Modelle) zur Abschätzung monatlicher PM10-Indizes, unter Verwendung großskaliger Einflussgrößen. Die Prädiktoren bilden hierbei die monatlichen Auftrittshäufigkeiten von 18 Zirkulationstypen einer optimierten Klassifikation. Die Eignung der verschiedenen Downscalingverfahren wird auf der Grundlage von Kreuzvalidierungen, die auf variierenden Subintervallen aus dem Zeitraum 1980-2011 als Kalibrierungs- bzw. Validierungssamples basieren, in Form adäquater Skill-Metriken (z.B. Mean Squared Skill Score) quantifiziert. Die höchste Güte der zirkulationsmuster-basierten Downscalingmodelle wird für monatliche $PM_{10}$-Konzentrationen an allen Stationen mit den Random-Forest-Modellen im Winter erreicht.

In einem weiteren Schritt erfolgt die Übertragung der geeignetsten Downscalingansätze auf verschiedene CMIP5-Modelle (ECHAM6, EC-Earth), um zu Abschätzungen möglicher zukünftiger $PM_{10}$-Konzentrationsänderungen für unterschiedliche Zeiträume (2021-2050, 2071-2100) und unter Zugrundelegung variierender Annahmen zur zukünftigen Entwicklung atmosphärischer Treibhausgaskonzentrationen (RCP 4.5, RCP 8.5) zu gelangen. Zu diesem Zweck werden die Zentroide der optimierten Zirkulationsmuster auf Projektionen der Klimamodelle (numerische Ensembles) übertragen und die daraus resultierenden Prädiktoren in den Downscalingmodellen verwendet. Neben den numerischen Ensembles für ECHAM6 wurden auch statistische Ensembles für die Downscalingmodelle in der Kreuzvalidierung generiert, um mögliche Modellunsicherheiten zu berücksichtigen. Es lassen sich langfristige Konzentrationsabnahmen im Winter an allen Stationen feststellen, die mit einer überwiegenden Häufigkeitszunahme von zonalen, zyklonal geprägten Zirkulationstypen vom historischen Modellzeitraum zu den Projektionen korrespondieren. Als weiteres maßgebliches Änderungssignal konnte eine Konzentrationszunahme im Sommer an den bayerischen Messstationen detektiert werden, die durch eine Häufigkeitsabnahme der zonalen, zyklonal geprägten synoptischen Situationen erklärt werden kann. In den Übergangsjahreszeiten dagegen zeigen sich geringer ausgeprägte Änderungstendenzen, die in den meisten Fällen insignifikant bleiben. Diese potentiellen Variationen der Partikelkonzentrationen bis zum Ende dieses Jahrhunderts konnten auch bei dem Vergleich der Abschätzungen aus den verschiedenen Klimamodellen beobachtet werden.

Abschließend wurden die Abschätzungen und die Performanz der generierten zirkulationstypen-

basierten Modelle mit lokalen Transferfunktionen, die im Rahmen des Projektes "Klimawandel und Feinstaubbelastung in Bayern"der Deutschen Forschungsgemeinschaft entwickelt wurden, verglichen. Innerhalb des Projektes wurde für die Modellierung täglicher $PM_{10}$-Werte ein zweistufiges Verfahren ausgearbeitet, das zunächst $PM_{10}$-relevante, lokale meteorologische Größen aus großskaligen atmosphärischen Feldern abschätzt, die anschließend als Einflussgrößen in statistische Transferfunktionen zur Abschätzung lokaler Feinstaubkonzentrationen eingehen. Aus dem Vergleich der Modellansätze lassen sich, trotz teilweiser ausgeprägter Unterschiede zwischen Klimamodellen, numerischen und statistischen Ensembles sowie Downscalingverfahren, die überwiegenden Konzentrationsabnahmen im Winter und -zunahmen im Sommer für alle Varianten feststellen. Die Modellgüte der lokalen Transferfunktionen für die Abschätzung täglicher $PM_{10}$-Konzentrationen zeigt im Wesentlichen eine bessere Performanz als die zirkulationstypen-basierten Modelle auf Basis des synoptischen Downscaling. Für die Modellierung monatlicher $PM_{10}$-Indizes ergibt sich dagegen eine vergleichbare bis bessere Modellgüte bei den lokalen Transfermodellen.

# 1. Introduction

## 1.1. Motivation

*"Clean air is considered to be a basic requirement of human health and well-being. However, air pollution continues to pose a significant threat to health worldwide. According to a WHO assessment of the burden of disease due to air pollution, more than 2 million premature deaths each year can be attributed to the effects of urban outdoor air pollution and indoor air pollution (caused by the burning of solid fuels). More than half of this disease burden is borne by the populations of developing countries."*

WHO 2005

Clean air is vital for all living organisms on earth, as this statement by the World Health Organization clarifies. Air pollution can be summarized as gaseous and particulate contaminants that are present in the atmosphere varying for example in size, shape, number, chemical composition, solubility and origin. Particulate air pollutants can be categorized into coarse, fine and ultrafine particles according to their medium diameter. They stem from both natural and anthropogenic sources. Natural sources of air pollutants, which form a natural background concentration, are for instance volcanoes, soil and rock debris, biomass burning or seas spray. Man-made air pollution is based on the burning of fossil fuel, industrial and transportation processes as well as volatile non-industrial sources like dust from roads or agriculture.

Former definitions of air pollution located the phenomenon only in urban and highly industrialized areas. Nowadays, it is clear that substances, resulting from both natural and anthropogenic sources, with concentrations high above their normal ambient levels, exists over the whole planet. Air pollutants are known to have a distinct effect on materials or living creature, without respecting any national frontiers (Seinfeld and Pandis, 2012). Quantities of emitted chemicals from all sources range from hundreds to millions of tonnes annually. With an increase of motorization and industrialization on earth, with rising numbers of humans and rapid urbanization, air pollution is one of the alarming global environmental problems of the 21th century with a considerable effect on human health in all stages of life.

This thesis focuses on $PM_{10}$, which is one of the most important air pollutants with an adverse impact on human health (Bayerisches Staatsministerium für Umwelt, 2006; Brunekreef and Holgate, 2002). Depending on the time scales of exposure, these effects range from changes in blood

Figure 1.1: Inhabitants of Beijing riding their bikes through the traffic with masks on during a high pollution event 2011 (Source: Greenpeace 2011).

parameter, cardiovascular, respiratory and pulmonary diseases as well as hospital admissions or even mortality. Especially elder and sick people, pregnant women as well as kids are affected. Ultrafine particles, e.g. $PM_{2.5}$ and $PM_1$, turned out to be even more critical. Unfortunately, there is still a lack of knowledge of the health effects of these ultrafine particle sizes caused by limited data availability due to complex techniques needed to measure them (Pope and Dockery, 2006; Rückerl et al., 2011). In contrast, $PM_{10}$ are part of operational networks since decades. In Bavaria/Germany for example, which is the target region of the present analysis, time series of measurements over 30 years exist. These series of measurements enable investigations on a long-term period.

Urban areas are particularly involved in increasing emission levels. Pictures from megacities, like Beijing or Mexico City, showing people wearing masks while walking in hazy streets during extreme smog events, circulate in press and illustrate the problem of urban air pollution. Figure 1.1 for example depicts people in Beijing on a high pollution event in 2011 riding their bikes through the traffic. The dense smog prevents the sunlight from shining through and impairs the visibility. As urban areas are especially vulnerable to high pollution events, a special focus of this thesis is set on urban aerosols. Urban air pollution has become critical over the globe in all major cities, especially in developing countries. Increasing emission levels in urban agglomerations are caused for example by growing vehicle particle load from a high number of older vehicles coupled with poor maintenance, inadequate infrastructure as well as low fuel quality. Additionally, urban areas are the economic centres of the countries with increasing industry, transportation and immigration.

The role of liquid and solid particles in the air, also known as aerosols, in the climate system

has been already a subject of research in the past years and statements about it are presented in the Fourth (AR4) and Fifth Assessment Report (AR5) of the Intergovernmental Panel on Climate Change (IPCC) (Stocker et al., 2013). In this emergent field of research, aerosols have been found to have an amplifying impact on climate through the absorption of incoming sunlight and thus a heating effect. The opposite, a negative impact with a cooling effect, emerges from a direct reflection of the incoming sunlight on the particles directly back into space. Both processes are called the direct effect of aerosols in the climate system. Aerosols act as cloud condensation nuclei for the formation of cloud droplets as well, which reflect the sunlight back into space. The latter is called indirect aerosol effect. Yet, these findings of the direct and indirect effect of aerosols in the climate system are stated with a high uncertainty in the reports of the IPCC.

Climate also affects particle concentrations. It is commonly known that air pollution is determined by both the amount of emissions and meteorological conditions with variations in space and time. A daily and weekly cycle of air pollution, for example, can be observed depending on the rush hour traffic with high pollution loads on working days in all countries. In winter time, as another example, a mixture of heating, high traffic load and stable atmospheric conditions with nearly no air mass exchange can lead to smog events in European cities. Particles emerging from photochemical reactions usually have higher concentrations in summer due to higher temperature on a local to regional scale. In street canyons in urban areas ventilation is needed, otherwise particles are accumulated and high pollution levels are reached in a minimum of time. As climate is changing readily, meteorological conditions on different scales will change until the end of this century as well. Hence, the question arises, whether particle concentrations will change due to climate change effects.

According to the current AR5 of the IPCC, the range in projections of local ozone and fine particle ($PM_{2.5}$) levels is primarily driven by emissions, rather than by physical climate change. As observational and modelling evidence indicates, climate change may alter removal processes by wet deposition or natural aerosol resources due to variations in precipitation or changes in chemistry and local emissions by increasing surface temperature (Stocker et al., 2013). Nevertheless, no confidence level is attached to the overall impact of climate change on $PM_{2.5}$ distributions. That fact evokes the need of further investigations with respect to climate change effects on local particle concentrations and robust models for reliable statements.

In order to contribute to these open research questions for the target region Bavaria in this thesis, influences of large-scale atmospheric conditions on urban particulate matter concentrations in Bavarian cities, measured for a 32-year period, are investigated at first. The analyses on a synoptic scale enable the evaluation of climatic impacts on air pollution as studies over the past decades

confirm. In a comprehensive study, objective circulation type classifications are optimized with respect to the target variable $PM_{10}$ to characterize those synoptic situations having a distinct effect on daily and monthly particle levels. Secondly, various statistical downscaling approaches, based on the characterized large-scale atmospheric conditions as influencing variables, are developed and compared in order to downscale particle concentrations in the recent period 1980-2011.

Nowadays much effort is set on the improvement of both short-term and long-term air quality prediction models and systems to forecast air pollution levels for the next few hours, days, weeks up to decadal time horizons. For short-term deterministic predictions, complex models, comprising an entire description of atmospheric chemistry and meteorological processes, provide promising results. Long-term predictions, based on climate-air-quality modelling systems, still need improvement with respect to computational and technical requirements for instance. Statistical downscaling techniques have turned out to be suitable to predict air quality levels from meteorological conditions on various time and spatial scales (Demuzere and van Lipzig, 2010a). On the basis of the downscaling models developed in the second part of this thesis, it is furthermore intended to estimate possible future climate-change-induced variations of particle concentrations from scenario runs of General Circulation Model (GCM) until the end of this century. With climate changing rapidly, these connections needs to be better understood in order to enable estimates of climate change related consequences for air quality management purposes.

The concept and main contributions of the present work are content of Section 1.2 and a thesis overview is given in Section 1.3.

## 1.2. Contributions

The main contributions of the thesis can be summarized as follows:

1. *Objective circulation type classifications optimized with respect to their synoptic skill for the target variable $PM_{10}$*: The general link between local particle levels and large-scale circulation dynamics - as reflected by Circulation Type Classifications (CTC) - has been proven in several studies. Thus far, only a few systematic attempts have been made to modify existing or to develop new classifications in order to improve their ability to resolve local particle concentrations. Hence, an iterative optimization, using a broad variety of set-ups, is performed to further characterize those synoptic situations having a distinct influence on local particulate matter with aerodynamic diameter $< 10\ \mu$m ($PM_{10}$) concentrations in Bavaria. The stated relationship is quantified by objective evaluation measures. Such an extended and systematic optimization of objective classifications with respect to the target variable $PM_{10}$ has not been done before. A selection of optimized seasonal synoptic CTC is derived for

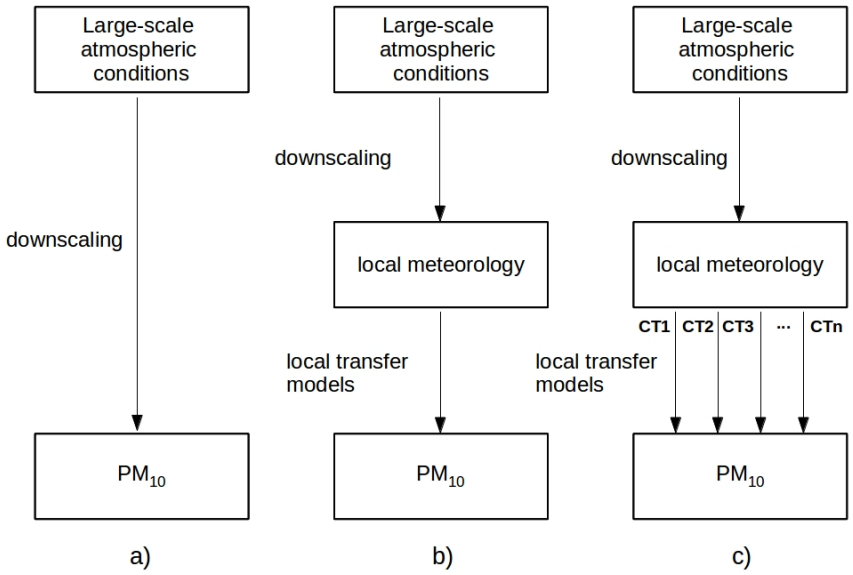


Figure 1.2: Scheme of three statistical downscaling approaches used in the project "Particulate Matter and Climate Change in Bavaria" (PACLIMBA) to investigate the influences of meteorology on various spatial scales on local $PM_{10}$ concentrations.

the application on statistical downscaling models. It has to be clearly stated, that no source apportionment or analysis of the influence of emissions on both measured and modelled data are conducted in this thesis. The main focus is set on the analysis of meteorological-climatological influences on local particle levels in Bavarian cities on various temporal and spatial scales.

2. *Linking seasonal large-scale atmospheric conditions to local $PM_{10}$ concentrations using various statistical downscaling methods*: Yarnal (1993) introduced two descriptive terms to illustrate the way atmospheric circulation, represented by weather and circulation type classifications, and smaller-scale environmental parameters can be related: the circulation-to-environment approach and environment-to-circulation approach. This thesis focuses on the circulation-to-environment methodology as depicted in Figure 1.2 (a). Classified large-scale atmospheric fields, represented by frequencies of occurrence of synoptic circulation patterns, are directly linked to smaller-scale variables, i.e. local $PM_{10}$ concentrations, by using a set of statistical downscaling approaches. Various methods exist in literature for statistical downscaling purposes. Especially regression-based methods have turned out to be an appropriate attempt for the analysis of the physical processes behind the relationship of predictors to predictands in the studies. A comprehensive selection of downscaling tools (Synoptic Downscaling, Multiple Linear Regression, Generalized Linear Models, Random Forests) is employed for estimating different $PM_{10}$ indices in the period 1980-2011 at 16

selected urban locations in Bavaria/Germany from monthly occurrence frequencies of optimized Circulation Types (CTs). The performance of the transfer models is objectively evaluated on the basis of various evaluation measures. The model skills are analyzed in three independent calibration and validation periods to detect the most suitable downscaling methodology, to identify CTs having a distinct influence on the target variable and to develop robust downscaling models for the application on future climate change projections.

3. *Estimation of future climate-change-induced variations of local $PM_{10}$ concentrations*: As it has become widely recognized and was described previously, climate change can affect air quality, particularly in the highly vulnerable urban areas. Reports investigating changes of Circulation Types (CTs) under future climate change conditions using GCM data get more numerous. Many studies focus on the short-time forecast of air pollution. For the prediction of long-term variations of air quality, some studies concentrate on the estimation of future climate-change-induced variations of air quality levels based on GCM for periods up to the year 2100. In this study, ensemble members from Atmosphere-Ocean Coupled General Circulation Models (AOGCM) from the current IPCC AR5 are applied to assess the potential effects of projected future changes in large-scale atmospheric circulation on $PM_{10}$ indices in the target region. First, selected CTs used in the downscaling models are assigned to gridded AOGCM data. These are, on the one hand, ensemble runs for a control period from 1980-2005 (historical runs) and, on the other hand, for two scenarios (RCP 4.5 and 8.5) differentiated in two time periods (2021-2050, 2071-2100). The occurrence frequencies of the resulting types are employed as predictors to model $PM_{10}$ indices. An estimation of future climate change induced variations of local $PM_{10}$ concentrations in the 16 Bavarian cities is therefore enabled. Instationarities between synoptic and local scale processes are taken into account by using statistical ensembles resulting from different selected calibration and validation periods. Uncertainties emerging from the usage of GCM projections are considered by numerical ensemble members, two future time periods as well as by the usage of different GCMs.

4. *Comparison of two quantitative approaches for estimating future climate-change-induced variations of $PM_{10}$ in Bavaria*: The presented work is conducted in the project "Particulate Matter and Climate Change in Bavaria" (PACLIMBA) funded by the German Research Foundation. In the framework of the project, quantitative relationships between daily and monthly $PM_{10}$ data at different Bavarian stations and the corresponding large-scale atmospheric circulation and local meteorological conditions are investigated. The downscaling approaches encompass the synoptic downscaling of daily $PM_{10}$ concentrations as well as several multivariate statistical models for the estimation of daily and monthly $PM_{10}$ indices as depicted in Figure 1.2 (a) - (c). All techniques use objective circulation type classifi-

cations that have been optimized with respect to their synoptic skill for the target variable $PM_{10}$. The described model approaches from Figure 1.2 are set up, compared and tested for a recent period 1980 to 2011. The most suitable downscaling procedures, in terms of model skill determined from cross-validation, are finally applied to projections of climate models to derive estimates of possible future climate-change-induced variations in $PM_{10}$ levels in Bavaria. In this thesis, model results from circulation-type based approaches (1.2 (a)) are compared and discussed with respect to local transfer models.

## 1.3. Thesis Overview

This thesis starts with a review of the literature in Chapter 2. An introduction of sources and health effects of particulate matter is presented together with an overview of existing studies determining the predictive relationship between meteorological variables on various spatial and temporal scales and particle concentrations. The following Chapter 3 comprises a brief description of the used data sets. The basic principles of the statistical methods and quantitative evaluation measures applied for the data analysis are content of Chapter 4. Chapter 5 contains a more detailed description of the unique $PM_{10}$ data basis, a trend analysis of particle concentrations in the period 1980-2011 as well as a regionalization of the measurement sites. A stepwise optimization of objective circulation type classifications with respect to the target variable $PM_{10}$ is performed and discussed in Chapter 6. Monthly occurrence frequencies of circulation types from selected classifications are used as predictors in statistical downscaling models to asses $PM_{10}$ indices (predictands) for the recent period 1980-2011. Results from the downscaling models are given in Chapter 7. Most suitable downscaling models, developed in Chapter 7, are applied on GCM runs to estimate future climate-change-induced variations of $PM_{10}$ concentrations in Chapter 8. Finally, a comparison with other quantitative approaches for estimating future particle levels, which are based on local meteorology as predictors in statistical downscaling models, is drawn in Chapter 9. The main conclusions emerging from the presented investigations of this thesis are given in Chapter 10 along with a brief outlook.

# 2. Review of the literature

In general, air pollution is described as gaseous, solid and liquid chemicals, that are emitted into the air. Gaseous pollutants include sulphur dioxide ($SO_2$), nitrogen oxides ($NO_x$), tropospheric ozone ($O_3$), carbon monoxide ($CO$), volatile organic compounds ($VOC$), hydrogen sulphide ($H_2S$), hydrogen fluoride ($HF$), and various gaseous forms of metals. Particulate matter (PM) is a mixture of solid or liquid particles in the air with varying sizes from a few nm to tens of $\mu$m, but larger than molecular dimensions. Aerosols are in addition defined as tiny solid or liquid particles in gas (Seinfeld and Pandis, 2012).

The size and chemical composition of particles determine their physical and chemical properties. Furthermore, they vary in number, shape, surface, area, chemical composition, solubility as well as origin (Pope and Dockery, 2006). PM is unique in its complexity and once emitted into the atmosphere, the properties are changed by different mechanisms until they are removed by dry or wet deposition. According to Seinfeld and Pandis (2012), *dry deposition* is defined as direct transfer of gaseous and particulate species to the Earth's surface without being removed by precipitation. In contrast, all processes in which airborne particles are transferred to the surface in aqueous form, for example by rain, snow or fog, are subsumed as *wet deposition*. The usual residence time of PM does not exceed several weeks in the lower atmosphere. The residence times of particles vary from only a few days to just a few weeks in the troposphere. Near the surface, the dominating removal processes are dry deposition and settling. Surpassing around 100 m above ground, the wet deposition is the main removal process (Seinfeld and Pandis, 2012).

A brief description of the health effects of PM is given in Section 2.1 followed by an introduction of sources of particles in Section 2.2. A broader discussion on particulate matter and climate respectively climate change is given in Section 2.3 starting with a general introduction of the relationship between particles and climate. Influences of meteorological conditions on air quality as represented by large-scale atmospheric conditions are discussed in Section 2.3.1 and local meteorological conditions in Section 2.3.2. Existing studies on forecast of particle levels are finally given in Section 2.3.3.

## 2.1. Health effects of particulate matter

According to the particle size, Particulate Matter (PM) can be categorized in ultrafine (< 100 nm), fine (< 2.5 $\mu m$) and coarse fraction (> 2.5 up to < 10 $\mu m$). In practical terms, PM with a particle size distribution of a median aerodynamic diameter < 10 $\mu m$ are also called $PM_{10}$ (or "thoracic" particles), that can penetrate into the lower respiratory tract of a human being (Heyder, 2004). Figure 2.1 shows the relationship between particle size (in diameter) and their deposition in the

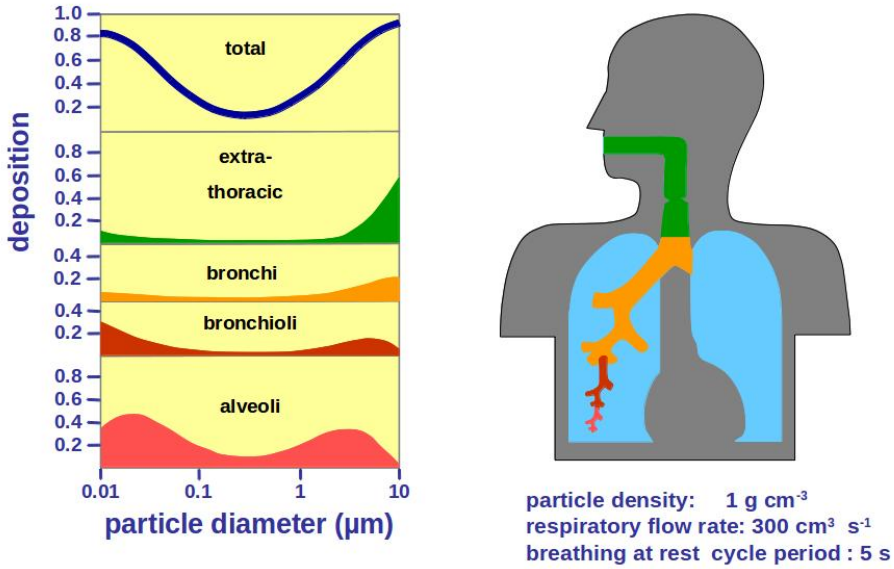


Figure 2.1: Particle size (in $\mu$m) and their deposition in the respiratory tract of a healthy adult marked by colours (adapted from Heyder 2004).

respiratory tract, marked by colours, of an healthy adult. $PM_{2.5}$ ("respirable" particles < 2.5 $\mu m$) can be infiltrated into the gas-exchange region of the lung, the bronchi and bronchioli parts, and $PM_1$ (< 1 $\mu m$) even into the blood with affecting and changing blood parameters, which is the alveoli part of the respiratory tract. Another classification of particle sizes divides them into the nucleation mode (< 10 nm), Aitken mode (10 - 100 nm), accumulation mode (0.1-2.5 $\mu m$) as well as the coarse mode (> 2.5 $\mu m$) (Seinfeld and Pandis, 2012).

Epidemiological studies over the past 20 years have proven adverse effects of $PM_{10}$ on human health, depending on the extent and duration of the exposure (Pope et al., 1995; WHO, 2006). Reviews on both short-term and long-term studies on air pollution and health effects have been presented for example by Brunekreef and Holgate (2002); Pope and Dockery (2006) or Rückerl et al. (2011). Particulate matter concentrations have been found to have serious effects on human health, for example cardiovascular diseases, changing blood parameters, reproduction as well as prenatal outcomes, hospital admissions, neurotoxic influences, respiratory and pulmonary effects or even mortality. Fine particles can even cause cancer and the risk of infant mortality increases with high pollution concentrations. In a comprehensive health impact assessment on $PM_{10}$ in 19 European cities, Medina et al. (2004) have investigated increasing mortality rates of population with high particulate matter exposure. Public health effects of critical particle levels depend on varying factors as size of particles, exposure in terms of spatial and temporal variations (short- and

long-term) for example.

The European Union (EU) inaugurates long- and short-term air quality standards of $PM_{10}$ for health protection in its Directive 2008/50/EC (E.U., 2008). According to these air quality standards, a daily average $PM_{10}$ concentration in air at a given station of 50 $\mu gm^{-3}$ must not exceed more than 35 times a year. Since 2011, sanctions were imposed on cities not in accordance with this air quality goals.

Given the current capacity of measurement techniques, it is still challenging to determine concentrations of the very fine particles like $PM_{2.5}$ or $PM_1$ (Kuttler, 2011a). The indirect and direct measurement of $PM_{10}$ in contrast are part of operational networks for time periods covering more than 30 years. This fact offers the opportunity for the well-founded statistical analysis of variations in air quality and their causes by a reliable estimation of statistical relationships between particles (predictands) and influencing parameters (predictors).

## 2.2. Sources of particles

Sources of PM can be categorized into four groups:

1. *Primary natural particles* stems from various biotic and abiotic sources, e.g. wind-borne dust, sea-spray, plants, radiological decomposition, forest fires, soil erosion or volcanoes (Seinfeld and Pandis, 2012).

2. *Secondary natural PM*, build by gas-to-particle conversion processes, emerge for example from gaseous activities of volcanoes, methane from wetlands or dinitrogen monoxide ($N_20$), nitrate from soils and organic aerosols from biogenic volatile organic compounds (VOC). Primary and secondary natural particles form a natural background concentration, which varies according to local sources or specific weather conditions (WHO, 2006; Umweltbundesamt, 2005; Seinfeld and Pandis, 2012).

3. Anthropogenic air pollution has increased rapidly since the industrialization. The enlargement of worldwide air pollution, resulting from the progressive use of fossil energy sources, the growth in manufacturing as well as use of various chemicals, has been accompanied by mounting public awareness of and concern about its adverse effects on health and the environment (WHO, 2006). *Primary anthropogenic particles* for example are formed and emitted directly at their origin. Large stationary sources are for example fossil fuel fired power plants, smelters, industrial boilers, petroleum refineries, and manufacturing facilities (Umweltbundesamt, 2005). Furthermore, these particles emerge from area and mobile

sources such as planes, ships and all forms of vehicles. The major aerosol classes of the primary anthropogenic aerosols can be summed up as industrial dust, black carbon and organic aerosols.

4. *Secondary anthropogenic PM* sources set gaseous components free. These are for example sulphur oxides ($SO_2$, $SO_3$), ammonia ($NH_3$) or nitrogen oxides ($NO_x$). Secondary particles are formed by complex chemical reactions (Umweltbundesamt, 2005).

The load of local particle concentrations are affected by the extent of natural and anthropogenic as well as by the level of precursor emissions. Major sources of particulate matter in Germany are, according to a recent report of the Federal Environment Agency, traffic and burning of fossil fuel and biomass especially in power industry, other industries and households (Umweltbundesamt, 2015). In German urban areas, basically traffic emissions (about 50%), especially diesel-powered vehicles, traffic abrasion products (25%) as well as long-ranged transportation processes (25%) have been identified to be the main sources (Umweltbundesamt, 2005). Currently, the annual mean concentrations for $PM_{10}$ in Germany show values around 10 to 18 $\mu g/m^3$ for rural areas, 20 to 30 $\mu g/m^3$ for urban background stations and 30 to 45 $\mu g/m^3$ in traffic related areas (Wichmann, 2008).

Urban areas are frequently burdened with enhanced air pollution and exceeding limit values particularly for $PM_{10}$ and smaller particle sizes (Schäfer et al., 2014). The main sources of urban aerosols are on the one hand natural ones and on the other hand emissions from industries, power generation, transportation processes or secondary formed material by gas-to-particle conversion (Seinfeld and Pandis, 2012). In their comprehensive study about sources of particles in European cities by Kiesewetter et al. (2015), comparatively high regional background contributions from natural, national and international sources are mainly combined with traffic emissions from domestic and transport vehicles. High pollution events are further intensified by the disposition of the street canyon, landscape or adverse weather conditions (Umweltbundesamt, 2015; Kiesewetter et al., 2015).

## 2.3. Particulate matter and climate

Aerosols have both a *direct* and an *indirect* effect on climate (Arneth et al., 2011). The *direct* effect occurs by scattering and absorption of solar radiation. Looking at the process of scattering, the incoming sunlight is reflected by the particles and the amount of solar radiation reaching the earth surface is reduced. As a results, a cooling effect for the climate is assumed. This is only the case for radiation that is scattered back in upward direction, which is back to space (Seinfeld and Pandis, 2012). Depending on the properties of the particles, they can absorb incoming solar radiation and therefore have a heating effect on climate. The *indirect* effect of aerosols in the climate

system is more complicated. Basically, aerosols act as condensation nuclei for cloud formation. Changes in population and sizes of cloud droplets, which leads to changes in cloud albedo and spatial extent, are dependent on particles (Seinfeld and Pandis, 2012).

The *direct* and *indirect* effect of aerosols on the global radiation and energy budget are content of the recent AR5 of the IPCC (Stocker et al., 2013). The Radiative Forcing (RF)[1] is the change in energy flux caused by a driver, and is calculated at the tropopause or at the top of the atmosphere. The total aerosol effect in the atmosphere is estimated with -0.9 [-1.9 to -0.1] W $m^2$ (medium confidence) and poses the largest uncertainty to the total RF estimate. Figure 2.2 depicts the estimation of the RF for both naturally and anthropogenic emitted atmospheric trace gases and aerosols. The best estimates of the net radiative forcing are shown as black diamonds with corresponding uncertainty intervals. The numerical values are provided on the right of the figure together with the confidence level in the net forcing (VH-very high, H-high, M-medium, L-low, VL-very low). Results show a negative forcing from most aerosols and a positive contribution from black carbon absorption of solar radiation. There is high confidence that aerosols and their interactions with clouds have offset a substantial portion of global mean forcing from well-mixed greenhouse gases.

Besides the fact that aerosols have a direct respectively indirect effect on climate through influencing the solar radiation, changes in climate also affect air quality. The temporal and spatial variability of local PM concentrations is on the one hand influenced by the amount of emitted natural and anthropogenic particles and on the other hand by varying meteorological and climatological conditions on the local to synoptic scales. In general, the quantitative relationship between meteorological conditions on different scales and local $PM_{10}$ concentrations has been proven in several studies so far. As it has been summarized by Demuzere et al. (2009) for example, emissions, as biogenic or dust related ones, may be dependent on climatic variables. On a local scale, they mention temperature, humidity measures, like relative or specific humidity, precipitation, which influences wet deposition processes, solar radiation fluxes and cloudiness, which have an influence on chemical processes. On a regional scale, short and long-term transport processes depend on surface turbulences and large-scale atmospheric circulation. Jacob and Winner (2009) furthermore have listed changes in air quality through perturbing ventilation rates, e.g. wind speed, mixing depth, convection, frontal passages, dry deposition, chemical production and loss rates, natural emissions and background concentrations and precipitation scavenging. The effect of temperature changes on local $PM_{10}$ concentrations in German urban area in context of global climate change has been discussed by Kuttler (2011a). An influence of temperature on $PM_{10}$ concentrations is

[1] The Radiative Forcing (RF) quantifies the strength of drivers, which are characterized as natural and anthropogenic substances and processes that change the Earth's energy budget. It was introduced in previous Assessment Reports (AR4) and is calculated in units watts per square metre (W $m^2$).

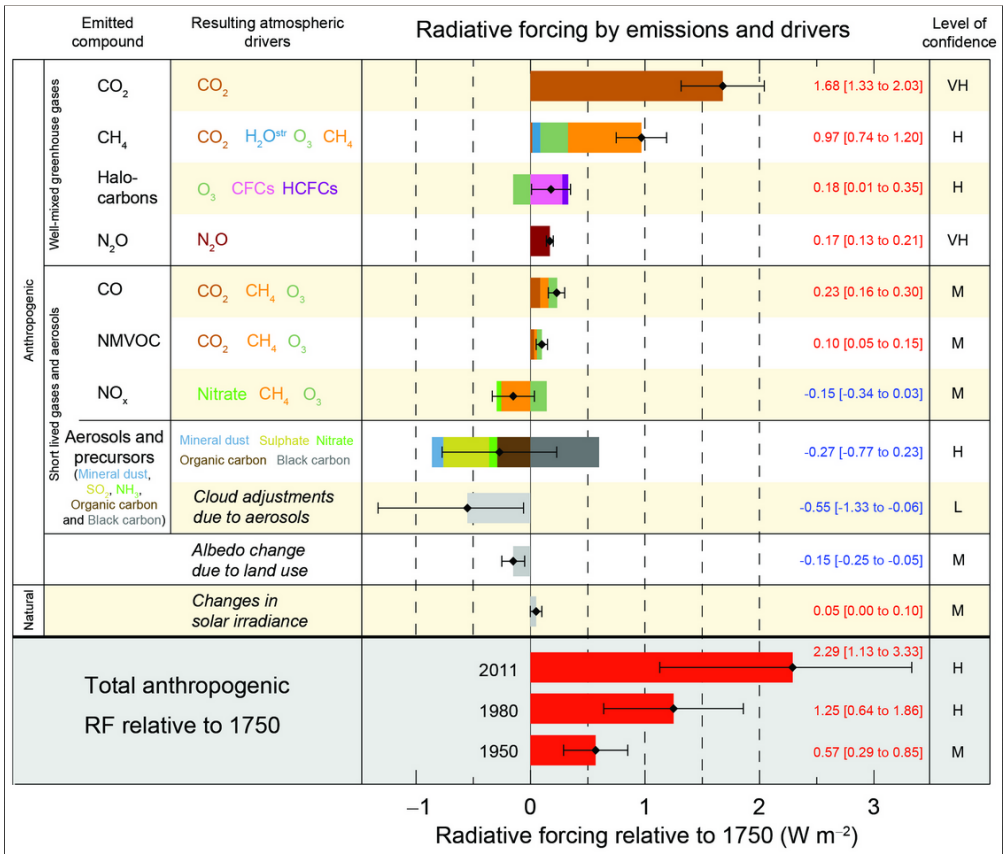


Figure 2.2: Radiative forcing and aggregated uncertainties for atmospheric trace gases and aerosols. Except for black carbon, which causes a tendentiously positive direct effect on the solar radiation, all aerosols and their precursors show a tendentiously negative RF with a high confidence level (Source: Stocker et al. (2013)).

stated therein, but with a large uncertainty. One has to keep in mind that the response of particulate matter on climate change processes is quite complicated to assess due to the diversity of PM components and compensating effects (Jacob and Winner, 2009).

Varying meteorological and climatological conditions on local, regional and synoptic scales are known to have an influence on spatial and temporal variations of local air quality such as $PM_{10}$ concentrations. With respect to public health effect of air pollutants, much attention is paid to improve the accuracy of short-term deterministic as well as statistical prediction models based on meteorological-climatological influences on the target variable. The development of robust long-term air quality prediction systems is currently a major concern (Stocker et al., 2013).

Interactions and relationships between the atmosphere, in the following represented by atmospheric circulation, and surface environment, for example air quality parameters, air temperature, precipitation, drought, and many others, are studied in the field of synoptic climatology. Classifi-

cations of weather and circulation types are a common tool in synoptic climatology to analyse and characterize large-scale atmospheric dynamics, to simplify large data sets in groups/classes/types/categories. Yarnal (1993) has worked out four factors, which all studies in the broad field of synoptic climatology have in common. First, the atmospheric circulation is classified. Mostly map patterns, showing pressure centres, or synoptic types, which represent weather properties, are used. Second, synoptic climatological studies link at the minimum two scales, e.g. large-scale atmospheric circulation and small-scale target variables. Thirdly, a main goal is to consider the effect of climate variability of the surface environmental parameters including seasonal, monthly or inter annual changes. Finally, the spatial unit of interest is on a regional scale. A general proceeding of all studies in this field can be depicted. Initially, the atmospheric circulation is classified in a way to structure and simplify the essential informations of the large-scale atmospheric conditions. From this level, a statistical link to smaller-scale environmental variables or phenomena is performed. Those studies still focus on a special region of interest and the effect of climatic variability (Yarnal, 1993; Yarnal et al., 2001).

The general relationship between large-scale circulation dynamics, as reflected by weather and circulation types CTs, and local to regional air quality data has been proven in various studies for different regions of interest. In the following Section 2.3.1, a selection of existing studies is summarized depicting the broad range of used classification methodology for describing the mentioned linkage in different regions and environments. For bridging the gap between the coarse resolution of the global, synoptic or regional scale data and local observations of air quality variables, statistical downscaling methods are a commonly used tool. In contrast to dynamical downscaling techniques, which are based on physical dynamics of a system, the used statistical downscaling approaches describe the relationship derived from observational data, e.g. reanalysis data, satellite data or other measurement techniques. Statistical downscaling methods are quite useful instruments with respect to computational requirements.

A brief overview of studies indicating the local and background contributions to air quality data based on empirical prediction models is given in Section 2.3.2. Existing reports have discussed model results for predicting several air quality parameters for various locations using a single method or combinations of statistical approaches. Literature presented in in Section 2.3.3 focuses on the prediction of particulate matter. The last part of this literature review is on forecast of air quality, again with a focus on statistical downscaling techniques.

### 2.3.1. Influences of large-scale atmospheric dynamics

Numerous studies investigating the relationship between synoptic circulation patterns, classified for example for a specific time, region of interest or from different predictor variables, and air pollution exist. The general proceeding is to arrange large-scale atmospheric fields of different variables, e.g. mean sea level pressure or geopotential height, using various statistical classification methods, for example cluster analysis, principal component analysis, leader algorithm, threshold based ones, and quantify the relation to a target surface variable afterwards. A review on classifications of atmospheric circulation patterns including recent applications and improvements have been given for example by Huth et al. (2008). An overview of existing weather and circulation type classifications for the European domain, with a brief introduction into the statistical algorithms behind, have been given by Philipp et al. (2010) or Philipp et al. (2014) for example. A selection of studies investigating the influence of large-scale atmospheric dynamics on air quality is presented in the following.

In an early study, McGregor and Bamzelis (1995) have shown results for the analysis of synoptic types classified with a principal component based approach and a cluster analysis to derive airmass types, which are analysed by their climatological, meteorological and air pollution characteristics for the period of 1992-1993 in Birmingham/UK. High pollution levels occur mainly under continental anticyclonic conditions in the area and low levels under strong westerly flows. Later on, another study by Buchanan et al. (2002) have confirmed these findings. They have analysed the influence of regional-scale circulation types (Jenkinson Daily Weather Types) on particle concentrations of Black Smoke and $PM_{10}$ in Edinburgh, UK for the two periods 1981-1996 and 1992-1996. Additionally, Buchanan et al. (2002) have computed air mass back trajectories. Results given there show especially anticyclonic weather types to elevate air pollution in UK through long-range transport from Europe. Based on a manual classification of four synoptic types with special focus on Greece, Triantafyllou (2001) have investigated the prevailing meteorological conditions during days with high concentrations of $PM_{10}$ from 1991-1994 in a mountainous industrial area. High pollution events have occurred during stagnant conditions in this study. A manual synoptic classification for the East Coast of New England has been applied on regional $PM_{2.5}$ concentrations from 1995-1999 by Keim et al. (2005). In summary, north to north-west weather types tend to have low $PM_{2.5}$ concentrations and transport from south to south-west high ones. Dayan and Levy (2005) have used as well a subjective manual classification of synoptic weather types to assess the dependence of $PM_{10}$ concentrations and visibility in Tel Aviv (Israel) on the large-scale situation for the period of 2000-2002. A persistent summer synoptic pattern over the east Mediterranean region was identified to have the lowest variability of $PM_{10}$ concentrations. Four synoptic types and five patterns for the local scale circulation have been distinguished by Flocas et al. (2009)

with a manual classification for the Greater Athens Area to investigate the synoptic and local scale atmospheric circulation that prevails during air pollution episodes in an urban Mediterranean area for the period of 1989-2004. They have concluded that highest air pollution levels are connected to anticyclonic conditions over northern Greece. Makra et al. (2006) have mentioned for example moderate winds or calm air with temperature inversions typically prevailing under anticyclonic conditions, leading to exceptionally high concentrations of air pollutants in Hungary. Therefore they have investigated a manual classification of characteristic sea level pressure patterns over the Carpathian basin, the so called Péczelys types, and air quality data for the period of 1997-2001. These findings were proven in another study using the same data set of observations. Makra et al. (2007) have classified 13 subjectively derived weather types based on Péczelys weather type classification to quantify the connection of large-scale circulation patterns and local meteorological parameters as well as particulate matter concentrations in Szeged, Hungary. Lesniok and Caputa (2009) have investigated the influence of subjectively derived circulation types over Poland on various air pollutants. They have found south-western, southern anticyclone circulation and the anticyclone centre and anticyclonic ridge to lead to increased pollution levels. Stefan et al. (2010) have shown that maxima of long-range transports of air pollutants occur with easterly circulation types in Eastern part of Europe, but may partly be also related to south-westerly circulation types in Central Europe. For the classification of main air circulation types they used 5 different statistical classification approaches and data of total suspended particles from 2001-2002 at 3 sites spread over Central and Eastern Europe.

As the brief overview depicts, the general relationship between local PM and large-scale circulation dynamics - as reflected for example by weather and circulation type classifications - has been proven in several studies so far. Nevertheless, only a few systematic attempts have been made to optimized weather and circulation type classifications concerning their influence and relationship to local air quality parameter, especially $PM_{10}$. Demuzere et al. (2010) for example have investigated the explanatory power of a variety of classifications with respect to surface ozone concentrations in Central Europe. Variations of weather and circulation type classifications included classification methods, domain size, input variables, multiple-day sequencing, seasons, conditioned towards temperature with several weights. They have stated the domain size and location, classified large-scale input parameters and the selection of an appropriate classification method to be the relevant parameters for classifying the large-scale atmospheric conditions having an influence on high ozone concentrations. In a recent study, Valverde et al. (2015) have worked out variants of circulation type classifications using a clustering technique for the Iberian Peninsula to study dynamics of $NO_2$ concentrations for a long-term period of 1983-2012. They have varied for example the number of types, domain size, temporal and spatial resolution of input data as well as the classification algorithm and concluded the domain size and classification approach to have the

highest influence for characterizing the synoptic situation. To my best knowledge, there has been no study investigating the optimization of weather and circulation type classifications in terms of air quality assessments in Germany and especially the target region Bavaria yet.

In order to estimate $PM_{10}$ concentrations (predictands) based on large-scale influencing variables as reflected by weather and circulation types (predictors), the general assumption is made that the relations may vary depending on the specific type (Huth et al., 2008). Various statistical downscaling methods exist to determine predictive relationships between meteorological and air quality variables. With respect to large-scale influencing parameters, Cheng et al. (2007a) have used an automated synoptic weather typing together with a robust orthogonal stepwise regression analysis, via principal component analysis, to develop air pollution prediction models for five air pollutants, measured from 1980-2000, in south-central Canada. As input variables, a combination of observed surface meteorological data and synoptic weather types has been used as predictors for the regression models. Environmental factors contributing the most to high pollution concentrations in the study area have been detected by robust orthogonal regression. These are dry weather situations, south-south-westerly winds, high air pressure, high temperatures as well as large interdiurnal temperature changes between different pressure levels. In an other study presented by Demuzere and van Lipzig (2010a), the ability of different regression approaches combined with the automated Lamb weather classification have been tested to hindcast air quality data from 2001-2006. The main goal of the latter study has been the development of a robust method for the improved projections of air-quality levels. For the multiple linear regression models a set of predictors from local meteorological observations and circulation patterns has been used. In Beck et al. (2014b), daily atmospheric Circulation Types (CTs), resulting from variants of classification methods, have been applied in three different statistical downscaling approaches for estimating various $PM_{10}$ indices for the period of 1980-2010 at 16 locations in Bavaria (Germany). Based on the promising results of the latter study, objective circulation type classifications optimized with respect to the target variable are used as predictors in different statistical downscaling models in the present study. Furthermore, most suitable approaches are employed to investigate future climate-change-induced variations of particle concentrations in Bavaria.

### 2.3.2. Local meteorological impacts

The influence of local meteorological conditions on air pollution is the topic of several existing studies. A broad variety and complex combination of meteorological variables on a small to regional scale has been detected to have a distinct effect on composition, propagation and extent of particulate matter. Some of the meteorological parameters are listed in the following, complemented after Beck et al. (2014b), with some exemplary studies in brackets:

- air temperature (Gietl and Klemm, 2009; Demuzere et al., 2009; Cheng et al., 2007a; Elminir, 2005; Stadlober et al., 2008);
- wind speed (Schäfer et al., 2014; Gietl and Klemm, 2009; Elminir, 2005; Triantafyllou, 2001; Stadlober et al., 2008; Barmpadimos et al., 2011);
- wind direction (Gietl and Klemm, 2009; Hooyberghs et al., 2005; Elminir, 2005; Smith et al., 2001);
- mixing layer height (Schäfer et al., 2006, 2014);
- boundary layer height (Hooyberghs et al., 2005; Holst et al., 2005);
- relative humidity (Elminir, 2005; Cheng et al., 2007a; Gietl and Klemm, 2009; Demuzere et al., 2009);
- air pressure (Demuzere et al., 2009; Gietl and Klemm, 2009; Cheng et al., 2007a);
- atmospheric stratification (Holst et al., 2005; Smith et al., 2001; Triantafyllou, 2001; Stadlober et al., 2008);
- global radiation (Demuzere et al., 2009; Pitz et al., 2008);
- cloud coverage (Hooyberghs et al., 2005; Demuzere et al., 2009) and
- precipitation (Holst et al., 2005; Stadlober et al., 2008; Demuzere et al., 2009; Barmpadimos et al., 2011).

One has to keep in mind that the particular influence of the variables varies for example with seasons, target region, measurement site characteristics (e.g. elevation, exposition, terrain) and measurement techniques. Besides these factors, the used analysis method as well as the combination of the influencing variables play an important role.

There is a broad range of statistical analysis techniques for quantifying, classifying and analysing the local and background contributions to air quality. On the basis of correlation analysis, Elminir (2005) has analysed the influence of wind speed, relative humidity and air temperature on urban air pollutants in Cairo (Egypt). Wind speed and relative humidity turned out to be the most important meteorological parameters influencing the behaviour of particles in this urban area. In a later study, Elminir (2007) has extended these results by analysing the seasonal variability of air pollutants and their connections to local meteorological conditions in the target region. They have concluded that particles vary with the seasons reaching highest pollution levels in winter time on the one hand. On the other hand, the influence of a meteorological variables on particle concentrations varies with

the seasons. Wind speed for example is negatively correlated to $PM_{10}$ concentrations in winter in Egypt and positively correlated in summer time. Schäfer et al. (2006) have presented a correlation analysis between mixing layer height and air quality data in summer and winter from measurements in German urban areas Hannover and Munich. In summary, a stronger correlation have been stated in winter time and for urban stations compared to rural ones. The apparent particle density of particulate matter concentrations in Augsburg (Germany) and the correlation between physical, chemical and meteorological parameters using a variable multiple regression model have been investigated by Pitz et al. (2008). They have found the mixing boundary layer height to play an important role in the daily cycle of urban air pollutants.

Jollois et al. (2009) have used Random Forests (RF), which are based on binary decision trees, mixtures of linear models as well as non-linear additive models for analysing the influences of local meteorological parameters on air pollutants in France. The selected predictors are daily minimum, maximum, mean temperature, daily maximum and mean wind speed, daily precipitation, daily mean atmospheric pressure, daily minimum, maximum and mean relative humidity, most frequently observed wind direction, wind direction associated with maximum wind speed and for some station the temperature gradient. For the RF approach, relative humidity has been found to play a minor role. Daily total precipitation and wind speed parameters have shown a decreasing effect on $PM_{10}$ concentrations at nearly all stations. Furthermore, daily mean atmospheric pressure, the temperature gradient as well as wind speed have been detected to have an increasing effect. In a study by Bobbia et al. (2011), various meteorological variables on a local scale have been used as predictors in RF models as well to detect those parameters having an impact on $PM_{10}$ pollution in Haute-Normandie (France). Selected predictors for the latter study are daily mean, maximum and minimum temperature, daily total precipitation, daily mean pressure, daily maximum and mean wind speed, daily most frequently observed wind direction and wind direction associated with daily maximum wind speed. Additionally, vertical differences of air temperature have been chosen as proxy for the mixing layer height. The results from this study can be summarized as follows: the effect of wind speed varies between the stations, precipitation has been found to have a marginal decreasing effect on air quality. The influence of temperature has been analysed to be non-linearly depending on the amplitude (hot and cold temperatures have a positive effect, medium ones zero to negative), pressure and temperature inversion lead to increasing particle levels.

For the source apportionment of $PM_{10}$, the relations between time series of measured particles and atmospheric properties are as well relevant. Enke et al. (2008) have presented a brief overview of four main methods to distinguish between $PM_{10}$ sources in the vicinity and from background sources, for example long-range transport: laboratory analysis of $PM_{10}$ components, upwind/downwind method, trajectory analysis and transport modelling. In this thesis, no source apportionment of

$PM_{10}$ concentrations in Bavaria is investigated. Therefore, no further literature is listed concerning this research field.

As already mentioned in the previous Section 2.3.1, some studies exist combining local meteorological observations and large-scale circulation patterns as predictors in statistical downscaling methods (Cheng et al., 2007a; Demuzere and van Lipzig, 2010a). Demuzere et al. (2009) for example have applied a set of local meteorological observations and objective Lamb Weather types as predictors in multiple linear regression models for analysing the relationship to air quality parameters measured from 2001-2006 in Netherlands. In another study, Dayan and Levy (2005) have combined seasonal meteorological conditions and synoptic circulation patterns to analyse the influence of meteorology at various spatial scales on particle levels in Tel Aviv.

In summary, different statistical downscaling methods exist to analyse predictive relationships between air pollution and a broad range of meteorological parameters on a local to regional scale. Most of the approaches are based on linear and non-linear regression algorithms, e.g. Multiple Linear Regression, Random Forests, Generalized Linear Models. Other common methods for this purpose are for example artificial neural networks, generalized additive models and fuzzy-logic-based models (Gietl and Klemm, 2009; Chaloulakou et al., 2003; McKendry, 2002; Hooyberghs et al., 2005; Barmpadimos et al., 2011), which are not used in the analysis presented in this thesis. Hence, studies applying these methods are not presented in more detail in this literature review.

### 2.3.3. Forecast and projection of air quality levels

Another focus of research concerning the influence of meteorological conditions on air quality data is the forecast and estimation of future air pollution levels, respectively. The time scale of forecast and projection ranges from daily, monthly up to estimations in context of future climate change conditions.

Stadlober et al. (2012) have listed multiple linear regression, generalized linear models, neural networks, discriminant analysis, multi-gene genetic programming, Kalman filtering as few statistical approaches used for the prediction on a shorttime scale. In their study, they have compared forecasts of daily $PM_{10}$ concentrations at several sites in Brno (Czech Republic) and Graz (Austria) based on multiple linear regression and generalized linear models using measurements of present day and meteorological forecast for the next day. The chosen meteorological parameters on a local scale are wind speed, precipitation, temperature for Graz and temperature and cloud cover for Brno. Both model approaches were found to be useful for predicting daily $PM_{10}$ concentrations. In an other analysis, Huebnerova and Michalek (2014) have compared two models for prediction of

daily average $PM_{10}$ (predictand) using a generalized linear model approach with observed data for temperature, wind speed, wind direction and cloud cover in Brno and predictions of the meteorological parameters as predictor variables. They have concluded a non-significant loss of prediction quality using the predicted meteorological data.

Future climate change projections from scenario runs of AOGCM are commonly used to analyse the impact of climate change on different variables on a local scale. Hence, it is necessary to overcome the spatial mismatch between GCM data and small-scale target variables, which are often point measurements. The two main methods are dynamical and statistical downscaling techniques.

As an example of a dynamical approach, Forkel and Knoche (2007) have studied the potential impact of global climate change on regional meteorology and near-surface ozone concentrations in central Europe and the effect of model resolution on the simulated quantities using a coupled climate-chemistry model. Nested simulations with a horizontal resolution of 60 km for Europe and 20 km for central Europe were performed for two time slices of about 10 years representing present-day and future climate conditions. The model results indicate that increased solar radiation due to decreased cloud cover, higher temperatures, and enhanced isoprene emissions promote the formation of tropospheric ozone in central Europe under future climate conditions.

Huth et al. (2008) have stated statistical downscaling to be a sufficient methodology to bridge the gaps between the coarse resolution of GCM and local variables. Some examples for the application of circulation-type-based downscaling models on GCM data are introduced in the following. Cheng et al. (2007b) have used air pollution prediction models, which have been developed using weather types in part I of the study (Cheng et al., 2007a), for application on GCM runs to estimate future synoptic situations and air pollution levels for four selected cities in Canada. First of all, the performance of downscaling model results for four main weather groups classified with observation data and downscaled GCM historical run for the period 1961-2000 have been compared. Afterwards, five emission scenarios have been used to assess future air pollution levels of various air quality parameters. Demuzere and van Lipzig (2010b) for instance have estimated future ozone concentrations in Netherlands from three scenario runs of a AOGCM using a synoptic-regression method described in Demuzere and van Lipzig (2010a) for the two periods 2051-2060 and 2091-2100. The regression model has been applied on a control run and the statistical downscaling tool has been evaluated utilizing observations beforehand. Yuval et al. (2012) have assessed future air quality in Israel by the application of a synoptic system classification on AOGCM data. By using this rather simple approach, climate change effects of the large-scale atmospheric situation have been determined through the varying frequencies of the appearance of the synoptic patterns in the model projections. The assumption of a constant relationship between the synoptic situation and

air pollution has been made. This presumption has been used as well by Demuzere and van Lipzig (2010b) or Cheng et al. (2007b). Thus far, only a few studies by Demuzere and van Lipzig (2010b) or Cheng et al. (2007b) for instance have investigated circulation-type-based downscaling models to estimate future climate-change-induced variations of air pollution levels, as this literature review revealed.

# 3. Data

The analyses presented in this thesis are based on different data sets, which are introduced in the following. The air pollution data basis, provided by the Bavarian Environment Agency/Landesamt für Umwelt (LfU), German Federal Environment Agency/Umweltbundesamt (UBA) and German Weather Service/Deutscher Wetterdienst (DWD), comprises $PM_{10}$ measurements at various stations for the period of 1980 to 2011. It is described in Section 3.1. Circulation Type Classifications (CTC) are performed using NCEP/NCAR reanalysis data set, which is content of Section 3.2. Future climate change scenarios until the end of this century are taken from several Atmosphere-Ocean Coupled General Circulation Models (AOGCM) projections based on different scenarios of the Fifth Phase of the Coupled Model Intercomparison Project (CMIP5). Scenarios and models are introduced in Section 3.3.

## 3.1. Particulate matter

Since 1974, continuous measurements from the Bavarian air quality monitoring network/ Lufthygienisches Landesüberwachungssystem Bayern (LÜB), run by the LfU, of air quality parameters like sulphur dioxide ($SO_2$), carbon monoxide (CO), nitrous gases ($NO_x$), ozone ($O_3$), particulate matter and several meteorological variables, e.g. wind speed, air temperature, precipitation, specific humidity, pressure, global radiation are available (Landesamt für Umwelt, 2013). The main tasks of this measurement network are the implementation of EU Air Quality standards according to EU directive 2008/50/EG (E.U., 2008) and the investigation of local and regional pollution loads in order to monitor trends and inform the public about critical values. Furthermore, high quality data sets for regional planning processes and research are provided. Hence, most of the stations are installed in urban areas in all major cities of Bavaria for monitoring air pollution.

The currently 50 stations, measuring the mass concentrations of particles in $\mu g/m^3$, are primarily situated in urban areas and are characterized, according to EoI (Exchange of Information (EU directive 2001/752/EC)), as rural and urban background stations as well as traffic-related ones. For the chosen analysis period 01/01/1980 to 31/12/2011, $PM_{10}$ measurements from 46 stations are available. A description of all sites is given in Table A.1. This 32-year period enables the analysis of long-term effects of both large-scale and local meteorological effects on local particle levels. As Table 3.1 illustrates, some measurement sites already measured before 01/01/1980. Yet, 01/01/1980 is selected as a starting date with a lot of stations having continuous data from this day on.

Table 3.1: $PM_{10}$ station information given by station name, ID, station type classified by EoI (see text) and measurement period.

| Name | ID | Type | measurement period | |
|---|---|---|---|---|
| | | | start | end |
| Ingolstadt/Rechbergstrasse | L1.1 | traffic | 01/07/1989 | - |
| Burghausen/Marktler-Strasse | L1.2 | urban background | 01/01/1976 | - |
| Trostberg/Schwimmbadstrasse | L1.14 | urban background | 01/05/1992 | - |
| Mehring/Sportplatz | L1.15 | rural background | 01/05/1977 | - |
| Andechs/Rothenfeld | L1.16 | rural background | 14/04/2003 | - |
| Kelheim/Regensburger-Strasse | L2.1 | traffic | 01/01/1975 | - |
| Landshut/Podewilsstrasse | L2.3 | traffic | 01/12/1985 | - |
| Neustadt/Eining | L2.6 | rural background | 01/03/1977 | - |
| Saal/Regensburger-Strasse | L2.9 | urban background | 01/08/1978 | - |
| Regen/Bodenmaiser-Strasse | L2.11 | urban background | 01/02/1989 | - |
| Passau/Stelzhamerstrasse | L2.12 | urban background | 05/04/2005 | - |
| Regensburg/Rathaus | L3.1 | traffic | 01/01/1975 | - |
| Weiden/Nikolaistrasse | L3.3 | urban background | 01/01/1980 | - |
| Schwandorf/Wackersdorfer-Strasse | L3.4 | urban background | 01/01/1980 | - |
| Tiefenbach/Altenschneeberg | L3.6 | rural background | 01/10/1983 | - |
| Sulzbach-Rosenberg/Lohe | L3.8 | urban background | 11/05/1999 | - |
| Bayreuth/Rathaus | L4.2 | traffic | 01/01/1978 | 01/05/2012 |
| Bamberg/Loewenbrücke | L4.3 | urban background | 01/01/1978 | - |
| Arzberg/Egerstrasse | L4.5 | urban background | 01/01/1980 | - |
| Naila/Selbitzer-Berg | L4.6 | urban background | 01/01/1986 | - |
| Coburg/Lossaustrasse | L4.7 | traffic | 01/02/1987 | - |
| Kulmbach/Konrad-Adenauer-Strasse | L4.8 | urban background | 01/10/1988 | - |
| Nürnberg/Bahnhof | L5.1 | traffic | 01/09/1986 | - |
| Nürnberg/Ziegelsteinstrasse | L5.2 | traffic | 01/01/1975 | 25/10/2012 |
| Fürth/Theresienstrasse | L5.5 | traffic | 01/01/1990 | - |
| Ansbach/Residenzstrasse | L5.12 | traffic | 01/07/1989 | - |
| Erlangen/Kraepelinstrasse | L5.14 | urban background | 01/04/2004 | - |
| Schweinfurt/Obertor | L6.3 | traffic | 01/01/1976 | - |
| Würzburg/Kardinal-Faulh.-Platz | L6.4 | traffic | 01/01/1975 | 31/12/2011 |
| Aschaffenburg/Bussardweg | L6.6 | urban background | 01/08/1978 | - |
| Augsburg/Königsplatz | L7.1 | traffic | 01/01/1975 | - |
| Kempten/Westendstrasse | L7.3 | urban background | 01/01/1976 | - |
| Lindau/Holdereggenstrasse | L7.4 | traffic | 01/01/1978 | - |
| Neu-Ulm/Gabelsbergerstrasse | L7.5 | urban background | 01/01/1978 | - |
| Augsburg/Bourges-Platz | L7.6 | urban background | 01/08/1986 | - |
| Augsburg/LfU | L7.8 | urban background | 27/07/2000 | - |
| München/Stachus | L8.1 | traffic | 01/01/1978 | - |
| München/Lothstrasse | L8.3 | traffic | 01/01/1978 | - |
| München/Johanneskirchen | L8.12 | urban background | 01/07/1993 | - |
| Augsburg/Karlstrasse | L14.1 | traffic | 01/07/2003 | - |
| Bayreuth/Hohenzollernring | L14.2 | traffic | 01/08/2003 | - |
| München/Prinzregentenstrasse | L14.3 | traffic | 01/07/2004 | 31/12/2011 |
| München/Landshuter-Allee | L14.4 | traffic | 01/07/2004 | - |
| Würzburg/Stadtring-Sued | L14.5 | traffic | 01/11/2005 | - |
| Nürnberg/Von-der-Tann-Strasse | L14.7 | traffic | 01/11/2006 | - |
| Oberaudorf/Inntal-Autobahn | L14.8 | traffic | 01/01/2008 | - |
| Schauinsland | | rural background | 01/01/1980 | - |
| Schmücke | | rural background | 01/01/1980 | - |
| Hohenpeissenberg | | rural background | 20/03/1996 | - |

During the measurement period from 1974 to 1999, data for total suspended particles have been collected. Since 01/01/2000, the instrumental set-up changed into measurement techniques for a direct measurement of particulate matter with a medium aerodynamic diameter $< 10\mu$m. In order to get a consistent $PM_{10}$ data set for the chosen period from 01/01/1980 to 31/12/2011, the values for total suspended particles have been converted into $PM_{10}$ data with a conversion factor 1/1.2 according to EU directive 1999/30/EG. Due to the fact that the measuring time steps changed from a daily mean for the period from 01/01/1979 to 31/12/1986 to a 3h-mean from 01/01/1987 to 31/12/1999 and 0.5h-mean from 01/01/2000 to 31/12/2007, daily mean $PM_{10}$ concentrations are calculated from the given data.

The used $PM_{10}$ data set is complemented by daily mean $PM_{10}$ measurements from rural background stations Schmücke (Thüringen) and Schauinsland (Baden-Württemberg) run by the UBA. These two sites are added as the representatives of background pollution schemes close to the border of Bavaria. The site Schauinsland is located on top of the same-named mountain in 1205 m elevation. Most of the time it is above the mixing layer height. Hence, local and long-range transported air masses can be measured (Umweltbundesamt, 2013). Station Schmücke, situated in a low range mountain region in 937 m a.s.l., collects air quality data from long-range transporting processes of western and eastern European regions. Local observations of the DWD at Mountain Hohenpeißenberg (1000 m a.s.l.) are as well added to the $PM_{10}$ data basis. Due to its position in a dense populated area and its elevation, Hohenpeißenberg is characterized as a rural background site.

In Table 3.1 all sites are listed by their station name, ID, station type according to EoI and the period of data availability. Most of the stations (around 47 %) are traffic-related, around 37 % are situated in urban background areas and the others in rural background. In Chapter 5, additional station informations are presented as well as descriptive statistics of the $PM_{10}$ data basis, a long-term trend analysis and a grouping of the selected measurement sites to $PM_{10}$ regions in Bavaria.

## 3.2. Circulation data

Daily gridded atmospheric fields (2.5° x 2.5° horizontal resolution) are provided by the reanalysis project of the National Center of Environmental Prediction (NCEP) and National Center for Atmospheric Research (NCAR) of the United States (Kalnay et al., 1996; Kistler et al., 2001). A frozen state-of-the-art analysis/forecast system is used to perform data assimilation from 1957 to present based on a synthesis of all available past data, e.g. from satellite, rawinsonde, land surface, ship or pibal measurements. The output variables are the result of a fixed analysis through time performed with the same model for 6 hour time steps. For classifying large-scale atmospheric fields, the daily

value on 12 a.m. of the 4-times daily runs of the chosen parameters is selected.

Depending on the degree to which they are influenced by the used observations and/or the model, the gridded output variables are categorized in four groups. The most reliable group are class A variables, which are strongly influenced by the observed data. The air pressure equivalent of geopotential height (in gpm), zonal ($u$ wind in m $s^{-1}$) and meridional ($v$ wind in m $s^{-1}$) wind components, temperature (in K) and relative vorticity (in $s^{-1}$) in 1000, 850 and 500 hPa levels as well as mean sea level pressure fields (in hPa) are selected from this group. Meteorological parameters classified with B are still affected by the observations, but the influence of the model is increasing. Here relative humidity (in %), specific humidity (in g $kg^{-1}$) and vertical velocity (in Pa $s^{-1}$) in 1000, 850 and 500 hPa levels are chosen. Reanalysis data from group C and D were not used in this work.

The selection of the enumerated large-scale meteorological variables is ensued by considering the influence of each of the parameters on local $PM_{10}$ concentrations. One indicator are existing studies on the influence of local and large-scale meteorological conditions on the particulate matter concentrations, as mentioned in Chapter 1. Additionally, the consideration of the role of one parameter on the formation, transportation or deposition of $PM_{10}$ is involved in the selection process. The wind components are, regarding the synoptic level, relevant for long range transport of the particles. The mean sea level pressure and geopotential height fields represent the general large-scale circulation. The humidity parameters indicate for example particle growing processes depending on the life of particles. Formation of secondary pollutants is influenced by the air temperature. Vertical velocity represents the down- or upward motion of air in the atmosphere and are therefore a measure for transportation processes. The relative vorticity represents the circulation in the upper-air and acts as a parameter for describing the general circulation. As a measure for the mixing layer height the air temperature differences in several pressure levels are calculated. The mixing layer height indicate the mixing volume of the air.

A drawback of the used NCEP/NCAR data set is the coarse resolution, because potential important processes on smaller scales, e.g. convective processes, are not covered in the data used for classifications. Apart from that the extracted reanalysis data offers some deciding advantages. NCEP/NCAR offers a consistent and reliable data base with a broad range of meteorological variables in different levels for the chosen analysis period of 01/01/1980to 31/12/2011. Additional advantages are the global coverage and continuous resumption of model output.

Large-scale atmospheric variables from the reanalysis are applied on weather and circulation type classifications in Chapter 6 and predictors in local downscaling models presented in Chapter 9.

## 3.3. CMIP5 climate models

Future climate change projections are taken from Atmosphere-Ocean Coupled General Circulation Models (AOGCM) of the Fifth Phase of the Coupled Model Intercomparison Project (CMIP5) used for the current Fifth Assessment Report (AR5) published by the Intergovernmental Panel on Climate Change (IPCC). The IPCC is an international institution for assessing climate variability and climate change and publishes the outcome in its Assessment Reports to inform the public (Stocker et al., 2013). These reports represent the current state of scientific knowledge relevant to climate change.

As it is summarized by Taylor et al. (2012), the main aim of the CMIP5 is to produce and provide a freely accessible state-of-the-art multi-model data set designed to advance the current knowledge of climate variability and climate change. The basis of the model experiments are the Representative Concentration Pathway (RCP) scenarios, a further developed approach compared to the former Special Report on Emission Scenarios (SRES) for the 4th IPCC Assessment Report (IPCC AR4). In general, socio-economic and emission scenarios are used in climate research to provide plausible descriptions of how the future may process with respect to a range of variables. Therefore, the RCP scenarios include for example socio-economic and technological changes, energy and land use. Emissions of greenhouse gases, such as nitrous gases ($N_2O$), methane ($CH_4$), halogens and $CO_2$, and air pollutants are also considered. These parameters can be applied as input data for General Circulation Model (GCM) runs and as a basis for assessments of possible climate impacts, mitigation strategies and associated costs. In order to compare various climate-change-related studies and for an easier communication of model results, commonly used scenarios are advantageous (van Vuuren et al., 2011).

In this thesis, projections based on the RCP4.5 and RCP8.5 scenarios are used to assess climate change effects for the period of 2005-2100. RCP4.5 is classified as medium stabilization or intermediate mitigation scenario with a representative concentration pathway, which results in a radiative forcing of approx. 4.5 W/m$^2$ until the end of this century relative to pre-industrial conditions. Radiative forcing in this case is defined as the additional difference of insolation (solar radiation that reaches the earths surface) absorbed by the earth and energy radiated back to space. A radiative forcing of 8.5 W/m$^2$ at year 2100 is simulated for the very high baseline emission scenario RCP8.5. Figure 3.1 indicates trends of the different scenarios for the radiative forcing (left), $CO_2$ emissions (middle) and 2100 forcing level of several greenhouse gases (right). Blue lines mark values for the RCP8.5 scenario, red for the RCP4.5. The forcing is put into relation to pre-industrial values. One has to keep in mind that an aerosol forcing by land use, dust or nitrate is not taken into consideration (van Vuuren et al., 2011).

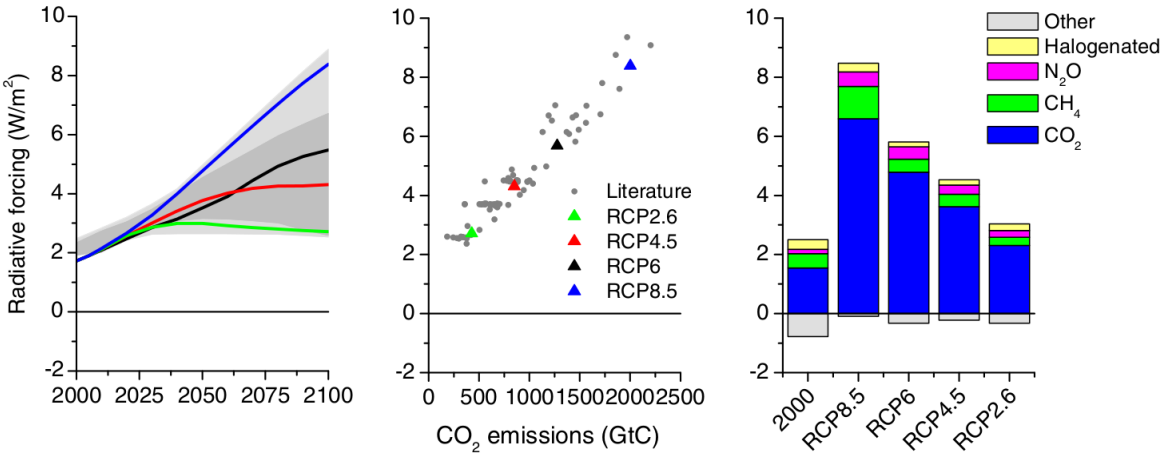


Figure 3.1: Representative Concentration Pathway (RCP) scenarios from the recent Fifth Assessment Report (AR5) of the IPCC. Trends in radiative forcing are given on the left hand side. Cumulative 21st century $CO_2$ emissions versus 2100 radiative forcing are shown in the middle figure. The 2100 forcing levels of several greenhouse gases are given on the right hand side. Grey area indicates the 98th and 90th percentiles (light/dark grey) of the literature. The dots in the middle graph also represent a large number of studies (Source: van Vuuren et al. (2011)).

Projections from two GCMs of the Fifth Phase of the Coupled Model Intercomparison Project (CMIP5) are used in this thesis. On the one hand, these are 3 ensemble runs from the Atmospheric Component of the MPI-M Earth System Model (ECHAM6) (Max-Planck-Institute Earth System Model Low Resolution (MPI-ESM-LR)) for control runs of the recent past (1980-2005), here referred to historical runs, and the two climate change scenarios (RCP4.5 and RCP8.5) for two periods of 2021-2050 and 2071-2100. The ECHAM6 model is a rather new version of the ECHAM model series and an advanced version of the ECHAM5 model in 1.9° x 1.9° horizontal resolution (Giorgetta et al., 2013; Stevens et al., 2013). The main differences between ECHAM6 and ECHAM5 concern computation of radiation schemes, surface albedo and the triggering conditions for convection processes. Data from the ECHAM6 model are taken for air temperature (AIR), zonal wind component (UWND), meridional wind component (VWND), mean sea level pressure (SLP), geopotential height (HGT), specific humidity (SHUM), relative vorticity (RVORT) and relative humidity (RHUM) in four pressure levels (1000, 925, 850, 500 hPa). In order to assign circulation types, classified with reanalysis data, on future climate change projections, the gridded fields of the GCM are regridded on the NCEP grid of 2.5° x 2.5° horizontal resolution.

Projections from the EC-Earth model are used on the other hand. The atmospheric model of EC-Earth version 2, which is a Numerical Weather Prediction Model (NWP) system of the European Centre for Medium-Range Weather Forecasts (ECMWF), forms the basis of the EC-Earth Earth-system model (Hazeleger et al., 2010). It is a coupled, state-of-the-art GCM from the CMIP5

project. The EC-Earth consortium is a collaboration of meteorologists and Earth-system scientists from 10 European countries. The standard configuration runs at T159 (1.1° x 1.1°) horizontal spectral resolution with 62 vertical levels. Data from one run in the historical period and two future climate change scenarios equivalent to RCP 4.5 and RCP 8.5 are chosen for mean sea level pressure, geopotential height and vertical velocity in 700 and 500 hPa levels, zonal and meridional wind components in 1000, 700, 500 and 300 hPa levels, specific humidity in 925, 850 and 700 hPa levels.

## 3.4. Local meteorological data

Table 3.2: Availability of different local meteorological variables at 16 long-term $PM_{10}$ stations for analyses period 1980-2011 marked as black crosses and for sub-periods as red crosses. Variables are wind speed (WS), cloud cover (CC), pressure (PRES), precipitation (PREC), sunshine duration (SUN), minimum temperature ($T_{min}$), maximum temperature ($T_{max}$), mean temperature ($T_{mean}$), relative humidity (RHUM), vapour pressure (VP).

| LfU | DWD | WS | CC | PRES | PREC | SUN | $T_{min}$ | $T_{max}$ | $T_{mean}$ | RHUM | VP |
|---|---|---|---|---|---|---|---|---|---|---|---|
| Ingolstadt | Kösching | X | X | X | X | X | X | X | X | X | X |
| Kelheim | Regensburg | X | X | X | X | X | X | X | X | X | X |
| Landshut | Weihenstephan-Dürnast | X | X | X | X | X | X | X | X | X | X |
| Regensburg | Regensburg | X | X | X | X | X | X | X | X | X | X |
| Weiden | Weiden | X | X | X | X | X | X | X | X | X | X |
| Schwandorf | Schwandorf | X | X | X | X | X | X | X | X | X | X |
| Bayreuth | Heinersreuth-Vollhof | X | X | X | X | X | X | X | X | X | X |
| Bamberg | Bamberg | X | X | X | X | X | X | X | X | X | X |
| Nürnberg Bahnhof | Nürnberg | X | X | X | X | X | X | X | X | X | X |
| Nürnberg Ziegelsteinstr. | Nürnberg | X | X | X | X | X | X | X | X | X | X |
| Fürth | Nürnberg | X | X | X | X | X | X | X | X | X | X |
| Schweinfurt | Arnstein | X | X | X | X | X | X | X | X | X | X |
| Würzburg | Würzburg | X | X | X | X | X | X | X | X | X | X |
| Augsburg | Augsburg | X | X | X | X | X | X | X | X | X | X |
| München Stachus | München-Stadt | X | X | X | X | X | X | X | X | X | X |
| München Lothstr. | München-Stadt | X | X | X | X | X | X | X | X | X | X |

In order to identify those meteorological parameters on a local to regional scale, which have a distinct impact on $PM_{10}$ concentrations in the target region Bavaria, a comprehensive set of variables has been used as potential predictors in local transfer models in the project "Particulate Matter and Climate Change in Bavaria" (PACLIMBA) (Beck and Jacobeit, 2015). The used data are provided by the DWD and NCEP/NCAR reanalysis project (Kalnay et al., 1996; Kistler et al., 2001). The NCEP/NCAR reanalysis data is described in Section 3.2. A brief introduction into the DWD data set is presented in the following.

Table 3.3: Distances between 16 $PM_{10}$ stations and assigned DWD measurement sites (in km).

| LfU | DWD | distance |
|---|---|---|
| Ingolstadt | Kösching | 32 |
| Kelheim | Regensburg | 20 |
| Landshut | Weihenstephan-Dürnast | 63 |
| Regensburg | Regensburg | 4 |
| Weiden | Weiden | 31 |
| Schwandorf | Schwandorf | 15 |
| Bayreuth | Heinersreuth-Vollhof | 45 |
| Bamberg | Bamberg | 47 |
| Nürnberg Bahnhof | Nürnberg | 17 |
| Nürnberg Ziegelsteinstr. | Nürnberg | 20 |
| Fürth | Nürnberg | 19 |
| Schweinfurt | Arnstein | 72 |
| Würzburg | Würzburg | 46 |
| Augsburg | Augsburg | 27 |
| München Stachus | München-Stadt | 18 |
| München Lothstr. | München-Stadt | 18 |

In Table 3.2, an overview of the availability of several meteorological variables from the DWD for 16 selected LfU measurement sites is shown. The stations have been selected through $\geq 90\%$ data availability for the chosen period 1980-2011. The meteorological parameters comprise daily values of wind speed (in m/sec), cloud cover (in percent), pressure (in hPa), precipitation (in mm), sunshine duration (in hour), minimum, maximum and daily mean air temperature (in degree Celsius), relative humidity (in %) and vapour pressure (in hPa). The names of the corresponding DWD stations are indicated as well, which are assigned as nearest measurement site in terms of the distance to a $PM_{10}$ station. Black crosses mark the availability over the whole analysis period of 1980 to 2011 and red crosses for sub-periods, respectively.

The distances between the air quality stations and assigned DWD measurement sites are given in Table 3.3. As it is indicated, distances vary fairly from a few kilometres up to 60-70 kilometres. In general, some meteorological parameters like pressure or temperature have a highly spatial representativeness. Humidity measures like precipitation or wind in contrast should be measured as close as possible to the corresponding air quality sites, as these variables represent small-scale processes.

Radiosonde ascension data have been taken from DWD stations München, Stuttgart, Meiningen and Kümmersbruck, additionally. The temperature gradients have been calculated from radiosonde measurements as differences between temperatures in 1000 hPa and 925 hPa levels. The 925 hPa level represents atmospheric processes in approx. 600-900 m.a.s.l. (Kraus, 2008). The nearest DWD station, according to the distance, has been assigned again to each $PM_{10}$ site.

Furthermore, data from the NCEP/NCAR reanalysis project for zonal and meridional wind components as well as temperature differences between 1000 hPa and 925 hPa level have been used as potential predictors. Data for each large-scale atmospheric variable at 6 grid points (7.5°-12.5° E, 47.5°-50° N in 2.5° x 2.5° horizontal resolution) covering Bavaria have been selected. Mean values of the two wind components as well as temperature differences have been calculated averaged over all six grid points. With a 2.5° x 2.5° horizontal resolution, the resolution of the NCEP/NCAR data

is comparatively coarse. Thus, this data represent primarily meteorological processes on a regional scale.

# 4. Methods

The basic principles and specific applications of the statistical methods used in this thesis are explained in the following. At first, Principal Component Analysis (PCA) in s-mode is introduced in Section 4.1, which is applied for grouping 16 selected measurement sites (see Section 3.1) into regions with similar temporal variability of $PM_{10}$.

Secondly, an overview of existing objective Circulation Type Classifications (CTC) for the European domain and the main statistical methodology behind the classifications are presented in Section 4.2. Selected classifications, which are explained in more detail in the Chapter, are applied on gridded reanalysis data to characterize the large-scale circulation having an influence on local particle concentrations.

Resulting large-scale Circulation Types (CTs) are used as predictors in statistical downscaling models to estimate local $PM_{10}$ indices. In Section 4.3, the downscaling approaches are introduced. Synoptic Downscaling (SD), sometimes referred to as reference class forecasting, is described in Section 4.3.1. The principle of a non-linear regression method based on decision trees, Random Forests (RF), is content of Section 4.3.2. Furthermore, two linear regression approaches, Multiple Linear Regression Analysis (MLR) and Generalized Linear Model (GLM), are used, which are introduced briefly in Section 4.3.3 and 4.3.4.

A broad variety of potential criteria exist to evaluate the performance of classifications and statistical downscaling methods. The robustness respectively performance of the resulting models are evaluated based on independent calibration and validation periods for selected objective evaluation measures, which are topic of Section 4.4.

## 4.1. Principal Component Analysis

Principal Component Analysis (PCA) is a quite popular multivariate statistical analysis technique in atmospheric sciences. The basic principles of the method are described in numerous statistical books, for example Bahrenberg et al. (2003); Wilks (2006); Wollschläger (2012) or Schönwiese (2013). It is mainly used for the reduction of a large data set into one containing fewer new variables, which are linear combinations of the original ones representing the maximum possible fraction of the variability contained in the original data basis.

The s-mode PCA (s for spatial) is a common tool for the identification of spatial patterns of temporal variability concerning different meteorological parameters (see for example Jacobeit (1993); Hertig and Jacobeit (2013); Huth (2002); Beck (2000)). In contrast to t-mode PCA, where grid-

ded spatial fields of parameters are the input data, time series of data are analysed using a s-mode PCA. The loadings of a Principal Component (PC), which represent the correlation coefficients between a particular PC and time series, are used to group stations with similar temporal variability.

In the present analysis, a s-mode PCA is used to generate relatively homogeneous groups of measurement sites in Bavaria/Germany with respect to temporal variation of daily mean $PM_{10}$ concentrations in the period 1980-2011. The results of the s-mode PCA are described in Section 5.5.

The formula behind the PCA can be found in the literature mentioned above. In general, PCA is based on the correlation matrix, in case of standardized variables, or the covariance matrix. The data matrix $M$ of the given input data is structured as follows: vectors reflecting time series of daily mean $PM_{10}$ stations are in columns, representing the spatial information (stations). The rows are as well values of $PM_{10}$ concentrations of each station as time related information (time units):

$$M = \begin{bmatrix} x_1 1 & x_1 2 & x_1 3 & ... & x_1 j \\ x_2 1 & x_2 2 & x_2 3 & ... & x_2 j \\ x_3 1 & x_3 2 & x_3 3 & ... & x_3 j \\ . & . & . & . & . \\ . & . & . & . & . \\ . & . & . & . & . \\ x_i 1 & x_i 2 & x_i 3 & ... & x_i j \end{bmatrix} \tag{1}$$

From this input matrix $M$, the correlation matrix $K_r$ is calculated with correlation coefficients $r_{ij}$, which reflect the correlation coefficients between time series of different measurement sites. Alternatively, the covariance matrix can be calculated instead of the correlation matrix (Bahrenberg et al., 2003):

$$K = \begin{bmatrix} r_1 1 & r_1 2 & r_1 3 & ... & r_1 j \\ r_2 1 & r_2 2 & r_2 3 & ... & r_2 j \\ r_3 1 & r_3 2 & r_3 3 & ... & r_3 j \\ . & . & . & . & . \\ . & . & . & . & . \\ . & . & . & . & . \\ r_i 1 & r_i 2 & r_i 3 & ... & r_i j \end{bmatrix} \tag{2}$$

The main task of PCA is to find linear combinations of PCs, which explain most of the variance of a target variable $X_i$:

$$X_i = A_{i1} * F_1 + A_{i2} * F_2 + A_{i3} * F_3 + ... + A_{iq} * F_q + \varepsilon \tag{3}$$

with $F_j$ indicating the PCs and $A_{ij}$ their weight (Schönwiese, 2013). $\varepsilon$ represents the unexplained residuals.

The first PC is that one explaining a maximum of the variance of the variables. The correlation coefficients between one PC and the variables are called loadings. The squared loadings represent the amount of variance of one variable explained by the PC (in %). The higher loadings represent spatial groups of variables ($PM_{10}$ stations) with similar time variations in the $PM_{10}$ time series (scores).

The sum of squared loadings of a PC is called Eigenvalue $\lambda$. The relation between Eigenvalue and the number of (standardized) variables represents the part of total variance explained by the PC. The second PC explains a maximum of the variance of those variables, which are not represented by the first. First and second PC are not correlated and hence orthogonal. The procedure proceeds for more PCs. If the first PC only explains a relatively small amount of the variance of a variable, the loading of the variable is higher for another PC.

All loading matrices resulting from the PCA are Varimax-rotated. This procedure is used, when the physical interpretation is the primary goal of the analysis, not the data compression. The procedure is explained in detail for example by Wilks (2006). The basic principle is to rotate the loadings without losing the orthogonality between them in order to extract a meaningful number of PCs, so called rotated PCs. Resulting PCs are easier to interpret and the sampling of the rotated loadings are more stable. As it is described by Wilks (2006), a major drawback of the rotating procedure is the fact, that the dominant-variance property of PCA is lost. This means for the first rotated PC for example, that it is no longer a distinct linear combination of the original data with the largest variance. Furthermore, the eigenvalue spectrum after the rotation is flatter. Additional lost emerges either for the orthogonality of the eigenvectors or for the uncorrelatedness of the resulting principal components, or both.

In this thesis, the PCA is applied on time series of $PM_{10}$ from the selected stations in Chapter 5.

## 4.2. Circulation type classifications for European domains

Classifications of atmospheric weather and circulation types are important tools in the field of synoptic climatology. Until the 1990s, main applications of these methods were on weather forecasting. Especially with the advantage of computers and their processing capacity, the usage of classifications broaden from weather prediction, including ensemble forecasting, to applications in climatology with analysing recent climate variations and validation of climate models as well as

downscaling approaches (Huth et al., 2008).

There are different attempts to categorize or group classification methods. A prior one divides them into two main groups of manual and automated classifications (Yarnal, 1993), an alternative way is the distinction between subjective and objective ones. A further division can be made between *circulation type classifications*, including only atmospheric circulation data like air pressure or geopotential height, and *weather type classifications* applying other large-scale atmospheric variables like temperature or humidity (Philipp et al., 2014). Yarnal et al. (2001) distinguish between manual typing classifications, correlation-based and eigenvector-based techniques. Especially the group of eigenvector-based methods include a broad variety of multivariate statistical approaches to classify like Principal Component Analysis (PCA), which seem to make a more precise categorization necessary. Huth et al. (2008) for example have presented a recent review of existing classification techniques and the basic statistical methods behind separated into three general groups: subjective (or manual), mixed (or hybrid) and objective (or automated) approaches.

Diverse CTC exist for the European domain using different statistical approaches (e.g. Principal Component Analysis, Empirical Orthogonal Functions, Cluster Analysis, Leader Algorithm) for the application in several fields of atmospheric sciences. In the framework of COST Action 733 "Harmonisation and Applications of Weather Type Classifications for European Regions" (hereafter referred to as Cost733), the main tasks have been the collection and creation of a large number of different CTC with focus on the circulation-to-environment approach (see Chapter 2). An inventory of existing methods for the European domain ended up in a widespread catalogue of 72 classifications schemes (Huth et al., 2008; Philipp et al., 2010, 2014). They have been categorized with regard to the main statistical approach they are based on. The COST Action 733 furthermore included a comparison of these methods in order to identify differences and to evaluate the performance of the different approaches.

An outcome of the COST Action is a dataset of classification catalogues, so called *cost*733*cat*, which have been compiled in a software package, *cost*733*class*. The software package allows an easy modification of the classifications concerning for example the input data or configuration variants. Philipp et al. (2014) give an overview of the included methods and their categorization in groups within the *cost*733*class* as well as a documentation and description of the particular approaches. A brief description of the classification groups and methods is given in the following.

The first group of CTC in the *cost*733*cat* are manual (or subjective) ones, which are based on the expert knowledge. Typical synoptic situations prevailing over a target region are taken into account to evaluate their effect on different surface climatic parameters. As these classifications are

established since decades, they are the basis of a lot of other methods and variants. Thus they could be denoted as general classifications. Examples for this group are the 29 *Hess-Brezowsky Grosswetterlagen (GWL)* after Hess and Brezowsky (1952) focusing on Central Europe, the *Carpathian based weather types (PEC)* after Péczely (1983) or the originally 26 *Lamb weather types (LMB)* for the target region Great Britain (Jones et al., 1993). Limitations of the 6 integrated manual classifications in the *cost*733*cat* are for example the presence of a category of unclassifiable days or the fact that the approaches are only usable for fixed regions (Philipp et al., 2014).

The second group are the so called threshold-based methods. Predefined values are applied to assign and separate circulation types. The threshold often represents zonal and meridional large-scale flow directions as well as vorticity (or high/low central pressure) fields. It is only possible to use the methods on one-dimensional pressure maps, not on multi-dimensional data sets, which can be seen as the main drawback of these methods. As a representative of this category, *Grosswettertypes or prototype classification (GWT)* is used for further analysis (Beck, 2000; Beck et al., 2007). Additional examples are the *Jenkinson-Collison classification (JCT)* by Jenkinson and Collison (1977) and the *Litynski advection and circulation types (LIT)* introduced by Litynski (1969).

In contrast to the introduced classifications using predefined types, the following groups of methods base on the idea to identify the circulation types by any structure in the input data set. One often used approach is the classification by Principal Component Analysis (PCA) (see also Section 4.1 for details of method). The implemented classification schemes using principal components are a s-mode variant called *Kruizinga* published by Kruizinga (1979), *t-mode PCA using obliquely (PCT) and orthogonally (PTT) rotated modes* and *Principal components extreme scores (PXE)* (Philipp et al., 2010).

A comparatively small number of CTC are based on leader algorithm, a predecessor of clustering techniques, which seek for key or leader patterns. For each type the number of elements with high similarity to the potential key pattern exceeding a certain threshold are counted. Representative classifications are *Classical leader algorithm by Lund (LUND)* invented by Lund (1963), using correlation coefficients as similarity measure, or *Kirchhofer types* from Kirchhofer (1974), which is based on the Kirchhofer score taking similarities in all parts of the given map into account.

Algorithms for cluster analysis include a first group of hierarchical cluster analysis classification methods including only agglomerative algorithms from the routine of Murtagh (1985). In the beginning each element is located in its own cluster. In order to find the pair of clusters to combine at each step, different kinds of similarity metrics are used, e.g. Wards method, single linkage, complete linkage, average linkage, MC Quittys Method, median method or centroid method (Philipp

et al., 2014). At the point, where only $k$ clusters are left, the procedure stops and, similar to leader algorithms based methods, no further optimization is done.

The last group separated in the *cost*733*cat* data set are the algorithms for optimizing partitions or optimization algorithms mainly based on non-hierarchical cluster analysis methods. In contrast to the hierarchical approach, existing groups may be split up again during the classification procedure for an optimal partitioning (Philipp et al., 2010, 2014). Selected classification methods from this methodological group are *k-means cluster analysis with Wards start partition (CAP)*, formerly known as *k-means by seeds from hierarchical cluster analysis of principal components (PCACA)*, which was introduced by Yarnal (1993) or *Simulated annealing and diversified randomization clustering (SANDRA)* by Philipp et al. (2007). Furthermore, *k-means with differing start partitions (CKM)* and *k-means with most differing start partitions (DKM)* are included (Enke and Spekat, 1997). The latter approach was mainly used in the presented analysis and is therefore described in more detail in the following. A few classifications are also performed using SANDRA algorithm and therefore this method is further described as well.

**Großwetter-Type or prototype classification (GWT)**

As a representative method of threshold based classifications, the *Grosswettertypes or prototype classification (GWT)* by Beck (2000) is selected for further analysis. The method can be seen as objective version of the *Hess-Brezowsky Grosswettertypen (GWT)*. Additional studies explaining the basic principles of this classification approach are for example Beck et al. (2007) or Philipp et al. (2010). In this thesis, the GWT is mainly used for comparison with optimized CTC.

Mean sea level pressure fields are categorized based on their varying degrees of zonality, meridionality and vorticity. Coefficients of zonality (Z), meridionality (M) and vorticity (V) for each day/case are calculated as spatial correlation coefficients between the respective mean sea level pressure field and three prototypical patterns, which represent idealized west-east, south-north and central low-pressure isobars over a target region. 10 types classified with GWT represent the means of particular combinations of these three coefficients, which leads to eight directional types according to the Z and M coefficients. Type 9 represents central high- and Type 10 central low-pressure types from maximum negative and positive V coefficient. 18 circulation types are classified by subdividing the directional circulation types into cyclonic and anticyclonic subtypes, 26 circulation types also include indifferent V coefficients.

Advantages of this method are the reproducibility and easy interpretation of circulation patterns. Furthermore, the processing on computer is quite fast. The main disadvantages are the fact that

only mean sea level pressure and geopotential height fields can be classified and the predetermination of rules and thresholds involves subjective decisions.

**K-means cluster analysis with most differing start partitions (DKM)**

As it is described by Enke and Spekat (1997), an initial weather situation $O_1$ is subjectively (randomly) selected. From all daily gridded input fields the seed for the following cluster is selected by most dissimilar weather patterns $O_2 ... O_n$ to the preceding. The normalized Euclidean Distance measure is used to assign weather patterns to a cluster. The seed for the third cluster has the highest sum of distances to the first two seed-patterns and so on. An iterative k-means clustering process is launched after the initial assignment of all days. The class assignment is done by iteratively exchanging objects, using the minimum distance method, until a stable state is reached. The two benefits from this classification approach are better separated centroids and a reduction of their internal variability. In contrast to *k-means cluster analysis using differing start partitions (CKM)*, which does not keep classes including less than 5% of all days, DKM also contains quite small classes (Philipp et al., 2010, 2014).

In the following analysis, DKM is used to optimize Circulation Type Classifications (CTC) with respect to the target variable $PM_{10}$. Concept and results of optimization are content of Chapter 6.

**Simulated annealing and diversified randomization (SANDRA)**

The classification method Simulated annealing and diversified randomization clustering method (SANDRA) was introduced by Philipp et al. (2007) and belongs to the algorithms for optimizing partitions based on non-hierarchical clustering. Drawbacks of the k-means cluster analysis, like the dependence of the results on the fixed starting partition and on the ordering of checks as well as reassignments, are reduced in this heuristic method. SANDRA enables to approximate a single global optimum in contrast to standard k-means clustering. On the one hand, the problem of the dependence on the starting partition is implemented by using randomization techniques for multiple variants of starting partitions. A random partition is, on the other hand, the basis for the clustering with simulated annealing technique. As Philipp et al. (2007) explain, each object, for example a gridded mean sea level pressure field, is checked at each iteration if it is assigned to an appropriate cluster. Otherwise it can be reassigned.

$$P = exp[(D_{old} - D_{new})/T] \tag{4}$$

Depending on the acceptance probability $P$, which is high in the beginning of the optimization

procedure and decreases in the progress with values between 0.0 and 1.0, assigned objects can be reassigned to other clusters ("wrong" reassignment) for an overall improvement. $D_{new}$ is the Euclidean distance between an object and a potential new cluster and $D_{old}$ the Euclidean distance between an object and its actual cluster (Philipp et al., 2010). A slow reduction of $P$ is enabled by a control parameter $T$ (similar like temperature), which has a huge value at first and is adjusted by a cooling factor $C$ (e.g. C=0.99).

$$T = T * C \tag{5}$$

From a given number of runs finally the best result according to within-type variance is chosen. In the application of SANDRA for this thesis, 100 runs are iterated. A major drawback of this classification approach is the computation time. Therefore, it was only applied to recalculate optimized conditioned classifications for more stable results.

## 4.3. Downscaling methods

The link between influencing meteorological variables (predictors) and air quality parameters (predictands) is, at various levels, ranging from small to local scale processes up to large-scale ones. Thus, methods are needed to bridge the gap between the scales (Yuval et al., 2012). Statistical downscaling approaches are useful techniques to obtain target variables on a local scale from regional to large-scale meteorological variables. An early review of downscaling techniques has been given by Wilby and Wigley (1997). They grouped them in four main categories, namely regression methods, weather pattern-based ones, stochastic weather generators and limited-area modelling. Nowadays, a broad variety of downscaling techniques exists. Studies investigating the influence of meteorology on air quality using variants of statistical downscaling techniques are already mentioned in Chapter 2. Many studies are using mixed or hybrid approaches of these methods. This is also the case for the presented analysis.

Regression based methods are one of the earliest statistical downscaling techniques. Linear or non-linear relationships between local or regional scale parameters (so called predictands), e.g. air quality data, temperature, precipitation, and coarser-resolved influencing variables (so called predictors), usually on a grid-scale like weather and circulation types, are investigated. In this thesis, three commonly used techniques, i.e. Multiple Linear Regression Analysis (MLR), Generalized Linear Model (GLM) and Random Forests (RF), are applied on the given data in order to compare the performance of methods to model primarily monthly $PM_{10}$ indices. Additionally, a simple statistical downscaling technique, here referred to as Synoptic Downscaling (SD), is used to model daily and monthly $PM_{10}$ indices.

### 4.3.1. Synoptic Downscaling

Synoptic Downscaling (SD), sometimes also referred to as reference class forecasting, is a quite straightforward and basic downscaling approach. For each CT of a classification, the long-term average $PM_{10}$ concentration is calculated. These conditionally averaged values are used to estimate daily mean $PM_{10}$ concentrations ($PM_{daily}$) for each day with the occurrence of the corresponding CTs (Beck et al., 2014b).

The performance of the SD is assessed by using time series of original and modelled daily $PM_{10}$ values to calculate different quantitative evaluation measures, e.g. coefficient of determination ($R^2$), Mean Square Skill Score (MSSS) and Heidke Skill Score (HSS). These skill scores are introduced in more detail in the following Section 4.4. From the daily $PM_{10}$ time series, monthly mean $PM_{10}$ concentrations ($PM_{mean}$) are determined as well as monthly exceedances of a daily mean $PM_{10}$ value of 50 $\mu g/m^3$ ($PM_{50}$).

### 4.3.2. Random Forests

Random Forests (RF), which are based on Classification and Regression Trees (CART) analysis, are a recently quite popular method for the prediction and quantification of the importance of influencing variables (predictors) on a target variable (predictand). It can be described as an ensemble approach using a form of nearest neighbour predictor.

RF have been introduced by Breiman (2001). The basic principle of this method can be summarized as follows: for the $k$-th tree, a random vector $\Theta_k$ is generated. It has the same distribution as past random vectors $\Theta_{1,...,}\Theta_{k-1}$ and is defined to be independent from them. A tree is growing using the training set and random vector $\Theta_k$. The result is a classifier $h(x, \Theta_k)$ with $x$ as input vector.

To sum it up, RF are defined as a classifier containing a collection of tree-structured classifiers $h$ with $k$ = 1,..., where the random vectors $\Theta_k$ are independent and identically distributed. Finally, each tree casts a unit vote for the most popular class of input variable $k$, which is realized in variable importance scores. These scores allow one to identify the most influential parameters. Observations (predictands) used for each tree are randomly selected and each split within each tree is created on the basis of a randomly selected set of predictors (Grömping, 2009). As Jollois et al. (2009) has stated, one has to keep in mind that no explicit model is defined, since a prediction model is build on the aggregation of regression trees.

There are some important advantages of this statistical downscaling approach. The non-parametric method is able to handle large data sets containing a lot of variables with relatively small numbers

of observations. Furthermore, RF provide an assessment of variable importance. The input data has not to be normally distributed and linear respectively non-linear relationships between observations $n$ and number of variables $p$ are taken into account. In contrast to linear regression, which works reasonably robust for a larger number of observations than number of variables ($n \gg p$), but not for the opposite case ($p \gg n$), RF work well for both cases (Grömping, 2009).

An overview of applications of RF in atmospheric science on air quality analysis is presented in Chapter 2. Recent studies applying RF for analysis of meteorological influences on various spatial and time scales on particulate matter are for example presented by Jollois et al. (2009); Bobbia et al. (2011) as well as Beck et al. (2014b).

In the study by Beck et al. (2014b), RF are used as downscaling tool with monthly occurrence frequencies of circulation types as predictors. Results discussed there assert the method to be feasible for the application. In accordance to these findings, RF are applied to monthly occurrence frequencies of CTs (predictors) to estimate monthly $PM_{mean}$ and $PM_{50}$ indices (predictands) in this thesis.

### 4.3.3. Multiple Linear Regression

MLR enables the analysis of a huge number of potential predictor variables (Wilks, 2006). According to Stahel (2008), it is important to keep in mind that the regression analysis is actually a method for describing the statistical relation between various quantitative or dichotomous variables $X_i$ ($i$ = 1,...,$m$) (predictors) and a quantitative criterion $Y$ (predictand) rather than the real influence. In order to avoid misunderstandings, the predictors $X_i$ are not called *independent* variables in the presented analysis, because in MLR, it is permitted to have correlations between the particular predictors (for the problem of multicollinearity see for example Bahrenberg et al. (2003); Stahel (2008)). An application-oriented introduction into MLR is given for example by de Sá (2007); Stahel (2008); Schönwiese (2013) or Toutenburg et al. (2006).

The model assumption for the MLR

$$\hat{Y} = b_0 + b_1 X_1 + b_2 X_2 + ... + b_m X_m \tag{6}$$

contains $\hat{Y}$, which represents the estimated variable $Y$ based on the regression equation. The values of $\hat{Y}$ differ from those of genuine $Y$ through the values of the residuals (Wollschläger, 2012; Bahrenberg et al., 2003). As equation 6 shows, each of the predictor variables has its own coefficient, analogous to the slope, $b$, and are often called regression parameters. $b_0$ is sometimes known as the regression constant or intercept. Parameters $b_0$ to $b_m$ are assumed by the empirical

data (Wilks, 2006). The coefficients $b_0$ to $b_m$ are commonly estimated by the method of least squares in order to get the function minimal. The main aim is to choose only those values for $X_i$, which fit as good as possible to the $Y$ (Bahrenberg et al., 2003).

In case of the intended analysis in this thesis, monthly occurrence frequencies of circulation types are used as predictors in MLR to estimate the predictand variable, here $PM_{10}$ indices.

In order to select a good set of predictors from the sample, a stepwise regression is performed based on the Akaike information criterion (Akaike, 1974), which is one commonly used screening procedure. Thereby, different predictor combinations are tested in a stepwise procedure in both directions. Smaller values of AIC indicate a higher information content (Wollschläger, 2012). In order to find the most appropriate model order, the AIC criterion regards the goodness of fit, as reflected in log-likelihoods, and a penalty that increases with the number of fitted parameters (Wilks, 2006). If no predictors are selected in the stepwise regression, the model is not used in the intended analysis.

Final sets of predictors are defined as those ones with most frequent numbers and types of predictors chosen in the exploratory MLR. Furthermore, only those models are considered, for which the basic assumptions of normality, homoscedasticity and independence of residuals are fulfilled, which underlie the MLR.

Daily $PM_{10}$ time series are in most of the cases not normally distributed. This was tested on the basis of a Kolmogorov-Smirnov-Test with $\alpha = 0.05$ (see for example Stahel 2008). However, monthly $PM_{10}$ values ($PM_{mean}$, $PM_{50}$) are generally normal distributed. Hence, the MLR is only used for monthly $PM_{10}$ indices in the following analysis.

Homoscedasticity, which means an equal variance of the residuals, is tested with a Breusch-Pagan-Test and the independence of the residuals with a Durbin-Watson-Test as described by Krämer and Sonnberg (1986) for example.

The model performances of the generated MLR are evaluated using the coefficient of determination ($R^2$) and Mean Squared Skill Score (MSSS) for original and modelled $PM_{10}$ indices.

### 4.3.4. Generalized Linear Models

GLM are extensions of traditional regression models that allow the mean to depend on the explanatory variables through a link function. The response variable can be any member of a set of

distributions called the exponential family. Different distributions exists, e.g. Normal, Poisson, Binomial and Gamma distribution. A good overview of regression approaches and especially GLM is given for example by Fahrmeir et al. (2009). In accordance to Stadlober et al. (2012) and Huebnerova and Michalek (2014), the Gamma distribution is assumed for monthly mean $PM_{10}$ data as predictands. For the application of GLM on estimating $PM_{50}$, the Poisson distribution turned out to be feasible as it is appropriate, when the dependent variable is a count of events.

Linear models for non-normally distributed variables have some characteristics in common, which can be generalized and described as follows (Fahrmeir et al., 2009). The conditional expectation value

$$\mu = E(y|x) \tag{7}$$

of target variable $y$ is linked to the linear predictor

$$\eta = x^{'}\beta \tag{8}$$

through a response function $h$ respectively a linkage function

$$g = h^{-1}, \tag{9}$$

which leads to

$$\mu = h(\eta), \eta = g(\mu). \tag{10}$$

$\beta$ is the parameter to be estimated. The distribution of the target variable $y$ (Normal-, Binomial-, Poisson-, Gamma distribution) can be described as density of a one parametric exponential function for all cases:

$$f(y|\theta) = exp\left(\frac{y\theta - b(\theta))}{\theta} + c(y,\phi,\omega)\right). \tag{11}$$

$\theta$ is called natural or canonical parameter, function $b(\theta)$ must fulfil the target that $f(y|\theta)$ can be normalized and derivations $b^{'}(\theta)$ and $b^{''}(\theta)$ exist. $\phi$ is the dispersion parameter and $\omega$ often a weight or other known parameter.

When the data is supposed to be Gamma $G(\mu,\nu)$ distributed, the coefficients $\theta(\mu)$ is $\frac{-1}{\mu}$, $b(\theta)$ is $-log(-\theta)$ and $\phi$ is $\nu^{-1}$. The expectation value

$$E(y) = b'(\theta) \tag{12}$$

is furthermore defined as $\mu = 1\frac{-1}{\theta}$ and the variance

$$Var(y) = b''(\theta)\phi/\omega \tag{13}$$

as $\mu^2 \frac{\nu^{-1}}{\omega}$.
Assuming the data to be Poisson $Po(\lambda)$ distributed, $\theta(\mu)$ is expected to be $log(\lambda)$, $b(\theta)$ as $exp(\theta)$ and $\phi = 1$. The expectation value is supposed to be $\lambda = exp(\theta)$ and the variance $\frac{\lambda}{\omega}$.

A stepwise procedure for both directions is used as well for the GLM to select predictor sets for the application in the intended analysis. If no predictors are selected in the stepwise GLM, the models are not used for further analysis.

The performance of the models for modelling $PM_{mean}$ and $PM_{50}$ is evaluated using $R^2$ and MSSS.

## 4.4. Evaluation methodology

*"Forecast verification is the process of assessing the quality of forecasts. [...] A wide variety of forecast verification procedures exist, but all involve measures of the relationship between a forecast or set of forecasts, and the corresponding observation(s) of the predictand. Any forecast verification method thus necessarily involves comparisons between matched pairs of forecasts and the observations to which they pertain."*

WILKS 2006

Forecast verification metrics are also known as skill scores, validation or evaluation measures. In general, they are defined as measures of the relative accuracy of forecasts between two forecasting systems with one of them acting as referencing system. "Positive" skill is hereby defined as a favourable difference in accuracy, which usually represents a minimum level of acceptable performance for a set of forecasts (Murphy, 1988). A good overview of several forecasting verification measures is given by Wilks (2006) or Jolliffe and Stephenson (2011).

When looking at the evaluation of Circulation Type Classifications (CTC), the question arises, how good do they perform in an explicit application or how good is the factor circulation type as a predictor (Schiemann and Frei, 2010). Huth et al. (2008) present a set of "classical" selected measures for determining the quality of classifications like the Explained Variance (EV). The two main investigations of the mentioned criteria in the overview are to evaluate the performance of the variable that is used for the CTC, for example pressure fields, or associated fields of determined meteorological variables, e.g. surface temperature, precipitation or air quality parameters. When looking at extreme values of skewed variables, the mentioned skill scores in Huth et al. (2008) have limitations. Therefore additional evaluation metrics are introduced here.

In the presented work, the performance of the statistical models is evaluated using a number of different scalar measures and skill scores introduced or adapted by different authors. These scores used as performance measure are the Explained Variance (EV) (in %), the Squared Pearson correlation coefficient ($R^2$), also known as coefficient of determination, MSSS based on mean squared error (MSE), Heidke Skill Score (HSS), Hit Rate (HR) and Brier Skill Score (BSS).

In order to evaluate and describe the influence of the classified circulation types on local $PM_{10}$ concentrations, their so called synoptic skill, the EV was chosen as a quantitative measure. It is calculated as the variance of $PM_{10}$ concentrations within circulation types (within sum of squares) related to the total variance of the $PM_{10}$ data set (total sum of squares). As it is described by Beck et al. (2013) for example, a higher value for EV marks a better discriminatory power of a classification for the analysed target variable:

$$EV = \frac{\sum_{k=1}^{K} N_k(\bar{a}_k - \bar{a})^2}{\sum_{i=1}^{N}(a_i - \bar{a})^2} \tag{14}$$

$K$ is the number of classes (circulation types) and $N$ the number of cases, $\bar{a}$ and $\bar{a}_k$ are the overall and type-specific mean values and $a_i$ is the value of the target variable for case $i$.

The product moment correlation coefficient after Pearson $r$ is a commonly used evaluation measure, describing the linear correlation between two variables $X$ and $Y$, resulting in a value between $-1 \leq r_{XY} \leq 1$:

$$r_{XY} = \frac{s_{XY}}{s_X * s_Y}. \tag{15}$$

$s_{XY}$ is the covariance between the two variables and $r_{XY}$ the normed covariance of $X$ and $Y$ regarding the standard deviations of the two variables. This results in

$$r_{XY} = r_{YX}. \tag{16}$$

The value 1 marks a positive correlation, 0 no correlation, and $-1$ a total negative correlation (Bahrenberg et al., 1999).

Murphy (1988) described the calculation of the MSSS, which is calculated by the mean squared error (MSE) for the model and climatology reference. $N$ is the number of cases, $y_i$ is the modelled value for case $i$, $a_i$ is the respective observed value and $\bar{a}$ is the mean over all $a_i$. MSSS values less than or equal to 0 imply a model quality worse or equal to climatology, while a maximum MSSS value of 1 indicates a perfect model (see also for example Jolliffe and Stephenson (2011) or Beck

et al. (2014a)). The formula for calculating the MSSS

$$MSSS = 1 - \frac{MSE}{MSE_{clim}} \tag{17}$$

contains the mean square error for the model, here referred to as MSE,

$$MSE = \frac{1}{N}\sum_{i=1}^{N}(y_i - a_i)^2 \tag{18}$$

and the mean square error for the climatology $MSE_{clim}$

$$MSE_{clim} = \frac{1}{N}\sum_{i=1}^{N}(\bar{a}_i - a_i)^2. \tag{19}$$

In order to test the model ability to reproduce several events such as critical $PM_{10} > 50\ \mu g/m^3$ per day, the HSS was applied on daily mean $PM_{10}$ series as described by Wilks (2006), Jolliffe and Stephenson (2011) or Beck et al. (2014a):

$$HSS = \frac{2(ad - bc)}{(a+c)(c+d) + (a+b)(b+d)}. \tag{20}$$

It is calculated using $a$ as number of observed events that are correctly modelled (so called hits). $b$ is the number of modelled events that are not observed (false alarms), $c$ is the number of events that are observed but not modelled (missed values) and $d$ is the number of non-events in both observations and model (correct negative). Perfect forecasts receive HSS equal 1, forecasts equivalent to the reference forecasts receive zero scores, and forecasts worse than the reference forecasts receive negative scores.

The HR is a quiet simple skill score to measure if an event of interest, here daily $PM_{10}$ concentrations $> 50\ \mu g/m^3$, occurs (Wilks, 2006). It is calculated as the ratio of correct forecasts $a$ to the number of times this event occurred $a + c$:

$$HR = \frac{a}{a+c}. \tag{21}$$

Schiemann and Frei (2010) introduce in their study a variant of the BSS, which was originally published by Brier (1950) as Brier Score (BS). The BSS is an evaluation measure for the occurrence of continuous variables for the exceedance/non-exceedance of a given threshold in dependency on a certain circulation type. Examples of studies using the BSS in context of the evaluation of CTs are Demuzere et al. (2010) or Beck et al. (2013).

According to Wilks (2006), the BS is essentially the mean squared error of the probability forecast and is calculated as follows:

$$BS = \frac{1}{N}\sum_{k=1}^{N}(y_k - o_k) \tag{22}$$

with $y_k$ indicating the forecast probability on a day $k$ ($k$ = 1,...N), in this context the empirical event frequency on day $k$. $o_k$ is the variable for the observations taking values 1/0 if an event occur (1) or does not occur (0) on that day $k$.
The BSS for CTC evaluation is calculated as follows:

$$BSS = \frac{\frac{1}{N}\sum_{k=1}^{N} N_i(y_i - \bar{o})^2}{\bar{o}(1-\bar{o})}. \tag{23}$$

If we assume $i$ = 1,...,N to be the number of CTs of a classification, $y_i$ is the relative frequency of the event for each type $i$. In the presented analysis these are number of days exceeding a daily mean $PM_{10}$ of 50 $\mu g/m^3$. Attributing a day $k$ to a CT $i$, $y_i$ can be considered as a prediction of the probability of the described $PM_{10}$ event to occur on a day $k$ (Demuzere et al., 2010). This prediction is available for all days $k$ = 1,...N. $N_i$ represents the frequency of each CT $i$ and $\bar{o}$ the binary indicator for the observations. $\bar{o}$ takes values 1/0 if an event occur/does not occur on that day $k$. The BSS varies between 0 and 1 with larger values indicating more skill.

Table 4.1: Three 20-year calibration and 12-year validation periods are defined to evaluate the performance of the models.

| Calibration | Validation |
|---|---|
| 1980 - 1999 | 2000 - 2011 |
| 1980 - 1989 + 2001 - 2011 | 1990 - 2000 |
| 1991 - 2011 | 1980 - 1990 |

In the context of this thesis, BSS is used to evaluate the occurrence of daily and monthly $PM_{10}$ indices for the exceedance or non-exceedance of the discrete value of $> 50$ $\mu g/m^3$ (BSS50) or the 80-, 90-, 95 and 98 - percentile of the $PM_{10}$ input data (BSS80, BSS90, BSS95, BSS98) on the prevailing circulation type.

For an independent verification of the performance of generated models, calibration and validation periods are used. There are different solutions for defining calibration and validation periods for the evaluation of the models. Table 4.1 indicates the selection of three 20 year calibration and 12 year fixed validation periods for the selected period of 1980-2011 used in further analysis. Beside the definition of fixed calibration and validation periods, other proceedings are for example the leave-one-out or similar cross-validation approaches or bootstrap resampling (Wilks, 2006).

# 5. $PM_{10}$ in study region Bavaria

Bavaria (47°16' - 50°34' N, 8°58' - 13°50' E) is a federal state, located in the southern part of Germany, covering an area of 70.551 $km^2$ with a population of around 12.5 million people. It borders in the south to Austria and Switzerland, in the east to Czech Republic. The capital city is München with a population of approx. 1.3 million. Other major cities are Nürnberg (503.000), Augsburg (270.000), Würzburg (135.200), Regensburg (132.500), Ingolstadt (123.000), Fürth (114.100) and Erlangen (104.700) (BayLfStaD, 2014).

The diverse topography includes parts of the Alps, with the highest altitude at Mount Zugspitze (2962 m) in the south, the Alpine foothills formed by glaciers with numerous lakes, the Eastern Bavarian central mountains as well as the Swabian-Franconian cuesta landscape with the lowest point at river Main (100 m). The two major rivers are the Danube and Main.

There are several reasons for choosing Bavaria as a study region for the intended analysis of the influences of meteorological conditions on local $PM_{10}$ concentrations in this thesis. On the one hand, a broad range of emission sources for particulate matter, from rural to urban areas with industry and traffic related sources as well as different altitudes and landscapes, are represented in the region. Furthermore, a long-range transport of particles from Eastern Europe to Bavaria, e.g. Czech Republic or Poland, can be observed. On the other hand, long-time series of $PM_{10}$, resulting from high quality measurements since 1974, are available. The long-time series are necessary to investigate the effect of climatic processes on local particles and to achieve statistically robust results.

In this Chapter, the main sources of particles as well as meteorological-climatological conditions in the study region are briefly introduced in Section 5.1. Afterwards, characteristics of the used $PM_{10}$ data basis concerning data availability, basic quality aspects, long-term trends and correspondence between locations are provided. Section 5.2 includes the selection of 16 long-term measurement sites for the period of 1980-2011 and descriptive statistics of the data basis. A discussion referring to the application of the $PM_{10}$ data set for the intended analysis are presented in Section 5.3. In order to analyse long-term trends of the $PM_{10}$ data set, a trend analysis is applied on the time series in Section 5.4. Finally, a s-mode Principal Component Analysis is used to group the 16 stations into Bavarian regions with similar time variability of $PM_{10}$ in Section 5.5.

## 5.1. Characteristics of the study region

In general, the composition of Bavarian particulate matter concentrations are a mixture of transregional background pollution (around 50 %), 25 % local traffic emissions and 25 % additional

emissions from urban areas. The highest emissions result from traffic emissions (38 %), home heating (27 %), industrial facilities (19 %), agricultural livestock farming (12 %) as well as handling of dusty goods (4 %). The traffic emissions mainly originate from road transportation (63 %), including 40 % emissions from heavy utility vehicles (Bayerisches Staatsministerium für Umwelt, 2006). The influences of local traffic emissions are dependent on the traffic load, types of vehicles or re-suspension of particles. Moreover, they are dependent on width and height as well as density of existing buildings in urban areas for instance. As it is described by Bayerisches Staatsministerium für Umwelt (2006), the composition of particulate matter in Bavaria at a main road is mainly of organic compounds (17 %), soot (13 %), nitrate (10 %), sulphate (12 %), ammonia (10 %) and others (38 %).

The amount of air pollution is on the one hand influenced by the extent of emissions and by local as well as large-scale meteorological conditions, on the other hand. Umweltbundesamt (2015) for example has mentioned cold winter in Germany, which lead to increased air pollution from home heating. A possible reason for the cold weather conditions are high pressure systems on a synoptic scale in winter over Europe, which are connected to low winds and stable conditions with nearly no air mass exchange and a particle accumulation. According to the climate classification of Köppen and Geiger, Germany is situated in a warm-temperate climate in the transition zone between the western European maritime and continental climate of eastern Europe (Schönwiese, 2003; Klimaforschungsverbund, 1996). The temperate maritime climate is characterized by mild winters and cool summers with humid conditions in contrast to continental climate, which is connected to long cold winters with snow and hot summers (StMUV, 2015).

The target region is located in the extra-tropical circulation with a dominant western flow direction of air masses. In general, the leading modes of variability of the extratropical circulation in both hemispheres are characterized by zonally symmetric or "annular" structures. Perturbations of opposing signs in geopotential height occur in the polar cap region and in the surrounding zonal ring centred near 45° latitude (Thompson and Wallace, 1999). The climate is influenced by the southern periphery of the northern European cyclones belt over the whole year and Mediterranean cyclones belt in September to May (Liedtke and Marcinek, 1996). Instabilities of meteorological-climatological conditions over Germany result from frequent changes of air masses of varying origin and properties, which are transported by frontal cyclonic systems with moving or quasi-stationary anticyclones. Western circulation patterns dominate throughout the year. Southern and eastern flow directions are the second and third frequent ones in the southern part of Germany (Liedtke and Marcinek, 1996).

In the recently published climate report of Bavaria by StMUV (2015), variations in the occurrence

frequencies of large-scale weather conditions have been discussed. Extreme weather situations caused by the large-scale atmospheric conditions have been mentioned as well as climate-change-induced variations of the extremes. An increase of hot, dry weather situations in summer has been detected for Bavaria since the seventies of the last century, which are connected to extremely dry vegetation periods. Furthermore, Vb weather conditions from the Mediterranean region have been observed to occur mostly in spring and autumn causing extreme precipitation events in Bavaria. A further description of the large-scale atmospheric conditions over Central Europe and the study region, which have a particular influence on particle concentrations, is presented in Chapter 6.

Spatial variations as well as local and regional differences in climatology mainly originate from diverse topography. The aforementioned manifold landscapes of Bavaria lead to small-scale influences and processes on local climate and meteorology. The main influencing factors are, beside the altitude and geographical position, land use, bodies of water as well as cold air areas (Klimaforschungsverbund, 1996). A detailed description of the climate of the particular landscapes is given by Liedtke and Marcinek (1996), Klimaforschungsverbund (1996) or StMUV (2015).

An annual mean temperature of 7.8 °C has been observed in Bavaria for the period of 1971-2000, with seasonal differences of 16.2 °C mean temperature in summer and 0.5 °C in winter. July is the warmest month and January the coldest (StMUV, 2015). Comparably large regional differences have been observed for annual total precipitation. The averaged value over the whole region is 945 mm, 1800 mm are achieved in the Alpine region. The averaged sunshine duration is 1586 hours.

## 5.2. Station description

Minimum 30 years of observations are commonly used for climate related analysis. The unique time series of continuous measurements from 16 stations spread over the study region, with over 90 % data availability for the period 1980-2011, enable analysis for a 32-years period, which is necessary for investigating climate-change-induced effects. Particulate matter data are provided by the Bavarian Environment Agency/Landesamt für Umwelt (LfU). A brief introduction of the data basis is presented in Chapter 3. The selected stations are (with station ID in brackets): Ingolstadt Rechenbergstrasse (L1.1), Kelheim Regensburger-Strasse (L2.1), Landshut Podewilsstrasse (L2.3), Regensburg Rathaus (L3.1), Weiden Nikolaistrasse (L3.3), Schwandorf Wackersdorfer-Strasse (L3.4), Bayreuth Rathaus (L4.2), Bamberg Löwenbrücke (L4.3), Nürnberg Bahnhof (L5.1) and Ziegelsteinstrasse (L5.2), Fürth Theresienstrasse (L5.5), Schweinfurt Obertor (L6.3), Würzburg Kardinal-Faulhaber-Platz (L6.4), Augsburg Königsplatz (L7.1), München Stachus (L8.1) and Lothstrasse (L8.3).

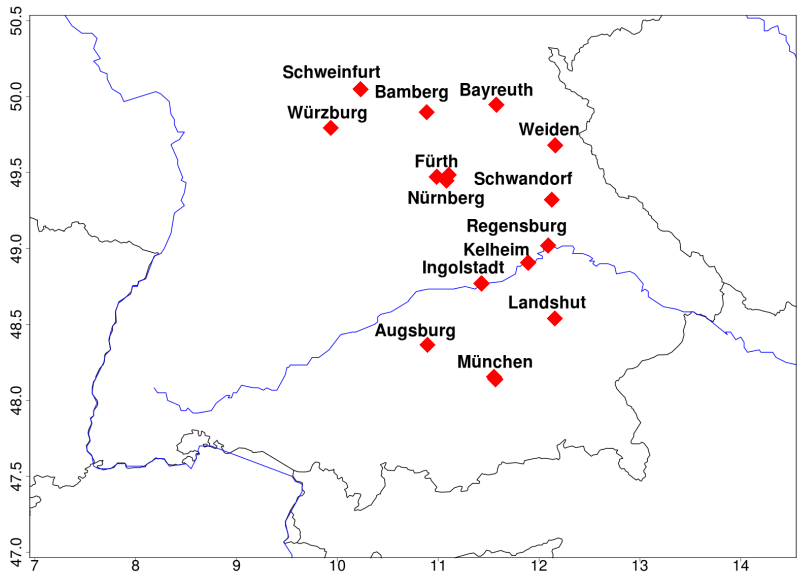


Figure 5.1: Locations of 16 selected $PM_{10}$ measurement sites run by the Bavarian Environment Agency (LfU).

Existing studies confirm that public health effects of high air pollution levels are particularly critical in urban areas (see Chapter 2). With urban regions being quite vulnerable to future climate change effects, a focus of this thesis is set on stations in Bavarian urban regimes. All measurement sites are situated in an urban environment and are characterized as urban background and traffic related ones according to EoI (Exchange of Information, EU directive 2001/752/EC). Thus, they are comparable. Additionally, the stations are spread over the whole target region and encompass all cities with more than 100.000 inhabitants. In Figure 5.1, the station locations are depicted.

Table 5.1: First and third quartiles (1st and 3rd Qu.), median, long-term mean and 99th percentile of daily mean $PM_{10}$ concentrations (in $\mu g/m^3$) from the period 1980-2011 at 16 long-term and three rural background stations (Schauinsland (Schau), Schmücke (Schmue), Hohenpeißenberg (MOHP)).

| ID | 1st Qu. | Median | Mean | 3rd Qu. | 99th P |
|---|---|---|---|---|---|
| Ingolstadt Rechenbergstrasse | 18.8 | 28.0 | 32.4 | 41.0 | 100.0 |
| Kelheim Regensburger-Strasse | 20.0 | 30.0 | 34.8 | 44.0 | 107.0 |
| Landshut Podewilsstrasse | 19.0 | 29.0 | 32.9 | 41.0 | 104.0 |
| Regensburg Rathaus | 22.0 | 34.0 | 37.7 | 48.0 | 109.0 |
| Weiden Nikolaistrasse | 20.0 | 31.0 | 38.0 | 48.0 | 130.0 |
| Schwandorf Wackersdorfer-Strasse | 19.0 | 29.0 | 34.4 | 44.0 | 115.0 |
| Bayreuth Rathaus | 20.0 | 29.0 | 33.9 | 43.0 | 108.1 |
| Bamberg Löwenbrücke | 18.0 | 27.0 | 32.7 | 41.0 | 112.0 |
| Nürnberg Bahnhof | 21.0 | 31.0 | 35.8 | 45.0 | 109.0 |
| Nürnberg Ziegelsteinstrasse | 20.0 | 28.0 | 32.2 | 40.0 | 91.3 |
| Fürth Theresienstrasse | 21.0 | 31.0 | 35.0 | 44.0 | 97.0 |
| Schweinfurt Obertor | 20.0 | 29.0 | 33.1 | 41.8 | 100.4 |
| Würzburg Kardinal-Faulhaber-Platz | 17.0 | 26.0 | 30.5 | 39.0 | 100.0 |
| Augsburg Königsplatz | 28.0 | 42.0 | 46.7 | 60.0 | 128.0 |
| München Stachus | 30.0 | 43.0 | 48.5 | 60.0 | 137.0 |
| München Lothstrasse | 18.0 | 27.0 | 31.9 | 40.0 | 103.0 |
| Schauinsland | 5.0 | 10.4 | 14.7 | 19.2 | 66.0 |
| Schmücke | 7.0 | 13.2 | 19.7 | 24.6 | 89.0 |
| Hohenpeißenberg | 6.5 | 9.4 | 10.9 | 13.6 | 32.1 |

Table 5.1 indicates descriptive statistical measures of the $PM_{10}$ data basis, including first and third quartile (1st and 3rd Qu.), mean, median as well as 99th percentile for the 16 long-term stations as well as three rural background stations. The minimum particle concentrations are not listed as they all tend to values $< 1 \mu g/m^3$ and are dependent on the detection limit of the measurement techniques. The rural background stations are shown for comparison. As already mentioned in the data description (see Chapter 3), the background stations are close to the Bavarian border (Schmücke in Thüringen, Schauinsland in Baden-Württemberg). Furthermore, they are of higher elevation compared to the urban sites.

As Table 5.1 illustrates, long-term mean $PM_{10}$ concentrations at the background sites are just half of the urban stations. Mean $PM_{10}$ concentrations are approx. 14.7 $\mu g/m^3$ at Schauinsland, 19.7 $\mu g/m^3$ for Schmücke and 10.9 $\mu g/m^3$ for Hohenpeissenberg in the considered measurement period. Comparably high long-term mean $PM_{10}$ concentrations are observed for instance at stations München Stachus (L8.1, 48.5 $\mu g/m^3$), Augsburg Königsplatz (L7.1, 46.7 $\mu g/m^3$) and Weiden Nikolaistrasse (L3.3, 38.0 $\mu g/m^3$). Conceivable reasons for this might be the exposition of the stations next to streets with high traffic load or the surrounding by relatively high buildings.

Values of the 99th percentile of $PM_{10}$ concentrations show even larger differences between background concentrations and urban air pollution. Approx. 137.0 $\mu g/m^3$ are for example observed at München Stachus compared to 31.1 $\mu g/m^3$ at nearby station Hohenpeissenberg, 112.0 $\mu g/m^3$ at station Bamberg compared to 89.0 $\mu g/m^3$ at Schmücke. Comparably small differences can be observed for values of the 1st quartiles, which range between 18 $\mu g/m^3$ and 22 $\mu g/m^3$, except for München Stachus (30 $\mu g/m^3$) and Augsburg Königsplatz (28 $\mu g/m^3$). A similar picture emerges for the 3rd quartiles with values between 39 $\mu g/m^3$ and 45 $\mu g/m^3$ with exceptional high values for Stachus and Königsplatz (60 $\mu g/m^3$).

Further analysis revealed differences in monthly mean $PM_{10}$ concentrations. In Figure 5.2, monthly mean $PM_{10}$ concentrations (in $\mu g/m^3$) are shown for 16 Bavarian stations for the period of 1980-2011. Maximum values are observed in winter (DJF) at all sites, which has also been the case at other European measurement sites, e.g. Netherlands (Demuzere et al., 2009) or Switzerland (Gehrig and Buchmann, 2003). High $PM_{10}$ pollution in winter is suspected to be a combination of increased home heating due to low temperatures or an enhanced occurrence of inversions and high pressure systems with nearly no air mass exchange, respectively. Other studies for example by Gehrig and Buchmann (2003), Elminir (2007) or Umweltbundesamt (2015) have confirmed that seasonal fluctuations of air quality parameters are not primarily caused by changing emissions over seasons, but mainly by meteorological effects. Additionally, Figure 5.2 depicts lowest $PM_{10}$ levels in summer. Decreasing emission levels due to moderate to warm temperatures combined with

frequent changes in the synoptic situation might be possible reasons for the lower particle levels. In spring, $PM_{10}$ concentrations reach higher values compared to autumn at nearly all stations.

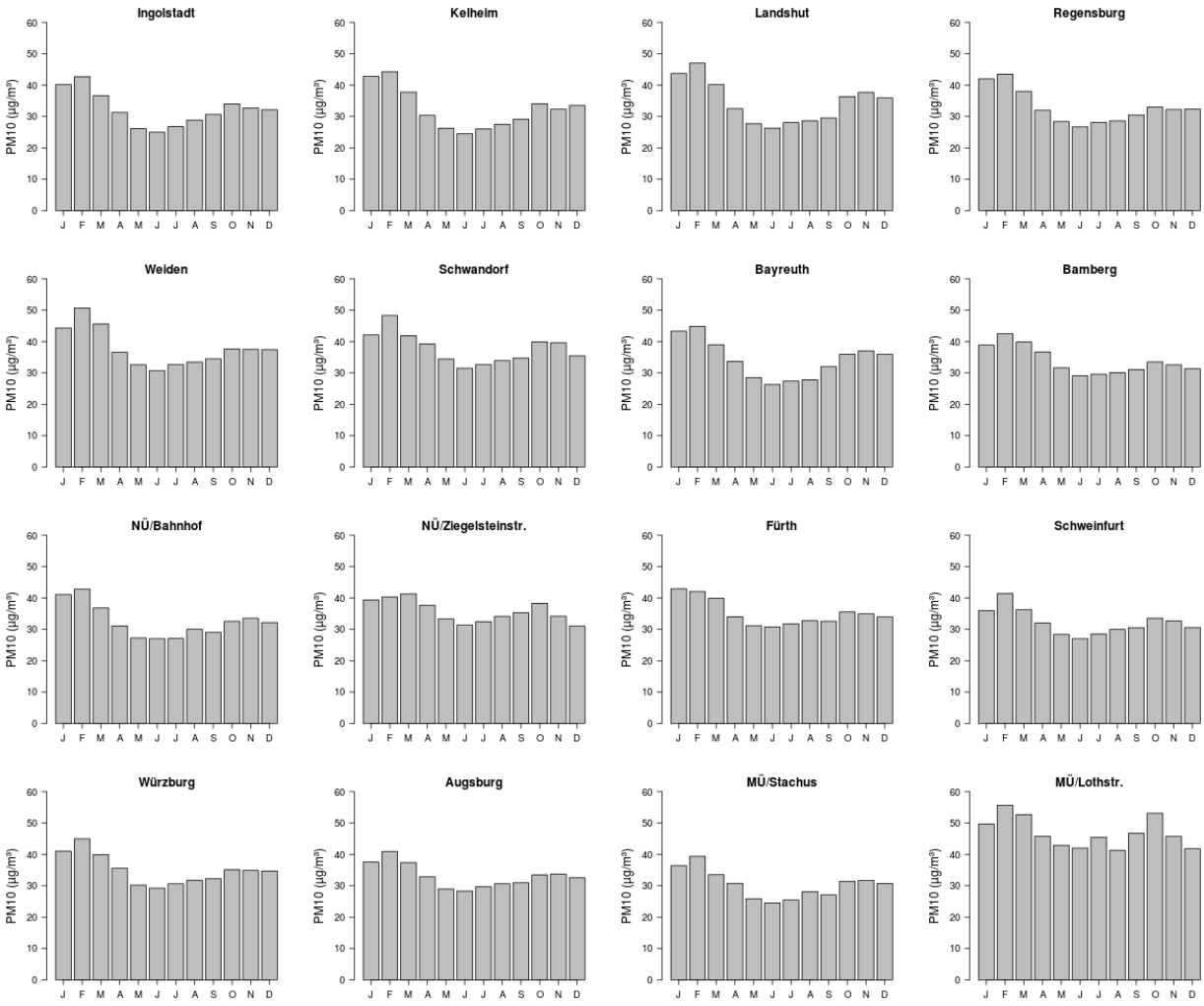


Figure 5.2: Barplots of monthly mean $PM_{10}$ concentrations at 16 Bavarian stations for the period 1980-2011.

According to the EU Directive 2008/50/EC, daily $PM_{10}$ concentrations must not exceed the critical load of 50$\mu$g/m$^3$ at more than 35 days per calendar year (E.U., 2008). As it is mentioned in Chapter 2, these air pollution loads are known to have critical health effects, for example on human respiratory tract and cardiovascular systems, especially in urban environments (WHO, 2006). The German Federal Environment Agency stated in a recent study the exceedance of the critical $PM_{10}$ load to happen especially at traffic exposed measurement sites in Germany in the past 10 years (Umweltbundesamt, 2015). Table 5.2 indicates the number of all days in 1980-2011 with daily mean $PM_{10}$ concentrations above 50 $\mu$g/m$^3$ at the Bavarian stations. München Lothstraße or Augsburg Königsplatz, for instance, exceed the critical particle load on approx. 35 % of all days,

Regensburg Rathaus and Weiden Nikolaistraße still on around 20 % of all days. München and Augsburg are categorized as traffic related stations compared to Regensburg and Weiden, which are classified as urban background ones (see Chapter 3). In this thesis, monthly exceedances of a daily mean $PM_{10}$ value of 50 $\mu g/m^3$ ($PM_{50}$) are additionally considered as critical particle load according to the EU Directive 2008/50/EC.

Table 5.2: Number of days exceeding a daily mean $PM_{10}$ concentration of 50 $\mu g/m^3$ at 16 measurement sites from 1980 - 2011.

| Station | No. of days with > 50 $\mu g/m^3$ |
|---|---|
| Ingolstadt Rechenbergstrasse | 13.9 |
| Kelheim Regensburger-Strasse | 16.3 |
| Landshut Podewilsstrasse | 13.8 |
| Regensburg Rathaus | 20.9 |
| Weiden Nikolaistrasse | 21.9 |
| Schwandorf Wackersdorfer-Strasse | 17.1 |
| Bayreuth Rathaus | 15.6 |
| Bamberg Löwenbrücke | 14.5 |
| Nürnberg Bahnhof | 17.5 |
| Nürnberg Ziegelsteinstrasse | 12.9 |
| Fürth Theresienstrasse | 17.1 |
| Schweinfurt Obertor | 13.7 |
| Würzburg Kardinal-Faulhaber-Platz | 12.9 |
| Augsburg Königsplatz | 35.0 |
| München Stachus | 35.2 |
| München Lothstrasse | 13.2 |

## 5.3. Discussion on $PM_{10}$ data basis

In this Section, some further aspects concerning the $PM_{10}$ data basis are discussed, which are important to keep in mind for the interpretation of any data analysis performed with the time series. First, a closer look on the meta data (documentation) of the stations should be taken provided by the LfU (Landesamt für Umwelt, 2013). Important informations like exact position, station type, ID, station location, instrumentation, measured parameters and starting date of measurements are given.

Second, the station location should be taken into consideration when using the $PM_{10}$ time series. The orientation and position of a station affect, for example, local and micro-climatological conditions and thus the measured particle concentrations. Figure 5.3 shows exemplary pictures of stations Weiden, Augsburg and München, which are classified as kerb site stations. The perspective of the photo Weiden Nikolaistrasse (a) is south-east oriented, Augsburg Königsplatz (b) and München Stachus (c) are north-east oriented (Landesamt für Umwelt, 2013). The photos illustrate some potential influences on the measurements caused by the station location.

(a) Weiden

(b) Augsburg

(c) München

Figure 5.3: Direct view of location of measurement sites Weiden Nikolaistrasse, Augsburg Königsplatz and München Stachus. Perspective of station Weiden is south-east oriented, for Augsburg and München it is north-east (Source: Landesamt für Umwelt 2013).

On the one hand, all stations are situated next to a road. The traffic load on the streets nearby a station, depending on number of vehicles per day and in total, is one example. The number of vehicles per day is an indicator for the exposure of a station. Unfortunately, exact numbers of traffic volume for the Bavarian stations are not provided by Landesamt für Umwelt (2013). On the other hand, the distance between the street and station plays a major role, as measurement sites nearby a road primarily monitor direct emissions, not background pollution levels. Furthermore, the surrounding vegetation has a remarkable influence on particle formation and deposition. Depending on the type of tree or plant, the vegetation emits primary particles or delivers substances for the formation of secondary particles. Station Weiden (a) is situated next to a main road and is surrounded by trees and buildings. Augsburg (b) in contrast is located between two main roads with high traffic loads. Station München (c) is built between two main roads with high traffic load as well. All depicted stations are located in densely populated areas. The named factors have a distinct influence e.g. on the particle load, chemical composition or particle formation, but also on

local meteorological and micro-climatological conditions.

Third, one should be aware of specific measurement techniques and changes in instrumentation for monitoring $PM_{10}$. As already mentioned in Chapter 3, the instrumental set-up changed from measurements of total suspended particles in the period of 1974-1999 to direct measurements of $PM_{10}$ since 2000. A commonly used conversion factor of 1/1.2, according to EU directive 1999/30/EG, has been applied on the time series to calculate $PM_{10}$ concentrations from the total suspended particles. The Bavarian Environment Agency, who provided the used data set, has already approved the usage of the recalculated $PM_{10}$ time series for data analysis and confirmed the application of quality test. Hence, no further homogenization of the used particulate matter data basis is applied.

## 5.4. Trend analysis

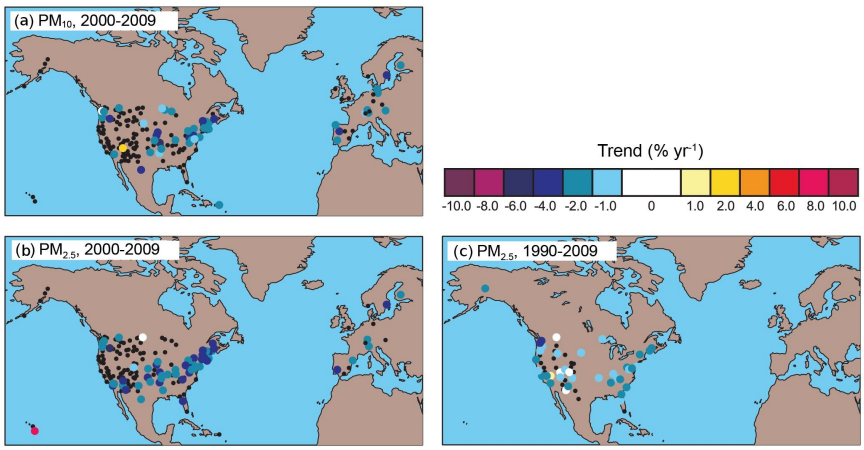


Figure 5.4: Trends in particle concentrations ($PM_{10}$, $PM_{2.5}$) in Europe and USA for two overlapping periods of 2000-2009 (a, b) and 1990-2009 (c). The trends are based on measurements from the EMEP and IMPROVE networks in Europe and USA (adapted from Stocker et al. 2013).

According to the Report of Working Group I from the 5th Assessment Report (AR5) published by IPCC 2013, a downward trend for $PM_{10}$ and $PM_{2.5}$ from the rural sites of the EMEP (European Monitoring and Evaluation Programme) and IMPROVE (Interagency Monitoring of Protected Visual Environments) network are monitored for Europe and USA (Stocker et al., 2013). Figure 5.4 illustrates the ascertained trends for two overlapping periods 2000-2009 (a, b) and 1990-2009 (c). Measurement sites with significant trends, here a trend of zero lies outside the 95% confidence interval, are given in colour, black dots mark stations with non-significant trends. In the period of 2000-2009, $PM_{2.5}$ has shown a significant averaged reduction of 3.9% $yr^{-}1$ at six of the analysed stations from the EMEP network for Europe. These trends are not significant at seven other mea-

surement sites. A significant downward trend of an averaged 2.6% yr $^{-}1$ of $PM_{10}$ is observed at 12 (out of 24) European sites from 2000-2009. As a primary cause of the decreasing particle levels, reduced emission levels have been stated.

In the recently published Air Quality Report 2015 of the German Federal Environment Agency (UBA), a decreasing trend of the $PM_{10}$ load since 2003 has been figured out for German measurement sites (Umweltbundesamt, 2015). Figure 5.5 depicts the development of annual mean $PM_{10}$ concentrations averaged over all UBA stations in three emission regimes (rural background, urban background, urban traffic related) for the period 2000-2014. The downward trend in particle levels since 2003 is illustrated for all regimes. Decreasing emission levels are suspected to cause the overall decreasing trend. Fluctuations may emerge from variations in weather conditions, e.g. the extreme hot summer in 2003 leading to a peak in $PM_{10}$ pollution. In order to compare the $PM_{10}$ trends presented in the AR5 and the current German Air Quality Report with long-term trends at Bavarian stations, a trend analysis is performed in this Section for the period 1980-2011.

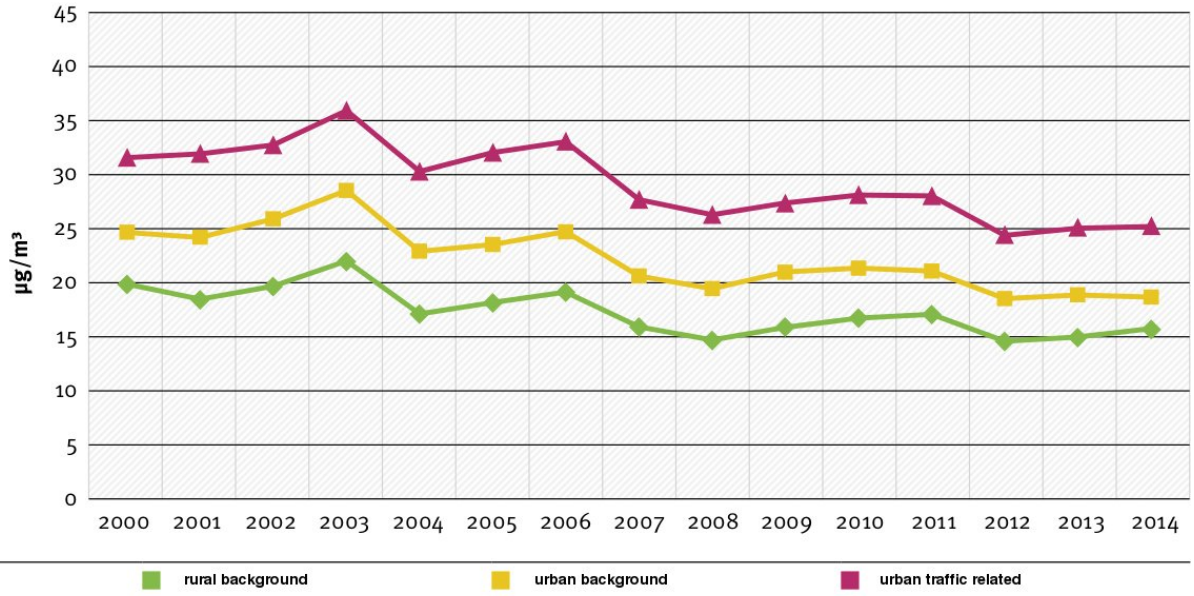


Figure 5.5: Development of annual mean $PM_{10}$ concentrations averaged over German stations for each air pollution regime for the period 2000-2014 (adapted from Umweltbundesamt 2015).

For the analysis of the long-term trend, a polynomial regression is applied. It is a linear regression describing the relationship between an independent variable $X_j$ and a dependent variable $Y$ as the $n$th polynomial:

$$Y = b_0 + b_1 * X + b_2 * X^2 + ... + b_n * X^n + \varepsilon \quad (24)$$

(Wollschläger, 2012). $\varepsilon$ marks a random unobserved error. In this thesis, a 3rd order polynomial trend is fitted on monthly mean $PM_{10}$ values at 16 stations. The significance of the trends is tested with a t-test using $\alpha = 0.05$ (Bahrenberg et al., 1999). A basic requirement of this test on the arithmetical mean of one or two samples is the normal distribution of the samples. Time series of monthly mean $PM_{10}$ values are found to be normally distributed as tested with a Kolmogorov-Smirnov-Test (see for example Bahrenberg et al. 1999).

Figures 5.6 and 5.7 illustrate time series of the monthly mean $PM_{10}$ concentrations (black dots) and the fitted 3rd order polynomial trend (blue line) at 16 stations. Significant trends are observed at all sites except Kelheim, Bayreuth, Fürth, Augsburg and München Lothstr ($\alpha = 0.05$). As Figures 5.6 and 5.7 indicate, variations in the long-term trend occur. A slightly decreasing trend of particle levels can be observed at nearly all stations, especially since the late 90ies. For stations Ingolstadt, Weiden, Schwandorf, Bamberg, NÜ Bahnhof, Fürth and MÜ Stachus an overall decrease of $PM_{10}$ is depicted. In contrast, increasing particle concentrations until the early 90ies are shown for stations Kelheim, Landshut, Regensburg, Bayreuth, NÜ Ziegelstr., Schweinfurt, Würzburg, Augsburg as well as MÜ Lothstr. followed by a decreasing tendency from the end of the 90ies. Thus, the observed $PM_{10}$ trends in Bavaria are comparable to trends analysed in the AR5 of the IPCC and in the air quality report of UBA.

A main focus of the investigations in this thesis is on estimating future climate-change-induced variations of monthly $PM_{10}$ concentrations. From the trend analysis of $PM_{10}$ presented in this Section for the observational period of 1980-2011, the question arises, whether the observed downward trend of $PM_{10}$ will proceed until the end of this century.

## 5.5. Regionalization of $PM_{10}$ stations by s-mode Principal Component Analysis

It is a common task in climatological research to analyse time series of climate elements in a given research domain to detect whether the data vary similar in time. Those measurement sites with related temporal variability of the data are grouped into spatial units, sometimes referred to as regions, to reduce the data set for instance (Huth, 2002). Several procedures exist for regionalization like Canonical Correlation Analysis, Principal Component Analysis or Cluster Analysis. Existing studies for example by Huth (2002), Beck (2000), Philipp et al. (2007) and Hertig and Jacobeit (2013) mainly used Principal Component Analysis to divide a research domain into regions within which the analysed climate element (temperature, precipitation) varies similarly in time.

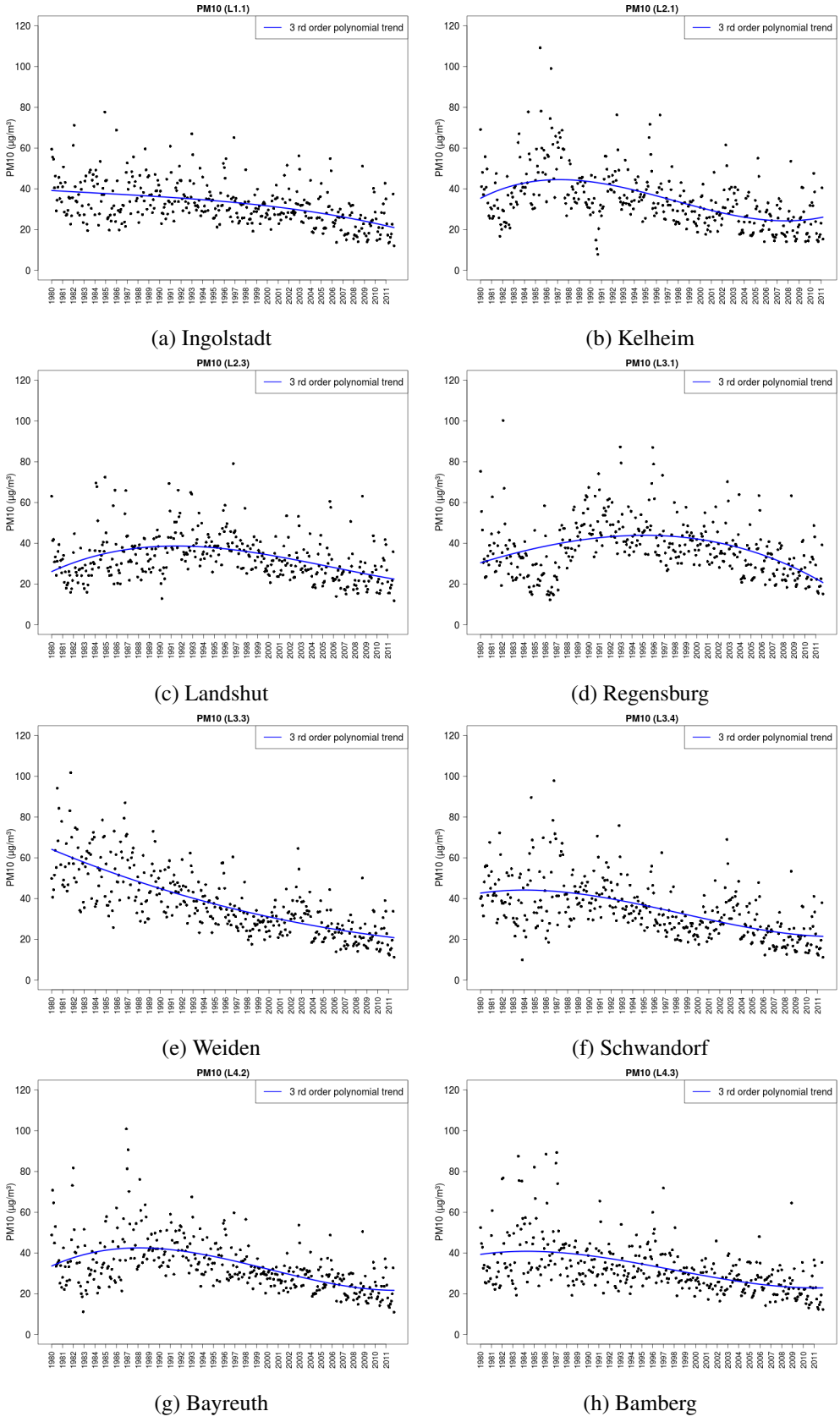


(a) Ingolstadt (b) Kelheim

(c) Landshut (d) Regensburg

(e) Weiden (f) Schwandorf

(g) Bayreuth (h) Bamberg

Figure 5.6: The long-term 3rd order polynomial trend for monthly mean $PM_{10}$ at stations Ingolstadt Rechenbergstrasse, Kelheim Regensburger-Strasse, Landshut Podewilsstrasse, Regensburg Rathaus, Weiden Nikolaistrasse, Schwandorf Wackersdorfer-Strasse, Bayreuth Rathaus, Bamberg Löwenbruecke over the period 1980-2011. Trends are significant ($\alpha = 0.05$) for all stations except Kelheim and Bayreuth.

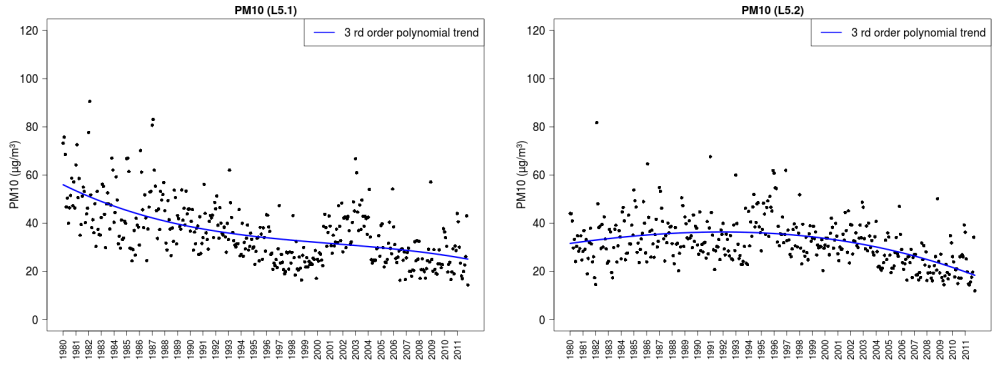


(a) NÜ Bahnhof




(b) NÜ Ziegelsteinstr.

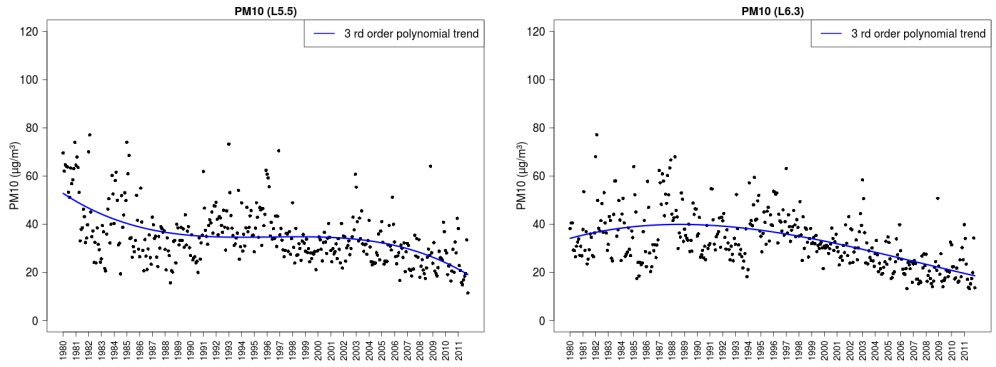


(c) Fürth




(d) Schweinfurt

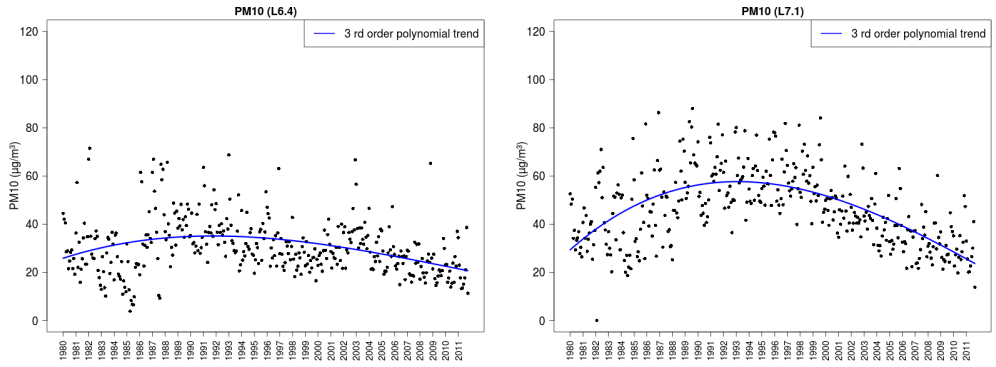


(e) Würzburg




(f) Augsburg

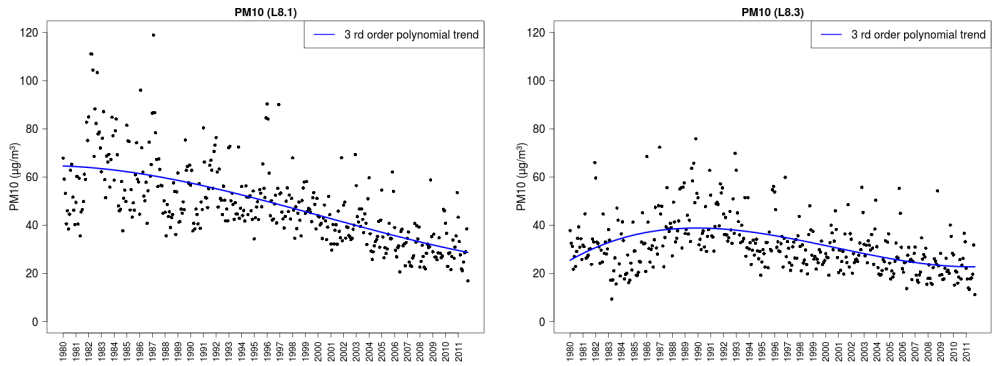


(g) MÜ Stachus




(h) MÜ Lothstr.

Figure 5.7: Same as Figure 5.6 for stations Nürnberg Bahnhof and Ziegelsteinstr., Fürth Theresienstrasse, Schweinfurt Obertor, Würzburg K.-Faulhaber-Platz, Augsburg Königsplatz, München Stachus and Lothstrasse over the period 1980-2011. Trends are significant ($\alpha = 0.05$) for all stations except Fürth, Augsburg and MÜ Lothstr.

As a further reduction of the $PM_{10}$ data basis is not necessary, time series of daily $PM_{10}$ concentrations from the 16 stations are grouped into $PM_{10}$ regions to investigate the correspondence between the sites and define Bavarian particulate matter regions. For the intended analysis, a s-mode Principal Component Analysis (PCA) is performed. The statistical principle of the PCA is introduced in Chapter 4. Main results are presented in the following.

First of all, a high-pass filter is applied on the daily $PM_{10}$ concentrations. The high-pass filter is a commonly used tool to detrend non-stationary time series (Schönwiese, 2013). By using a high-pass filter, relatively low frequencies are filtered to work out relatively high frequencies, which are more interesting for analysing $PM_{10}$ data. The implementation of the filter is based on the right decision of the number of the filtering weights $w_k$. Thus, the selection of number of weights represents a compromise between as much weights as possible, for the best filtering result, and a preferably small reduction of the time series (Schönwiese, 2013). A number of weighting factors of 7 turned out to be appropriate from several tested variants.

According for example to Schönwiese (2013), the filtering of a time series $a_i$ with the filtering weights $w_k$

$$\widetilde{a_i} = \sum_{k=-m}^{+m} w_k \cdot a_{i+k} \tag{25}$$

and $i = 1+m, ...n-m$ and $k = -m, -m+1, ..., 0, 1, ..., m$ is applied. For the filtering of the $PM_{10}$ data set, a 7-day filter is performed. The filtered time series are further used as input data for the PCA.

First, an exploratory correlation-based s-mode PCA is conducted using 2 to 10 Varimax-rotated Principal Components (PC). In general, the number of PCs should be smaller than the number of original variables. Only PCs explaining most of the variance, according to values of Explained Variance, are selected containing the maximum possible fraction of the variability of the original input data. The Explained Variance is introduced in Chapter 4. Secondly, the dominance test is used to select an appropriate number of varimax-rotated PCs as described for example by Jacobeit (1993) or Philipp et al. (2007). In general, the dominance criterion gives an estimate of the number of PCs. Furthermore, all extracted PCs are still realistic manifestations of the particle time series and not just constructed groups resulting from the algorithm. As it is introduced by Philipp et al. (2007), each PC resulting from each rotation is tested with respect to a loading dominating at least one input variable. Additionally, two conditions have to be fulfilled for an extracted PC. The loading of the PC must be greater than one standard deviation above all other loadings and the loading must be the uniquely leading one for this object. Finally, five PCs are extracted based on the dominance criterion representing 91.5 % of the Explained Variance.

Each PC is identified with one of the regions and stations are assigned to that region for whose PC they have the highest loading (Huth, 2002). In Table 5.5, an overview of the maximum rotated loadings of each station on the associated PC is given. As values in Table 5.5 show, the coefficients are generally high with values > 0.5. Relatively high correspondence appears between spatially adjacent stations.

Table 5.3: Rotated loadings of each station on the assigned Principal Component (PC) marked by numbers.

| ID | PC | maximum loading |
|---|---|---|
| Ingolstadt Rechenbergstr. | 2 | 0.65 |
| Kelheim Regensburger Str. | 2 | 0.74 |
| Landshut Podewilsstr. | 2 | 0.70 |
| Regensburg Rathaus | 2 | 0.63 |
| Weiden Nikolaistr. | 4 | 0.75 |
| Schwandorf Wackersdorfer-Str. | 4 | 0.59 |
| Bayreuth Rathaus | 4 | 0.62 |
| Bamberg Löwenbrücke | 3 | 0.63 |
| Nürnberg Bahnhof | 5 | -0.51 |
| Nürnberg Ziegelsteinstr. | 5 | -0.62 |
| Fürth Theresienstr. | 5 | -0.58 |
| Schweinfurt Obertor | 3 | 0.75 |
| Würzburg Kardinal-Faulh.-Platz | 3 | 0.77 |
| Augsburg Königsplatz | 1 | -0.77 |
| München Stachus | 1 | -0.85 |
| München Lothstr. | 1 | -0.83 |

Figure 5.8 illustrates station locations and the assignment to the 5 PCs in colours. PC 1 (orange) represents southern Bavarian urban agglomerations. Station München Lothstr. is selected as the representative station with the highest loading of -0.83. PC 2 (red) includes measurement sites in the Danube valley with station Kelheim as the representative one (loading of 0.74). Furthermore, PC 3 (green) indicates stations north-west to the Franconian Jura. Schweinfurt has the highest loading of 0.75 on PC 3. PC 4 (blue) includes cities in the north-eastern part of Bavaria with Weiden as the representative site. A loading of 0.75 is reached here. The stations of PC 5 (purple) are situated in Middle Franconian urban area with Nürnberg Ziegelsteinstr. as station with highest loading (-0.62).

In the following, further characteristics of the five regions are discussed based on monthly mean $PM_{10}$ concentrations averaged over period 1980-2011 for the representative stations in Figure 5.9. Graphs are shown for München Lothstr. (orange, PC 1), Kelheim (red, PC 2), Schweinfurt (green, PC 3), Weiden (blue, PC 4) and Nürnberg Ziegelsteinstr. (purple, PC 5). PC 1 includes three stations in a densely populated area with high traffic load and enhanced particle pollution. Highest mean particle levels are observed for this region compared to the other ones with two major peaks in autumn (October, November) and winter (January, February). Furthermore, a smaller peak is observed in summer (June, July), when local temperatures reach maximum values, which is depicted in Figure 5.9. Minimum $PM_{10}$ concentrations can be observed in August.

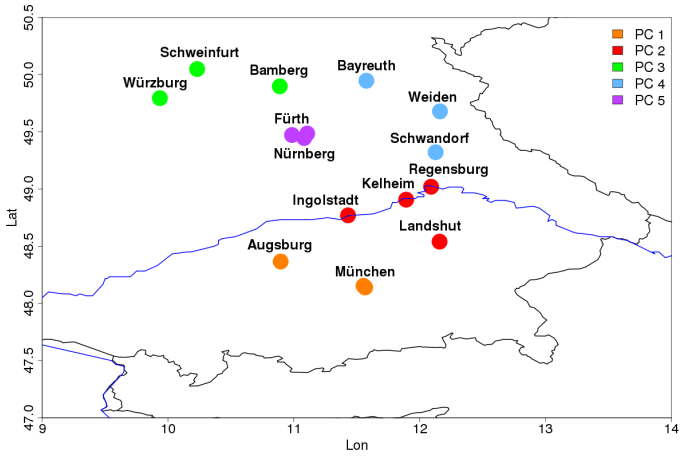


Figure 5.8: Map of $PM_{10}$ data grouped by a s-mode PCA. Different colours mark assignment of each station to one of the five Principal Components (PCs).

Lowest mean $PM_{10}$ levels over all seasons and all stations are observed at Kelheim (PC 2) and Schweinfurt (PC 3) with only one distinct peak in winter (January, February) and minimum concentrations in July. Differences between the measurement sites occur in January as particle concentrations reach higher values at station Kelheim. PC 2 and PC 3 comprise mid-size Bavarian cities with an average $PM_{10}$ load throughout the year.

As it was previously mentioned, stations of PC 4 are situated in the north-eastern part of Bavaria. The annual cycle of the representative station Weiden, illustrated in Figure 5.5 as blue graph, shows a similar particle regime as for station Nürnberg, but with a pronounced peak in winter (February, March). Compared to PC 2 and 3, the overall pollution reaches higher values. A possible explanation of enhanced $PM_{10}$ concentrations at station Weiden might be a transport of polluted air masses from eastern Europe. However, stations of PC 5 are situated in a densely populated urban area causing increased air pollution.

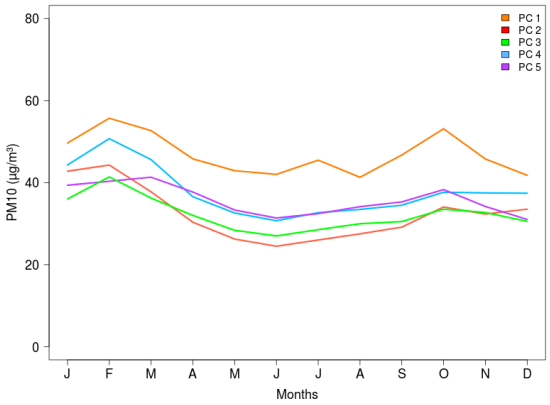


Figure 5.9: Monthly mean $PM_{10}$ averaged over the period 1980-2011 for five stations representing five PCs.

Depending on analysis presented in this thesis, the five stations are used as the representative ones for the whole data set on the one hand. Other contributions are investigated for each of the 16 stations separately, on the other hand.

# 6. Objective circulation type classifications optimized with respect to $PM_{10}$ concentrations

The large-scale atmospheric conditions over Central Europe and Germany are mainly influenced by the southern component of northern European cyclonic activities and partly from cyclonic activities in the Mediterranean region of the extra-tropical circulation. Frequent changes in weather conditions are the consequence of variations between cyclonic and anticyclonic activities, which transport air masses from diverse origin and characteristics. South-west, north-west and northern synoptic systems dominate throughout the year, but their frequency of occurrence varies with the seasons, depending on the manifestation of weather patterns with other flow directions (Liedtke and Marcinek, 1996). In the recent period 1991-2000 for example, the frequency of occurrence of zonal, cyclonic weather patterns increased in Bavaria in winter months (StMUV, 2015).

In this Chapter, those large-scale atmospheric conditions, as reflected by
Circulation Type Classifications (CTC), are identified, which are best suited to capture variations in concentrations of particulate matter with aerodynamic diameter $< 10\ \mu$m ($PM_{10}$) at Bavarian measurement sites. Thus far, only few systematic attempts have been made to modify consisting or to develop new weather and circulation type classifications in order to improve their ability to resolve local $PM_{10}$ concentrations. Similar studies, dealing with variations of existing classifications to analyse the connection between specific synoptic patterns and air quality parameters, exist for other dependent variables, e.g. surface ozone (Demuzere et al., 2010) or $NO_2$ (Valverde et al., 2015). In these studies, classification variants include for example methods, number of types, spatial domain, temporal and horizontal resolution, different input variables and classifications conditioned towards the target variable.

In accordance to Beck et al. (2014b), it is assumed that specific large-scale CTs distinctly affect different particle concentration levels. Different classifications are applied on gridded NCEP/NCAR reanalysis data set (see Section 3.2) and resulting circulation types are evaluated concerning their discriminative power for daily particle concentrations by objective evaluation measures. Based on evaluation results, a selection of classifications is conducted and the resulting CTs are applied on different statistical downscaling methods in the following analysis.

In the framework of the COST Action 733 "Harmonisation and Applications of Weather Type Classifications for European Regions" (*cost*733), introduced in Section 4.2, various statistical classification techniques for the European domain have been collected, developed and compared resulting in a *cost*733 dataset and software package. Depending on the method, the software allows modifications of the classification schemes, for example with respect to the spatial domain, large-scale

input variables in several pressure levels, temporal variations, number of types and sequencing as well as weighting of target variables. Hence, various versions of existing classification schemes can be tested and adjusted according to the target variable.

The intended optimization is based on existing classification methods from the software package. An introduction to the main basic statistical principles is given in Section 4.2, particularly for the selected approaches used in this thesis.

The explanatory power of all classifications in terms of daily $PM_{10}$ concentrations is quantified using the Explained Variance (EV) (in %), which is defined as ratio of the sum of squares of differences within classes (circulation types) and the total sum of squares (Beck and Philipp, 2010). Another skill score applied in this study is a variant of the Brier Score (BS) introduced by Brier (1950), here the Brier Skill Score for the number of days exceeding $PM_{10}$ concentrations of 50 $\mu g/m^3$ (BSS50). This metric determines a binary probability forecast for a certain threshold to be exceeded ("event") or not ("non-event") and achieves values between 0 and 1. For the intended analysis, the BSS50 has to be interpreted as it is described by Jolliffe and Stephenson (2011) with increasing values of BSS indicating a forecast benefit with respect to the climatological forecast. Both skill scores are additionally described more detailed in Section 4.4.

This Chapter starts with an overview of the used variants of weather and circulation type classifications in Section 6.1. Results from the optimization of CTC are presented in Section 6.2, which includes analysis concerning the selection of a classification method and spatial domain in Section 6.2.1. The influence of different large-scale meteorological variables and combinations of them on the target variable are discussed in Section 6.2.2. Classifications conditioned towards particulate matter data are presented in Section 6.2.3. The Chapter ends with a summary of selected classifications in Section 6.3, which are used in further analysis.

## 6.1. Variants of circulation type classifications

The concept for optimizing objective Circulation Type Classifications (CTC) to reduce the within-type variability of the weather and circulation types with respect to the particulate matter is depicted in Figure 6.1. The scheme illustrates the selected parameters starting with some basic configurations to more complex ones.

In general, Philipp et al. (2014) stated from their comprehensive study of varying classifications for different purposes that there is no statistical reason to prefer one of the classification algorithms in general. Depending on the intended application, a broader set of classification methods needs to

be compared. In Beck et al. (2014b), no distinct CTC has been found to be especially suitable for the application on local $PM_{10}$ concentrations in Bavaria. Thus, the first variations include several classification methodologies, which are explained more detailed in Section 4.2. The selected classifications are performed utilizing mean sea level pressure fields from the NCEP/NCAR reanalysis data set. A data description is given in Chapter 3.2.

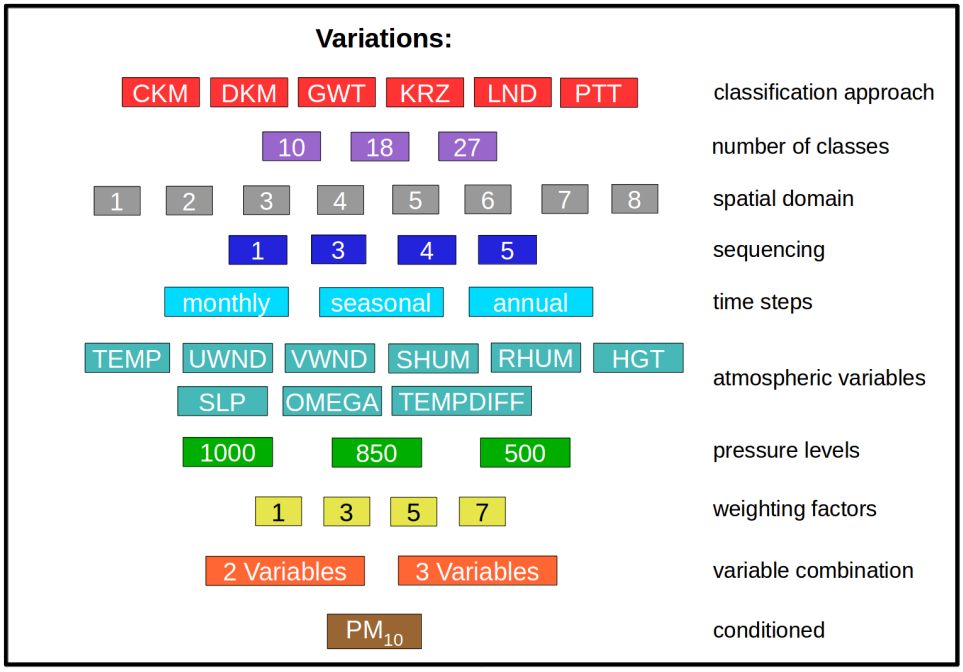


Figure 6.1: Scheme illustrating the distinct variations for optimizing circulation type classifications. Abbreviations of classification approaches are explained in detail in Chapter 4 and for large-scale atmospheric variables in Chapter 3.

Finding an optimum number of types to cover the important features of the synoptic situation are intensively discussed in several existing studies, e.g. Huth et al. (2008), Beck and Philipp (2010), Philipp et al. (2010). One crucial point concerning the selection is the sensitivity of evaluation metrics against the number of classes. Beck and Philipp (2010) for example investigate the dependence of several skill scores like the EV, Pseudo-F-Index, Within-type standard deviation, Confidence Interval of the mean or Faster Silhouette Index on the number of classes of different classifications methods. They stated the impact of number of types to be more important concerning the evaluation measures than the classification method itself.

In the present analysis, different number of classes, depending on the classification method (10, 18, 26 respectively 27 types), are tested to find an optimum number to capture important features of the synoptic situation. 10 types represent a rather small number of types. The differences between the atmospheric states can be easily conceive with a small number, but the homogeneity within

classes can be maximized with higher numbers (Huth et al., 2008). Therefore, 18 up to 26/27 classes can capture a broader range of specific events or separate individual classes in more detail. The selected number of classes for the stated purpose is also used in existing studies evaluating, for example, the performance of CTCs as a result from the COST733 Action (Demuzere et al., 2010; Beck and Philipp, 2010; Philipp et al., 2014). Initial classifications performed in this study revealed a number of 18 types to be a good compromise that allows to capture differences between the synoptic situations and an increasing homogeneity within classes (see Figure A.1).

Another variation for optimizing CTCs is the usage of eight different spatial domains. Figure 6.2 illustrates the locations of the spatial sub-samples centred over the target region Bavaria with 2.5° to 17.5° E, 45° to 55° N by 2.5° for the smallest (Number 1) and 32.5° W to 52.5 ° E, 27.5° to 72.5° N by 2.5° for the biggest (Number 8) one. The smaller domains consider mainly the atmospheric state over Central Europe. The bigger domains can even capture whole dynamical systems in the atmosphere like the North Atlantic Oscillation with interactions between the Azores high-pressure and Iceland low-pressure system.

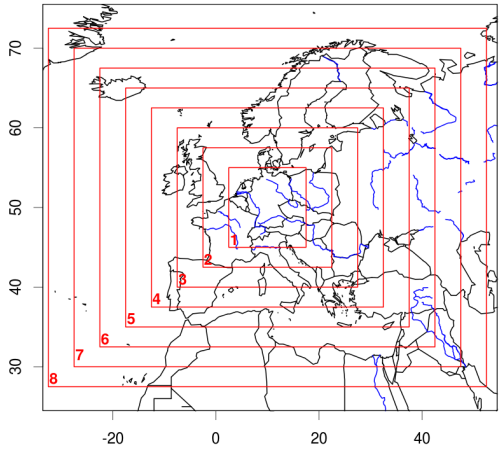


Figure 6.2: Eight domain sizes centred over the target region Bavaria.

There are several options for time-related variations depicted in Figure 6.1. One option is not to use only single-day fields of a large-scale variable, but also sequences of fields, which can be quite useful for applications dealing with parameters like air temperature. As mentioned in Philipp et al. (2014), each element is not only described by the atmospheric conditions of an actual day, here called 1-day-sequence, but also by the state of the three preceding days (3-day-sequence) or more. The data matrix structure for pattern sequence analysis is described for example in Philipp (2009): the fields of an large-scale atmospheric parameter like mean sea level pressure (SLP) of the previous days are chained to the SLP field of a key day. With this improved feature of classifications, the history of a circulation pattern is taken into account. This is of special interest, because the same circulation pattern can have different influences on a surface parameter depending on the synoptic situation that preceded it (Huth et al., 2008). Particulate matter concentrations are not implicitly categorized as persistent local parameters, but steady atmospheric conditions over several days with nearly no air mass exchange for example may have an influence on the accumulation of particles. The usage of pattern sequence

analysis comprise a broader range of possible evolution types for large-scale atmospheric conditions and therefore was tested as a variant.

Exploratory studies in context of the thesis furthermore included variations with respect to 1-, 3-, 4- and 5-day sequences using the DKM classification for domain 3 and mean sea level pressure fields. Demuzere et al. (2010) for example stated a variable behaviour of classifications of air temperature with respect to surface ozone data for 4- and 10-day sequencing. As results by Beck et al. (2014b) indicate, no specific temporal sequence-length can be stated for the CTC optimized with respect to particulate matter concentrations. These findings are in accordance to results from analysis conducted here. A comparison of values for EV for the named variants indicated a small, but not systematic increase of the evaluation metric. As a consequence, no sequencing is used in the presented analysis.

Further time-related configurations included modulations in time steps, e.g. annual, seasonal and monthly ones. Annual classifications over the whole period of 1980-2011 allow the definition of weather and circulation types, which in general have an influence on local daily mean $PM_{10}$ concentrations in Bavaria. As already mentioned in Section 5.2, there are seasonal and monthly trends of local $PM_{10}$ concentrations in the European region. Beck et al. (2014b) ascertained seasonal classifications to have the highest synoptic skill between CTs and particulate matter concentrations in Bavaria. Monthly, seasonal and annual variants of CTCs were tested in this study and the findings of Beck et al. (2014b) can be confirmed. Hence, classifications are optimized on a seasonal basis.

In a next step, varying large-scale input variables in different pressure levels (1000, 850, 500 hPa), obtained from the NCEP/NCAR reanalysis project, are classified using DKM with domain 3 and seasonal time steps. The parameters are, as described in the selection process in Section 3.2, air temperature (AIR), zonal wind component (UWND), meridional wind component (VWND), specific humidity (SHUM), relative humidity (RHUM), geopotential height (HGT), mean sea level pressure (SLP), vertical velocity (OMEGA) and temperature differences (TEMPDIFF) between 1000 hPa and 925 hPa as well as 1000 hPa and 850 hPa. Combinations of two and three variables with varying weighting factors (1,3,5,7) are classified with a standardization beforehand. For more than one input dataset, each set can be weighted relatively to the others. By including the weighting factors, it is possible to increase the importance of a specific field during the classification. Finally, the values count more or less assessing the similarity between the observations.

As a final step, the so far optimized weather type classifications are run comprising the target variable. In the presented study, the so called conditioned classifications are performed including the daily mean $PM_{10}$ concentrations with varying weighting factors ranging from 0 to 20. Several

studies deduced, CTC conditioned towards the target variable could be useful as a downscaling procedure (Demuzere et al., 2010; Huth et al., 2008). This variant is tested by using only $PM_{10}$ concentrations of 5 stations, which represent the Bavarian $PM_{10}$ regions (see Section 5.5). These are Kelheim (L2.1), Weiden (L3.3), Nürnberg Ziegelsteinstrasse (L5.2), Schweinfurt (L6.6) and München Lothstrasse (L8.3).

All resulting classifications described in this Chapter are evaluated concerning their discriminatory power for local $PM_{10}$ concentrations at the measurement sites, their synoptic skill. As it has been described previously in this Chapter, these are the Explained Variance (EV) (in %) and the Brier Skill Score for the number of days exceeding $PM_{10}$ concentrations of 50 $\mu g/m^3$ (BSS50). To assess the performance of the optimized variants of classifications, the selection of the "best" classifications has been defined as that one with the maximum value of EV and BSS compared to the others.

## 6.2. Results

In this Section the discriminatory power of the baseline configuration of classifications with respect to the surface target variable is presented. These are varying classification approaches using only mean sea level pressure as input variable for three numbers of classes and eight different domain sizes. Additionally, 1- to 5-day sequencing has been tested. After selecting a method, a domain size and the number of types, the dependence of synoptic skill on further optimization steps is investigated. A brief discussion on differences between the used evaluation metrics is also presented.

### 6.2.1. Spatial domain

Existing studies, for example by Stefan et al. (2010) or Demuzere et al. (2010), have stated the domain size to play an important role for deriving weather and circulation types. Beck et al. (2013) concluded that differences in the discriminatory power of CTC due to varying spatial domain sizes reach similar magnitude than those related to distinct classification approaches.

Varying classification methods, e.g. k-means cluster-analysis-based ones (CKM, DKM), Großwettertype (GWT), Kruizinga- (KRZ) , Lund- (LND) and a Principal-Component-based classification (PTT), are applied on mean sea level pressure fields for eight spatial domains. Resulting values of Explained Variance (EV) (in %) from these steps are shown as Box-Whisker-Plots in Figure 6.3 for daily mean $PM_{10}$ concentrations, integrated over 18 CTs in winter (DJF) from 1980 - 2011 at 16 stations. Upper/lower whiskers indicate the 1.5 interquartile range (IQR) from the upper/lower quartile, the box covers the interquartile range, defined as the central 50 % of the data, and the

black line within the box marks the median. Box-Whisker-Plots are useful exploratory methods for showing the range of the data from maximum to minimum values as well as for examining the skewness and spread (Wollschläger, 2012; Jolliffe and Stephenson, 2011).

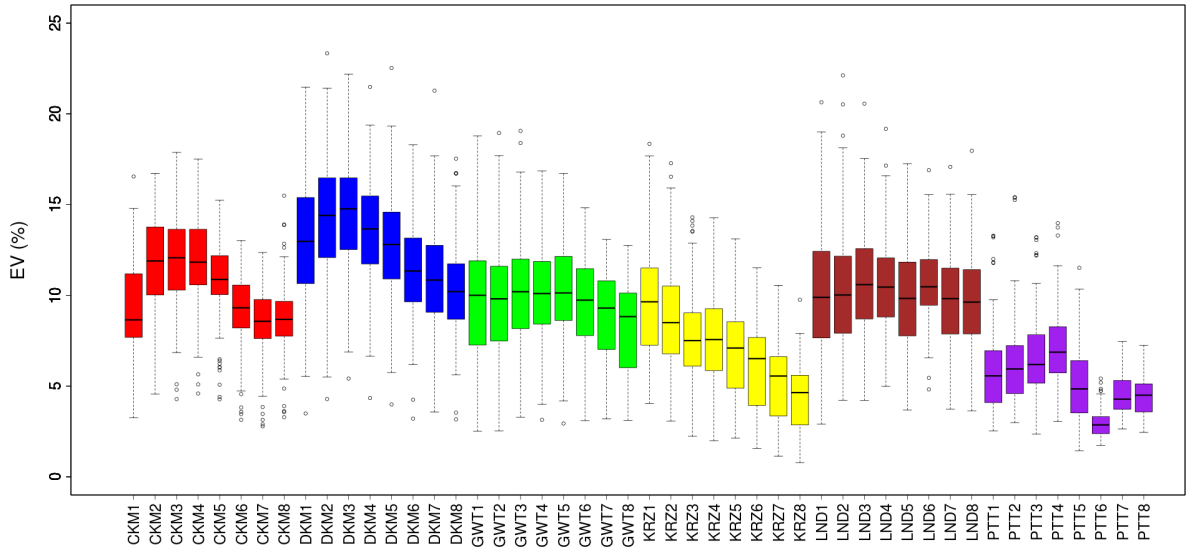


Figure 6.3: Box-Whisker-Plots show the values of Explained Variance (EV) (in %) for daily mean $PM_{10}$ concentrations at the 16 selected stations in winter 1980 - 2011 using varying classification methods of mean sea level pressure fields for eight domains sizes marked by numbers (see text for further explanation). Abbreviations of classification methods and number of domain sizes are given along the *x*-axis. Upper/lower whiskers indicate the 1.5 interquartile range from the upper/lower quartile.

In general, the values of EV for all approaches and domain sizes reach values up to 24 % maximum. By comparison, highest values of EV appear for cluster-analysis-based classification DKM for a mid-size domain (number 3) ranging from 7.5° - 27.5° E and 40° - 60° N. Especially cluster-analysis-based classifications (CKM, DKM) tend to capture variations of particle concentrations better than other methods. These findings are comparable to other studies investigating the effect of domain sizes applied on CTC targeting on variables of European measurement sites. Beck et al. (2013), who have used temperature measures and precipitation as target variable, or Demuzere et al. (2010) for surface ozone, found small to mid-size domains to be best suited for classifications using optimization algorithms. Values of EV decrease independently from the classification method with a larger spatial domain, except the LND classification. As it is also concluded by Demuzere et al. (2010), a sensitivity of the used algorithm with respect to the spatial domain can be stated.

In order to obtain the characteristics of the atmospheric circulation having an influence on local

$PM_{10}$ concentrations, mean sea level pressure composites of 18 types resulting from both GWT and DKM classification are shown in Figure 6.5 and 6.6. Daily mean sea level pressure fields for the period of 1980-2011 are classified using the Großwetter-Type or prototype classification for the spatial domain 7.5° - 27.5° E and 40° - 60° N. Therefore, gridded NCEP/NCAR reanalysis data are used.

Bar charts of occurrence frequencies of the 18 types during the period of 1980-2011 are shown in Figure 6.4 (a) as well as daily mean $PM_{10}$ concentrations at station Augsburg Königsplatz (L7.1) for each type (b). Bar charts are a useful way to analyse and compare the distribution of variables revealing the frequency of occurrence of each category. As it is described by Jolliffe and Stephenson (2011), the mode of a bar chart is the value occurring most frequently.

Results from the classification performed with GWT revealed type 9 to be the most frequent pattern over Bavaria, a western anticyclonic circulation with daily mean $PM_{10}$ concentrations around 50 $\mu gm^3$. The south-east cyclonic situation (type 7) has the highest pollution level with daily mean $PM_{10}$ concentrations around 70 $\mu gm^3$. Similar particulate matter concentrations appear for the southern cyclonic and anticyclonic types (8 and 16) and for the central high pressure pattern (18) with around 63 up to 69 $\mu gm^3$.

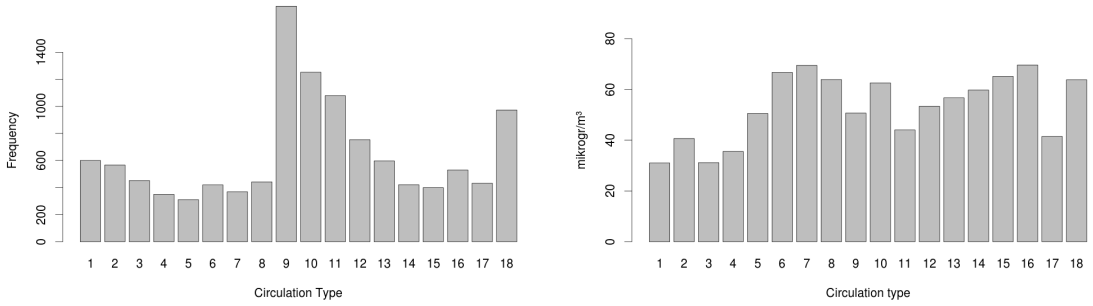


(a) Occurrence frequencies (b) Daily mean $PM_{10}$

Figure 6.4: Barplots indicating occurrence frequencies of 18 circulation types classified with Großwetter-Type or prototype classification (GWT) given in Figure 6.5 (a) and daily mean $PM_{10}$ concentrations ($\mu gm^3$) of each type at station Augsburg Königsplatz (b) for the period 1980-2011.

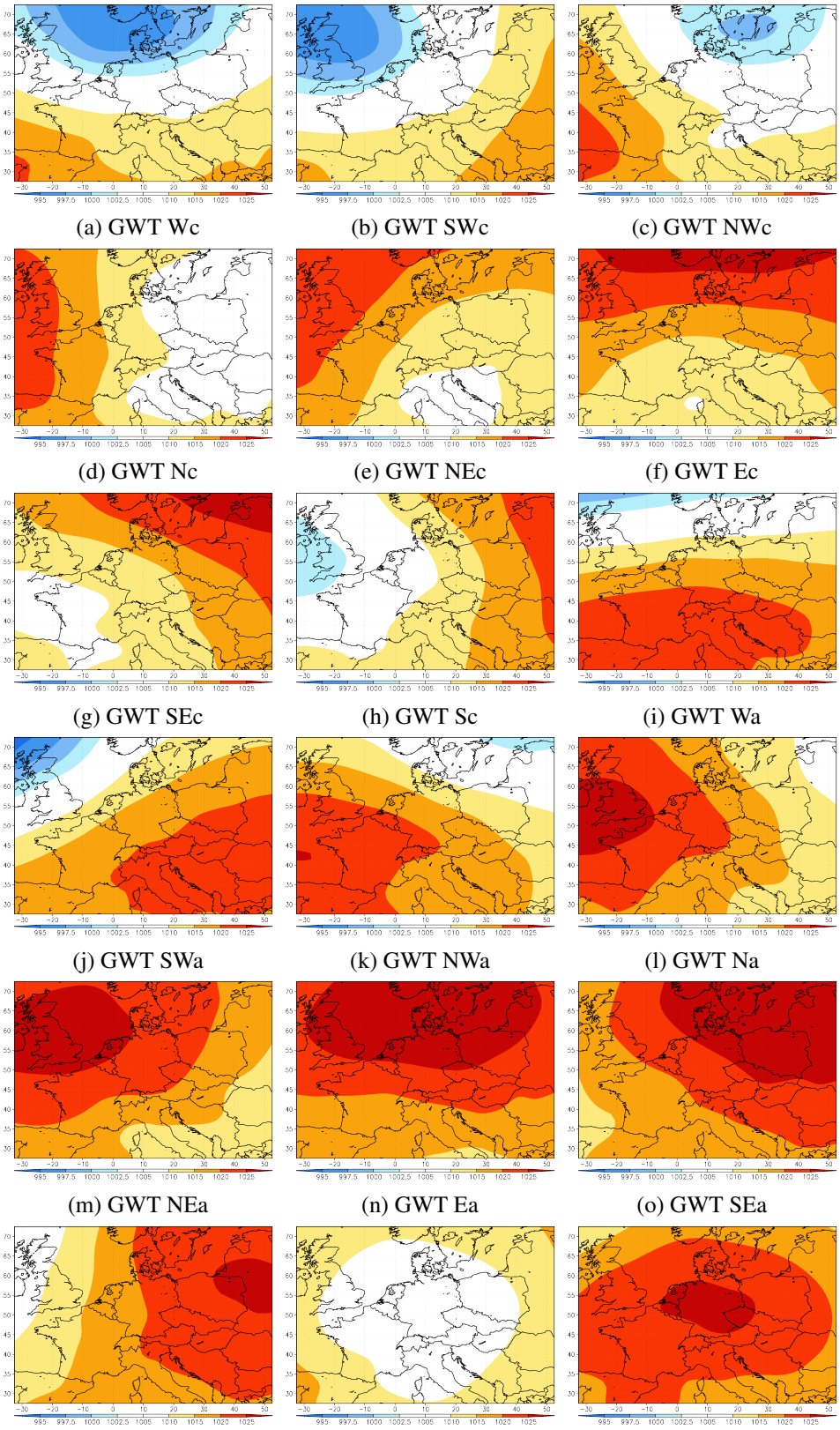

(a) GWT Wc (b) GWT SWc (c) GWT NWc

(d) GWT Nc (e) GWT NEc (f) GWT Ec

(g) GWT SEc (h) GWT Sc (i) GWT Wa

(j) GWT SWa (k) GWT NWa (l) GWT Na

(m) GWT NEa (n) GWT Ea (o) GWT SEa

(p) GWT Sa (q) GWT L (r) GWT H

Figure 6.5: Mean sea level pressure (hPa) composites for 18 circulation types resulting from the GWT classification applied to daily SLP (1980-2011) for the spatial domain 7.5°-27.5° E and 40°-60° N. The patterns are named by their large-scale flow characterization (N = North, W = West, E = east, S = south, c = cyclonic, a = anticyclonic, L = central low pressure, H = central high pressure). Composites are shown for illustrative region 32.5° W-52.5° E and 27.5°-72.5° N.

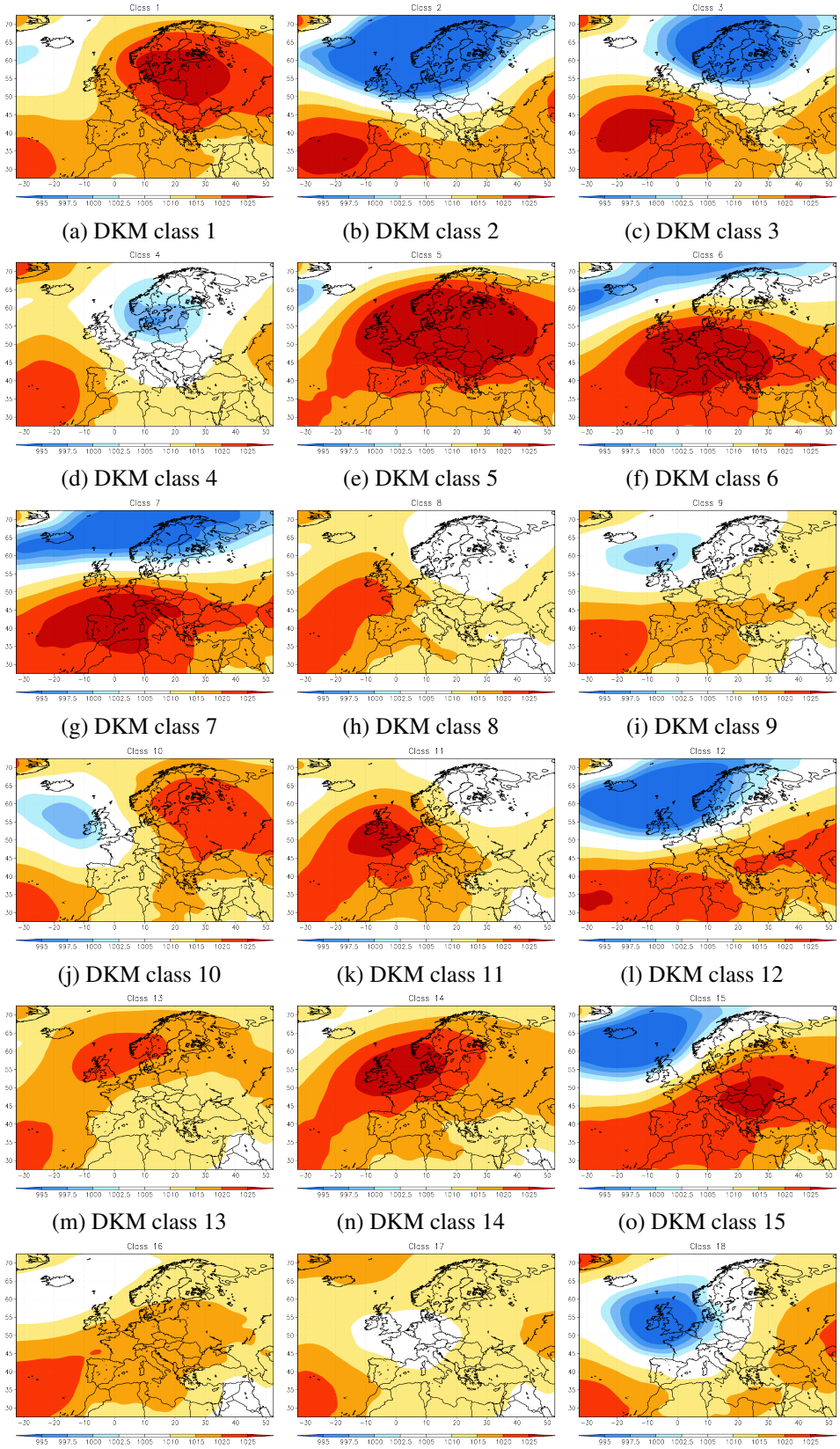

(a) DKM class 1 (b) DKM class 2 (c) DKM class 3

(d) DKM class 4 (e) DKM class 5 (f) DKM class 6

(g) DKM class 7 (h) DKM class 8 (i) DKM class 9

(j) DKM class 10 (k) DKM class 11 (l) DKM class 12

(m) DKM class 13 (n) DKM class 14 (o) DKM class 15

(p) DKM class 16 (q) DKM class 17 (r) DKM class 18

Figure 6.6: Mean sea level pressure (hPa) composites for 18 circulation types resulting from the DKM classification applied to daily SLP fields (1980-2011) for the spatial domain 7.5°-27.5° E and 40°-60° N. Composites are shown for illustrative region 32.5°-52.5° E and 27.5°-72.5° N.

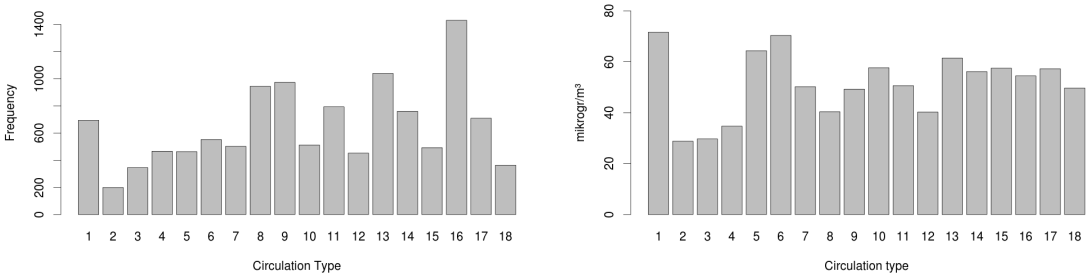


(a) Occurrence frequencies

(b) Daily mean $PM_{10}$

Figure 6.7: Barplots indicating occurrence frequencies of 18 circulation types classified with K-means cluster analysis with most differing start partitions (DKM) given in Figure 6.6 (a) and daily mean $PM_{10}$ concentrations ($\mu gm^3$) of each type at station Augsburg Königsplatz (b) for the period 1980-2011.

Figure 6.6 illustrates mean sea level pressure composites (in hPa) of 18 circulation types over Bavaria classified with DKM using gridded daily NCEP/NCAR reanalysis data for the period of 1980-2011. In addition, bar charts of occurrence frequencies of the classes are indicated in Figure 6.7 (a) as well as mean $PM_{10}$ concentrations ($\mu gm^3$) at station Augsburg Königsplatz (L7.1) for 18 CTs in (b). In accordance to the types resulting from GWT classification, the frequent type 16 is as well a south-west flow. Mean $PM_{10}$ concentrations resulting here are around 54 $\mu gm^3$. The highest pollution levels are connected to type 1 (approx. 71.6 $\mu gm^3$), a south-east pattern, type 6 representing a central high pressure field (approx. 70 $\mu gm^3$) and type 15 as a south-west situation with 57.5 $\mu gm^3$.

Additionally, the composites of both classifications elucidate the main features of the statistical algorithm behind. The GWT approach enables an easy interpretation of the patterns as they are previously defined by thresholds. Figure 6.5 illustrates these predefined patterns, which are categorized by their large-scale flow characterization (N = North, W = West, E = east, S = south, c = cyclonic, a = anticyclonic, L = central low pressure, H = central high pressure). DKM, in contrast, enables a more precise characterization of synoptic situations having an influence on the target variable. Some composites of DKM show similar synoptic situations with small modifications, e.g. Class 13 and 14 or Class 2 and 12).

### 6.2.2. Classified input variables

The DKM algorithm enables classifications including additional input variables and combinations of them, which are assumed to have a distinct effect on particulate matter as stated in Chapter 3.2. A comprehensive selection of daily gridded large-scale atmospheric variables in three pressure levels from the NCEP/NCAR reanalysis project is chosen for exploratory analysis on their effect

on particulate matter concentrations on a local scale. These are air temperature (AIR) (in Kelvin), zonal wind component (UWND) and meridional wind component (VWND) (in m $s^{-1}$), vertical velocity (OMEGA) (in Pa $s^{-1}$), relative humidity (RHUM) (in %), specific humidity (SHUM) (in g $kg^{-1}$) and geopotential height (HGT) (in gpm) in 1000, 850 and 500 hPa levels. Furthermore, mean sea level pressure (SLP) (in hPa) is included. As a proxy for the mixing layer height, temperature differences between 1000 and 925 hPa as well as 1000 hPa and 850 hPa (TEMPDIFF925, TEMPDIFF850) are calculated.

In order to reduce the number of input variables, classifications with DKM, three numbers of classes and eight domain sizes using only one of the named atmospheric input parameters are run. They are evaluated in terms of their explanatory power for daily $PM_{10}$ concentrations at the 16 Bavarian stations using the Explained Variance (EV) as an evaluation metric.

In this preliminary study, SLP, AIR in 1000 hPa, geopotential in 1000 and 500 hPa, RHUM in 1000 and 850 hPa, UWND in 1000 and 500 hPa, VWND in 500 hPa and OMEGA in 1000 and 850 hPa yield out to have the highest values for EV at all stations and all seasons. Possible effects of these parameters on transportation, deposition or formation of local particulate matter concentrations are briefly discussed in the following.

AIR in 1000 hPa is known to be a relevant factor for the formation of secondary particles, which is the case near the surface. The wind components are responsible for transportation of particles. On a synoptic scale, especially in higher pressure levels, the long-distance transport of particles plays a major role (Seinfeld and Pandis, 2012). SLP, HGT and OMEGA fields represent the general circulation over a target region indicating the transport of air masses. The humidity parameters, as reflected by relative and specific humidity, act as measures for particle growing processes and deposition. Relative humidity in 850 hPa for example represents the level of clouds of medium height. The other atmospheric parameters analysed in this step showed on the one hand comparably small values for EV in general and on the other hand high variations with respect to stations and seasons. The mixing layer height for example is relevant in winter months on a large-scale, but not in other seasons. This is in accordance with findings for example by Schäfer et al. (2006), who resumed the influence of this variable to be high in winter time on a local scale.

Based on the pre-selection of variables, further classifications are performed using combinations of two up to three parameters including different weighting factors (1,3,5,7) for 18 types and spatial domain 3. In case of classifications of multiple variables, they are standardized in the classification process. As results from the study by Beck et al. (2014b) revealed, most distinct connections between CTs and $PM_{10}$ occur especially in winter (DJF). Furthermore, seasonal classifications

showed best performance compared to annual and monthly classifications. Hence, seasonal classifications with varying input variables are utilize in the presented analysis.

Table 6.1 illustrates values for EV for daily mean $PM_{10}$ in winter (a) and summer (b) for the period 1980-2011 at 16 measurement sites for best performing optimized seasonal classifications (best CTC). The classifications are characterized by their input variable combination (parameter:level:weight). In comparison to classifications performed with SLP using GWT, reaching maximum values of around 24 % for EV (see Section 6.2.1), optimized CTC in winter achieve around 30 % and in summer similar by depending on the specific measurement site. Classifications including large-scale fields of air temperature in 1000 hPa, relative humidity in 1000 and 850 hPa as well as zonal wind in 500 hPa turned out to have the highest influence on local $PM_{10}$ concentrations at nearly all stations in winter.

The combination of input variables, pressure levels and weighting factors vary more in the other seasons. In summer, the combination of air temperature in 1000 hPa and weight 7, geopotential in 500 hPa (factor 5) as well as relative humidity in 1000 hPa (factor 5) dominates over all stations with reaching highest values of EV up to 33 %. This is illustrated in Table 6.1 (b). In contrast, the skill of the second best classification decreases in summer remarkably from around 28.6 % to 19.4 % at station Kelheim for example, which it is not shown here.

Table 6.1: Weighted variable combinations, combined as parameter:level:weight, with corresponding values of Explained Variance (EV) (in %) for daily mean $PM_{10}$ in winter (a) and summer (b) 1980-2011 at each of the 16 stations for best optimized CTC performed with DKM and 18 types.

| Station | (a) winter (DJF) | | (b) summer (JJA) | |
|---|---|---|---|---|
| | | EV (%) | | EV (%) |
| Ingolstadt Rechenbergstr. | air:1000:3_rhum:850:5_uwnd:500:7 | 26.4 | air:1000:7_hgt:500:5_rhum:1000:5 | 30.5 |
| Kelheim Regensburger-Str. | air:1000:7_rhum:1000:3_omega:850:7 | 20.9 | air:1000:7_hgt:500:5_rhum:1000:5 | 28.6 |
| Landshut Podewilsstr. | air:1000:3_rhum:850:5_uwnd:500:7 | 21.6 | air:1000:7_hgt:500:5_rhum:1000:5 | 24.6 |
| Regensburg Rathaus | air:1000:3_rhum:850:5_uwnd:500:7 | 24.5 | air:1000:7_hgt:500:5_rhum:1000:5 | 34.8 |
| Weiden Nikolaistr. | air:1000:7_rhum:1000:3_uwnd:500:3 | 23.2 | air:1000:7_hgt:500:5_rhum:1000:5 | 30.2 |
| Schwandorf Wackersdorfer-Str. | hgt:1000:7_rhum:1000:5_uwnd:500:3 | 22.5 | air:1000:7_hgt:500:5_rhum:1000:5 | 26.8 |
| Bayreuth Rathaus | air:1000:7_rhum:1000:3_uwnd:500:3 | 25.4 | air:1000:7_hgt:500:5_rhum:1000:5 | 30.7 |
| Bamberg Löwenbrücke | air:1000:7_rhum:1000:5_uwnd:500:3 | 26.5 | air:1000:7_hgt:500:5_rhum:1000:5 | 29.8 |
| Nürnberg Bahnhof | air:1000:7_rhum:1000:3_uwnd:500:3 | 24.3 | air:1000:7_hgt:500:5_rhum:1000:5 | 23.4 |
| Nürnberg Ziegelsteinstr. | shum:1000:3_uwnd:500:3_omega:850:5 | 27.8 | air:1000:7_hgt:500:5_rhum:1000:5 | 33.5 |
| Fürth Theresienstr. | air:1000:7_rhum:1000:3_uwnd:500:3 | 27.1 | air:1000:7_hgt:500:5_rhum:1000:5 | 27.1 |
| Schweinfurt Obertor | air:1000:3_shum:1000:7_uwnd:500:7 | 21.5 | air:1000:7_hgt:500:5_rhum:1000:5 | 33.3 |
| Würzburg Kardinal-Faulhaber-Pl. | shum:1000:3_rhum:850:5_uwnd:500:7 | 29.5 | air:1000:7_hgt:500:5_rhum:1000:5 | 31.0 |
| Augsburg Königsplatz | shum:1000:5_rhum:850:7_uwnd:500:5 | 27.4 | air:1000:7_hgt:500:5_rhum:1000:5 | 32.0 |
| München Stachus | air:1000:7_rhum:1000:5_uwnd:500:3 | 21.7 | air:1000:7_hgt:500:5_rhum:1000:5 | 32.6 |
| München Lothstr. | shum:1000:3_rhum:850:5_uwnd:500:7 | 30.3 | air:1000:7_hgt:500:5_rhum:1000:5 | 28.1 |

In accordance to Table 6.1, results of BSS50 for the best performing CTC in winter (a) and summer (b) at each of the 16 stations are presented in Table 6.2. As it is shown here, results for winter

are comparably high in contrast to summer. A possible reason might be a higher occurrence frequency of number of days exceeding a daily $PM_{10}$ value $> 50\ \mu g/m^3$ in the cold season. Due to high emissions of particles in the heating season combined with a distinct influence of large-scale atmospheric high pressure fields with nearly no air mass exchange in winter months, the critical air pollution concentration is reached faster. Independently from station and season, resulting best performing classifications, depicted in Table 6.2, vary stronger with respect to classified input variables compared to those selected by maximum skill of EV. Mostly, air temperature, geopotential height, humidity measures as well as zonal wind are used.

The skill of classifications in other seasons reach lower values compared to winter for both evaluation metrics, especially when looking at the synoptic skill measured by BSS50. In spring the maximum value of EV is 27 % and in autumn around 26 %, for the BSS50 0.17 and 0.15.

As the evaluation results revealed, the dominating input variables having an influence on local particulate matter data are AIR in 1000 hPa, RHUM in 1000 and 850 hPa, SHUM in 1000 hPa as well as UWND in 500 hPa through all seasons and all stations. These parameters seem to have an important influence on particle formation, transportation and deposition throughout the year. In the transitional seasons, no dominating variable combination can be stated for autumn, but AIR in 1000 hPa, RHUM in 850 hPa and UWND in 500 hPa appear quite often in spring.

Table 6.2: Weighted variable combinations, combined as parameter:level:weight, with corresponding values of Brier Skill Score for the number of days exceeding $PM_{10}$ concentrations of $50\ \mu g/m^3$ (BSS50) for daily mean $PM_{10}$ in winter (a) and summer (b) 1980-2011 at each of the 16 stations for best optimized Circulation Type Classifications (CTC) performed with DKM and 18 types.

| Station | (a) winter (DJF) | | (b) summer (JJA) | |
|---|---|---|---|---|
| | | BSS50 | | BSS50 |
| Ingolstadt | hgt:500:1_shum:1000:7_rhum:850:3 | 0.18 | hgt:500:5_shum:1000:1_uwnd:500:3 | 0.08 |
| Kelheim | hgt:500:1_shum:1000:7_rhum:850:3 | 0.15 | hgt:500:5_shum:1000:1_uwnd:500:3 | 0.04 |
| Landshut | air:1000:3_rhum:850:5_uwnd:500:7 | 0.14 | rhum:1000:5_uwnd:1000:7_omega:1000:1 | 0.06 |
| Regensburg | air:1000:3_rhum:850:5_uwnd:500:7 | 0.20 | air:1000:7_hgt:500:5_rhum:1000:5 | 0.18 |
| Weiden | air:1000:5_rhum:1000:1_uwnd:1000:1 | 0.20 | air:1000:7_hgt:500:5_rhum:1000:5 | 0.13 |
| Schwandorf | air:1000:1_hgt:500:7_omega:1000:7 | 0.17 | shum:1000:3_rhum:1000:3_uwnd:500:7 | 0.07 |
| Bayreuth | shum:1000:3_uwnd:500:1_omega:1000:1 | 0.17 | air:1000:5_rhum:1000:1_omega:1000:7 | 0,10 |
| Bamberg | air:1000:7_rhum:1000:1_omega:1000:7 | 0.20 | rhum:1000:1_uwnd:500:3_omega:850:7 | 0.14 |
| Nürnberg B. | air:1000:5_hgt:500:7_rhum:1000:1 | 0.18 | shum:1000:7_rhum:850:5_omega:850:7 | 0.10 |
| Nürnberg Z. | air:1000:7_hgt:1000:1_rhum:1000:1 | 0.16 | shum:1000:1_rhum:1000:3_uwnd:1000:1 | 0.09 |
| Fürth | air:1000:7_rhum:1000:1_omega:1000:3 | 0.17 | air:1000:7_hgt:500:5_rhum:1000:5 | 0.09 |
| Schweinfurt | air:1000:5_hgt:1000:7_rhum:1000:1 | 0.15 | air:1000:7_hgt:500:5_rhum:1000:5 | 0.11 |
| Würzburg | shum:1000:3_rhum:850:5_uwnd:500:7 | 0.2 | hgt:500:5_shum:1000:3_rhum:850:5 | 0.11 |
| Augsburg | hgt:500:1_rhum:850:1_uwnd:1000:7 | 0.21 | air:1000:7_hgt:500:5_rhum:1000:5 | 0.22 |
| München S. | shum:1000:1_rhum:1000:5_uwnd:500:3 | 0.2 | air:1000:7_hgt:500:5_rhum:1000:5 | 0.2 |
| München L. | air:1000:5_rhum:850:3_uwnd:500:3 | 0.2 | air:1000:5_hgt:1000:5_uwnd:500:1 | 0.04 |

### 6.2.3. Circulation types conditioned towards $PM_{10}$

Recent studies have shown that the integration of the target variable into classifications could be a benefit with respect to the usage as a downscaling tool (Huth et al., 2008; Schiemann and Frei, 2010; Demuzere et al., 2010). The weighting property included in the *cost*733 software enables an increasing importance of a specific field during the classification procedure. A weighting factor of 1 for $PM_{10}$ means the variables as an equal importance compared to the other classified parameters. A weight of 3, for example, triples the importance (Demuzere et al., 2010).

In the present analysis, best performing optimized seasonal classifications, according to values of EV, are selected for 5 representative stations with the highest loading on one of the five Bavarian $PM_{10}$ regions (see Section 5.5). These stations are Kelheim (L2.1) representing region 2, Weiden (L3.3) for region 4, Nürnberg Ziegelsteinstraße (L5.2) as the representative for region 5, Schweinfurt (L6.3) for region 3 and München Lothstraße (L8.3) for region 1. Table 6.3 illustrates the assignment of the 16 stations to one of the $PM_{10}$ regions. As it has been previously described in Section 5.5, nearby stations are grouped into regions of three stations except PC 2, which represents 4 stations.

The classifications, which include combinations of three variables with specific weighting factors, are run again including the target variable. Daily mean $PM_{10}$ concentrations are only available as point measurements, but the *cost*733*class* software enables classifications using both gridded and non-gridded data (Philipp et al., 2014). Resulting conditioned classifications are evaluated in three calibration and validation periods and best classifications are selected by maximum value of EV in one of the three validation periods. Finally, conditioned classifications are chosen for each of the five stations and each season.

Table 6.3: Assignment of 16 measurement sites to one of the five $PM_{10}$ regions.

| Station | Region |
|---|---|
| Ingolstadt | 2 |
| Kelheim | 2 |
| Landshut | 2 |
| Regensburg | 2 |
| Weiden | 4 |
| Schwandorf | 4 |
| Bayreuth | 4 |
| Bamberg | 3 |
| Nürnberg B. | 5 |
| Nürnberg Z. | 5 |
| Fürth | 5 |
| Schweinfurt | 3 |
| Würzburg | 3 |
| Augsburg | 1 |
| München S. | 1 |
| München L. | 1 |

In order to increase the importance of $PM_{10}$, weighting factors from 0 - 20 are tested. One has to keep in mind that an increasing magnitude of the weighting factor of a variable contains the risk of an overfit. Results for Explained Variance using conditioned classifications towards $PM_{10}$ with weighting factors up to 20, which are not shown here, showed values $> 90\%$ for EV. In accordance to studies conducted by Demuzere et al. (2010), who developed conditioned classifications towards surface ozone, factors $< 10$ are selected for the target variable. Another strategy to test the performance of classifications is to classify the conditioned variants in the 20-year calibration period and to assign the resulting CTs in the 11-year validation period.

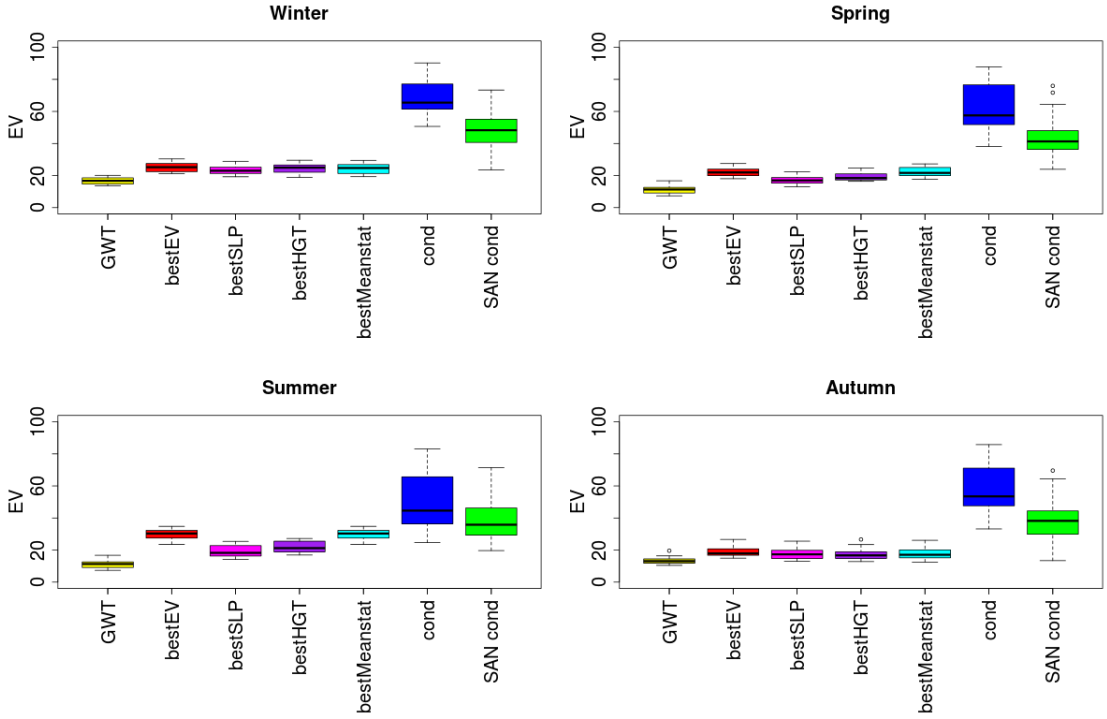


Figure 6.8: Box-Whisker-Plots of EV (in %) for daily $PM_{10}$ averaged over 16 stations for seasonal classifications with GWT, best performing optimized classification for each station (bestEV) and including mean sea level pressure (bestSLP) as well as geopotential (besthgt) as one classified input variable of a combination of three, best performing classifications averaged over all stations for each season (bestmeanstat), conditioned classifications using DKM (cond) and SANDRA (SAN cond).

A final optimization step of the resulting sample of conditioned classifications is to reclassify them with the Simulated annealing and diversified randomization (SANDRA) algorithm. This classification scheme, which is introduced in Section 4.2, uses a diversified random algorithm with heuristic simulated annealing algorithm to approximate a single global optimum with the possibility of a temporary *wrong* re-assignment. The latter enables a removal of objects from their nearest cluster for a further optimization (Philipp et al., 2014).

The overall increase of EV using conditioned classifications is depicted in Figure 6.8 by Box-Whisker-Plots. Results of EV are averaged for 16 stations for a comprehensive set of seasonal classifications. GWT is included as an example of a barely optimized classification for comparison. Best performing optimized classification for each station (bestEV) and classifications including mean sea level pressure (bestSLP) and geopotential height (besthgt) as one of three input variables, best performing classification averaged over all stations for each season (bestmeanstat), conditioned classifications using DKM (cond) and SANDRA (SAN cond) are utilize.

Comparing the evaluation results presented in Figure 6.8, highest skill appear for the conditioned classifications. As the median of the boxplots, marked with a black line, indicate, results for the optimized unconditioned classifications (bestEV, bestHGT, best SLP, bestmeanstat) are similar in each season except summer, where skills vary stronger. Differences in skill also appear between stations, especially at the basis of conditioned classifications.

## 6.3. Summary

In this Chapter, a stepwise optimization of objective Circulation Type Classifications (CTC) with respect to the target variable $PM_{10}$ at 16 urban measurement sites in Bavaria has been conducted. A characterization of those synoptic situations, which have a distinct influence on local particle concentrations, has been outlined. A representative classification approach, a k-means cluster-analysis-based method (DKM), has been mainly used to implement the optimization steps. Several skill scores, namely the Explained Variance (EV) and BSS50, have been applied as objective evaluation measures to quantify the influences of the generated classifications on daily mean $PM_{10}$ concentrations.

The initial variations included varying spatial and temporal settings as well as modified numbers of classes. A mid size domain (7.5° - 27.5° E, 40° - 60° N), 18 number of circulation types and seasonal classifications turned out to have the highest skill.

Taking into account the outcome of the first steps, further attempts towards the optimization of CTC have been made. The analysis have included seasonal time steps, varying meteorological input parameters on several pressure levels (1000, 850 and 500 hPa) and combinations of two to three of these variables with different weighting factors (1,3,5,7). All classification variants have been evaluated again. Finally, the best and second best performing classification, according to maximum values of the used evaluation measures EV and Brier Skill Score for the number of days exceeding $PM_{10}$ concentrations of 50 $\mu g/m^3$ (BSS50), have been selected for each station and

season. Additionally, the best performing classification using mean sea level pressure as well as geopotential as one input variable have been chosen for each station and season.

In general, the systematic optimization of objective CTCs has helped to further characterize those synoptic situations over Central Europe, which have a distinct effect on local $PM_{10}$ concentrations in Bavaria. The following large-scale atmospheric variables have been detected to have an influence over all seasons and stations, as they occur mostly in the best performing classifications independently from the seasons: air temperature in 1000 hPa, relative humidity in 1000 and 850 hPa, mean sea level pressure, geopotential height in 500 hPa, specific humidity in 1000 hPa as well as vertical velocity in 1000 hPa. Air temperature near the surface can foster the formation of secondary particles, which is especially relevant in summer. In winter, low temperatures may indicate continental cold air masses from eastern Europe, which are mainly connected to stable high pressure conditions over Central Europe and nearly no air mass exchange. Humidity measures represent those synoptic situations having an influence on the wet deposition of particles. The wind components and vertical velocity mark transportation processes of small particles on different scales as well as atmospheric turbulences and mixing conditions. Geopotential height and mean sea level pressure fields characterize the high and low pressure patterns over the target region.

Finally, the best performing optimized classification, according to EV, has been classified again using seasonal time series of daily target variable of five representative measurement sites as fourth input data. The $PM_{10}$ data have been added into the conditioned classifications with varying weighting factors (0 - 10). This optimization step has lead to a distinct increase of the skill of the classifications. As the DKM classification method is by design a potentially unstable approach, the conditioned classifications have been run again with the SANDRA algorithm, which is based on a heuristic algorithm, here the simulated annealing.

A few general characteristics of the synoptic situations having an influence on daily $PM_{10}$ concentrations have been found. South-east patterns and central high pressure fields have turned out to dominate high pollution events in Bavaria. Air temperature in 1000 hPa, relative humidity in 1000 and 850 hPa as well as zonal wind in 500 hPa appeared mostly in the selected optimized classification variants. Maximum values of EV have reached 30 % in winter and up to 33 % in summer at single stations. Averaged over all stations and classifications variants, the influence of seasonal synoptic weather types dominates in winter. In the other seasons, the connections are quite variable and reach comparatively low skill.

From this first contribution of the thesis, a comprehensive set of classifications for each station and season has been selected for the assessment in further analysis:

- classifications using only SLP as input variable classified with GWT and DKM for comparison;
- optimized CTC reaching highest and second highest values of the selected skill scores EV and BSS50;
- optimized classification for each season reaching highest averaged values of EV at all stations;
- optimized CTC reaching highest values of EV with SLP and HGT as one of three input variables;
- optimized conditioned classifications towards 5 representative stations classified with DKM and SANDRA.

Daily and monthly occurrence frequencies of the selected weather types are used in the next Chapter 7 as influencing variables (predictors) in several statistical downscaling models to estimate daily and monthly $PM_{10}$ indices.

# 7. Relating large-scale atmospheric circulation to local $PM_{10}$ indices using statistical downscaling models

A general relationship between the synoptic conditions, derived from optimized Circulation Type Classifications (CTC), and local $PM_{10}$ concentrations at 16 measurement sites in Bavaria has been determined in Chapter 6. In order to model local $PM_{10}$ concentrations based on the large-scale atmospheric conditions, characterized in the previous analysis for a recent period 1980-2011, it is necessary to bridge the gap between the spatial scales. For this purpose, statistical downscaling approaches are useful instruments to quantitatively assess these connections.

A broad variety of methods exists to model predictive relationships between meteorological influencing variables, on various temporal and spatial scales, and air quality parameters. As it has been summarized for instance by Demuzere and van Lipzig (2010a), artificial neural networks, generalized additive and fuzzy-logic based models or regression-based methods are therefore used. Regression-based approaches are commonly used tools for downscaling in atmospheric science due to their small computational time and straightforward implementation (Wilby and Wigley, 1997). Linear and multiple linear regression, generalized linear models as well as non-linear methods are examples for the latter. Studies by Cheng et al. (2007a), Demuzere and van Lipzig (2010a) or Beck et al. (2014b) have revealed remarkable results for downscaling local air quality parameters from the large-scale circulation using linear and multiple linear regression algorithms as well as non-linear regression-based ones. Furthermore, recent studies using statistical downscaling techniques for assessing air quality levels in European regions have revealed promising results, especially in winter (December, January, February), when air pollution levels reach highest values.

In Beck et al. (2014b), daily Circulation Types (CTs), which have been classified by using three non-optimized classification methods, and their monthly occurrence frequencies have been used as influencing variables (predictors) in three different downscaling approaches to estimate monthly indices of $PM_{10}$ for the period 1980-2011 at 16 selected stations in Bavaria (Germany). The applied downscaling methods are Synoptic Downscaling (SD), Multiple Linear Regression Analysis (MLR) and Random Forests (RF) for modelling monthly mean $PM_{10}$ concentrations ($PM_{mean}$) as well as monthly exceedances of a daily mean $PM_{10}$ value of 50 $\mu g/m^3$ ($PM_{50}$). According to the 2008/50/EC directive, critical particle concentrations of $> 50$ $\mu g/m^3$ on a day must not exceed 35 days per year. Hence, the index $PM_{50}$ represents high pollution events. Some important conclusions can be drawn from the study by Beck et al. (2014b) for the intended analysis in this thesis. First of all, no optimal circulation-type based statistical downscaling approach exists for modelling $PM_{10}$ indices in Bavaria. Variations of model performance with respect to considered stations and seasons have been shown. Hence, it is necessary to develop downscaling models for each station

and each season, separately. The generated models have performed best in winter months in the study. Additionally, the regression-based downscaling methods have achieved higher model skill compared to the SD approach and for modelling $PM_{mean}$ compared to $PM_{50}$.

The main purpose of this contribution is to establish quantitative relationships between large-scale CTs and local $PM_{10}$ indices at 16 selected sites in Bavaria (Germany). For that purpose, advanced statistical downscaling techniques are used. Section 7.1 comprises an introduction of the downscaling model set-up. The basic principles of the statistical methods are briefly discussed in Chapter 4. Daily and monthly occurrence frequencies of CTs resulting from objective CTC that have been optimized with respect to their synoptic skill for the target variable $PM_{10}$ in Chapter 6, are applied as predictors in the downscaling models. All downscaling approaches are evaluated via cross-validation using varying subintervals of the 1980-2011 period as calibration and validation periods, respectively. Results from the downscaling of daily mean $PM_{10}$ concentrations ($PM_{daily}$), monthly mean $PM_{10}$ concentrations ($PM_{mean}$) and monthly exceedances of a daily mean $PM_{10}$ value of 50 $\mu g/m^3$ ($PM_{50}$) are presented in Section 7.2. A comparison and discussion of the evaluation results of the best performing models in cross-validation with respect to applied downscaling techniques, considered stations, seasons and classifications are given. CTs selected as predictors in best performing models are also studied in Section 7.2. The Chapter ends with a summary in Section 7.3.

## 7.1. Downscaling model set-up

As it is proposed in the introduction, this thesis focuses on the meteorological-climatological influences on particle concentrations at Bavarian measurement sites. In order to eliminate the interference of non-climatic variabilities in time series of daily $PM_{10}$ concentrations, the 3rd order polynomial trend is fitted on each particular time series. A brief description of the polynomial regression is given for example by Wollschläger (2012). Afterwards, the differences between the daily values and the polynomial trends are calculated. The anomalies to the long-term averaged $PM_{10}$ concentrations are added. The detrending procedure is applied on time series of $PM_{mean}$ and $PM_{50}$ as well. The filtered time series are used for the application in statistical downscaling models in the following.

In order to model daily mean $PM_{10}$ concentrations ($PM_{daily}$), variants of Synoptic Downscaling (SD) are employed. An introduction to the basic principles of the method is presented in Chapter 4. First, the long-term averaged $PM_{10}$ concentrations are calculated for each circulation type of a classification. For a particular day when a certain CT occurs, its conditional value is applied to estimate $PM_{daily}$. If a CT has a mean $PM_{10}$ concentration of 30 $\mu g/m^3$ for example, this value is

used for every single day the type appears resulting in a time series of daily modelled $PM_{10}$ values.

Various quantitative measures are applied to evaluate the model performance. Skill Scores used to measure the model performance to estimate $PM_{daily}$ are the coefficient of determination ($R^2$), Mean Squared Skill Score (MSSS), Heidke Skill Score (HSS) and Hit Rate (HR). The evaluation metrics are further described in Chapter 4. $R^2$ as well as MSSS are accuracy measures evaluating observed and modelled series of continuous variables (Wilks, 2006). However, HSS and HR quantify the ability of the models to reproduce certain events. In this thesis, days exceeding a critical $PM_{10}$ concentration of 50 $\mu g/m^3$ are considered as such events. The different models are calibrated in three independent 20-year time periods and validated in corresponding validation periods to achieve robust model results. Calibration and validation periods are listed in Table 4.1 in Chapter 4.

In Figure 7.1, boxplots illustrate results for different skill scores of modelling daily mean $PM_{10}$ concentrations ($PM_{daily}$) at Augsburg Königsplatz in winter (DJF) and summer (JJA) using SD in three validation periods. The x-axis depicts selected optimized and non-optimized CTC applied in the analysis, which are further described in Chapter 6. The classifications comprise non-optimized (non-opt.) classifications performed only with mean sea level pressure fields using Großwetter-Type or prototype classification (GWT) as method. Optimized unconditioned (opt.uncond.) classifications as well as conditioned ones (cond.), classified with K-means cluster analysis with most differing start partitions (DKM) and Simulated annealing and diversified randomization (SANDRA) (SAN cond.), are additionally applied. Skill scores depicted in Figure 7.1 are $R^2$, MSSS, HSS and HR.

Comparably high skill is determined for the downscaling models in winter, which is shown in Figure 7.1. In summer in contrast, the skill of the models is less pronounced and more variable. Furthermore, increasing model skill is observed with respect to a further optimization of the classifications. All evaluation measures approve these findings. As results for HSS and HR indicate, a huge skill spread, especially in summer months, remarks a weak performance of the downscaling models on a daily basis to model certain particle events. Nevertheless, positive skill is determined for all model variants and skill scores. For further analysis, $R^2$ and MSSS are chosen as skill scores as they can be applied for evaluating monthly $PM_{10}$ indices as well.

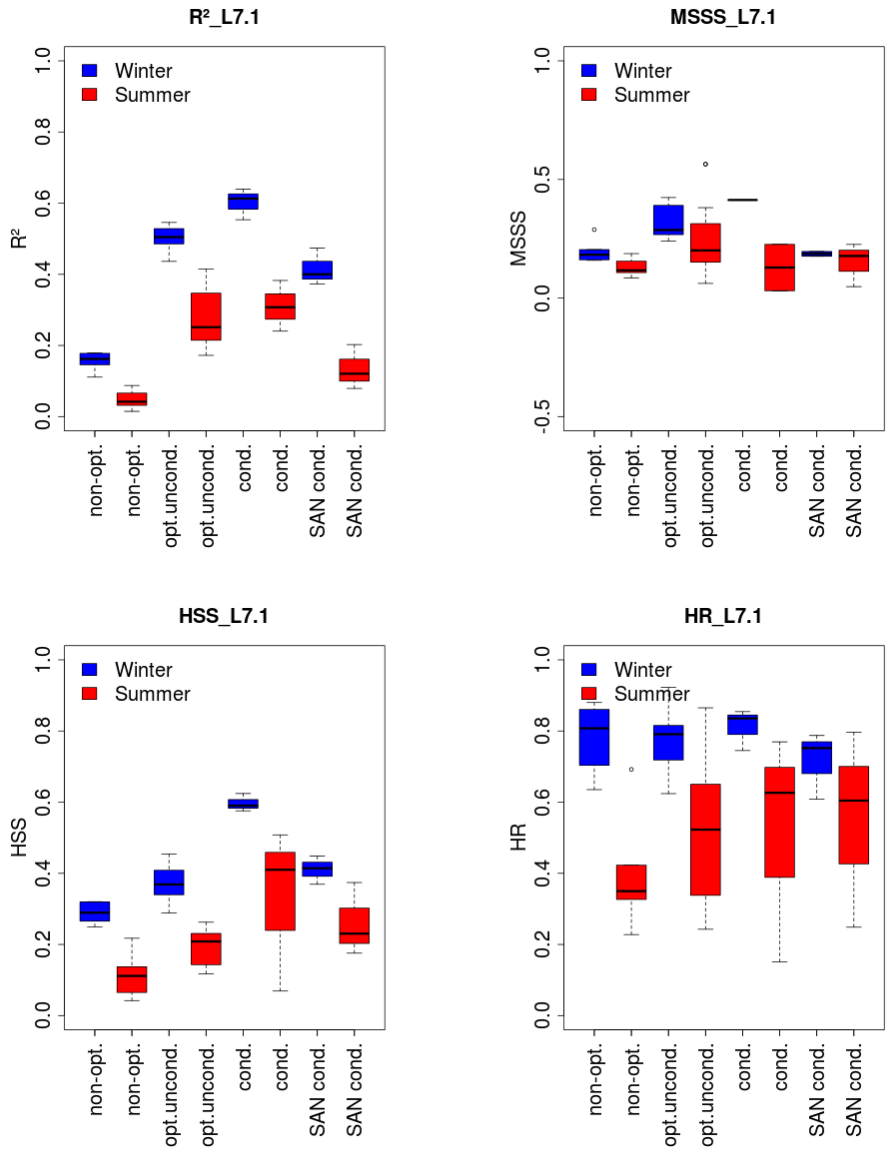


Figure 7.1: Boxplots including three values of coefficient of determination ($R^2$), Mean Squared Skill Score (MSSS), Heidke Skill Score (HSS) and Hit Rate (HR) of modelling $PM_{daily}$ in winter (DJF, blue) and summer (JJA, red) at Augsburg Königsplatz for three validation periods. SD is used for various classifications: non-optimized classifications (non-opt.), optimized unconditioned (opt.uncond.), conditioned with DKM (cond.) and SANDRA (SAN cond.). The 1.5 Interquartile Range from the upper/lower quartiles is marked by upper/lower whiskers.

In a next step, variations of the SD are tested to improve the model skill. These variants comprise the median instead of mean or a randomly selected value from the set of $PM_{10}$ concentrations of a particular CT. In their study, Cheng et al. (2007a) have included air pollution concentration anomalies on the previous day as a predictor and achieved reasonable results. Hence, additionally tested experiments of SD take the $PM_{10}$ concentrations on the previous day into account. Two

variants are explored:

1. Each CT is categorized with above or below average $PM_{10}$ concentrations compared to the overall mean $PM_{10}$ in the calibration period. 36 possible combinations result, which can appear on a given day. This implies that the CT on a given day is combined with an above or below average CT on the previous day before. $PM_{10}$ concentrations for this CT are summarized to a new subset. A randomly selected $PM_{10}$ value from this subset is used for modelling, here referred to as random previous day (RandomPR).

2. For the second variant, the same procedure as in variant 1 is used, but instead of randomly selecting a value, an average over all $PM_{10}$ concentrations from the subset is taken (mean previous day (meanPR)).

The named configurations are compared based on 18 CTs resulting from non-optimized classifications using mean sea level pressure classified with DKM and GWT for each station and season. The model skill is assessed in cross-validation by $R^2$. In Figure 7.2, barplots show validation results for München Lothstraße as an example. Results for the other respresentatives of Bavarian $PM_{10}$ regions are shown in Figures A.2-A.5. Each bar marks results of one validation period. The black line indicates the mean of $R^2$ averaged over all validation periods. Colours mark the classification method, namely DKM (red) and GWT (blue). In general, the model performance reaches highest skill in winter compared to other seasons. Variations of model performance can be observed between the validation periods. SD using mean and median of $PM_{10}$ concentrations reach similar skill. MeanPR, as a variant considering the $PM_{10}$ concentrations on the previous day, reaches comparably high model skill. Hence, this approach is included for the modelling of $PM_{daily}$ in the following analysis.

On the one hand, it is interesting to consider the particle concentrations on the previous day as a predictor. On the other hand, the synoptic situation on the previous day is an additional important influencing factor. The synoptic conditions may be, for example, an indicator of stable (blocking) large-scale atmospheric conditions resulting in nearly no airmass exchange and an accumulation of $PM_{10}$ on a considered day.

Two more variants of SD are carried out. Both take the large-scale atmospheric situation on the previous day into account, which are represented by circulation types from seasonal GWT classifications. The reason for the selection of CTs resulting from GWT is the possibility of an easy differentiation in cyclonic/anti-cyclonic conditions and high pressure/low pressure patterns. Hence, CTs are categorized with respect to large-scale atmospheric conditions indicating a potential $PM_{10}$-fostering synoptic situation (e.g. high pressure, anticyclonic patterns) or $PM_{10}$-reducing one (e.g.

low pressure, cyclonic patterns), depending on large-scale patterns and vorticity characteristics.

In the first variant, 18 CTs are subjectively categorized into 9 cyclonic and 9 anticyclonic types. The modelling procedure of $PM_{daily}$ is accomplished as follows: for a considered day with a specific circulation type from any classification, the CT on the previous day is classified as cyclonic or anticyclonic. 36 possible combinations result with specific mean $PM_{10}$ values for the modelling procedure. The second variant is based on the same technique dividing the CTs into high pressure and low pressure patterns.

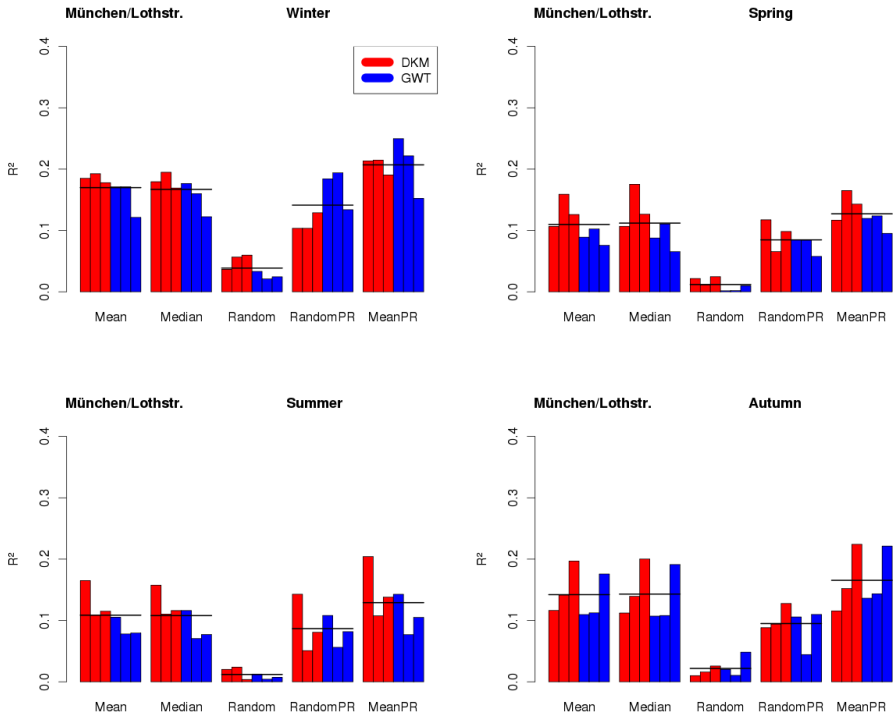


Figure 7.2: Barplots indicating $R^2$ for three validation periods marked by bars. Mean, median and randomly selected $PM_{10}$ values as well as two modifications including the $PM_{10}$ concentrations on the previous day marked as random PR and meanPR (see text for further explanation) are used as Synoptic downscaling variants based on seasonal non-optimized classifications of sea level pressure classified with GWT (blue) and DKM (red) at München Lothstrasse (L8.3). Averaged $R^2$ over three validation periods are marked as black line.

In order to model monthly $PM_{10}$ indices ($PM_{mean}$, $PM_{50}$), various regression-based approaches are used. These are Multiple Linear Regression Analysis (MLR), Generalized Linear Model (GLM) as well as Random Forests (RF). Chapter 4 comprises a description of the statistical principles of the methods. Furthermore, selected variants of the SD are applied for modelling $PM_{mean}$. The downscaling model performance of all regression-based models are evaluated using $R^2$ and MSSS,

which is determined between the observed and modelled $PM_{10}$ series in cross-validation.

The MLR is a commonly used downscaling tool in atmospheric science. This approach has been applied for the analysis of large-scale meteorological influences on air quality by other studies previously (see for example Beck et al. (2014b) or Demuzere and van Lipzig (2010a)). One has to keep in mind that an assumption for using MLR is the normal distribution of the input data. As it is tested in Chapter 5, the assumption is fulfilled for monthly $PM_{10}$ time series. A stepwise regression, using the Akaike criterion (Akaike, 1974) for predictor selection, is performed in the calibration periods based on monthly occurrence frequencies of 18 CTs as potential predictors. A set of predictors from the screening is applied in the corresponding independent validation period to predict monthly mean $PM_{10}$ concentrations ($PM_{mean}$) and monthly exceedances of a daily mean $PM_{10}$ value of 50 $\mu g/m^3$ ($PM_{50}$).

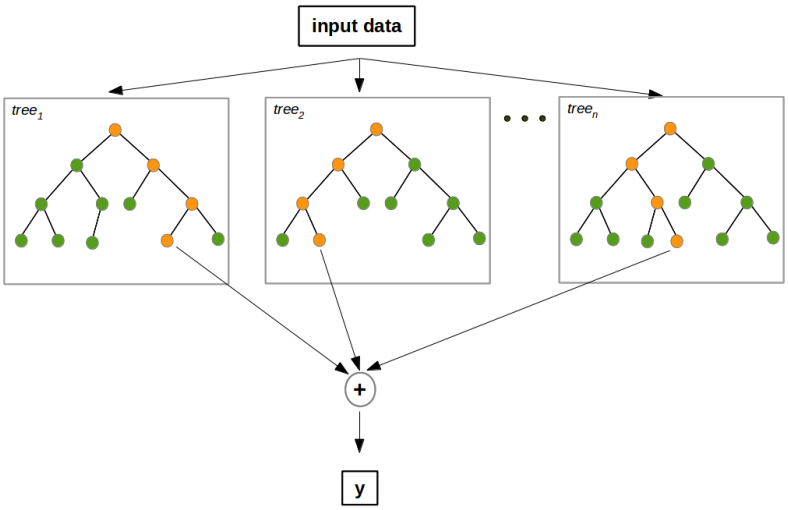


Figure 7.3: General architecture of Random Forests based on randomized ensembles of decision trees (adapted from Nguyen et al. (2013)). Predictor selection is marked in orange.

Generalized Linear Model (GLM) are a more flexible variant based on linear regression. Compared to MLR, the data is not assumed to be normally distributed, but various distributions can be adjusted. As it is described in Chapter 4, a Gamma distribution is applied to model $PM_{mean}$. For the application of GLM to hindcast $PM_{50}$, a Poisson distribution revealed to be feasible. The general proceeding of modelling $PM_{10}$ indices is similar to the one described for MLR models.

Random Forests (RF) are based on Classification and Regression tree analysis (CART). The two main advantages of the method are that the input data is not assumed to be normally distributed in

comparison to MLR and linear as well as non-linear relationships between predictors and predictands are captured. In this developed version of CART, a combination of binary decision trees is determined for random sub-samples of the observation data first. Secondly, the best split at each node is determined on the basis of a random sub-sample of explanatory variables. Figure 7.3 illustrates a scheme of the general architecture of Random Forests with a certain number of trees ($n_{tree}$) and the predictor selection marked in orange. In the present analysis, monthly occurrence frequencies of 18 CTs are applied as potential predictors for modelling the $PM_{10}$ indices using a quite high number of trees (5000) for robust results.

## 7.2. Results

As it is stated in the research objectives, the study investigates circulation-type-based downscaling models, which are best suited to capture the relevant links between large-scale atmospheric conditions and local $PM_{10}$ concentrations in the observational period 1980-2011. Hence, the downscaling approaches introduced previously are applied for each station and each season, separately, to examine and compare the potential of each method for the intended application on climate model data. The performance (robustness) of all variants of approaches is evaluated in cross-validation, in order to achieve reliable performance ratings to detect the most suitable downscaling approaches. $R^2$ and MSSS are employed as evaluation measures between observed and modelled time series.

### 7.2.1. Modelling daily $PM_{10}$

Minimum values of $R^2$ between modelled and observed seasonal time series of daily mean $PM_{10}$ concentrations ($PM_{daily}$) at stations Weiden Nikolaistraße (a) and München Lothstraße (b), resulting from 3 validation periods for various downscaling methods and classifications, are depicted in Figure 7.4. Results for other representatives of Bavarian $PM_{10}$ regions are illustrated in Figures A.6-A.7. The used downscaling techniques are Synoptic Downscaling (SD) using mean $PM_{10}$ (black points), SD considering cyclonic/anticyclonic pressure patterns on the previous day (SD-GWT CYC/ANT, green), SD considering high/low pressure patterns on the previous day (SD-GWT HP/LP, red) and SD taking mean $PM_{10}$ concentrations on the previous day (SD-PMT, blue) into account. The x-axis represents various classifications, which are used for the modelling. These are a non-optimized classification (GWT), optimized (bestBSS, bestSLP, bestallstat) as well as optimized conditioned (cond., SANcond.) ones. For a detailed description of the classifications see Chapter 6.

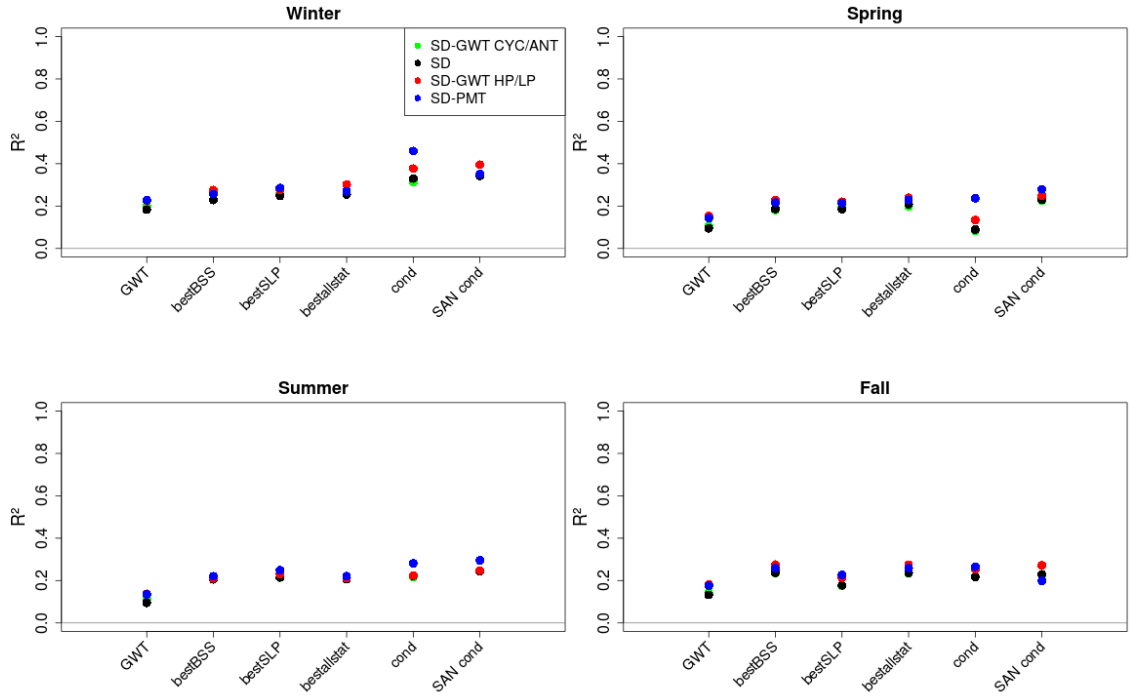


(a) Weiden

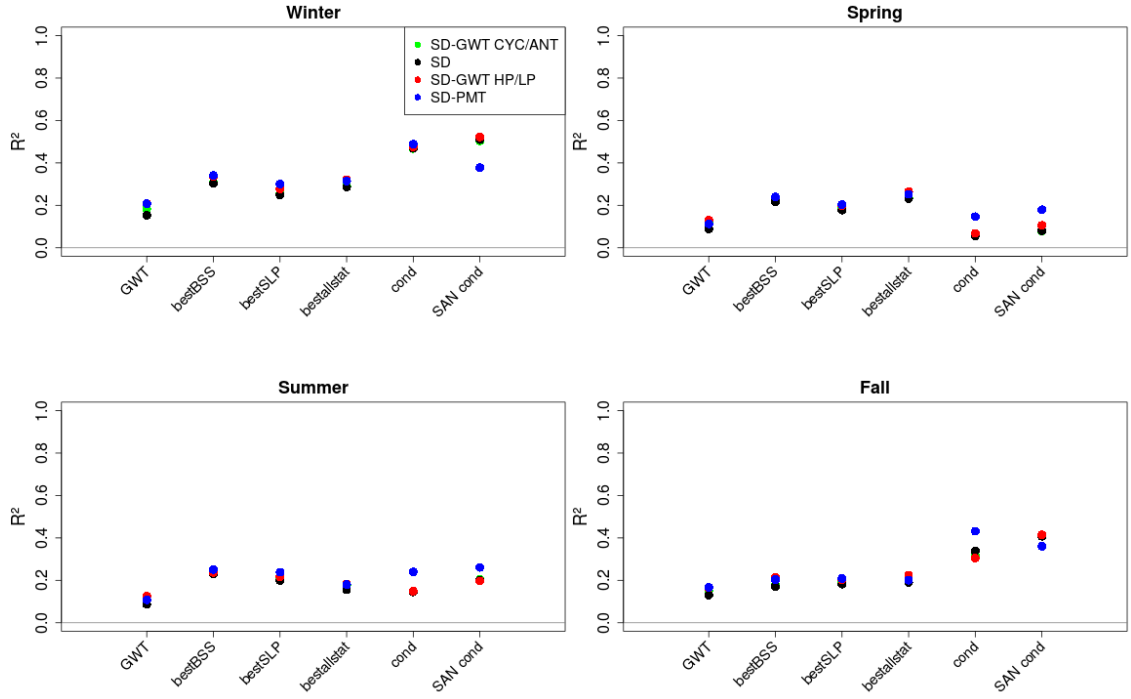


(b) München

Figure 7.4: Minimum values of $R^2$ from 3 validation periods between modelled and observed seasonal $PM_{daily}$ values at station Weiden Nikolaistraße (a) and München Lothstraße (b) using various downscaling methods (see text for further explanation) and the representative non-optimized (GWT), optimized unconditioned (bestBSS, bestSLP, bestallstat) as well as optimized conditioned (cond., SANcond.) classifications.

Results shown in the two figures revealed maximum values in winter at both stations. A possible reason for this might be, as it is also mentioned for example by Beck et al. (2014b), a stronger influence of the large-scale atmospheric conditions on local meteorological parameters in the region of interest in winter, which in turn influence local particle concentrations. In other seasons, the connection is less pronounced, especially in summer. An explanation for the latter might be the fact that local meteorological conditions are stronger influenced by local processes in boreal summer than by the large-scale atmospheric conditions.

Further variations in skill appear depending on the classification used for predictors. The overall skill increases with further optimization of the classification, but larger variations of the results occur between methods and stations. A comparison of the results for the considered downscaling methods show the highest skill for SD-GWT HP/LP and SD-PMT approaches over all seasons, stations and considered classifications, which can be seen in Figure 7.4. SD-GWT HP/LP and SD-PMT are selected as methods for further analysis. It can be concluded that these variants of Synoptic Downscaling approaches tested in the study increase the model skill.

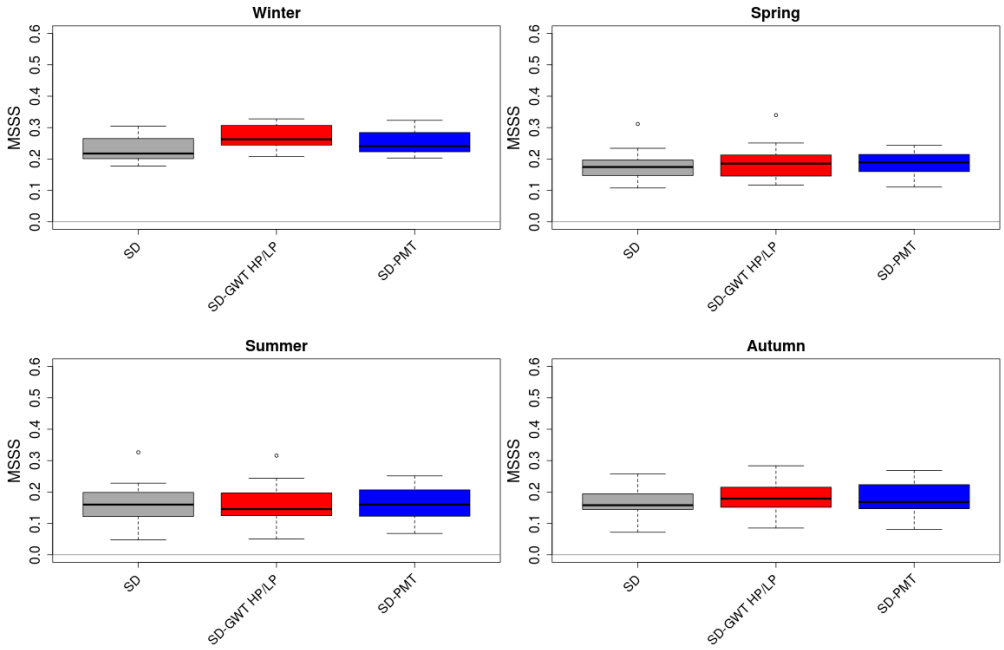


Figure 7.5: Boxplots of Mean Squared Skill Score (MSSS) for modelling seasonal $PM_{daily}$ for three validation periods and all stations using best performing classifications and three SD variants. The 1.5 Interquartile Range from the upper/lower quartile is marked by upper/lower whiskers.

Validation results also vary between the stations. As values of $R^2$ in Figure 7.4 indicate and as it has been determined by Beck et al. (2014b), it is necessary to consider the transfer model for each station, separately.

From the discussed results, a further selection of methods and classifications is carried out. Results are shown in Figure 7.5. Mean Squared Skill Score (MSSS) for three selected variants of the SD approach (SD, SD-GWT HP/LP and SD-PMT) are given as boxplots for modelling seasonal $PM_{daily}$ for three validation periods and all stations. Results for MSSS are considered for best performing classifications at each station and for each season separately, averaged over the three validation periods. Although the skill for the models is positive in all seasons and for all downscaling models, the values for MSSS are quite small. It can be concluded that the modelling of $PM_{daily}$ using circulation-type-based downscaling methods delivers insufficient model skill for the intended application on future climate change scenarios to estimate daily $PM_{10}$ concentrations. As results in Beck et al. (2014b) have shown, higher skill can be expected from the modelling of monthly $PM_{10}$ values.

### 7.2.2. Modelling monthly $PM_{10}$ indices

Validation results of estimating seasonal monthly mean $PM_{10}$ concentrations ($PM_{mean}$) , presented as minimum values of $R^2$ from three validation periods, at stations Weiden Nikolaistraße and München Lothstraße are illustrated in Figure 7.6. Results for other representatives of the Bavarian $PM_{10}$ regions see Figures A.8-A.9. Monthly occurrence frequencies of 18 Circulation Types (CTs), resulting from various classifications, are used as predictors in several statistical downscaling models. The applied transfer model approaches comprise three variants of Synoptic Downscaling (SD) for modelling time series of daily $PM_{10}$, which are aggregated to $PM_{mean}$. In addition, three regression-based methods are applied, namely Random Forests (RF-M), Multiple Linear Regression (MLR) and Generalized Linear Models (GL-M).

Similar to model results of $PM_{daily}$ discussed previously, variations in the model skill for $PM_{mean}$ occur with respect to statistical downscaling methods, considered classifications, seasons and stations. Highest model skill can be observed in winter compared to other seasons. The overall skill of the downscaling models for $PM_{mean}$ reaches higher values of $R^2$ compared to $PM_{daily}$, which is concluded by Beck et al. (2014b) as well for models based on non-optimized classifications. Results of seasonal and monthly downscaling models presented in the study by Beck et al. (2014b) are interpreted with respect to maximum values of skill scores in cross-validation. In comparison to results in the named study, the skill of estimating $PM_{mean}$ based on optimized classifications presented in this thesis reaches higher maximum skill. Nevertheless, distinct variations of $R^2$ emerge depending on the used downscaling approach and considered classifications. Hence, a further selection of classifications and methods is performed in the following.

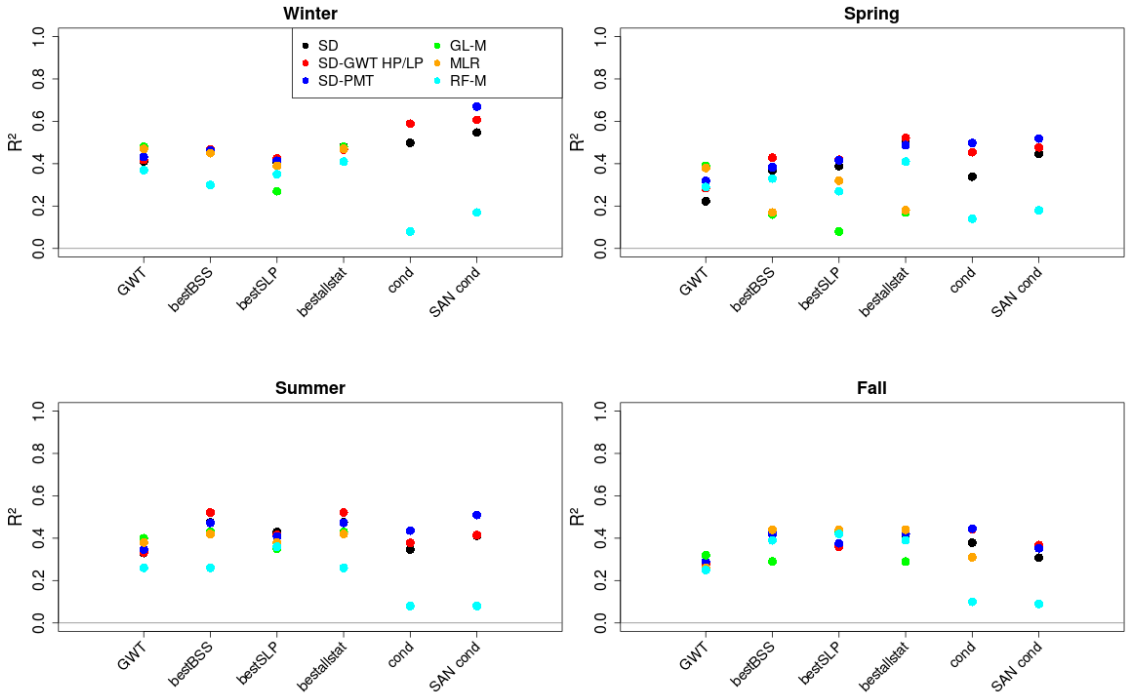


(a) Weiden

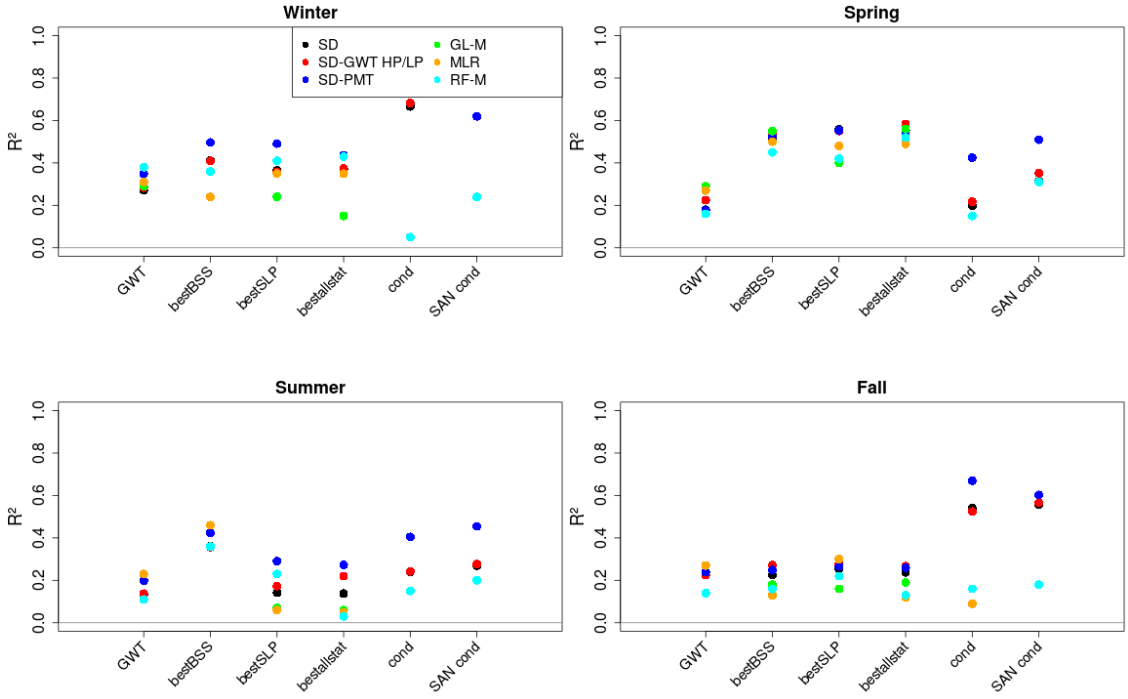


(b) München

Figure 7.6: Minimum values of $R^2$ from 3 validation periods between modelled and observed seasonal $PM_{mean}$ at stations Weiden Nikolaistraße (a) and München Lothstraße (b) using various downscaling approaches (SD = Synoptic Downscaling with mean $PM_{10}$, SD-GWT HP/LP = SD considering high/low pressure patterns on the previous day, SD-PMT = SD considering mean $PM_{10}$ concentration on the previous day, GL-M = Generalized Linear Model, RF-M = Random Forest Model, MLR = Multiple Linear Regression) and the representative classifications.

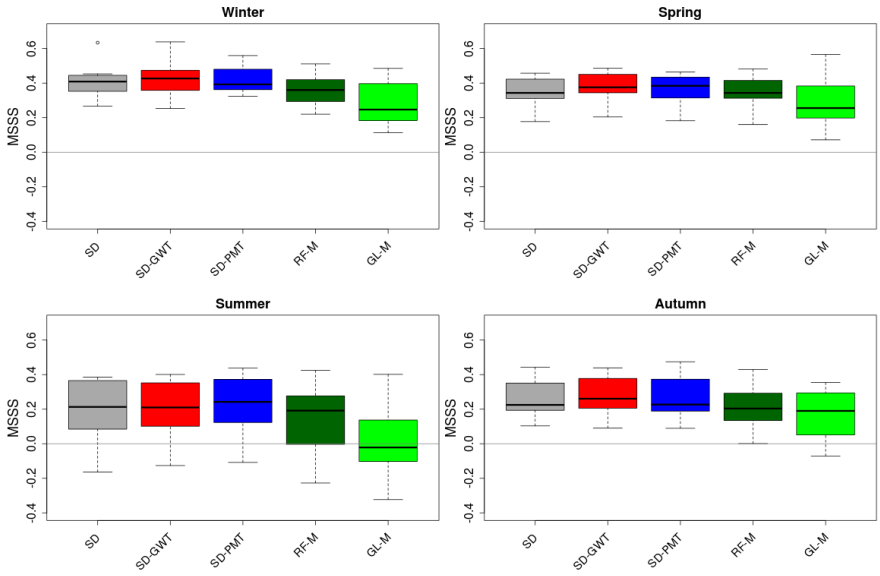


Figure 7.7: Boxplots of MSSS averaged over 16 measurement sites of best performing circulation-type-based downscaling models for modelling seasonal $PM_{mean}$ using various downscaling approaches. The 1.5 Interquartile Range from the upper/lower quartile is marked by upper/lower whiskers.

In accordance to maximum skill of Mean Squared Skill Score (MSSS) in three validation periods for each season and each station, the best performing model is selected for each downscaling approach. In Figure 7.7, MSSS calculated for all stations for modelling seasonal $PM_{mean}$ are depicted for best performing circulation-type-based downscaling models. Throughout the seasons, stations and methods, a comparably high skill appears for the RF-M compared to the GLM. As results for MLR showed similar to less pronounced skill compared to the other regression-based models, the models are not used for further analysis. RF-M are selected as the representative regression-based models.

In a last step, $PM_{50}$ is estimated in order to test the downscaling approaches to capture high pollution events. As the SD method is not suitable for modelling certain events or extreme values, the modelling of $PM_{50}$ is performed using RF-M and GLM. In Figure 7.8, boxplots of MSSS for best performing models of RF-M and GLM in cross-validation and 16 stations are presented for four seasons. In correspondence to results discussed in Beck et al. (2014b), an overall lower model skill for $PM_{50}$, compared to results of estimating $PM_{mean}$, is observed. A possible reason for the differences in model performance might be the fact that CTC capture values near or equal to 0 insufficiently, which appear more often using $PM_{50}$ resulting from months without a day exceeding the critical value of 50 $\mu g/m^3$ (Beck et al., 2014b). Furthermore, the critical $PM_{10}$ events appear quite rarely at some stations leading to a reduced data availability as well as gaps in the time series, which causes a weak performance of the downscaling models, especially in summer. As Figure 7.8

illustrates, higher model skill is reached for RF-M compared to GLM. Hence, RF-M are selected for the intended application on climate model data in next steps of this thesis.

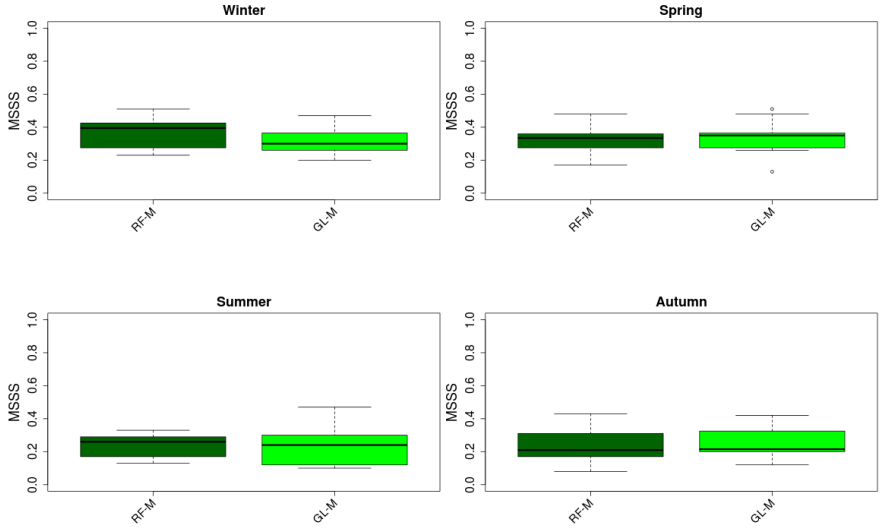


Figure 7.8: Boxplots of mean squared skill score from three validation periods for 16 measurement sites of best performing circulation-type-based downscaling models for modelling seasonal $PM_{50}$ using two regression-based approaches (RF-M, GL-M). The 1.5 Interquartile Range from the upper/lower quartiles is marked by upper/lower whiskers.

### 7.2.3. Circulation types selected as predictors

In this Section, a closer look is taken on those CTs, which are selected as predictors in most suitable downscaling procedures to model $PM_{mean}$. Centroids of the CTs, which have been selected as predictors in RF-M in calibration, are analysed for each station and each season to characterize features of the atmospheric circulation having an influence on local particle levels in Bavaria.

Table 7.1 shows an overview of CTs chosen as predictors in best performing RF-M at five stations representing the five Bavarian $PM_{10}$ regions (Kelheim Regensburger Str., Weiden Nikolaistr., Nürnberg Ziegelsteinstr., Schweinfurt Obertor, München Lothstr.) in winter for the period 1980-2011. CTs are characterized by their pressure patterns and thus the main flow directions of air masses: N = North, W = West, E = east, S = south, c = cyclonic, a = anticyclonic, L = central low pressure, H = central high pressure. As Table 7.1 illustrates, central high pressure conditions as well as anticyclonic patterns with a western flow direction are mainly chosen as predictors for winter months. On the one hand, air masses with western flow directions dominate in boreal win-

ter, particularly in the target region, and are connected to relatively low $PM_{10}$ concentrations (see Chapter 6). On the other hand, high pressure patterns are linked to comparably high particle levels, but appear less frequent.

Table 7.1: Circulation types (CTs) selected as predictors in best performing downscaling models for period 1980-2011 at five selected $PM_{10}$ stations in winter (DJF). The patterns are named by their large-scale flow direction (N = North, W = West, E = east, S = south, c = cyclonic, a = anticyclonic, L = central low pressure, H = central high pressure).

| Station | CTs |
|---|---|
| Kelheim | H (CT3, CT6, CT7, CT8, CT18), Wa (CT4, CT13), Wc (CT1, CT12) |
| Weiden | H (CT5, CT10, CT12, CT14, CT16, CT17), L (CT2, CT7), SWa (CT8), SEa (CT3) |
| NÜ/Ziegelstr. | H (CT5, CT10, CT12, CT14, CT16, CT17), L (CT2, CT7), SWa (CT8), SEa (CT3) |
| Schweinfurt | H (CT5, CT11, CT17), Wa (CT4, CT12), NWa (CT7, CT14, CT16), SWa (CT15), SEa (CT9) |
| MÜ/Lothstr. | H (CT1, CT5, CT8, CT11), Wa (CT4), NWa (CT14), SWa (CT6, CT15), SEa (CT9) |

For comparison, CTs used as predictors in summer are given in Table 7.2. In general, the circulation characteristics having an influence on local particle concentrations are more variable in this season. Nevertheless, high pressure fields dominate as predictors, which in turn are connected to high particle concentrations on a local scale. These patterns occur more often in summer compared to winter. Western flow directions of air masses are less dominant compared to winter situations in Central Europe.

Table 7.2: Same as Table 7.1 for summer (JJA).

| Station | CTs |
|---|---|
| Kelheim | H (CT2, CT5, CT7, CT9, CT16), Wa (CT10, CT13, CT14), NWa (CT11), SEa (CT14) |
| Weiden | H (CT6, CT7, CT12, CT13), Wa (CT2, CT3, CT5, CT14), SEa (CT4) |
| NÜ/Ziegelstr. | Nc (CT4), Ec (CT6), SEa (CT7), Sc (CT8), NWa (CT11), Ea (CT14), SEa (CT15), Sa (CT16), L (CT17), H (CT18) |
| Schweinfurt | Nc (CT4), NEa (CT5), SEa (CT7), Wa (CT9), NWa (CT11), Na (CT12), Ea (CT14), SEa (CT15), Sa (CT16), L (CT17) |
| MÜ/Lothstr. | H (CT2, CT6, CT10, CT12), Wa (CT7, CT10, CT13, CT14), NWa (CT7) |

## 7.3. Summary

The primary aim of the present investigations is to quantify the relationships between the large-scale atmospheric circulation and local $PM_{10}$ concentrations at 16 measurement sites in Bavaria for the period 1980-2011. Monthly occurrence frequencies of 18 Circulation Types (CTs), resulting from seasonal optimized unconditioned and optimized conditioned Circulation Type Classifications (CTC), as well as non-optimized ones for comparison (see Chapter 6), are used as influencing variables (predictors) in a variety of statistical downscaling techniques to model daily mean $PM_{10}$ concentrations ($PM_{daily}$), monthly mean $PM_{10}$ concentrations ($PM_{mean}$) and monthly exceedances

of a daily mean $PM_{10}$ value of 50 $\mu g/m^3$ ($PM_{50}$) for each season and station, separately.

The selected modelling approaches comprise variants of Synoptic Downscaling (SD) for estimating $PM_{daily}$. Three regression-based techniques, Multiple Linear Regression Analysis (MLR), Generalized Linear Model (GLM) and Random Forests (RF), as well as SD are applied for estimating monthly mean $PM_{10}$ concentrations ($PM_{mean}$). RF-M as well as GLM are used for the modelling of monthly exceedances of a daily mean $PM_{10}$ value of 50 $\mu g/m^3$ ($PM_{50}$). All downscaling approaches are evaluated via cross-validation using varying subintervals of the 1980-2011 period as calibration and validation periods, respectively. $R^2$ and Mean Squared Skill Score (MSSS) are mainly used as evaluation metrics. The most suitable, in terms of model skill determined from cross-validation, downscaling procedures are finally selected.

From this comprehensive set of circulation-type-based downscaling models, variations in skill are observed with respect to downscaling methods, considered classifications, seasons, stations and target $PM_{10}$ indices. As it is mentioned in Demuzere and van Lipzig (2010a), deficiencies in regression-based models might be caused by an inadequate representation of predictor variables and the tendency of nearly all downscaling methods to resolve only some part of the total variance. Variations of model results revealed a necessity to select the best performing circulation-type-based downscaling method for each season and each station separately.

In the present analysis, highest model skill is achieved in boreal winter (DJF). A possible explanation for that fact might be a greater influence of the synoptic conditions on local particle levels in winter as well as higher emission levels of $PM_{10}$ in this season due to increased heating and traffic load. The model performance varies considerably in other seasons, especially in summer, when small scale processes are more dominant compared to synoptic conditions (Beck et al., 2014b).

SD considering high/low pressure patterns on the previous day and SD taking mean $PM_{10}$ concentration on the previous day into account achieved highest model skills for modelling $PM_{daily}$. In addition, positive, but less pronounced model skill is determined for downscaled $PM_{daily}$, with maximum MSSS of approx. 0.3 in winter averaged over best performing models at 16 stations, compared to monthly $PM_{10}$ indices. In order to achieve higher model skill, time series of $PM_{daily}$, resulting from the SD models, are aggregated to $PM_{mean}$, which leads to maximum values of MSSS of around 0.6 for best performing models in winter.

Model results for the most suitable approaches for downscaling $PM_{mean}$ and $PM_{50}$ revealed positive skill in all seasons in cross-validation. Furthermore, higher skill is achieved for estimating $PM_{mean}$ compared to $PM_{50}$. Maximum values of MSSS are approx. 0.5 in winter for $PM_{50}$.

A specific analysis of those CTs, which are selected as predictors in best performing downscaling models for each season and selected stations, exposed mainly synoptic conditions with a western flow of air masses as well as high pressure patterns in winter over Bavaria. However, circulation characteristics of selected predictors are dominated by high pressure conditions in summer. Variations in patterns are more pronounced in summer as well as in transitional seasons. Finally, a general applicability of the developed downscaling models for estimating future climate-change-induced variations of monthly $PM_{10}$ concentrations can be concluded from results presented in this Chapter.

# 8. Estimation of future climate-change-induced variations of $PM_{10}$ concentrations

As pollution levels tended to exceed internationally accepted guidelines, they have been widely recognized by policy makers. In the past 20 years, a focus was set on the estimation of tropospheric ozone levels in Europe (Demuzere and van Lipzig, 2010b). Observations of different air pollutants like particulate matter, sulphur dioxide or nitrogen oxides are available. Time series of various air quality parameters enable the improvement of air prediction models, and thus the forecast of critical air pollutants for human health such as particulate matter with aerodynamic diameter < 10 $\mu$m ($PM_{10}$) (Carmichael et al., 2008).

Future air pollution levels are affected by several factors including changing natural and anthropogenic emission levels, human activities like agriculture or forestry and a growing world population. Moreover, changes in global and regional climate are recognized to influence air pollution concentrations (Cheng et al., 2007b). Forecast of air quality is of increasing importance, for instance with respect to better management of national and international air resources. As various studies revealed, predicting possible short and long term impacts of air pollution on public health and on the environment is of major concern as well as the projection of future climate-change-induced variations of air pollution levels (Yuval et al., 2012; Carmichael et al., 2008).

Several approaches exist for estimating future climate-change-induced variations of air quality levels. Chemical transport models for instance are meanwhile able to predict urban air pollution parameters with a spatial resolution < 1 kilometre. Some of them cover the globe with a horizontal resolution < 50 km. These dynamical downscaling tools consider emission levels, transport and transformation as well as removal processes for various pollutants. Nevertheless, chemical transport models are limited to asses the feedbacks between meteorological and air quality components, bridging the gap between urban/local to global scale and are limited by computational efficiency (Carmichael et al., 2008).

Scenarios from Atmosphere-Ocean Coupled General Circulation Models (AOGCM) are commonly used for predicting future climate conditions and climate changes until the end of this century. The model data is of coarse resolution, which evokes the need to bridge the gap between the scales by so called downscaling techniques. Statistical (empirical) downscaling techniques are often used tools for that purpose in atmospheric science. An early review of downscaling techniques on the basis of GCM is given by Wilby and Wigley (1997) for example. Another review on empirical downscaling techniques in synoptic climatology is presented by Yarnal et al. (2001). In contrast to other downscaling techniques, statistical downscaling methods are comparably easy to

apply and are able to provide information on a station-scale of a target variable from large-scale atmospheric predictor variables.

All statistical downscaling methods refer to the same basic concept of quantifying relations between large-scale predictors and local target variables regarding observational data and an application on GCM output afterwards (Wojcik, 2015; Wilby et al., 2004). Statistical downscaling models are employed as well to forecast air pollution levels. Cheng et al. (2007b) for example have used within-weather-group air pollution prediction models to estimate future air quality levels of various parameters, e.g. ozone, carbon monoxide, nitrogen dioxide, sulphur dioxide and suspended particles. Yuval et al. (2012) have studied future air quality in a changing climate scenario in Israel by assigning various synoptic patterns, classified with reanalysis data, on GCM data. Future air quality levels have been assessed by synoptic forecasts based on a monthly synoptic pollution coefficient for each air quality variable (sulphur dioxide, nitrogen dioxide, ozone, particulate matter).

In this thesis, statistical downscaling techniques are also applied to estimate future climate-change-induced variations in monthly particle levels at 16 measurement sites in Bavaria. The downscaling models are based on the identified relationships between the large-scale atmospheric conditions over Europe (predictors) and local $PM_{10}$ concentrations at the stations (predictands). In a first step, centroids of large-scale atmospheric fields, derived from best performing Circulation Type Classifications (CTC) for each season and each station from previous analysis (see Chapter 7), are assigned by the minimum Euclidean distance to corresponding gridded data from the Atmospheric Component of the MPI-M Earth System Model (ECHAM6) (Stevens et al., 2013) and EC-Earth model (Hazeleger et al., 2010). In this context, projections of two climate change scenarios, RCP4.5 and RCP8.5, for two time steps 2021-2050 and 2071-2100 are used. A detailed description of the climate model data basis is content of Section 3.3.

Secondly, monthly occurrence frequencies of 18 Circulation Types (CTs), resulting from an optimized classification conducted in the aforementioned analysis, are employed as predictors in robust downscaling approaches for estimating future levels of monthly mean $PM_{10}$ concentrations ($PM_{mean}$) and monthly exceedances of a daily mean $PM_{10}$ value of 50 $\mu g/m^3$ ($PM_{50}$). For that purpose, suitable downscaling models have been selected for each season and station. The downscaling model set-up and model validation are discussed in previous Chapter 7.

Differences between observed (measured $PM_{10}$ concentrations) and modelled time series from the historical period of ECHAM6, resulting from GCM model bias, are considered by using a bias correction method proposed by Cheng et al. (2007b). The bias corrected time series in the recent period 1980-2005 are used for a more precise estimation of future air pollution concentrations. In

accordance to the removal of the bias in the observational period, a bias correction is applied on the modelled time series of the projections as well, assuming a similar model bias in the future and the present-day climate (Demuzere and van Lipzig, 2010b).

Relationships between predictors and predictands are assumed to be stationary in the intended analysis, implying that the quantitative relations are not changing over time. In reality, many atmospheric processes are not stationary. The stationary assumption is one of the primary uncertainties in statistical downscaling (Wojcik, 2015). Nevertheless, a lot of methods for analysing time series are based on the assumption of stationarity (Wilks, 2006). For the historical (control) period 1980-2005, stationarity can be estimated by means of an ensemble of statistical models each derived for different calibration sub-periods.

This Chapter is structured as follows. In Section 8.1, a description of the application of best performing statistical downscaling models on future climate change scenarios is presented. A brief discussion on the validation of GCM is given in Section 8.2 based on the analysis of the representation of modes of variability in ECHAM6 data. Uncertainties emerging from GCM model biases as well as downscaling models are addressed in Section 8.3. Results from downscaling models on the basis of ECHAM6 data are content of Section 8.4.1. First, results from the estimation of future monthly mean $PM_{10}$ concentrations ($PM_{mean}$) and monthly exceedances of a daily mean $PM_{10}$ value of 50 $\mu g/m^3$ ($PM_{50}$) levels are presented in Section 8.4.1. Second, differences in frequencies of occurrence of $PM_{10}$ relevant large-scale atmospheric patterns between the historical period and projections are presented in Section 8.4.2. Finally, a comparison between estimations of $PM_{10}$ indices, resulting from ECHAM6 and EC-Earth, are conducted in Section 8.4.3. The chapter ends with a summary in Section 8.5.

## 8.1. Application of downscaling models on GCM projections

Huth et al. (2008) have summarized four different strategies to compare circulation patterns of two climate data sets. In this thesis, for example, these are Circulation Types (CTs) resulting from NCEP/NCAR reanalysis data and GCMs.

1. In a first procedure, classifications are determined for each data set separately. Dominant CTs can be detected for the particular data sets with this method. However, a comparison may be misleading due to unstable classification results from the method itself or by circulation patterns, which are not assigned to a class or form small classes.

2. Another strategy is to predefine CTs independently from the two climate data sets and assign the types afterwards. The main advantage of this approach is the independence of the

classification from the climate data set for a comparison, but in reverse the real structure in the particular data sets may be not captured.

3. As a third approach, CTs are classified on the basis of one data set and are assigned on the other one.

4. In the fourth method, two data sets are combined into one data set and CTs are determined concurrently.

A standard procedure to estimate future climate-change-induced variations of a target variable, based on statistical downscaling techniques, is to calibrate the models with observations. In this thesis, these are large-scale atmospheric fields from NCEP/NCAR reanalysis data (see Section 3.2 for data description). Afterwards, they are applied on GCM projections. This corresponds to the third approach outlined by Huth et al. (2008) as well as the description of the procedure for similar analysis discussed by Wojcik (2015).

In the following, centroids from selected Circulation Type Classifications (CTC) are assigned to gridded large-scale atmospheric fields of corresponding variables from General Circulation Model (GCM) data. The CTCs result from a previously described optimization towards the target variable $PM_{10}$ in Chapter 6. A further selection of the best performing classifications for the application in downscaling models for each station and season is discussed in Chapter 7.

The assignment of the centroids is conducted using the *cost*733 software package from the COST Action 733 "Harmonisation and Applications of Weather Type Classifications for European Regions" introduced in Section 4.2. To this end, Circulation Types (CTs), classified with reanalysis data, are assigned to the large-scale atmospheric fields from the ECHAM6 and EC-Earth model using the minimum Euclidean distance. As it is described by Wilks (2006) for example, the Euclidean distance is a quite simple conventional distance measure between two points $x$ and $y$ with $K$ indicating the dimensions:

$$\|x-y\| = \sqrt{\sum_{k=1}^{K} (x_k - y_k)^2}. \tag{26}$$

For each object of the GCM dataset, the Euclidean distances between the object and centroids of 18 CTs are calculated. An assignment of the object to a class number is ensued to that one with the minimum distance.

Resulting monthly occurrence frequencies of 18 CTs are used in different statistical downscaling models as predictors to estimate various $PM_{10}$ indices (predictands). Results in Chapter 7 have revealed only small skills for circulation-type-based downscaling models in validation with respect

to the prediction of $PM_{daily}$, independently from the downscaling techniques. However, higher skill can be reached by modelling monthly $PM_{10}$ indices by aggregating daily modelled time series. To this end, two variants of Synoptic Downscaling (SD) have been chosen to model time series of daily mean $PM_{10}$ concentrations ($PM_{daily}$) in Chapter 7. The basic statistical principles behind the SD are explained in Chapter 4. SD regarding mean $PM_{10}$ concentrations on the previous day (SD-PMT) have been selected as well as SD considering high/low pressure patterns on the previous day (SD-GWT HP/LP). They appeared to be most suitable for downscaling $PM_{daily}$ with respect to values of evaluation measures in cross-validation in Chapter 7.

Random Forests (RF) are selected as the representative regression-based technique to model $PM_{mean}$ and $PM_{50}$. In Chapter 7, the RF models turned out to be most suitable for predicting monthly particle levels with respect to model skill in the validation. The basic statistical principles of RF are introduced in Chapter 4. In summary, the relative importance of regressor variables (predictors) is assessed on the basis of Classification And Regression Trees (CART) (Grömping, 2009).

The downscaling models are calibrated in three 20-year calibration periods on the one hand and over the whole period 1980-2005 on the other hand, on the basis of observational data, to consider statistical ensembles. Afterwards, the models are applied on the GCM data. The differences between ECHAM6 downscaled and observed particle concentrations are addressed by performing a bias correction introduced by Cheng et al. (2007b). Thus, a better assessment of future $PM_{10}$ levels is enabled. Estimated future levels of particle concentrations from ECHAM6 projections, which are as well bias corrected, are regarded for the representative stations in Section 8.4.1.

In their study, Cheng et al. (2007b) have investigated the changes in frequencies of occurrence of distinct weather groups by calculating the differences of percentage occurrence of these groups in the historical and projected period as well as for observations. They have concluded a minor decreasing trend of air pollution related weather groups for their study area south-central Canada. Huth et al. (2008) have analysed the changes of frequencies of circulation patterns over central Europe between reanalysis and GCM data based on two classification methods. They have found increasing frequencies of occurrence of westerly circulation patterns in autumn and winter seasons. Furthermore, (Demuzere and van Lipzig, 2010b) have investigated differences in frequencies of occurrence of circulation patterns between reanalysis and GCM data. Especially changes in western patterns have been discussed to be significant. In the following analysis, changes in frequencies of occurrence of seasonal $PM_{10}$ compounding or weaken CTs between the recent period and future scenarios are assessed in Section 8.4.2.

As it is addressed for example by Wojcik (2015), the performance of GCM may vary with respect

to seasons or modelled large-scale atmospheric parameter. Hence, multi-model ensembles should be used to consider the differences of climate model projections in downscaling application. In this thesis, a comparison of estimations from ECHAM6 and EC-Earth is conducted in Section 8.4.3. Downscaling models are run for both climate models on the basis of the best performing classification averaged over all 16 stations in a season. The bias correction of the modelled time series in historical period and projections is applied on all resulting time series of $PM_{mean}$ and $PM_{50}$.

## 8.2. GCM validation

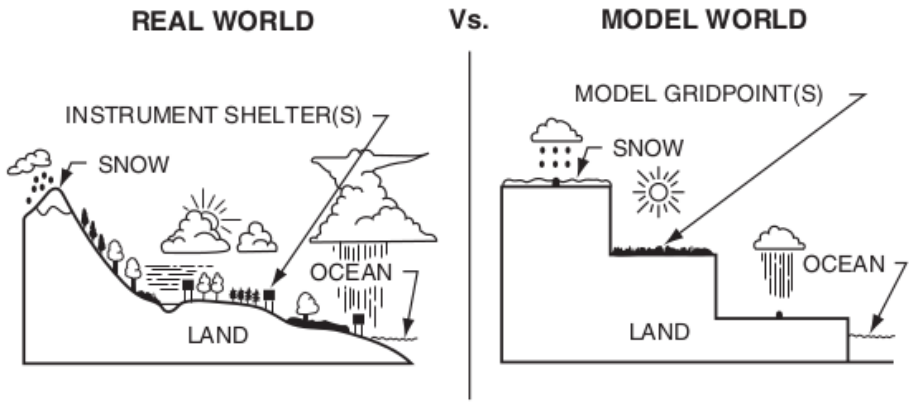


Figure 8.1: Sketched illustration of reality (left) and model world (right) as represented in numerical weather prediction models (Source: Wilks 2006).

Numerical models simplify the reality by representing the world as a grid, parametrize processes or homogenize surface conditions (Wilks, 2006). Figure 8.1 schematically illustrates the complex processes of the real word (left) and their representation in a numerical weather prediction model (right). An improvement of GCM performance over the past years has been ascertained by recent studies (Gleckler et al., 2008; Rahmstorf et al., 2012). Nevertheless, model biases occur, which have to be taken into account when using climate model data. In case of the used ECHAM6 model for instance, Stevens et al. (2013) have outlined biases occurring with respect to the representation of small-scale physical processes, e.g. clouds or convection.

In a comprehensive study by Brands et al. (2013), the ability of seven Earth System Models (ESMs) from the Fifth Phase of the Coupled Model Intercomparison Project (CMIP5) (Taylor et al., 2012) to reproduce present climate conditions in Europe and Africa has been investigated. As reference for an evaluation of daily circulation, temperature and humidity parameters, ECMWF reanalysis data have been used. Main results from this study have revealed a largely overestimated meridional pressure gradients during boreal winter and spring in most of the ESMs, which lead to pronounced

moist and mild conditions in continental Europe. Serious circulation biases and an underestimation of the duration of wintertime has been stated for the ESM projections, which are suspected to result from ESM errors in the historical period for Europe.

In their project on "WEather Patterns, CycloneTRAcks and related precipitation EXtremes" (WETRAX) for the Alpine region, Hofstätter et al. (2015) have investigated the representation of dominant modes of variability (spatial patterns and corresponding time coefficients) of the atmospheric circulation in GCM data. To this end, gridded mean sea level pressure fields from NCEP/NCAR renalysis as well as three historical runs of ECHAM6 have been used in s-mode Principal Component Analysis (PCA) to extract and compare five modes of variability for the period 1951-2005. A further description of the PCA is given in Chapter 4. An overall good representation of the spatial patterns of the modes of variability from the reanalysis in climate model projections has been ascertained. The loadings of the extracted Principal Components, which indicate the correlation coefficients between mean sea level pressure time series of a grid point and time coefficients of a pattern, have shown small differences. Values of Explained Variance (see Chapter 4 for further explanation of the evaluation measure) for both reanalysis and GCM have achieved values around 65 %. In summary, results from this comprehensive study have proven a general applicability of the analysed GCM for further investigations based on the atmospheric circulation as performed in this thesis.

Moreover, differences between reanalysis and climate model data may arise from GCM model biases in simulating different large-scale present-day climate variables. GCMs deliver quite reliable results in terms of reproducing long-term pressure fields, i.e. mean sea level pressure (SLP) or geopotential height (HGT). Other large-scale atmospheric parameters, such as AIR, zonal wind component (UWND), meridional wind component (VWND) or relative humidity (RHUM), tend to higher model biases (Wojcik, 2015). In the latter study by Wojcik (2015), the reliability of several CMIP5 models in reproducing seasonal large-scale atmospheric circulation patterns over Europe and the North Atlantic, represented by gridded mean sea level pressure (SLP) and geopotential height (HGT) of the 500 hPa level, has been investigated. NCEP/NCAR reanalysis data have been used as reference values. In summary, variations of the reliability of climate models have been ascertained between the different models, seasons and considered atmospheric parameters.

In order to investigate differences between NCEP/NCAR reanalysis and ECHAM6 of $PM_{10}$ relevant large-scale atmospheric parameters (air temperature (AIR) in 1000 hPa, geopotential height (HGT) in 500 hPa, mean sea level pressure (SLP), zonal (UWND) and meridional (VWND) wind component in 500 hPa, relative humidity (RHIM) in 1000 hPa), time averaged spatial means of these variables are calculated for a mid-size domain (7.5°-27.5° E, 40°-60° N) and the recent period

1980-2005. Table 8.1 indicates comparably small differences between reanalysis and ECHAM6 for SLP as well as air temperature. These findings are in accordance to other studies, e.g. Wojcik (2015) or Rahmstorf et al. (2012). In comparison, values of geopotential height, wind components and relative humidity indicate larger variations. It should be noted that results of model realizations differ as well, which are illustrated in Table 8.1. Nevertheless, these differences are less pronounced compared to the previously stated contrasts between reanalysis and GCM.

Table 8.1: Time averaged spatial mean of daily gridded fields from various large-scale atmospheric variables, i.e. air temperature (AIR) in 1000 hPa (in K), geopotential height (HGT) in 500 hPa (in gpm), mean sea level pressure (SLP) (in hPa), zonal wind component (UWND) in 500 hPa (in m $s^{-1}$), meridional wind component (VWND) in 500 hPa (in m $s^{-1}$), relative humidity (RHUM) in 1000 hPa (in %), centred over the target region (7.5° - 27.5° E and 40° - 60° N) for the period 1980-2005 from NCEP/NCAR reanalysis and 3 historical runs of ECHAM6.

| Variable | NCEP | Hist1 | Hist2 | Hist3 |
|---|---|---|---|---|
| AIR | 285.94 | 285.59 | 285.54 | 285.38 |
| SLP | 1015.83 | 1014.79 | 1014.93 | 1014.64 |
| RHUM | 74.29 | 65 | 64.42 | 64.34 |
| HGT | 5606.46 | 5579.08 | 5577.92 | 5574.49 |
| UWND | 8.34 | 9.18 | 9.38 | 9.35 |
| VWND | -0.78 | -0.11 | -0.05 | 0.17 |

## 8.3. Quantifying model uncertainties

For quantifying potential uncertainties arising from intern model variability of the climate models, several model runs (realizations) are applied in this thesis, if provided by the data basis, as numerical ensembles. Jolliffe and Stephenson (2011) or Wilks (2006) for example describe the general idea of ensemble forecasting as the iteration of a model on the basis of perturbed initial states of the atmospheric conditions. The analysis of the resulting forecast ensemble focuses on the phase-space propagation. Three ensemble runs are available for the ECHAM6 model in the historical period (1980-2005) and for the two scenarios (RCP4.5, RCP8.5). Furthermore, two time periods (2021-2050, 2071-2100) of the projections are distinguished. Future $PM_{10}$ concentrations are estimated from the ensemble mean.

Another strategy to consider numerical model uncertainties is the usage of multi-model ensembles. Jolliffe and Stephenson (2011) for example have applied a combination of model output from several GCMs combined to a multi-model ensemble in their study, with the aim to take model uncertainties into account. In this thesis, model runs from ECHAM6 and EC-Earth are applied. Model results are compared and discussed for a better assessment of future particle levels in Bavaria. For

EC Earth, only one model run has been available in the historical period and for the climate change scenarios.

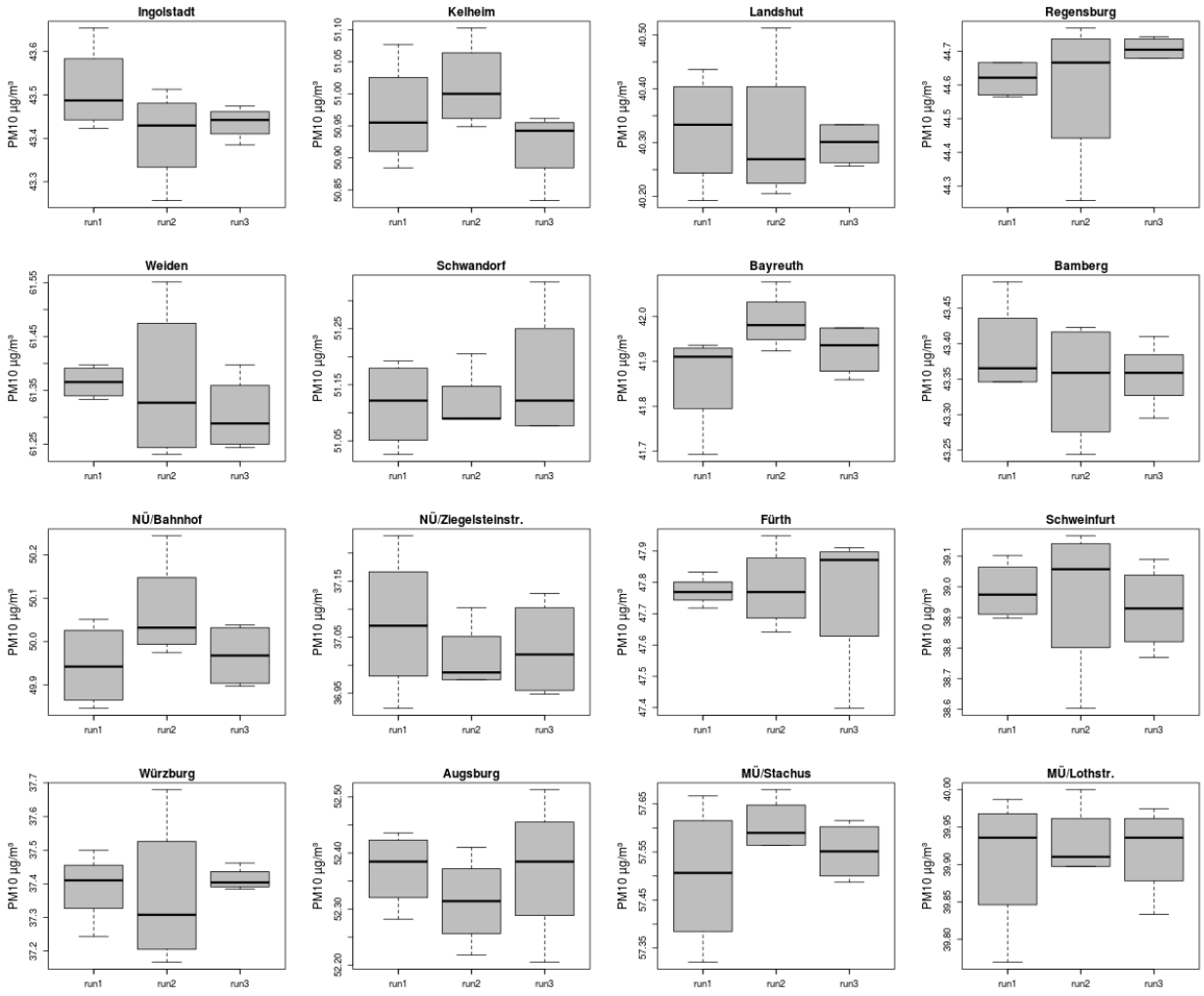


Figure 8.2: Boxplots of $PM_{mean}$ levels in winter (DJF) from RF-M estimated for numerical and statistical ensemble members at 16 measurement sites in Bavaria in the historical period 1980-2005. The 1.5 Interquartile Range from the upper/lower quartile is marked by upper/lower whiskers.

Additional uncertainties may emerge from the downscaling approaches for the circulation-type-based projection of future particle levels. In Chapter 7, the models have been calibrated in three independent 20-year periods and validated in corresponding 10-year validation periods to generated robust transfer models. In order to take these uncertainties into account, statistical ensembles are considered. To this end, four statistical ensemble members are calculated for each downscaling model. The first time period for calibration period is 1980-2011. The other sub-periods are three different 20-year periods for calibrations and validations in independent 11-year time frames. The used calibration periods are 1980-1999, 1980-1989 + 2001-2011 as well as 1991-2011. The corresponding validation periods are 2000-2011, 1990-2000 and 1980-1990.

Figure 8.2 shows boxplots of estimated levels of monthly mean $PM_{10}$ concentrations ($PM_{mean}$) (in $\mu g/m^3$) modelled with circulation-type-based Random Forests (RF) models (RF-M) in winter (DJF) at 16 Bavarian measurement sites. Best performing CTC are used as predictors, which are assigned to ensemble runs of ECHAM6 in the historical period (1980-2005) for the statistical ensemble members. As results in Figure 8.2 indicate, variations of model results occur between the numerical ensembles, which can be seen by the position of the median marked by the black line in the boxplots. A reason for this are differing initial starting conditions for the three historical runs described by Giorgetta et al. (2013) for instance.

The modelled spread of particle levels, resulting from the statistical ensembles, are even bigger than differences between the realizations of the climate model. A possible explanation for that could be type-internal variabilities of the CTs, which result from the objective classifications that have been optimized with respect to their synoptic skill for the target variable $PM_{10}$ for each season and at each station, separately. Demuzere and van Lipzig (2010b) have mentioned deficiencies in the model data sets, limited capability of regression-based methods to capture higher percentiles as well as scale-dependency of the predictor variables as additional reasons. In this study, future particle levels are assessed by using ensemble means of numerical and statistical ensembles.

## 8.4. Results

### 8.4.1. Downscaled future $PM_{10}$ levels

Differences between daily and monthly $PM_{10}$ concentrations from observations in 1980-2005 and modelled time series from ECHAM6 historical runs, resulting from a possible GCM bias, are addressed in the following. For that purpose, standard deviations of $PM_{mean}$ time series from observations and best performing RF models with NCEP and ECHAM6 in 1980-2005 are calculated and compared.

In Table 8.2, standard deviations of $PM_{mean}$ time series are given for 5 selected stations in winter from observations (obs) and best performing RF models based on NCEP and ECHAM6 data in the period 1980-2005. Results reveal usually smaller values from the modelled time series of NCEP and ECHAM6 compared to the observations. In order to minimize the mentioned differences between observations and models and adjust the bias for a more accurate estimation of future particle concentrations, a bias correction is applied on the modelled time series from ECHAM6 in the following.

Table 8.2: Standard deviations of $PM_{mean}$ time series in winter at five stations, representing Bavarian $PM_{10}$ regions, from observations (obs) and best performing RF models averaged over three validation periods based on NCEP and ECHAM6 data (1980-2005).

| Station | obs | NCEP | ECHAM6 |
|---|---|---|---|
| Kelheim | 6.3 | 1.9 | 0.8 |
| Weiden | 15.5 | 4.7 | 2.2 |
| NÜ Ziegelsteinstr. | 11.5 | 3.5 | 2.0 |
| Schweinfurt | 11.5 | 3.5 | 2.8 |
| MÜ Lothstr. | 12.7 | 3.5 | 3.2 |

A bias correction between the observed and modelled time series in a recent period is suggested by Cheng et al. (2007b). Daily or monthly model predictions for the GCM historical runs after correction ($PM_{hist-new}$) are assessed by using daily or monthly model prediction for the climate model historical runs before correction ($PM_{hist-old}$). Standard deviations of observations ($Std_{PM_{Obs}}$) and model predictions in the historical period ($Std_{PM_{hist-old}}$) as well as mean concentrations of observations ($\overline{PM}_{Obs}$) and model predictions from historical runs ($\overline{PM}_{hist-old}$) are included in the correction (Cheng et al., 2007b):

$$PM_{hist-new} = (PM_{hist-old} - \overline{PM}_{hist-old}) \frac{Std_{PM_{Obs}}}{Std_{PM_{hist-old}}} + \overline{PM}_{Obs} \; . \tag{27}$$

Estimations of future climate-change-induced variations of monthly $PM_{10}$ indices, i.e. monthly mean $PM_{10}$ concentrations ($PM_{mean}$) and monthly exceedances of a daily mean $PM_{10}$ value of 50 $\mu g/m^3$ ($PM_{50}$), are presented in the following. Future levels of particles are assessed by statistical circulation-type-based downscaling models using ECHAM6 data for two scenarios (RCP4.5, RCP8.5) and time periods (2021-2050, 2071-2100).

According to the removal of the bias in the first step, a bias correction is applied on the modelled time series from the GCM scenarios for a more accurate adjustment of future air pollution levels

as well. As it has been employed by Cheng et al. (2007b), differences in overall means ($\overline{PM}$) and standard deviations ($Std$) of time series after ($hist-new$) and before ($hist-old$) bias correction of historical runs are used, assuming a similar model bias for historical climate and future projections of GCM:

$$PM_{future-new} = (PM_{future-old} - \overline{PM}_{hist-old}) \frac{Std_{PM_{hist-new}}}{Std_{PM_{hist-old}}} + \overline{PM}_{hist-new} \; . \tag{28}$$

$PM_{future-old}$ are the time series before correction. $PM_{future-new}$ are resulting bias corrected future daily model predictions, which are aggregated to model monthly $PM_{10}$ indices.

In order to test the significance of differences in the central tendency between the GCM historical period and projections, a Wilcoxon-Mann-Whitney rank-sum test with alpha = 0.05 is performed. In this classical non-parametric test, variables do not need to be normally distributed. The null hypothesis $H_0$ indicates that the two data samples have been drawn from the same distribution (Wollschläger, 2012). For a sample 1, $R1$ is defined as the sum of the ranks of the elements of this sample in a pooled distribution of the ranks within $n$ observations (Wilks, 2006). $R2$ are the sum of the ranks of the elements from a sample 2:

$$R1 + R2 = 1 + 2 + 3 + 4 + ... + n = \frac{(n)(n+1)}{2}. \tag{29}$$

If $H_0$ is true, the two samples are drawn from the same distribution. In that case, if numbers of observations $n1 = n2$, $R1$ and $R2$ will be similar in magnitude. If the null hypothesis is true and sample sizes are not equal, $R1/n1$ and $R2/n2$ should be similar in magnitude (Wilks, 2006). Results of estimated future climate-change-induced variations of $PM_{mean}$ and $PM_{50}$ are presented and discussed in the following.

#### $PM_{mean}$ levels

Initially, bias-corrected estimations of future $PM_{mean}$ levels (in $\mu g/m^3$) are conducted using two variants of the Synoptic Downscaling (SD) approach. These are SD considering mean $PM_{10}$ concentration on the previous day (SD-PMT) and SD considering high/low pressure patterns on the previous day (SD-GWT HP/LP). The methods are described in more detail in Chapter 7. In a first step, daily $PM_{10}$ time series are estimated from the occurrence of CTs on a considered day, which are connected to certain $PM_{10}$ levels. Secondly, the daily values are aggregated to $PM_{mean}$. Hereinafter, modelling results for the two SD approaches are discussed on the basis of SD-PMT as the representative method for selected stations.

In Figures 8.3 - 8.5, seasonal $PM_{mean}$ levels, modelled by SD-PMT, are shown for five selected

$PM_{10}$ stations. The stations are used as the representative ones for five $PM_{10}$ regions in Bavaria, which have been defined in Chapter 5. The measurement sites are Kelheim Regensburger Strasse, Weiden Nikolaistrasse, Nürnberg Ziegelsteinstrasse, Schweinfurt Obertor as well as München Lothstrasse. Star symbols mark statistical significance (alpha = 0.05) of differences of central tendency between respective projection and historical periods assessed by a Wilcoxon-Mann-Whitney-Test. Estimated particle levels are averaged over four statistical and three numerical ensemble members. Model results for RCP4.5 in two time periods are illustrated in orange and for RCP8.5 in red. Results for the historical period (1980-2005) are depicted in green for comparison.

As Figures 8.3-8.5 illustrate, decreasing $PM_{mean}$ levels are estimated for winter (DJF), especially in the second projection period of 2071-2100. These changes can be observed at all depicted stations. Results for other stations are depicted in Figures A.10-A.15. Furthermore, the modelled variations are primarily significant in the second time period of 2071-2100 for scenario RCP8.5 at nearly all stations.

A possible explanation for the decrease of local particle concentrations in winter are an increase of western circulation patterns over Europe projected by the ECHAM6 model. In general, western circulation patterns lead to air mass exchanges in the target region and thus are connected to relatively low $PM_{mean}$ values. With an increasing occurrence frequency of the western patterns, monthly particle concentrations decrease in whole Bavaria. The changes in frequencies of occurrence of $PM_{10}$ relevant circulation types are discussed in more detail in the following Section 8.4.2.

In summer (JJA) however, increasing $PM_{mean}$ levels are estimated at most of the stations, as depicted in the figures. The differences of particle concentrations between historical period and scenarios are more pronounced compared to changes in winter. As the figures indicate, the stated deviations are only in some cases significant in summer. An increase of frequencies of occurrence of high pressure patterns in summer month might be a reason for the increasing particle levels. High pressure patterns over Europe are connected to relatively high particle concentrations due to stagnating air masses with nearly no air mass exchange. Furthermore, they foster, for example, higher temperatures at a local scale, which are connected to the formation of secondary particles. An increase of high pressure systems in Europe in the summer months leads to rising air pollution in Bavarian cities.

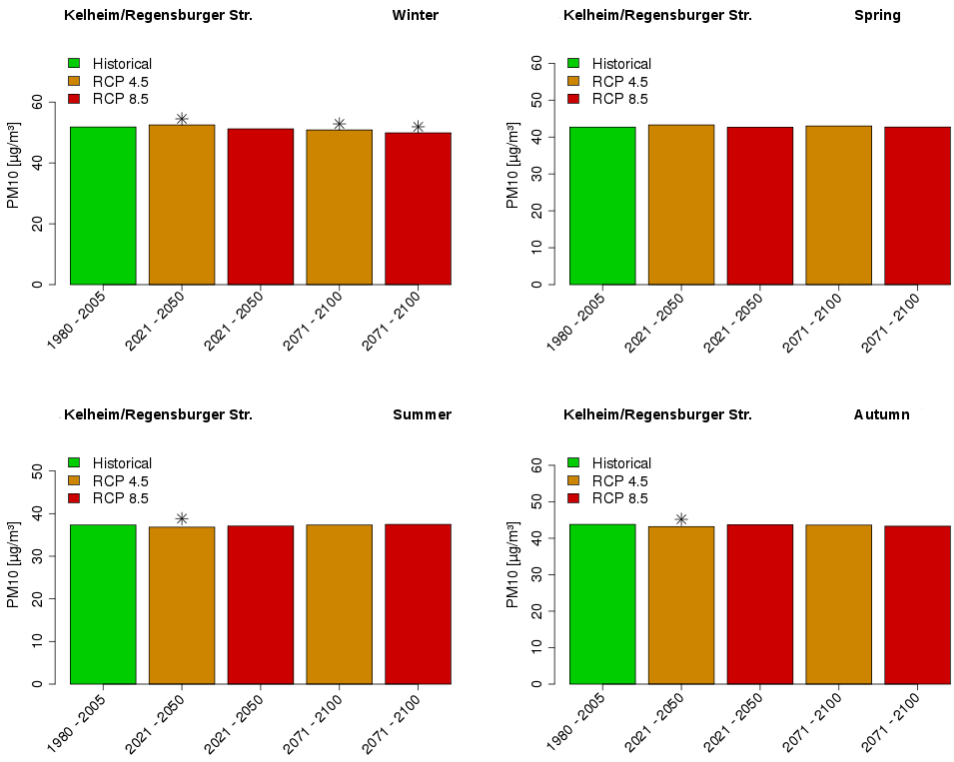


(a) Kelheim

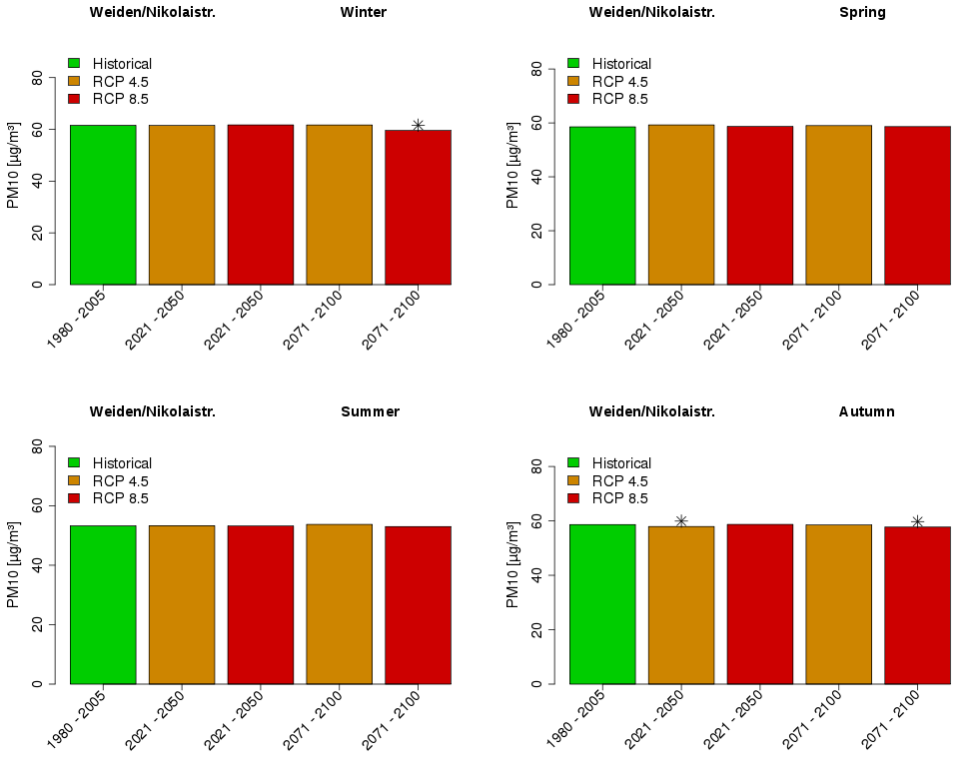


(b) Weiden

Figure 8.3: Modelled seasonal $PM_{mean}$ levels (in $\mu g/m^3$) at station Kelheim Regensburger Str.(a) and Weiden Nikolaistr. (b). Estimations are based on three numerical ensemble members from ECHAM6 scenarios (RCP4.5, RCP8.5) for two time periods (2021-2050, 2071-2100) using four statistical ensemble members and the downscaling approach SD-PMT. Stars mark statistical significance (alpha = 0.05) of differences between particular scenario and historical period.

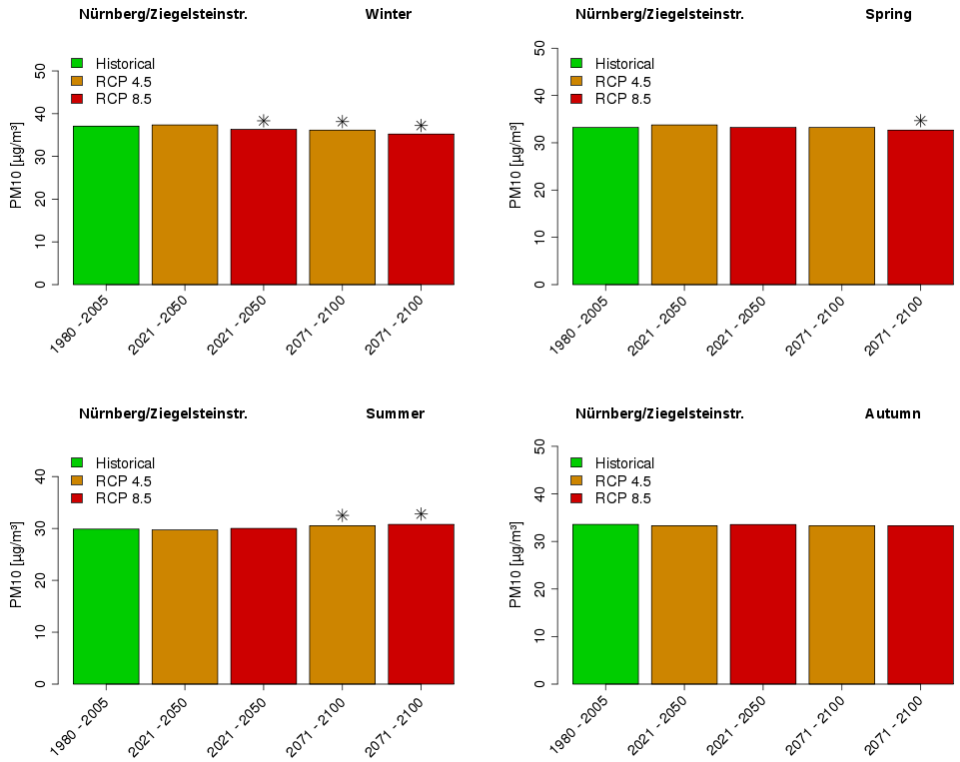


(a) Nürnberg

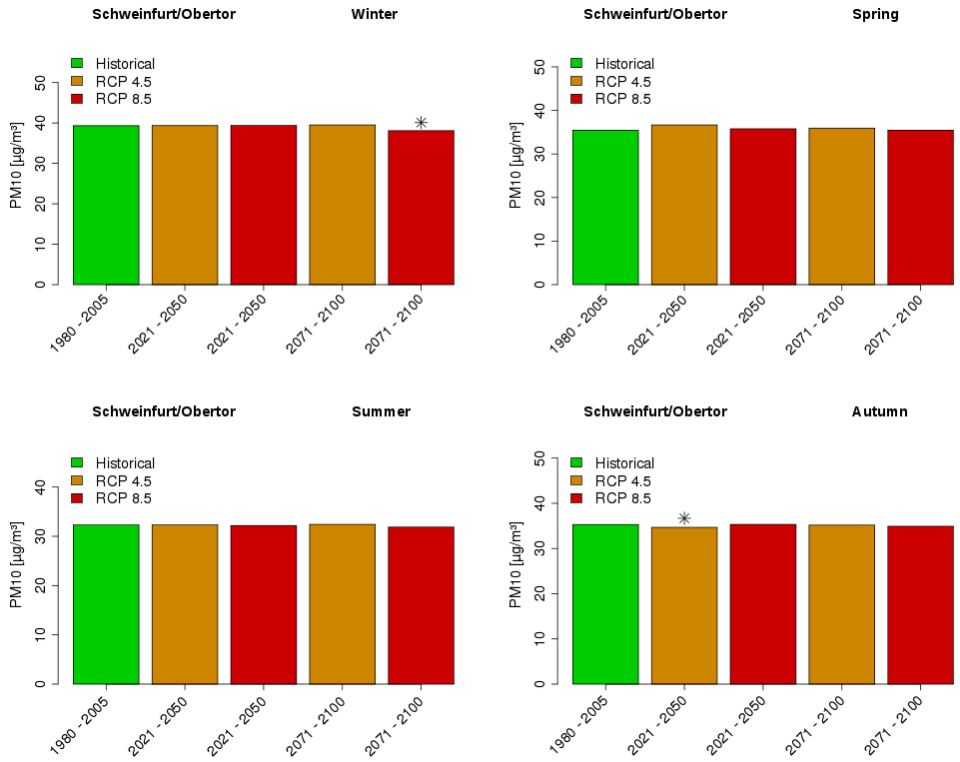


(b) Schweinfurt

Figure 8.4: Same as Figure 8.3 for stations Nürnberg Ziegelsteinstr. (a) and Schweinfurt Obertor (b).

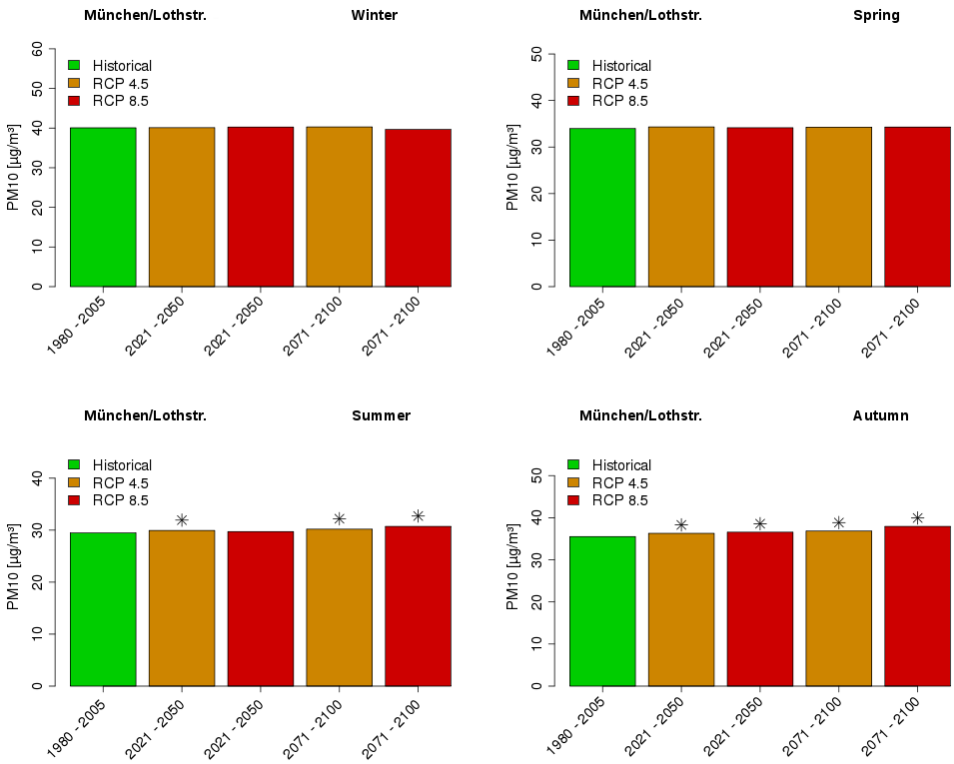


Figure 8.5: Same as Figure 8.3 for station München Lothstr.

Changes in future $PM_{mean}$ levels are less pronounced in the transitional seasons spring (MAM) and autumn (SON)) as Figures 8.3 - 8.5 illustrate. Differences between historical period and scenarios remain in almost all cases insignificant. These findings can be noticed at nearly all stations. Similar conclusions revealed from previous analysis in Chapter 6 and 7: the relationship between the large-scale atmospheric conditions, represented by circulation types, and local particle concentrations are less pronounced in spring and autumn compared to winter for instance.

Barplots indicating estimations of $PM_{mean}$ levels resulting from the downscaling based on Random Forests (RF) (RF-M), using ECHAM6 projections, are shown in Figures 8.6-8.8. Additionally, results for other stations are given in Figures A.16-A.33. Predictions are presented for four seasons and five representative stations. Orange bars depict results for RCP4.5 scenario and red bars for RCP8.5 in two time periods (2021-2050, 2071-2100). $PM_{mean}$ levels for the historical period (1980-2005) are illustrated in green bars.

In general, the estimated changes of $PM_{mean}$ levels modelled by RF-M are more variable compared to results from the SD-PMT approach, as Figures 8.6 - 8.8 depict. In summer for example, RF-M as well as SD-PMT estimated an increase of particle concentrations, but the increase is insignificant in most of the cases and less pronounced for the RF-M.

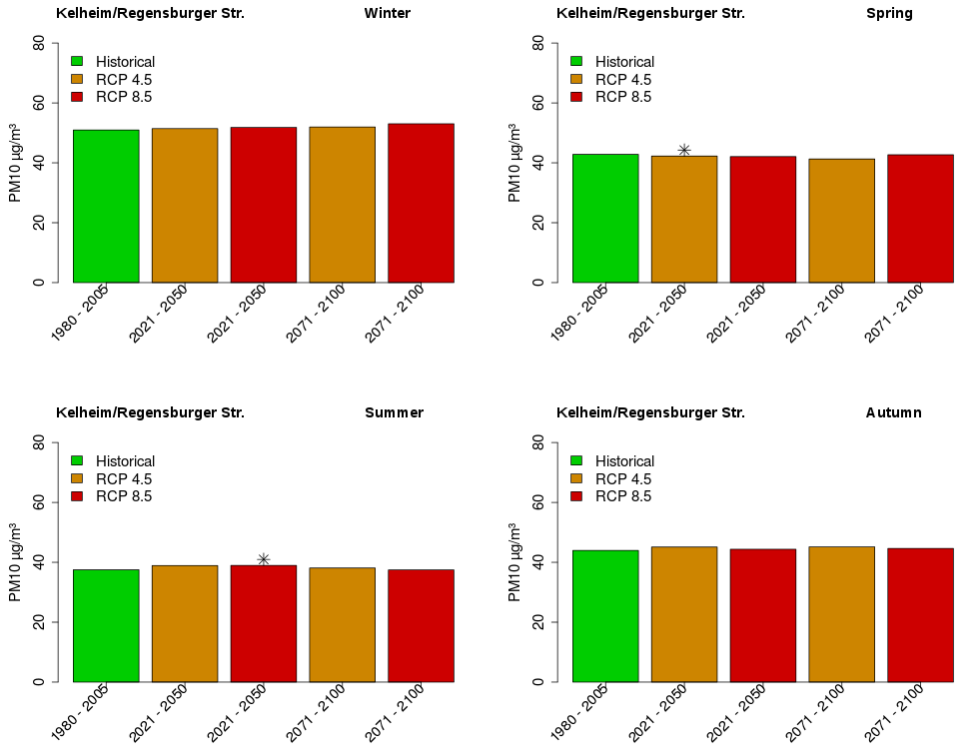


(a) Kelheim

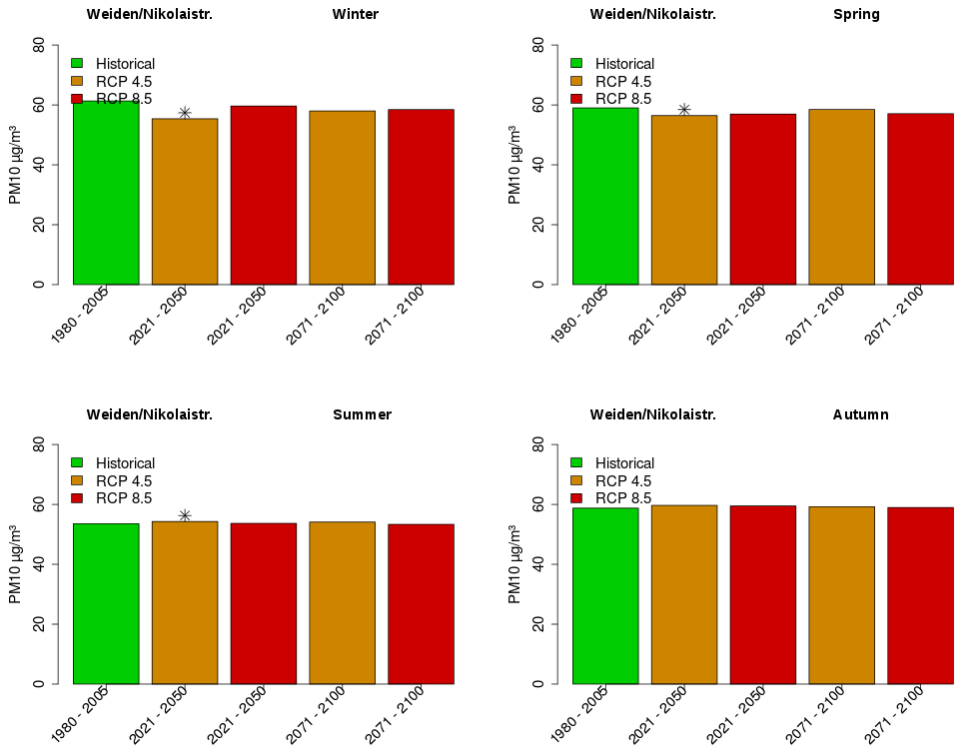


(b) Weiden

Figure 8.6: Modelled seasonal $PM_{mean}$ levels (in $\mu g/m^3$) at stations Kelheim Regensburger Str. and Weiden Nikolaistr. Estimations are based on ECHAM6 scenarios (RCP4.5, RCP8.5) for two time periods (2021-2050, 2071-2100) using Random Forests (RF). Stars mark statistical significance (alpha = 0.05) of differences between particular scenario and historical period.

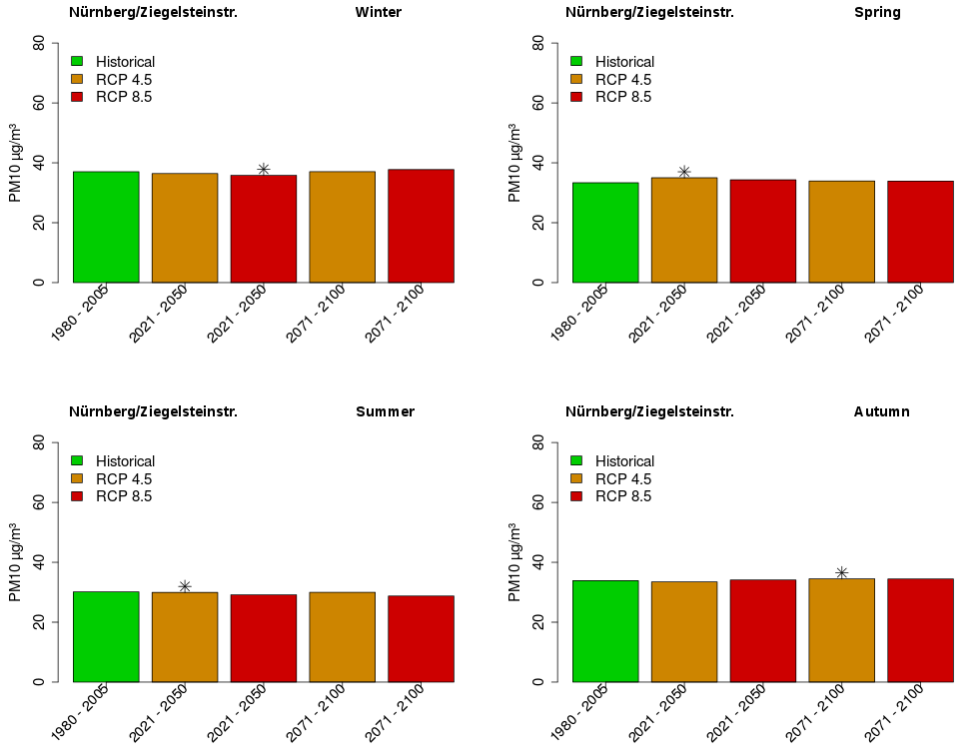


(a) Nürnberg

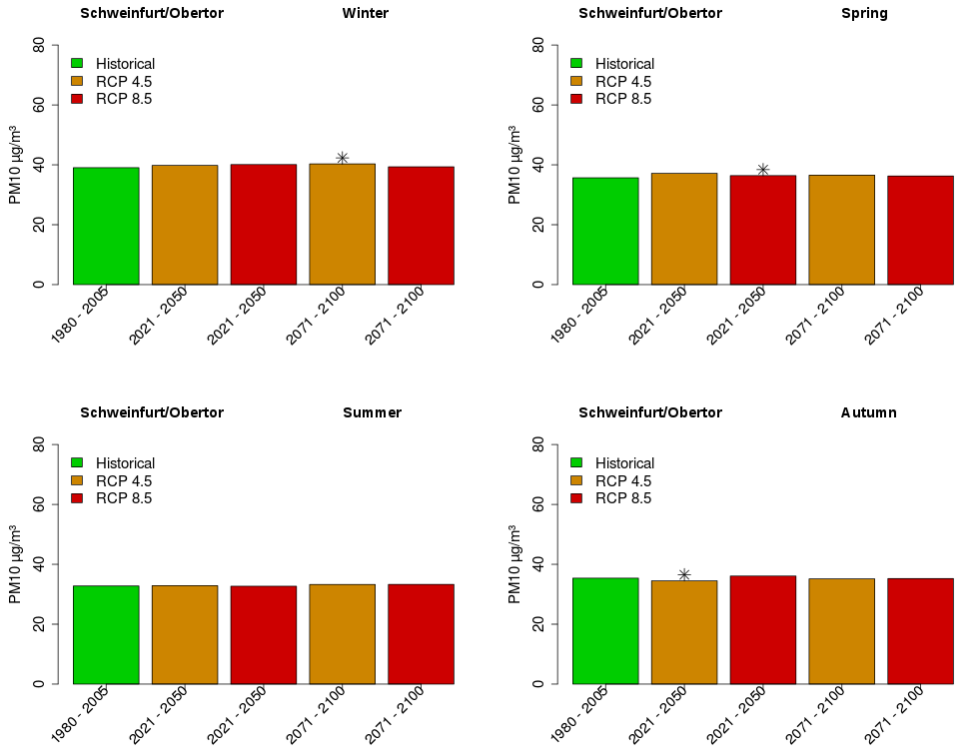


(b) Schweinfurt

Figure 8.7: Same as Figure 8.6 for stations Nürnberg Ziegelsteinstr. and Schweinfurt Obertor.

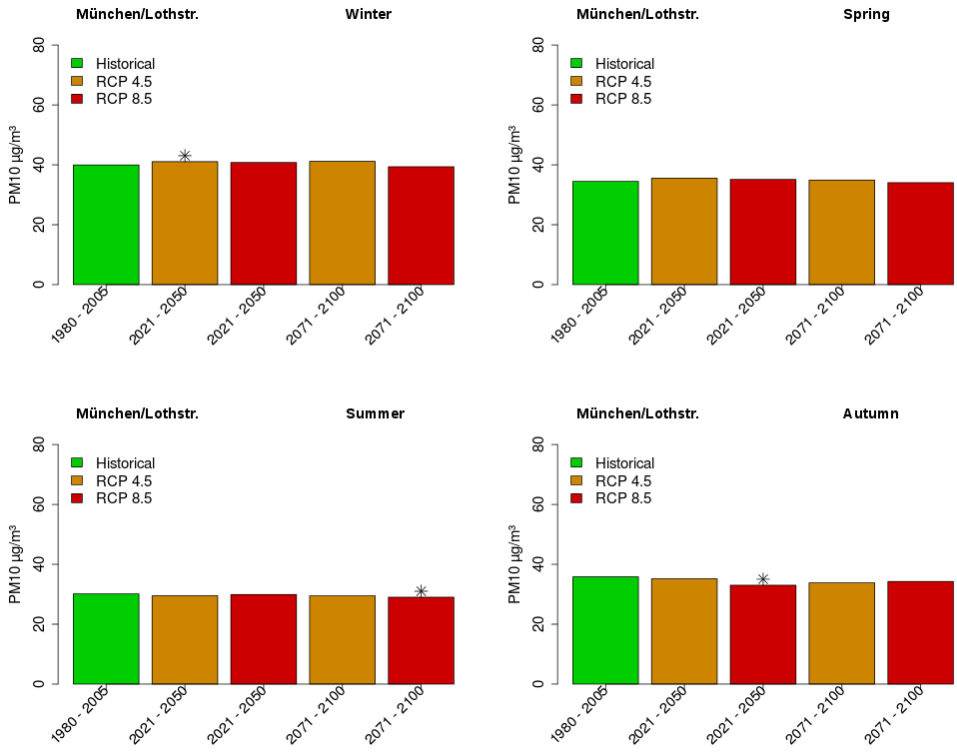


Figure 8.8: Same as Figure 8.6 for station München Lothstr.

In winter, stronger variations of particle levels are predicted by RF-M compared to SD-PMT. $PM_{mean}$ concentrations decrease at nearly all stations until the middle of the century (2021 - 2050). In contrast to the estimations conducted by SD-PMT, the particle concentrations increase at some stations by the end of the century (2071 - 2100). In the transitional seasons, the changing signal of particle levels is indifferent for the RF-M, which is similar to the results for SD-PMT.

### $PM_{50}$ levels

Estimations of future climate-change-induced variations of monthly exceedances of a daily mean $PM_{10}$ value of 50 $\mu g/m^3$ ($PM_{50}$) are shown in Figures 8.9-8.11 for stations Kelheim, Weiden, Nürnberg Ziegelsteinstr., Schweinfurt as well as München Lothstraße. Results for other stations are presented in Figures A.22-A.27. The $PM_{50}$ time series are estimated on the basis of the same model set-up used for modelling $PM_{mean}$. In general, the model skill of downscaling $PM_{50}$ concentrations is usually smaller compared to the skill of downscaling models for estimating $PM_{mean}$ in cross-validation. This has been proven in Chapter 7.

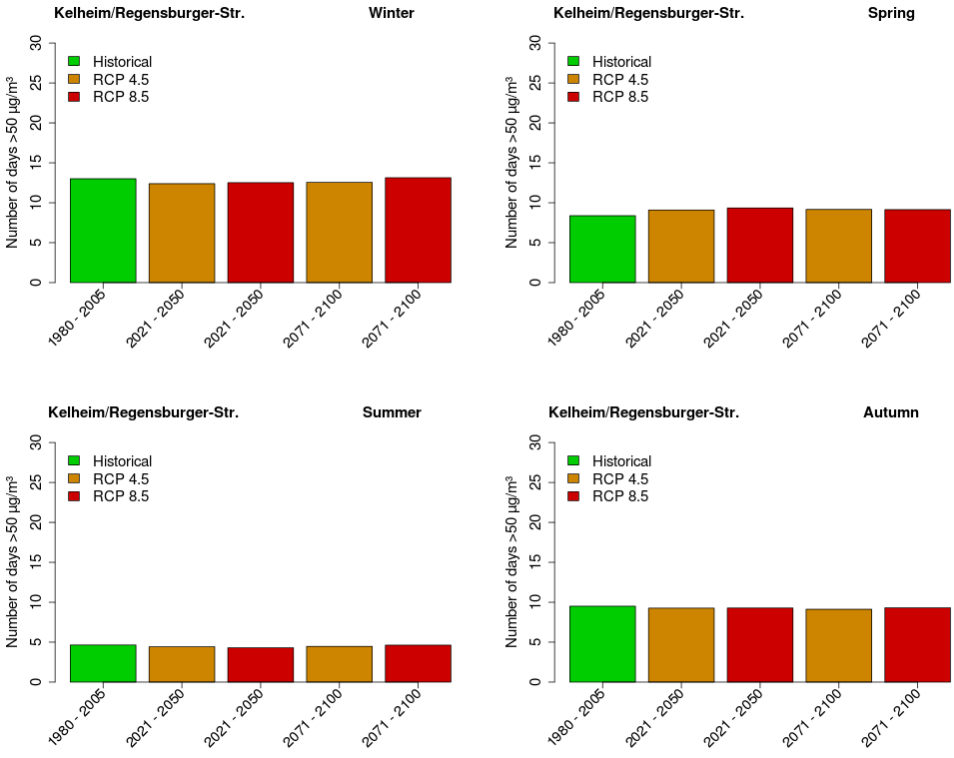


(a) Kelheim

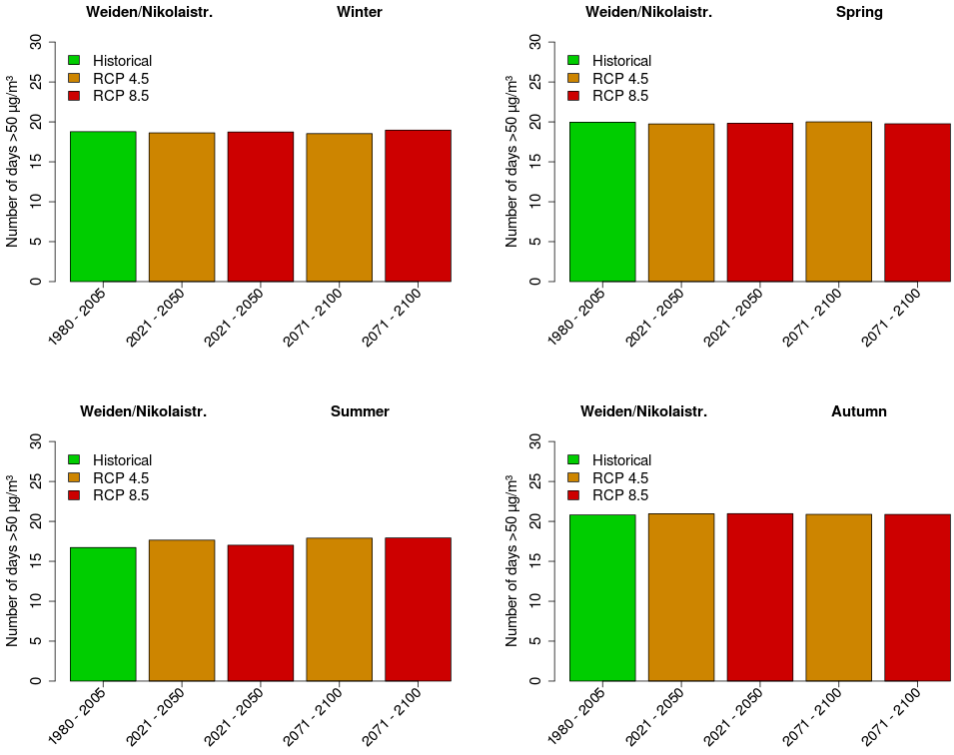


(b) Weiden

Figure 8.9: Modelled seasonal $PM_{50}$ at stations Kelheim Regensburger Str. and Weiden Nikolaistr. Estimations are based on ECHAM6 scenarios (RCP4.5, RCP8.5) for two time periods (2021-2050, 2071-2100) using RF-M. Stars mark statistical significance (alpha = 0.05) of differences between central tendency of particular scenario and historical period.

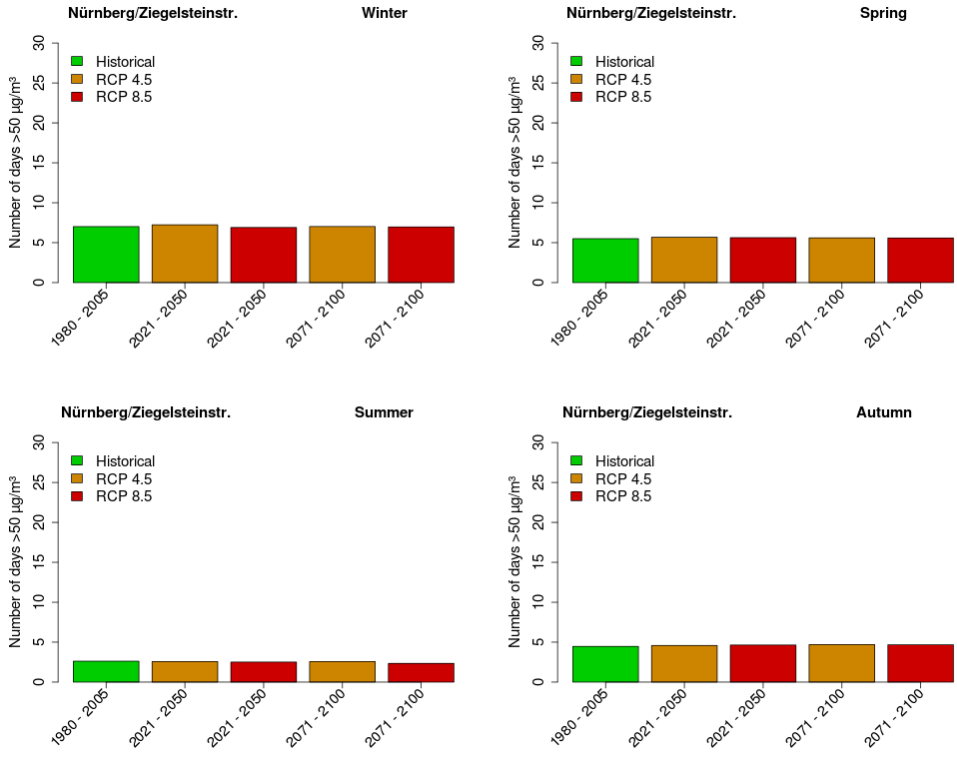


(a) Nürnberg

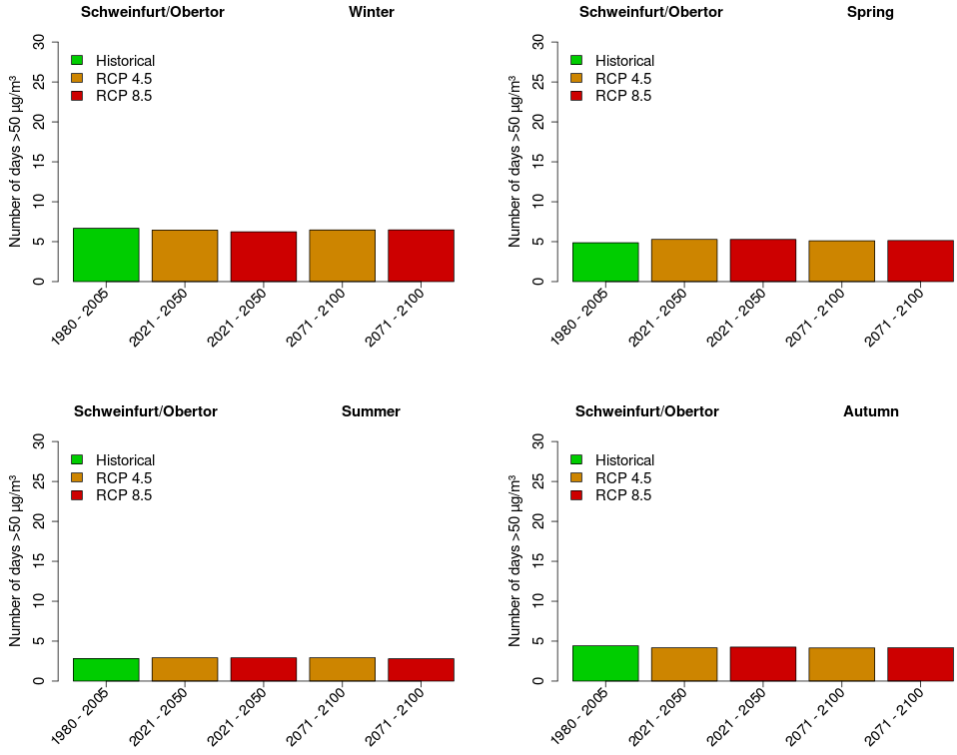


(b) Schweinfurt

Figure 8.10: Same as Figure 8.9 for stations Nürnberg Ziegelsteinstr. and Schweinfurt Obertor.

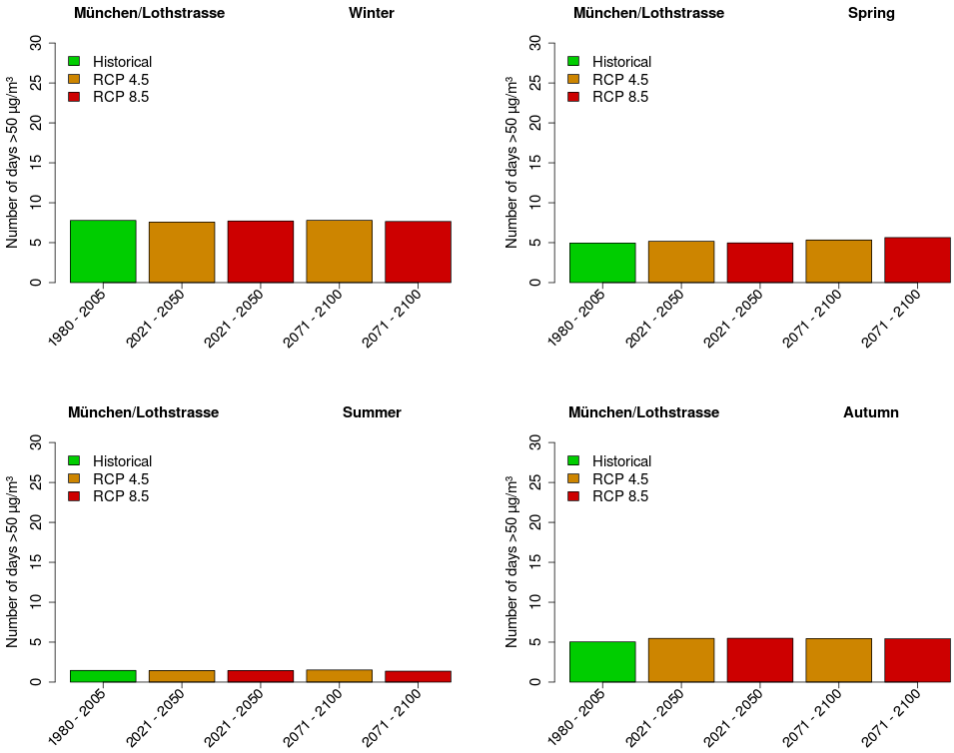


Figure 8.11: Same as Figure 8.9 for station München Lothstr.

Variations of $PM_{50}$ levels are less pronounced compared to $PM_{mean}$ as the figures reveal. Differences between recent and future $PM_{50}$ levels remain insignificant in most of the cases. Possible explanations could be on the one hand the limited performance of the regression-based models to capture higher percentiles and small influences of large-scale atmospheric conditions on this high pollution events on the other hand. Natural and anthropogenic emissions are suspected to cause $PM_{50}$ events in the past as well as in future.

$PM_{50}$ concentrations vary more with the seasons, but the overall seasonal variations are comparably to $PM_{mean}$. An overall decrease of $PM_{50}$ concentrations in winter can be concluded. A possible reason for the decrease of high pollution events in winter months are changes in frequencies of $PM_{10}$ fostering synoptic systems. An increasing frequency of occurrence of western circulation patterns until the end of the century can cause a decrease of high pressure systems, which lead to high pollution events in winter.

However, an increase of $PM_{50}$ events can be observed in summer, but differences between historical period and scenarios are smaller compared to $PM_{mean}$ levels. As it has been previously stated, an increase of high pressure systems over Europe supports high temperatures on a local scale in summer, which can lead to the formation of secondary particles. In the transitional seasons (spring, autumn), the changing signals of $PM_{50}$ levels are rather small.

The application of different emission scenarios, i.e. the moderate RCP4.5 scenario and the stronger RCP8.5, have a variable impact on the predicted levels of $PM_{mean}$ and $PM_{50}$. On the one hand, the differences of estimated particle variations between the two scenarios are comparably small considering the huge differences in the assumptions of the scenarios. On the other hand, differences between predicted $PM_{mean}$ concentrations in the historical period and RCP8.5 are not stronger compared to RCP4.5 as it might be assumed. This is also illustrated in Figures 8.3 - 8.8.

### 8.4.2. Changes in frequencies of occurrence of CTs

Demuzere and van Lipzig (2010b) identified changes in frequencies of occurrence of those large-scale atmospheric patterns favouring high ozone levels as one main effect for variations of the predicted air quality parameter until the end of this century. In this thesis, the effect of changes in frequencies of $PM_{10}$ relevant circulation types on future variations of particle concentrations at Bavarian urban locations are investigated. To this end, changes in frequencies of occurrence of $PM_{10}$ relevant circulation types between a recent period (1980-2005) and future RCP scenarios from ECHAM6 are considered. As it has been shown previously, variations of local particle concentrations occur most distinctly in winter and summer in Bavaria. Hence, the frequency changes are primarily discussed for these two seasons.

In the recently published Climate Report by the Bavarian government, changes in the frequencies of occurrence of weather patterns over Bavaria between the observational period 1991-2000 and climate change scenarios until the end of this century have been briefly discussed (StMUV, 2015). An increase of western cyclonic patterns in winter, with increasing humid conditions due to the transport of maritime air masses, have been estimated for the period 2071-2100. Eastern high pressure patterns in contrast, which are connected to cold, dry weather conditions in winter, have been predicted to occur less frequent. In summer, a decrease of western cyclonic patterns, which lead to humid conditions in summer, and an increase of anticyclonic high pressure patterns have been modelled.

In Figure 8.12, relative differences (in %) of frequencies of 18 Circulation Types (CTs) in winter (DJF), resulting from the best performing classification at station Kelheim, are illustrated as one example. The selected classification comprises a large-scale atmospheric variable combination of geopotential height in 500 hPa, specific (in 1000 hPa) and relative humidity (in 850 hPa). To this end, future changes of CTs are discussed on the basis of the geopotential height field and associated mean sea level pressure fields near the surface.

Differences are calculated between the ensemble means in historical period and scenarios RCP4.5 (blue) and RCP8.5 (red) in two time periods (2021-2050, 2071-2100). In order to assess, whether these differences are significant over all types for a season, a $\chi^2$ test (chi-square goodness of fit test) is applied for a significance level of alpha = 0.05. Bahrenberg et al. (1999), for example, describe the calculation of the test statistic as

$$\chi^2 = \sum_{i=1}^{k} \frac{(BH_i - TH_i)^2}{TH_i}. \tag{30}$$

$k$ is the number of classes in a sample, $BH_i$ is the number of observations of type i and $TH_i$ the theoretical frequency of type i, if the null hypothesis is valid.

In general, differences in overall frequency distributions between all scenarios in two time steps and historical periods of circulation types from ECHAM6 data remain insignificant.

Type 4 for instance, illustrated in Figure 8.13 (a) as composite of geopotential heights in 500 hPa, is a cold air trough with a north-western air mass flow near the ground over the target region. It appeared quite often in winter in the period 1980-2005 and is connected to comparably small mean $PM_{10}$ concentrations of around 40 $\mu gm^3$. The frequency of type 4 increases in all scenarios and time steps in winter. This might lead to decreasing particle levels in winter as western patterns are known to be connected to air mass exchanges with transportation of particles.

Circulation type 11 in contrast, which is linked to relatively high mean $PM_{10}$ concentrations of around 65 $\mu gm^3$, did not appear quite often in the past in winter months. The pattern is a high ridge in 500 hPa (see Figure 8.13 (b)) with a high pressure component near the surface in the target region. Its frequency decreases especially by the end of the century (2071 - 2100) for both scenarios.

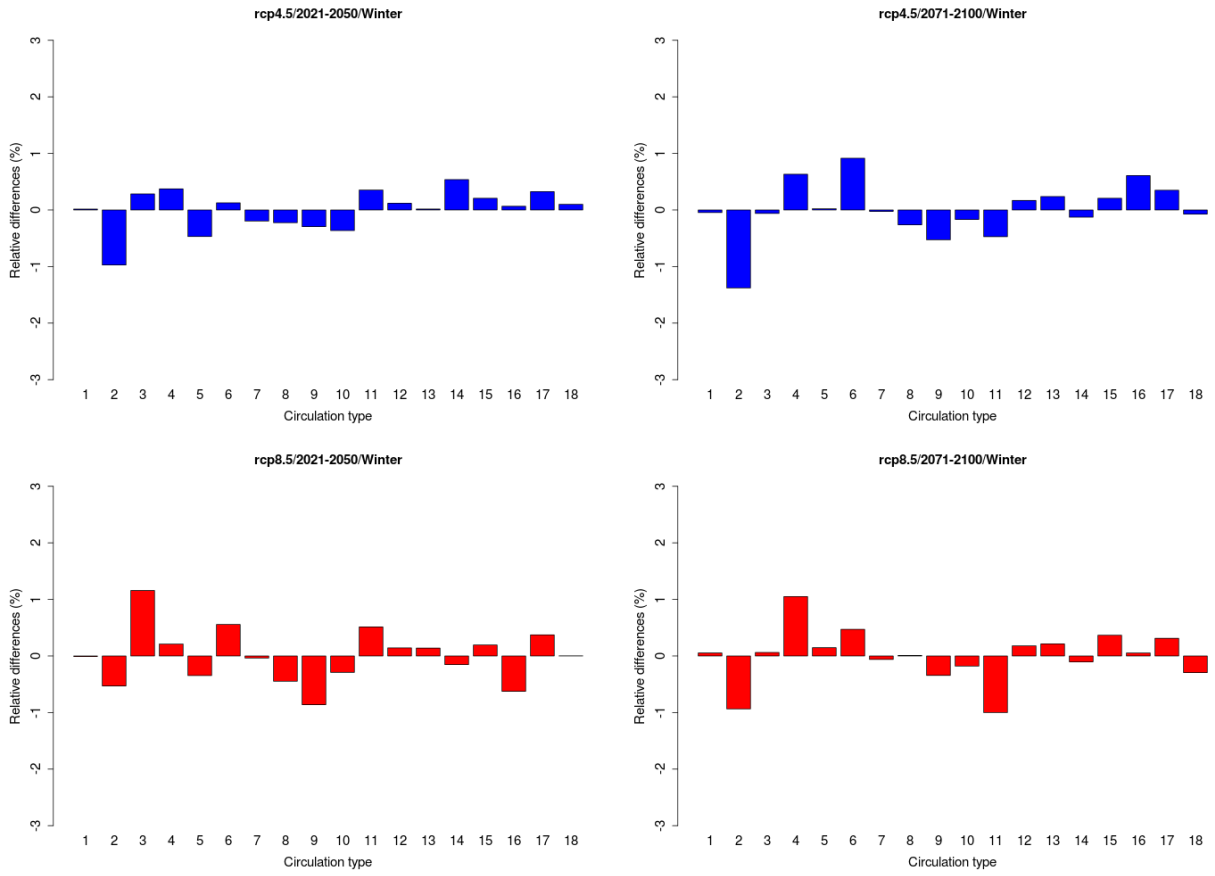


Figure 8.12: Relative differences (in %) between frequencies of occurrence of 18 circulation types from the best performing classification at station Kelheim in winter for ensemble means in historical period (1980-2005) and projections from ECHAM6. Scenarios are RCP4.5 (blue) and RCP8.5 (red) in two time periods of 2021-2050 and 2071-2100.

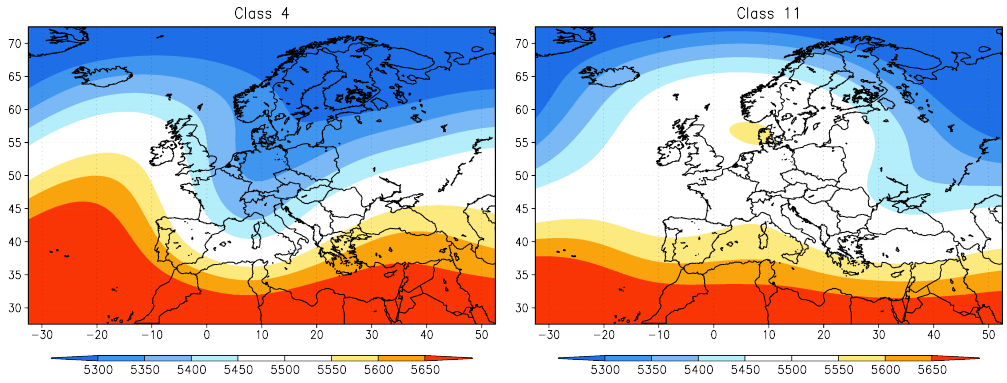


(a) Class 4 (b) Class 11

Figure 8.13: Composites of geopotential height fields in 500 hPa for type 4 (left) and type 11 (right) of best performing classification at station Kelheim in winter.

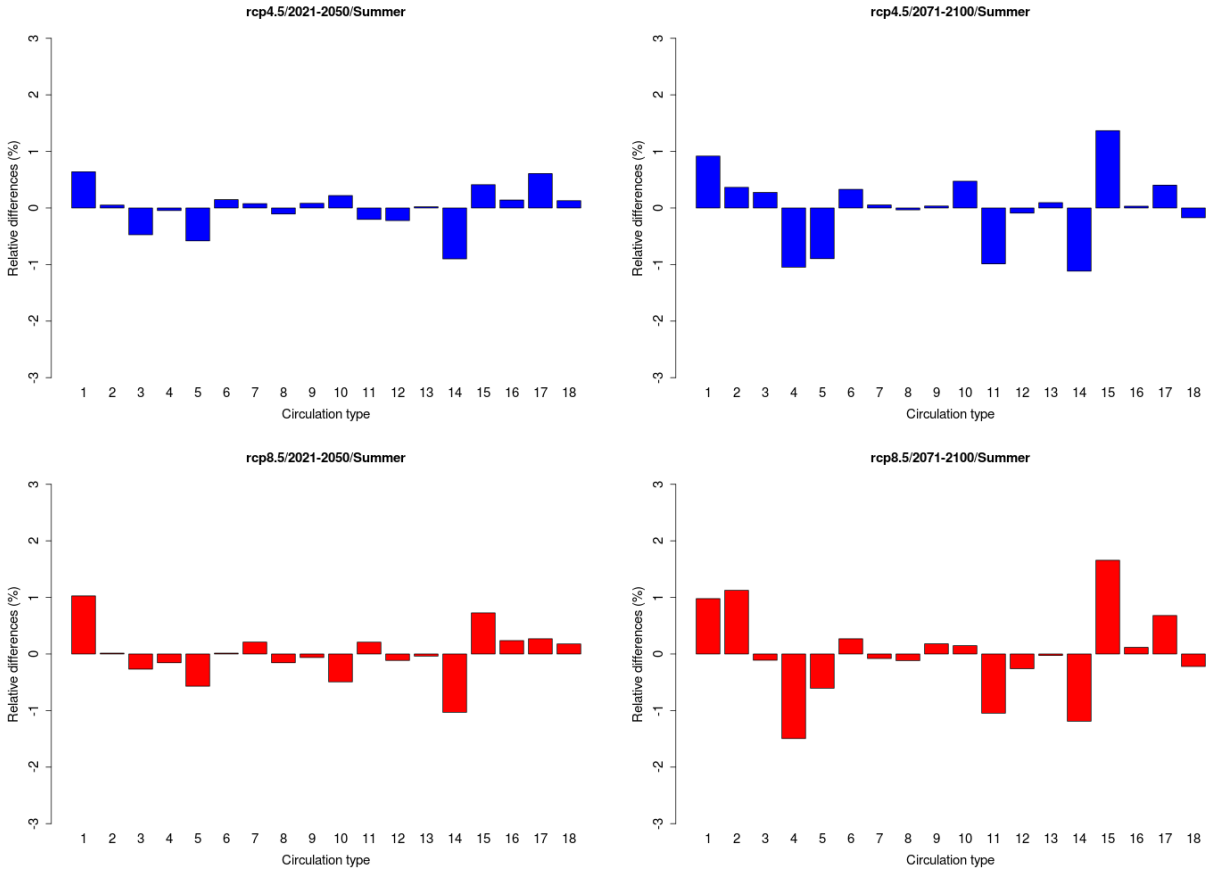


Figure 8.14: Relative differences (in %) between frequencies of occurrence of 18 circulation types from the best performing classification at station Kelheim Regensburger Str. in summer for ensemble means in historical period (1980-2005) and projections from ECHAM6. Scenarios are RCP4.5 (blue) and RCP8.5 (red) in two time periods 2021-2050 and 2071-2100.

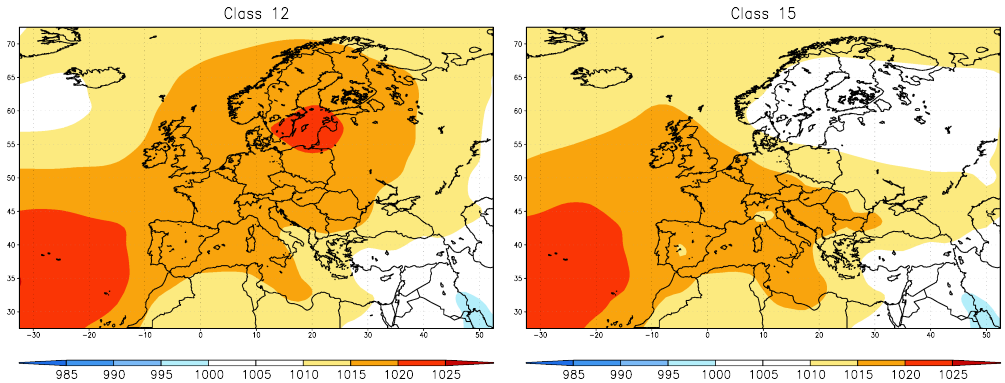


(a) Class 12 (b) Class 15

Figure 8.15: Composites of mean sea level pressure for type 12 (left) and type 15 (right) of the best performing classification at station Kelheim in summer.

The summer situation at Kelheim is depicted in Figure 8.14. Geopotential heights in 500 hPa, specific humidity in 1000 hPa and zonal wind component in 500 hPa are included in the best performing classification. The $\chi^2$ test revealed no significant changes in frequencies of the 18 CTs. Type 12, which appeared most frequent in the past and is related to relatively high mean particle concentrations of around 48 $\mu$gm$^3$, represents a high pressure ridge over Europe between the Baltic states and the Azores. It is connected to stable conditions with nearly no air mass exchange in Bavaria. Hence, particles can accumulate. Higher temperatures near the surface can foster the formation of secondary particles, additionally. The composite of mean sea level pressure of this pattern is shown in Figure 8.15 (a). As relative differences in Figure 8.14 illustrate, only small changes emerge for this type until the end of the century.

Regarding type 15, however, distinct relative differences can be observed, especially for the scenarios in the second time period 2071-2100. This high pressure ridge over the Azores, which is shown in Figure 8.15 (b) as mean sea level pressure composite, is associated to mean $PM_{10}$ concentrations of around 33 $\mu$gm$^3$.

The high pressure ridge involves sunny conditions in Bavaria with relatively high local temperatures as well, which leads to the previously described consequences for particle transport and formation. The increase of high pressure ridges on the one hand and little changes in frequencies of occurrence of other high pressure ridges might be the reason for increasing particle levels in summer discussed in the previous Section 8.4.1.

The analysis of $PM_{10}$ relevant circulation types from best performing classifications at other measurement sites revealed similar results. $PM_{50}$ are almost entirely influenced by high pressure systems in winter and summer. As detected changes in estimated $PM_{50}$ concentrations in previous Section 8.4.1 illustrated, these high pollution events seems to be driven by high emissions rather than from climate-change-induced variations of the synoptic situation.

### 8.4.3. Estimations of particle levels from different climate models

In order to verify the estimated particle levels from the ECHAM6 model, a comparison of future $PM_{mean}$ concentrations assessed from ECHAM6 and EC-Earth model runs is presented in the following. A brief description of the EC-Earth model is given in Chapter 3. Due to limited access of model realizations from EC-Earth, only one model run for a few large-scale atmospheric variables could be used for the application in the intended analysis. 18 circulation types resulting from best performing seasonal classifications averaged over all stations are used for the predictions, not the best performing classifications at each station applied in the previous analysis. The reason for that

is the limited availability of large-scale atmospheric parameters from EC-Earth.

In Figure 8.16, barplots illustrate estimated $PM_{mean}$ levels at station Kelheim (a) and Nürnberg Ziegelsteinstr. (b) in winter and summer from RF models performed with EC-Earth (left) and ECHAM6 (right). Stars mark statistical significance (alpha = 0.05) of differences in central tendency between historical runs (1980 - 2005) in green and two scenarios RCP4.5 (orange) and RCP8.5 (red) in two time periods (2021 -2050, 2071-2100) tested with a Mann-Whitney-Test. In general, estimated changes of particle levels are less pronounced and more variable for the RF models using EC-Earth data. A possible explanation could be the usage of circulation types from best performing classifications averaged over all stations and not the specific classification ascertained for each season and station separately. In winter for example, only decreasing $PM_{mean}$ concentrations at station Kelheim are significant. In summer months, the stated signal of increasing particle levels from previous analysis is also relatively small at both stations shown in Figure 8.16. Results for other stations from EC-Earth based estimations are given in Figures A.28-A.33.

As results of $PM_{mean}$ concentrations from the application of circulation types in SD-PMT models in Figure 8.17 indicate, which are assigned to ECHAM6 and EC-Earth data, a stronger changing signal of particle levels can be concluded for the ECHAM6 data. Increasing particle concentrations are less pronounced for EC-Earth-based estimations. One reason for that fact might be the limited availability of EC-Earth model realizations or less pronounced climate change signals in the data.

In order to achieve robust statements from the estimation of future climate-change-induced variations of $PM_{10}$ concentrations in Bavaria from climate models, an application of the circulation-type-based downscaling models should be conducted with a multi-model ensemble from models of the CMIP5 for instance. As results presented in this Section revealed, no distinct changing signals until the end of this century could be concluded by the comparison of only two models. The limited access of data from the EC-Earth model enabled some exploratory analysis, which should be extended to achieve robust statements from model comparison.

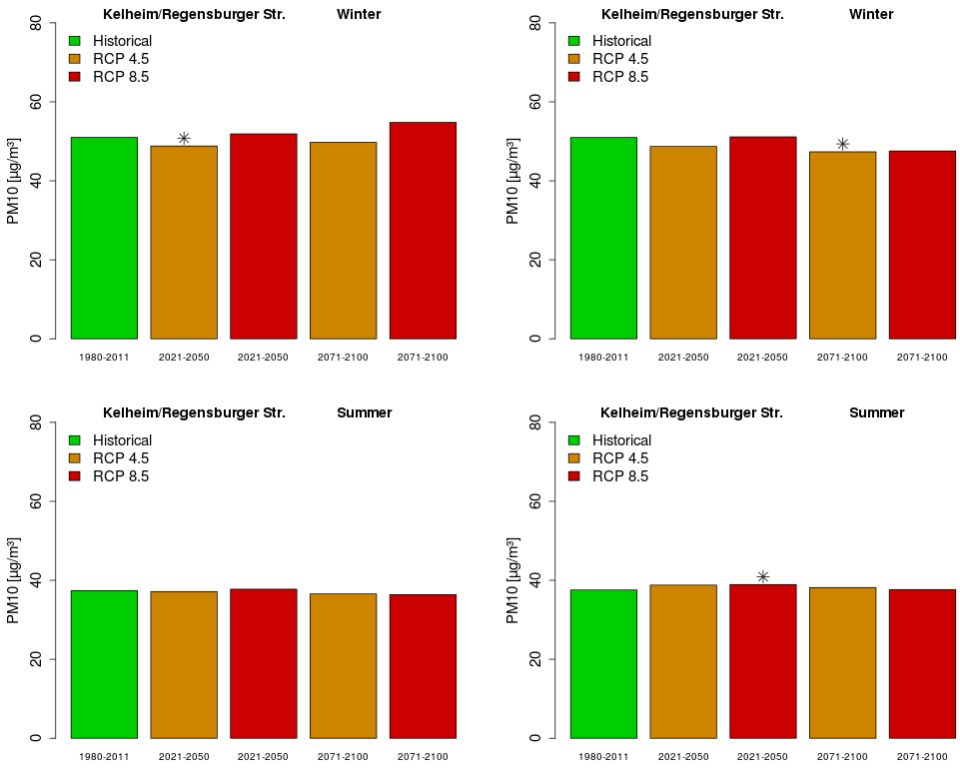


(a) Kelheim

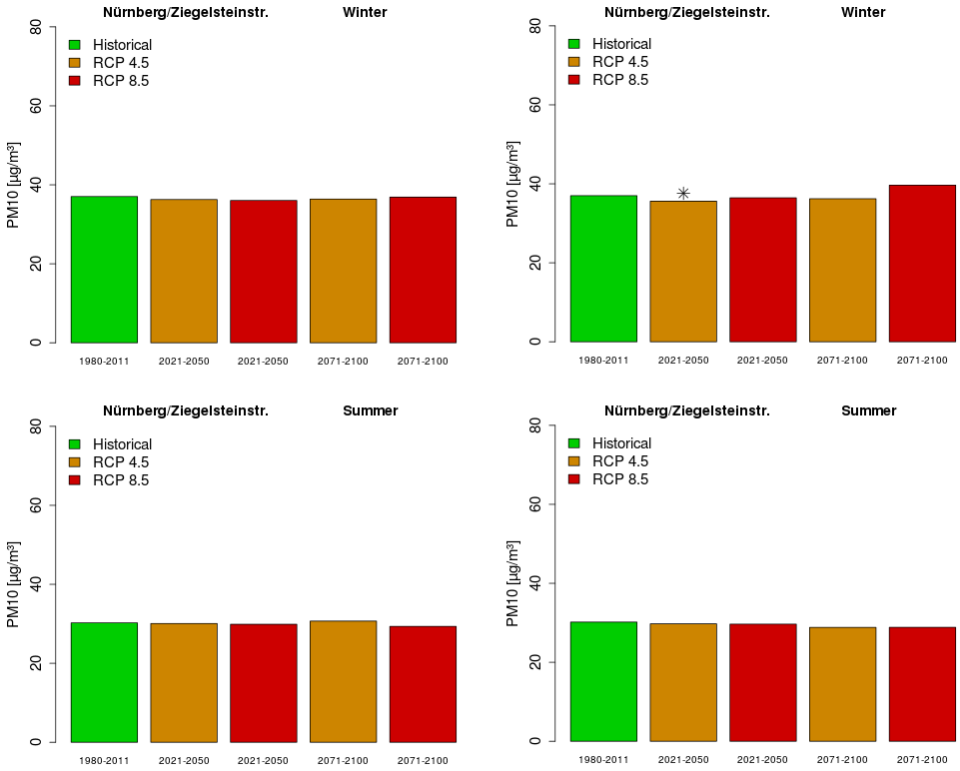


(b) Nürnberg

Figure 8.16: Modelled seasonal $PM_{mean}$ at stations Kelheim and Nürnberg Ziegelsteinstr. Estimations are based on one run of EC-Earth (left) and ensemble mean of ECHAM6 (right) for two scenarios (RCP4.5, RCP8.5) in two time periods (2021-2050, 2071-2100) using RF-M for winter and summer. Stars mark statistical significance (alpha = 0.05) of differences between central tendency of particular scenario and historical period.

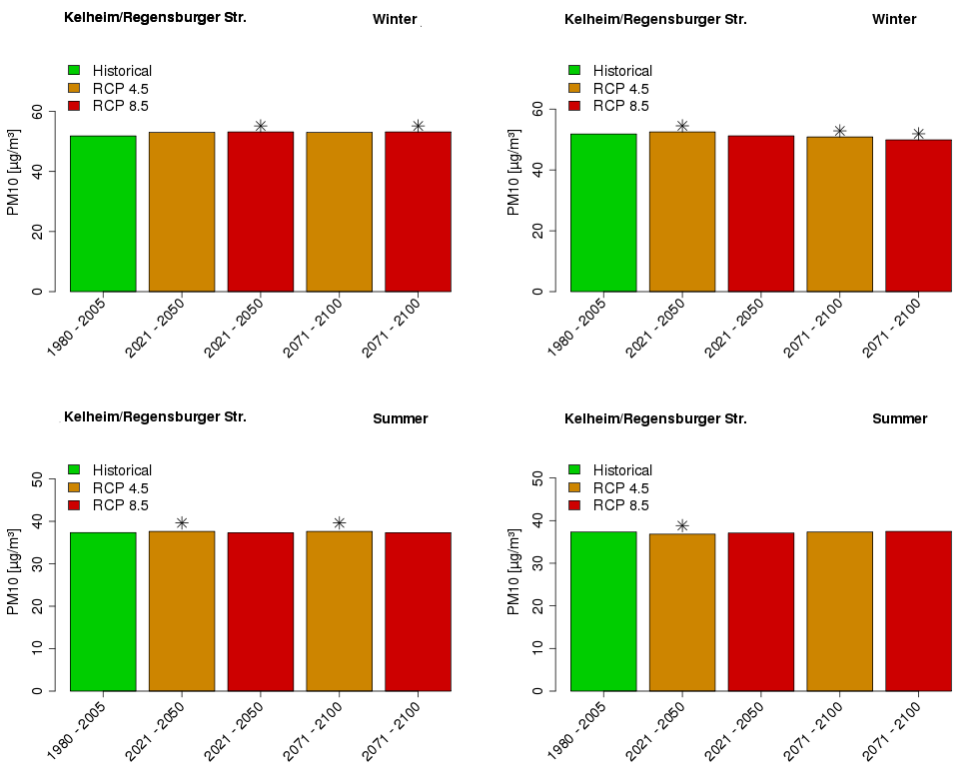


(a) Kelheim

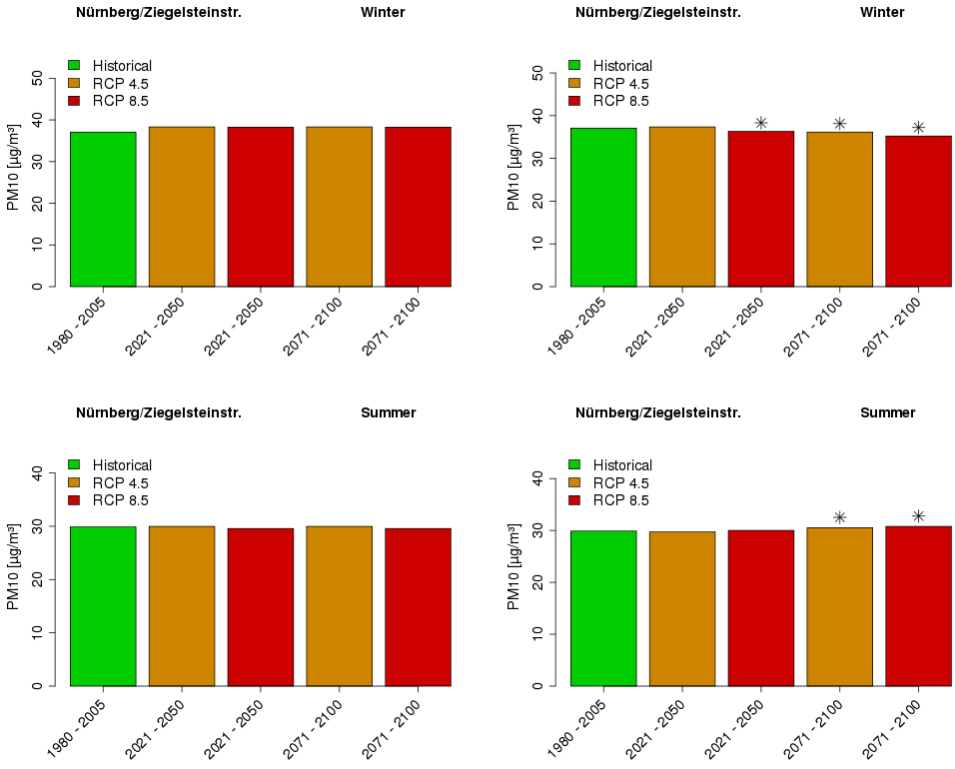


(b) Nürnberg

Figure 8.17: Same as Figure **??** for SD-PMT.

## 8.5. Summary

In this Chapter, most suitable circulation-type-based downscaling models, which have been developed according to highest model skill in cross-validation in this thesis, are used to estimate future climate-change-induced variations of monthly $PM_{10}$ concentrations. To this end, objective circulation type classifications for each season and each station, that have been optimized with respect to their synoptic skill for the target variable $PM_{10}$ in Chapter 6, are assigned to gridded large-scale atmospheric fields from Global Climate Model data (ECHAM6, EC-Earth). For that purpose, model data for two scenarios (RCP4.5, RCP8.5) in two time periods (2021-2050, 2071-2100) as well as in a control period of 1980 to 2005 (historical runs) are considered. Resulting circulation types are applied as predictors in Synoptic Downscaling and Random Forest Models to estimate monthly mean $PM_{10}$ concentrations ($PM_{mean}$) and monthly exceedances of a daily mean $PM_{10}$ value of 50 $\mu g/m^3$ ($PM_{50}$) levels (predictands) at 16 measurement sites in Bavaria.

In order to take potential model biases, resulting from climate models and downscaling approaches, into account, numerical ensembles are utilized from three runs of ECHAM6 on the one hand. On the other hand, statistical ensembles are regarded from varying subintervals of the 1980-2011 period as 20-year calibration and 11-year validation periods. Furthermore, a bias correction proposed by Cheng et al. (2007b) has been applied on the modelled $PM_{10}$ time series. The bias correction takes differences between the downscaled $PM_{10}$ distribution quantities from the General Circulation Model (GCM) and observed $PM_{10}$ distribution quantities into account (Demuzere and van Lipzig, 2010b).

Results from the estimation of differences of $PM_{mean}$ and $PM_{50}$ levels between the historical period and scenario periods have been discussed for selected measurement sites. Significant changes of the central tendency of the modelled time series have been tested with a Mann-Whitney-test. Changes in frequencies of occurrence of particle fostering synoptic situations until the end of this century have been presented afterwards. Furthermore, estimated $PM_{mean}$ levels from ECHAM6 and EC-Earth-based models have been compared in this Chapter.

In summary, the assessment of future climate-change-induced variations of monthly $PM_{10}$ levels revealed mostly decreasing concentrations in winter and increasing ones in summer. Changes are more variable and less pronounced in the transitional seasons spring and autumn. Differences in estimations occur between considered scenarios and time steps and statistical ensemble members. Furthermore, differences in the results appear between the stations. As a possible reason for this less pronounced consistency of the estimations, a relevant internal variability of the circulation-types, which are used as predictors, could be assessed, which are suspected to remain although the

CTC have been optimized in previous steps.

The decrease of particle levels in winter in Bavaria could be explained by an increase of zonal, cyclonic circulation patterns until the end of the century over Europe. These synoptic situations, which are connected to relatively low $PM_{10}$ levels, are characterized by humid conditions and a frequent change of air masses. Hence, the wet deposition or transport of particles might be potential consequences. In summer, decreasing frequencies of occurrence of these zonal, cyclonic types have been detected together with an increase of anticyclonic high pressure systems. Consequently, events fostering high temperatures near the surface in the target region could lead to the formation of secondary particles for instance and thus increasing particle levels in the future. The detected changes in frequencies of occurrence of $PM_{10}$-relevant synoptic situations in Bavaria are in accordance to modelled variations of circulation patterns published in the recent Climate Report of the Bavarian government (StMUV, 2015).

The comparison of estimated $PM_{mean}$ concentrations from statistical models based on two different climate models ECHAM6 and EC-Earth revealed similar tendencies of future variations in winter and summer. Due to limited access of data from the EC-Earth model, including only one realisation for a small selection of large-scale atmospheric parameters, it was not possible to consider the best performing circulation type classifications for each season and each station in the downscaling models. Consequently, the best performing classification averaged over all stations for one season has been considered leading to less pronounced changing signals for future $PM_{mean}$ and $PM_{50}$.

# 9. Comparison of two quantitative approaches for estimating future daily $PM_{10}$ concentrations

A broad range of local meteorological variables has been detected by several studies to have an influence on particle concentrations. A literature review on this topic is presented in Chapter 2. Depending on the landscape or exposition of the target region, the layout of the street canyon and locations of the measurement sites for example, the set of local meteorological parameters having an influence on local particle levels vary. Kiesewetter et al. (2015) for example have found atmospheric mixing conditions in the boundary layer to play an important role on local air pollution levels in major European cities. Seasonal differences of local meteorological influences on $PM_{10}$ have been ascertained by Demuzere et al. (2009) for several stations in Netherlands. Precipitation for instance has been detected to be negatively correlated to particle concentrations in winter as well as wind speed over the whole year. In German cities, relative humidity, temperature and wind have been detected to have a remarkable influence on $PM_{10}$ levels by Gietl and Klemm (2009) or Kuttler (2011a). According to Schäfer et al. (2006) or Schäfer et al. (2014), the mixing layer height as well as wind speed have an important influence on local $PM_{10}$ concentrations in German cities.

In the framework of the project "Particulate matter and climate change in Bavaria" (PACLIMBA), funded by the German Research Foundation (DFG), quantitative relationships between daily and monthly $PM_{10}$ concentrations at different Bavarian measurement sites and the corresponding large-scale atmospheric conditions as well as local meteorological variables are established by statistical downscaling models. As it has been discussed in Chapter 7 of this thesis, statistical downscaling techniques, based on large-scale atmospheric circulation types as predictors, are not able to model daily exceedances of critical daily particle levels (Synoptic Downscaling) or are not suitable to model daily $PM_{10}$ concentrations at all, which is the case for the regression-based downscaling techniques (Multiple Linear Regression Analysis (MLR), Generalized Linear Model (GLM), Random Forests (RF)).

Transfer models using local meteorological parameters as predictors have been developed for four seasons and 19 Bavarian $PM_{10}$ stations as an alternative for the assessment of daily particle levels in the project (Beck and Jacobeit, 2015). Objective circulation type classifications, generated in this thesis, are integrated into the local transfer models as well. The main goals of these models are to gain a powerful method for prediction and variable importance quantification by computing marginal effects of each meteorological variable on the $PM_{10}$ concentrations. Furthermore, the identification of the most influential local meteorological parameters is investigated (Beck and Jacobeit, 2015).

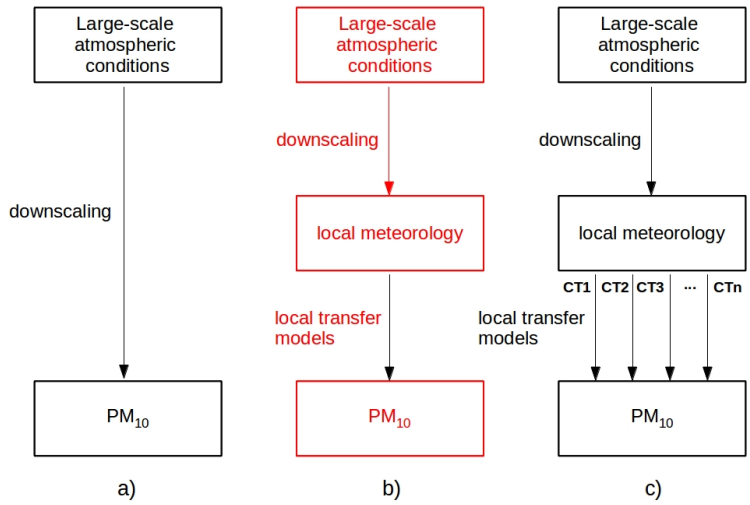


Figure 9.1: Same as Figure 1.2. In variant (b), marked in red, local meteorological predictors are downscaled from objective circulation type classifications and applied in transfer models to predict particle levels.

In Figure 9.1, the concepts of three statistical downscaling approaches, applied in the project, are depicted. Results from the estimation of daily and monthly $PM_{10}$ indices, using objective circulation type classifications as predictors in seasonal downscaling models, which have been optimized with respect to their synoptic skill for the target variable $PM_{10}$, are presented in Chapter 6 - 8 of this thesis. The general proceeding is depicted in Figure 9.1 (a). Concerning the other approaches, which are illustrated in Figure 9.1 (b) - (c), daily $PM_{10}$ concentrations are assessed by regression-based transfer models using local meteorological variables as predictors, which themselves are downscaled from the large-scale atmospheric conditions. All downscaling approaches have been evaluated via cross validation using varying subintervals of the 1980-2011 period as calibration and validation periods, respectively. The most suitable downscaling procedures, defined in terms of model skill determined from cross validation, are finally applied to CMIP5 climate model data for the large-scale atmospheric conditions in the future.

As it has been shown by Demuzere and van Lipzig (2010a) for example, the skill of the local transfer models could increase by developing and applying these models for each specific circulation type separately. This approach is conducted in the PACLIMBA project as well (see Figure 9.1 (c)). For this purpose, circulation-type-based local transfer models are generated and evaluated with respect to their model skill in two variants. First, the models are considered for each circulation type of an optimized classification separately and second, Circulation Types (CTs) are aggregated into groups, e.g. CTs connected to particle concentrations above average. The statistical-functional

link between these local meteorological predictors and the target variable $PM_{10}$ are calculated using the same statistical methodology as in the downscaling variant 1.2 (b). No systematic improvement of the model skill has been identified for transfer models based on separate CTs (Beck and Jacobeit, 2015). However, the model skill increases by combining CTs into $PM_{10}$-fostering, $PM_{10}$-indifferent and $PM_{10}$-reducing synoptic situations, which have been considered as additional exploratory variables. Modelling results from the second approach 9.1 (b) (marked in red) are mainly compared and discussed with results from the first attempt 9.1 (a) in this Section.

This Chapter is structured as follows. First, a brief introduction of the model set-up of the downscaling models using local meteorological predictors are given in Section 9.1. Secondly, results of the different models are discussed with respect to selected large-scale and local meteorological predictors in Section 9.2.1 as well as model skill of the validation in Section 9.2.2. A comparison of estimated future particle levels are presented in Section 9.2.3. This Chapter ends with a summary in Section 9.3.

## 9.1. Downscaling models including local meteorological variables

In order to identify those meteorological parameters on a local to regional scale, which have a distinct impact on $PM_{10}$ concentrations in the target region Bavaria, a comprehensive set of variables has been used in the project PACLIMBA (Beck and Jacobeit, 2015). The selection of potential predictors for the intended analysis is based on the one hand on parameters, which have been found to have an influence on particle concentrations in existing studies (see Chapter 2). These are for instance temperature measures or wind parameters. On the other hand, a preferably broad range of possible predictors, in dependence of data availability for the selected period 1980-2011, have played a major role. The used data are provided by the DWD and NCEP/NCAR reanalysis project (Kalnay et al., 1996; Kistler et al., 2001). The NCEP/NCAR reanalysis data is described in Chapter 3.2 as well as a brief introduction into the DWD data set.

In a first step, a correlation analysis has been performed using the comprehensive set of meteorological variables to select significant predictors for the intended application in the local transfer models (Beck and Jacobeit, 2015). Results from the seasonal predictor screening are compared to large-scale atmospheric variables mainly occurring in best performing objective CTC in the following Section 9.2.1.

CTs, resulting from objective circulation type classifications that have been optimized with respect to the target variable $PM_{10}$ in Chapter 6 for each season and each station, are aggregated into $PM_{10}$-fostering, $PM_{10}$-indifferent and $PM_{10}$-reducing synoptic situations. They have been consid-

ered as additional exploratory variables in the downscaling models.

The statistical modelling of daily mean $PM_{10}$ concentrations ($PM_{daily}$) has been employed by regression-based methods using local meteorological variables as predictors. The selected approaches are Multiple Linear Regression Analysis (MLR), Generalized Linear Model (GLM) and Random Forests (RF) (Beck and Jacobeit, 2015). The statistical principles of these methods are introduced in Chapter 4. The three regression-based methods have been applied in circulation-type-based downscaling models of monthly $PM_{10}$ indices in this thesis as well, which are presented in Chapter 7. All approaches have been utilized in existing studies for the assessment of meteorological influences on local $PM_{10}$ concentrations, yet. Jollois et al. (2009) or Bobbia et al. (2011), for instance, have successfully applied RF models for the analysis of local and background contributions to local particle concentrations in France. In their comprehensive study, Stadlober et al. (2012) have used MLR models as well as GLM to estimate $PM_{10}$ values in European cities.

The performance of the local transfer models has been evaluated in the same calibration and validation periods on the basis of the same skill scores ($R^2$, MSSS) as for circulation-type-based downscaling models. The quantitative evaluation measure are further described in Chapter 4. The used calibration periods are 1980-1999, 1980-1989 + 2001-2011 as well as 1991-2011 and the corresponding validation periods 2000-2011, 1990-2000 as well as 1980-1990. RF models have been found to have the highest skill in nearly all models (Beck and Jacobeit, 2015). The most suitable local transfer models, according to the highest model skill in the validation periods, are used to estimate future particle levels on the basis of climate change projections from the Atmospheric Component of the MPI-M Earth System Model (ECHAM6) (Giorgetta et al., 2013; Stevens et al., 2013), afterwards. To this end, ensemble runs of RCP4.5 and RCP8.5 scenarios are taken for two periods (2021-2050, 2071-2100). In Chapter 3, a more detailed data description of the ECHAM6 model data is given.

In order to estimate local meteorological parameters (in this case predictands) from the large-scale atmospheric fields (predictors) of the ECHAM6 climate model runs, statistical downscaling models have been assessed. In a first step, Principal Components (PCs) of various daily gridded large-scale atmospheric fields of the NCEP/NCAR reanalysis data set have been used as predictors in RF models (Beck and Jacobeit, 2015). The Principal Component Analysis is described in more detail in Chapter 4. Mean sea level pressure, geopotential heights (1000, 850, 700 hPa), omega (1000, 850 hPa), zonal and meridional wind components (1000, 850, 700 hPa) relative and specific humidity (1000 hPa) as well as air temperature (1000, 925, 850 hPa) have been chosen for this purpose. The models have been evaluated and compared for several calibration and corresponding validation periods from 1980 to 2011 in a second step. To this end, a set of most suitable predictors

from the large-scale atmospheric parameters have been selected for each local meteorological predictand (Beck and Jacobeit, 2015). The RF models have been run with ECHAM6 data afterwards to model future daily levels of the local meteorological parameters. Finally, these estimated local meteorological variables are used as predictors in local transfer models to predict future particle levels.

Resulting model combination RF-GLM for example represents a RF model, which is used to estimate local meteorological variables from large-scale atmospheric fields in a first step. In a second step, these local meteorological variables are used as predictors in a GLM model to estimate daily mean $PM_{10}$ concentrations ($PM_{daily}$) (Beck and Jacobeit, 2015). Highest model skill has been achieved for seasonal RF-GLM models as well as RF-RF models, which are a combination of RF models for the downscaling of local meteorological predictors and estimation of particle levels in cross-validation. Furthermore, RF-RFCT models have reached comparably high model skill. Aggregated circulation types ($PM_{10}$-fostering, $PM_{10}$-indifferent, $PM_{10}$-reducing CTs) have been regarded as potential predictors in this variant of RF-RF models. Model skill of the RF-GLM, RF-RF and RF-RFCT models are compared to results from circulation-type-based Synoptic Downscaling models in Section 9.2.2. The used variants of the Synoptic Downscaling approaches are introduced in more detail in Chapter 7.

A comparison of estimated seasonal daily particle levels from ECHAM6 ensemble runs for the two scenarios and time steps from the large-scale downscaling and local transfer models are discussed in Section 9.2.3.

## 9.2. Results

### 9.2.1. Large-scale and local predictors

In a first step, correlation analysis have been performed between seasonal daily mean $PM_{10}$ concentrations ($PM_{daily}$) at different long-term Bavarian measurement sites and seasonal daily values of the introduced local meteorological variables to detect potential predictors for the intended application in downscaling models including local meteorological variables (Beck and Jacobeit, 2015). Therefore, the Spearman rank correlation analysis has been applied, which is a robust non-Gaussian variant of the Pearson correlation analysis using the ranks of the data instead of the original data (Wilks, 2006). The Spearman correlation coefficient $r_{rank}$ for a sample size $n$ is defined as

$$r_{rank} = 1 - \frac{6 \sum_{i=1}^{n} D_i^2}{n(n^2 - 1)} \tag{31}$$

with $D_i$ marking the difference in ranks between the $i$th pair of data values. If a particular data value appears more than once, an averaged rank is calculated from all these equal values before assessing $D_i$. The coefficient varies between -1 and 1, with values of $\pm 1$ indicating a perfect positive or negative correlation and 0 indicating no connection (Wilks, 2006).

The subsequent analysis have been conducted by using $PM_{10}$ time series from those Bavarian measurement sites with $\geq 90$ %, which results in 19 stations (including additional sites Burghausen/ Markler Str. (L1.2), Arzberg/Egerstr. (L4.5) and Neu-Ulm/Gabelsbergerstr. (L7.5)) (Beck and Jacobeit, 2015). Corresponding local meteorological variables have been used from the DWD data set. In Figure 9.2, boxplots of Spearman correlation coefficients between seasonal daily particle levels at 19 stations and seasonal daily values of different meteorological variables are shown for winter (DJF) and summer (JJA). The parameters are cloud coverage, vapour pressure, mean sea level pressure, mean, maximum and minimum air temperature, precipitation, sun duration, wind speed, temperature gradients between 1000 hPa and 925 hPa (Tdiff925-1000), zonal (Uwnd1000) and meridional (Vwnd1000) wind components in 1000 hPa from NCEP/NCAR reanalysis and temperature differences between 1000 hPa and 925 hPa from radiosonde measurements (RS925-1000). Independently from the season or the station, precipitation, vapour pressure, cloud coverage, Tdiff925-1000 as well as temperature parameters (mean, maximum and minimum) have been selected as significant predictors in the models (Beck and Jacobeit, 2015). All parameters have been used in further local transfer models except RS925-1000, which has been replaced with Tdiff925-1000.

As it is shown in Figure 9.2, the algebraic sign of Spearman R between $PM_{10}$ and temperature indices varies with respect to the season. In winter for example, negative correlations between the averaged temperature and particle levels indicate a decreasing particle load with rising temperatures. In mid-latitude winter, cold temperatures on a local scale are known to be connected to large-scale atmospheric conditions with nearly no air mass exchange. These are, for example, strong high pressure systems over Russia, which can cause an accumulation of particles on a local scale. In summer, higher temperatures foster the formation of secondary particles, which is the reason for a positive correlation illustrated in Figure 9.2. Precipitation is relevant for the wet deposition of particles in winter, but the correlation coefficients are comparatively small. Higher negative correlation coefficients appear for the wind components. Local and regional winds are responsible for the transportation and relocation of $PM_{10}$. Temperature differences between 1000 hPa and 925 hPa (Tdiff925-1000), which are a proxy for the mixing layer height, are positively correlated in both seasons. As it is described by Schäfer et al. (2006) for example, the mixing layer height is a proxy for the air pollution near the surface due to the dilution of particles, which are emitted or formed. They have found a stronger connection between the mixing layer height

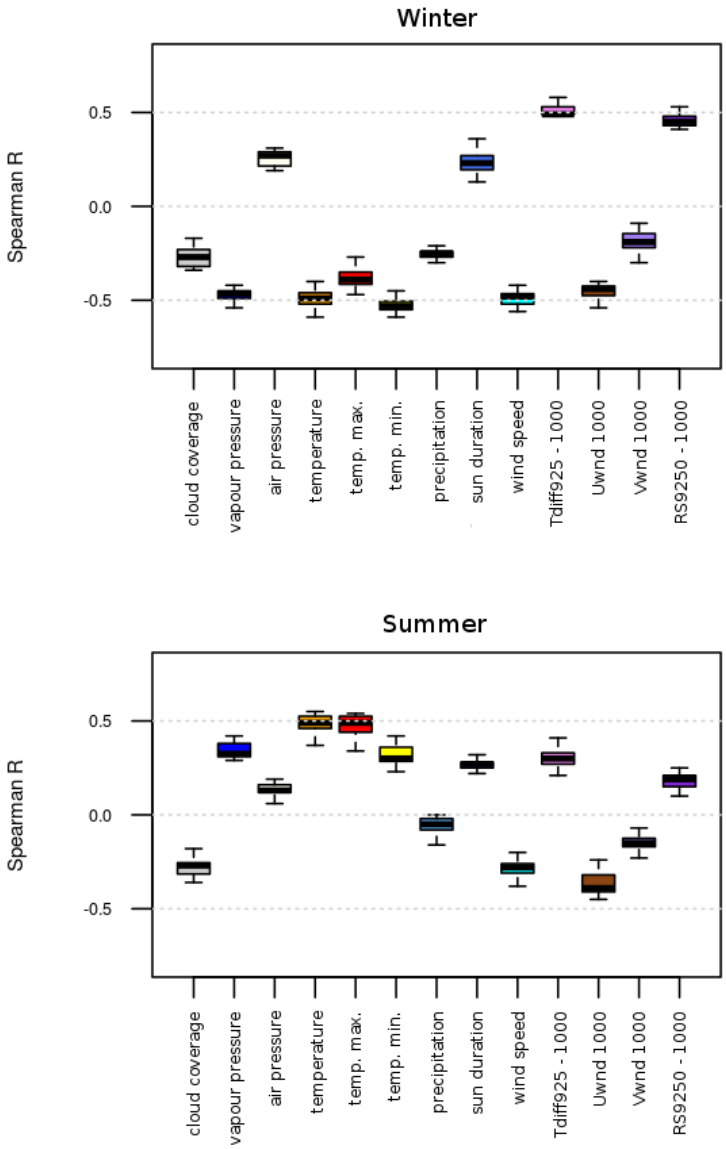


Figure 9.2: Boxplots of spearman correlation coefficients between $PM_{daily}$ and daily values of various local meteorological predictors in winter and summer from 19 Bavarian measurement sites (adapted from Beck and Jacobeit 2015).

and $PM_{10}$ in winter compared to summer at German measurement sites. This is in accordance to higher correlation coefficients in winter compared to other seasons between Tdiff925-1000 and RS925-1000, respectively, and $PM_{10}$ at Bavarian stations depicted in Figure 9.2.

In Chapter 6, the stepwise optimization of seasonal objective circulation type classifications with respect to local $PM_{10}$ concentrations at 16 stations is discussed. Classifications on the basis of a weighted combination of three different large-scale atmospheric variables have turned out to have

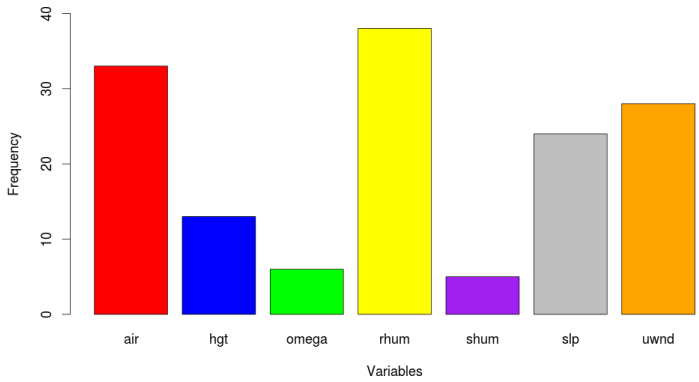


Figure 9.3: Barplots of occurrence frequencies of different large-scale atmospheric parameters in best performing seasonal circulation type classifications. Variables are air temperature in 1000 hPa (air), geopotential height in 500 hPa (hgt), vertical velocity in 1000 hPa (omega), relative humidity in 1000 and 850 hPa (rhum), specific humidity in 1000 hPa (shum), mean sea level pressure (slp) and zonal wind in 500 hPa (uwnd).

the highest discriminative power for local daily $PM_{10}$ concentrations according to objective evaluation measures. From a comprehensive set of large-scale parameters, air temperature in 1000 hPa (air), geopotential height in 500 hPa (hgt), vertical velocity in 1000 hPa (omega), relative humidity in 1000 and 850 hPa (rhum), specific humidity in 1000 hPa (shum), mean sea level pressure (slp) and zonal wind in 500 hPa (uwnd) have been selected as most important influencing variables throughout the seasons and stations. For each of the 16 stations and for each season, the best performing objective classifications have been finally used as predictors in downscaling models to estimate daily particle levels in Chapter 7. In Figure 9.3, the occurrence frequencies of the named large-scale atmospheric variables in seasonal best performing classifications are indicated. Relative humidity in two levels, temperature as well as zonal wind component appear mostly in the classifications. As it was previously summarized, these variables have reached a relatively high correlation on a local scale, too. Hence, an influence of temperature, relative humidity and zonal wind component in various spatial scales on local $PM_{10}$ concentrations at Bavarian measurement sites can be concluded from the analysis.

### 9.2.2. Comparison of model skill in validation (1980 - 2011)

In order to assess daily mean $PM_{10}$ concentrations ($PM_{daily}$) from large-scale atmospheric circulation and local meteorological conditions, several statistical downscaling approaches have been developed for the period 1980-2011. For the circulation-type-based models, these are variants of Synoptic Downscaling (SD). These type-specific mean values are used to model time series of daily particle levels in the corresponding validation period. Best performing objective circulation type classifications are implemented in the models. A variant of SD, SD-PMT considers $PM_{10}$ con-

centrations on the previous day and SD-GWT the synoptic situation on the previous day, whether it is a high pressure or low pressure pattern. Best performing seasonal local transfer models are mainly based on Random Forests (RF) and Generalized Linear Model (GLM) to estimate $PM_{daily}$ from local meteorological variables. As it was previously described in this Chapter, local meteorological parameters are downscaled from the large-scale circulation using Random Forests (RF) models in a first step. Secondly, local particle concentrations are assessed from these local meteorological parameters using RF models (RF-RF, RF-RFCT) as well or GLM (RF-GLM) (Beck and Jacobeit, 2015).

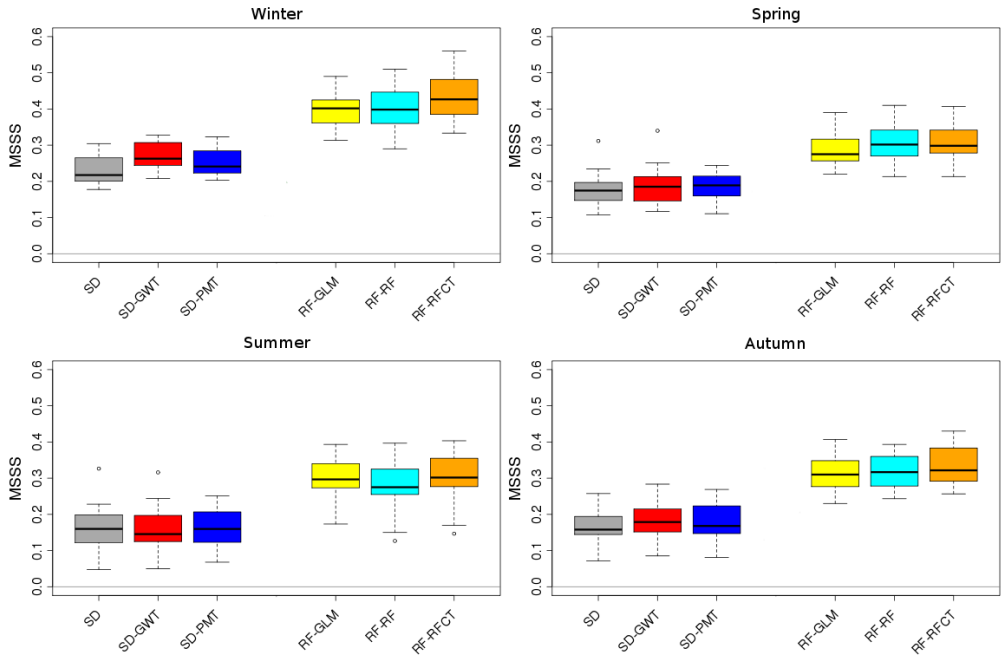


Figure 9.4: Boxplots of Mean Squared Skill Score (MSSS) for estimating seasonal $PM_{daily}$ at all stations and for three validation periods. See text for further explanation of used methods depicted as x-axis (adapted from Beck and Jacobeit 2015).

In Figure 9.4, boxplots of Mean Squared Skill Score (MSSS), assessed for $PM_{daily}$ at the different stations in three validation periods, are shown for three variants of SD and local transfer models (RF-RF, RF-GLM, RF-RFCT). As it is illustrated in Figure 9.4, positive skill can be stated for all model approaches at all stations and for all seasons. Nevertheless, values of MSSS are comparably low for SD in contrast to the local transfer models. Maximum values of MSSS are achieved in winter with values around 0.3 for SD-GWT and SD-PMT and > 0.55 for RF-RFCT. Furthermore, lower skill can be stated for all models in summer as well as for the transitional seasons.

As validation results have revealed, the downscaling models including local meteorological variables as PM-predictors are more suitable for modelling $PM_{daily}$. The model skill of the SD ap-

proaches are not sufficient for modelling daily particle levels based on ECHAM6 data in a next step. A higher model skill can be achieved by aggregating the resulting daily time series from the SD to monthly $PM_{10}$ for example. This has been done for the modelling of monthly $PM_{10}$ concentrations from SD models in Chapter 7.

### 9.2.3. Assessment of future particle levels until 2100

For the estimation of future daily mean $PM_{10}$ concentrations ($PM_{daily}$) from local transfer models and $PM_{mean}$ levels from SD models at Bavarian measurement sites, the best performing approaches from the validation have been applied on three ensemble runs of the ECHAM6 model for two scenarios (RCP4.5, RCP8.5) in two time periods (2021-2050, 2071-2100) as well as on ensemble runs in the control period 1980-2011 (historical). Statistical ensembles have been generated by applying the climate model data on the downscaling models based on the whole analysed period 1980-2011 and three sub-calibration periods, additionally. The numerical and statistical ensembles have been used to consider model uncertainties resulting from GCM data on the one hand and from the downscaling models on the other hand.

A bias correction of the modelled $PM_{10}$ time series have been performed in accordance to Cheng et al. (2007b). A more detailed description of the bias correction is given in Chapter 8. Differences between the central tendency of estimated particle levels in the historical period and future climate change scenarios have been tested by a Mann-Whitney Test with significance level of alpha = 0.05. The principle of this test is introduced in Chapter 8 as well.

In Figure 9.5 - 9.9, seasonal estimated daily $PM_{10}$ (RF-RFCT) and monthly $PM_{10}$ (SD-PMT) levels are depicted for representatives for Bavarian $PM_{10}$ regions Kelheim (Figure 9.5), Weiden (Figure 9.6), Nürnberg (Figure 9.7), Schweinfurt (Figure 9.8) and München (Figure 9.9). Modelled time series are assessed for three numerical and four statistical ensemble members. Stars mark significant changes of particle concentrations between historical period (1980-2011) and scenarios.

In general, a decreasing tendency of $PM_{10}$ levels has been estimated in winter and increasing ones in summer for almost all model approaches and stations. As Figures 9.5 - 9.9 illustrate, these changes are mostly significant for the local transfer models (RF-RFCT) in contrast to the SD-PMT approach. In the transitional seasons, future climate-change-induced variations of particle concentrations are more variable compared to winter and summer projections and no clear decreasing or increasing tendency can be concluded.

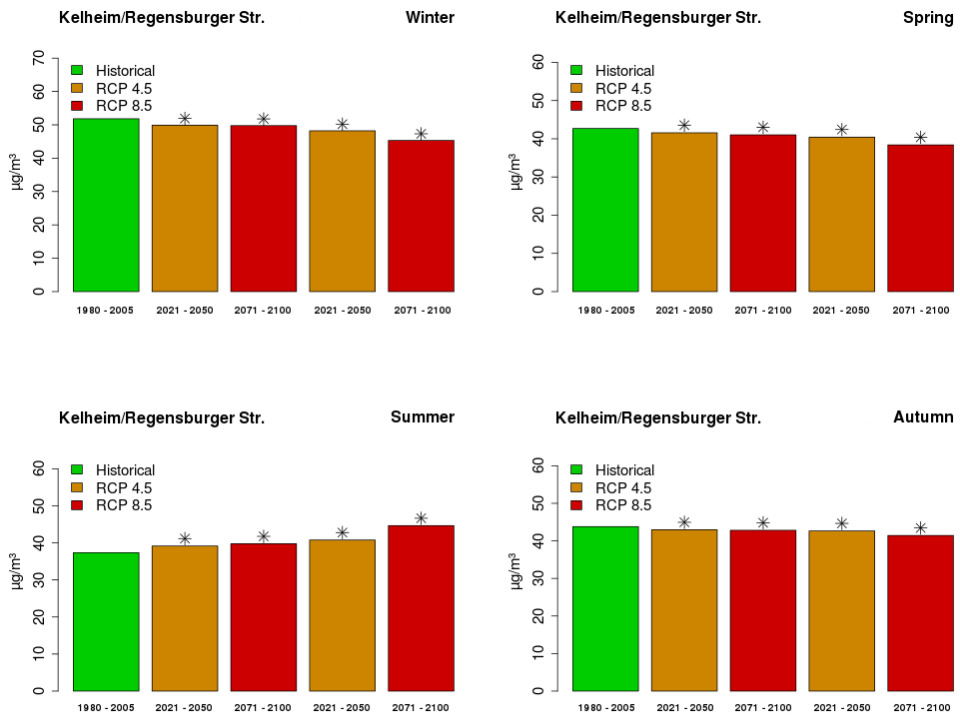


(a) Kelheim RF-RFCT

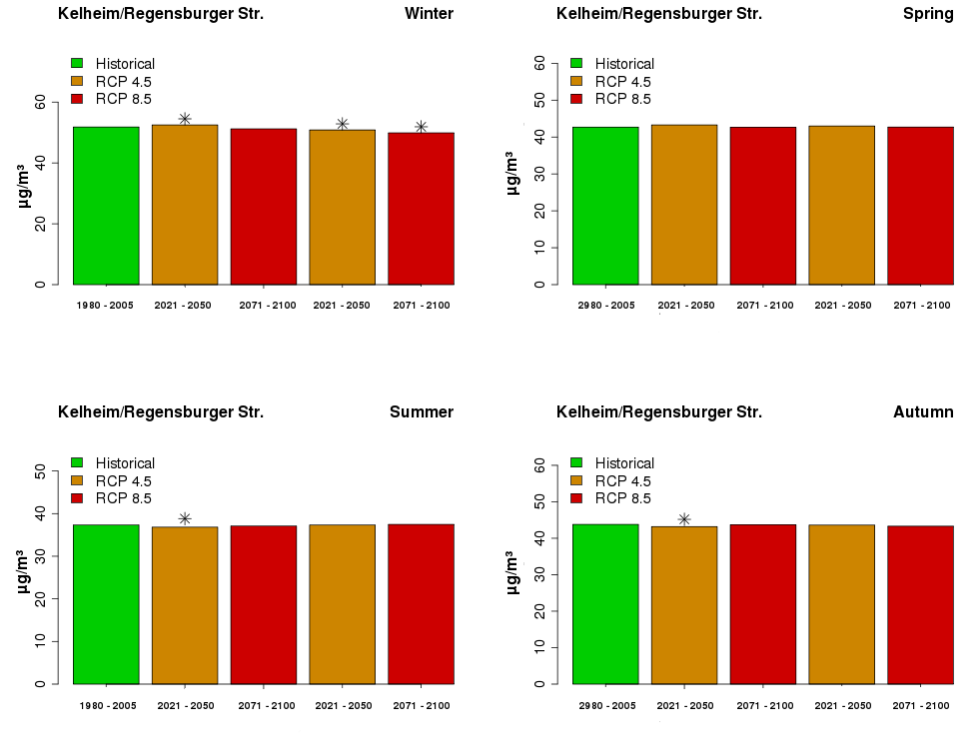


(b) Kelheim SD-PMT

Figure 9.5: Modelled seasonal $PM_{mean}$ levels (in $\mu g/m^3$) at station Kelheim Regensburger Str. Estimations are based on ECHAM6 scenarios (RCP4.5, RCP8.5) for two time periods (2021-2050, 2071-2100) using local transfer models (RF-RFCT) and the Synoptic Downscaling variant (SD-PMT). Stars mark statistical significance (alpha = 0.05) of differences between particular scenario and historical periods (adapted from Beck and Jacobeit 2015).

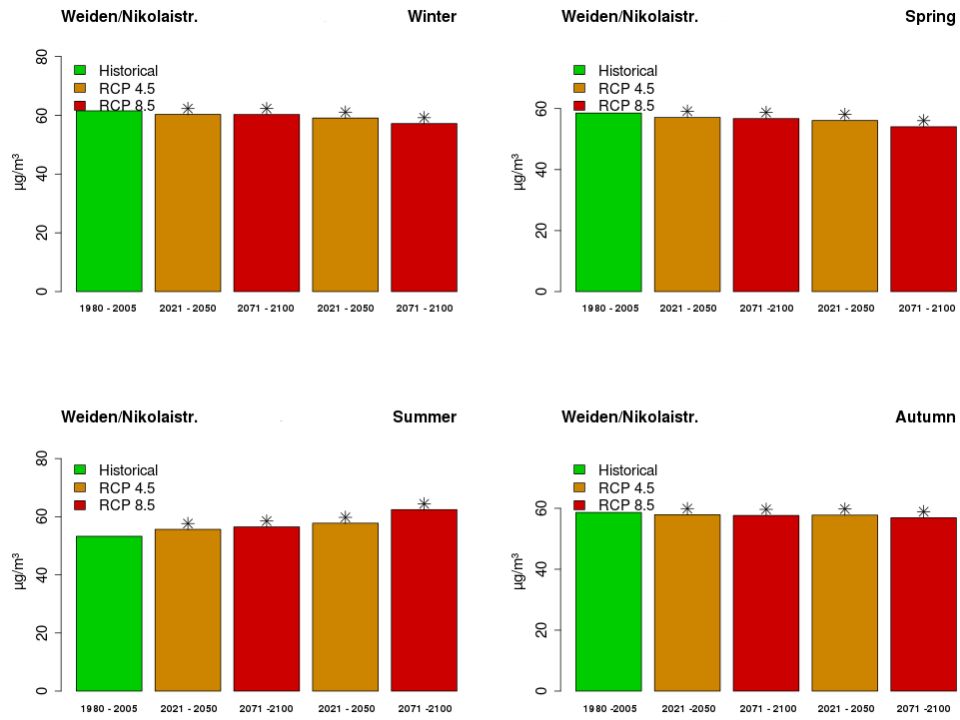


(a) Weiden RF-RFCT

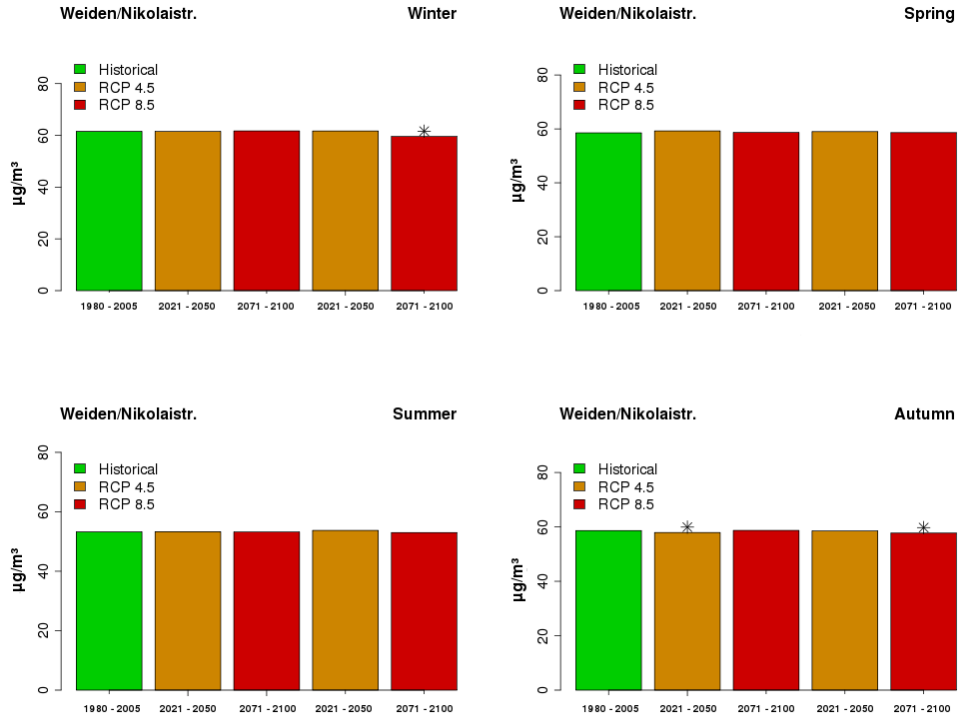


(b) Weiden SD-PMT

Figure 9.6: Same as Figure 9.5 for station Weiden Nikolaistraße (adapted from Beck and Jacobeit 2015).

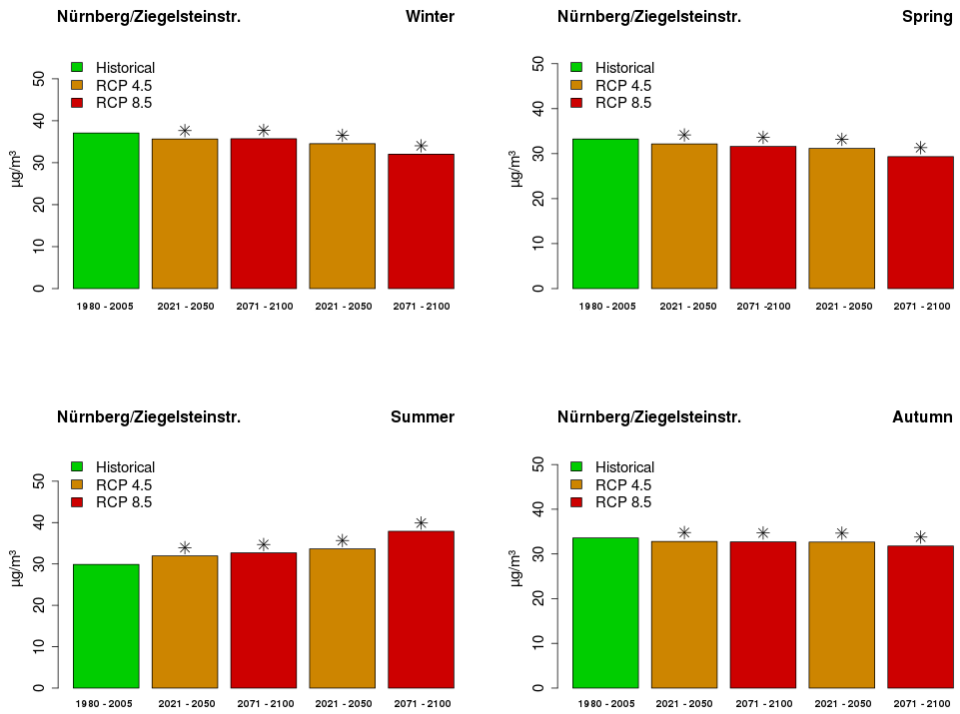


(a) Nürnberg RF-RFCT

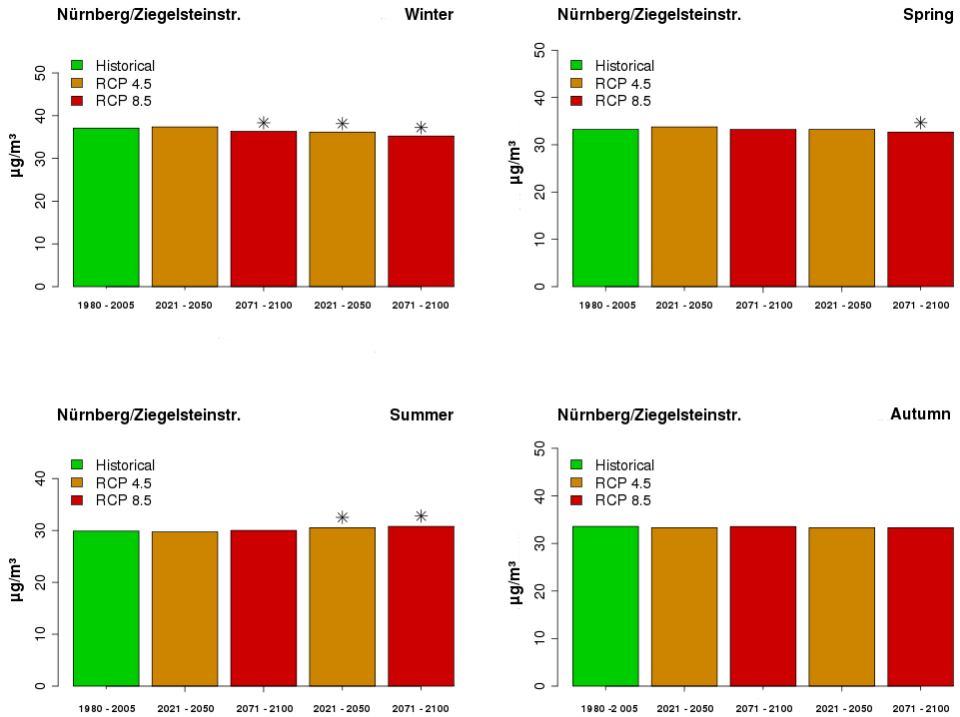


(b) Nürnberg SD-PMT

Figure 9.7: Same as Figure 9.5 for station Nürnberg Ziegelsteinstraße (adapted from Beck and Jacobeit 2015).

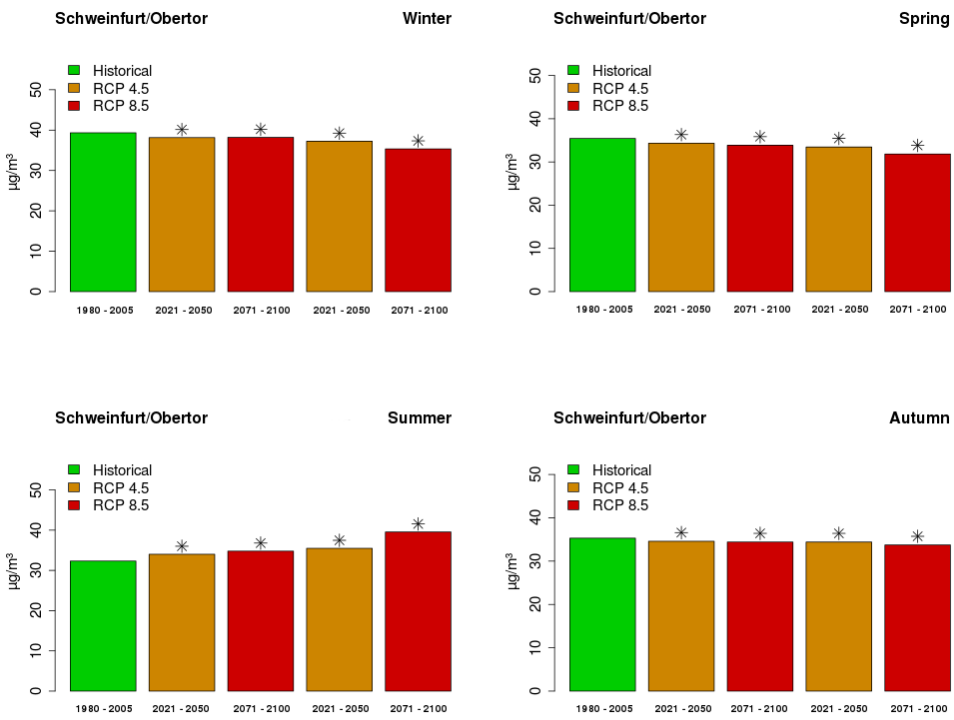


(a) Schweinfurt RF-RFCT

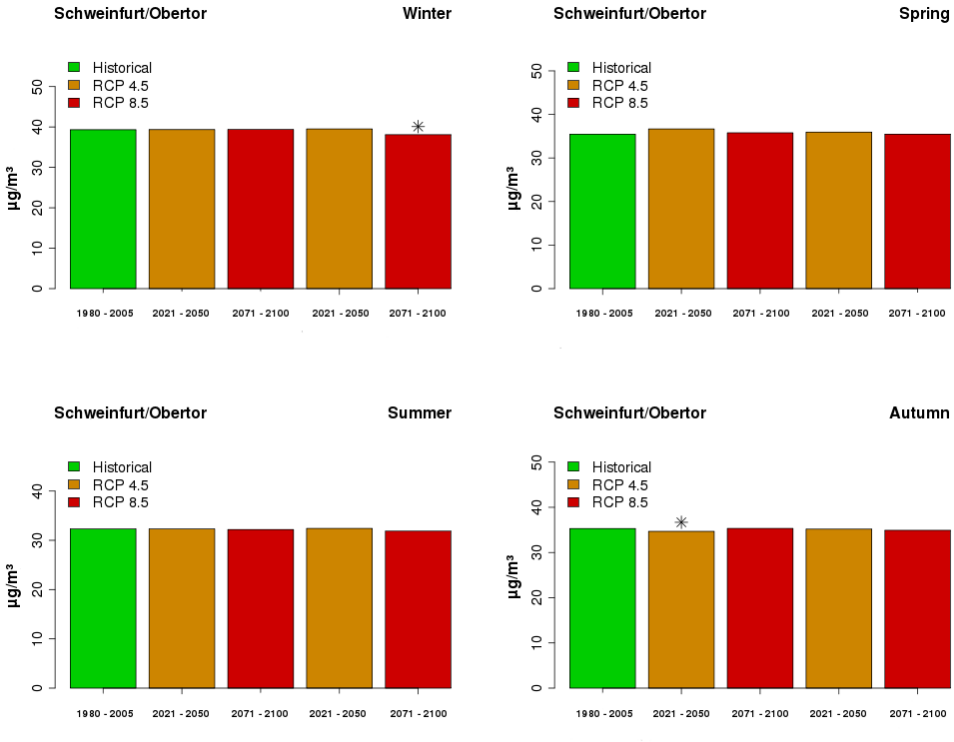


(b) Schweinfurt SD-PMT

Figure 9.8: Same as Figure 9.5 for station Schweinfurt Obertor (adapted from Beck and Jacobeit 2015).

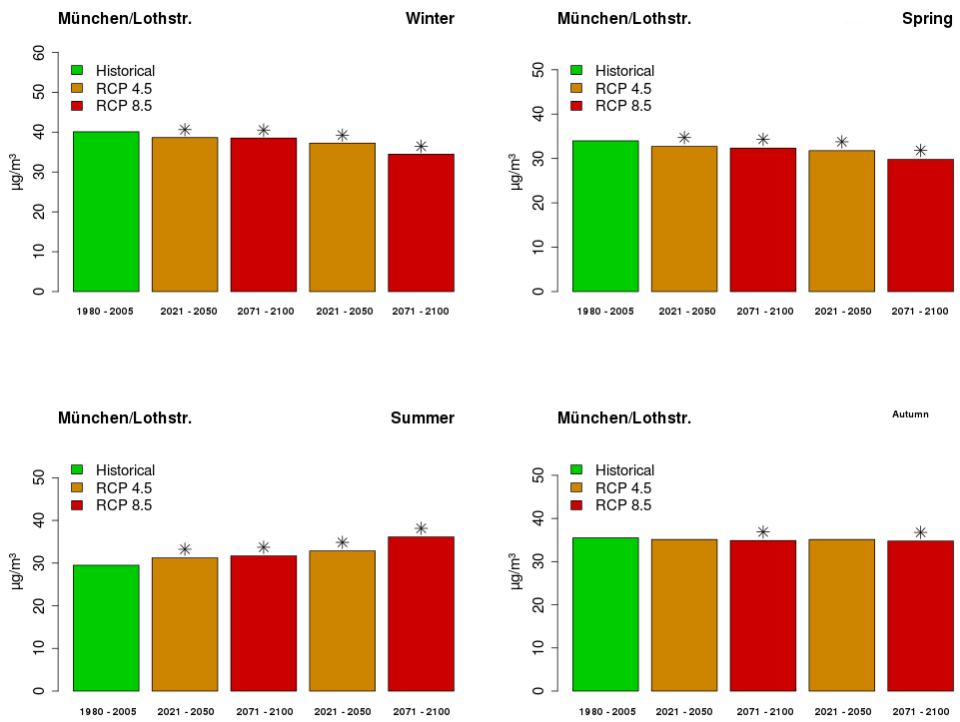


(a) München RF-RFCT

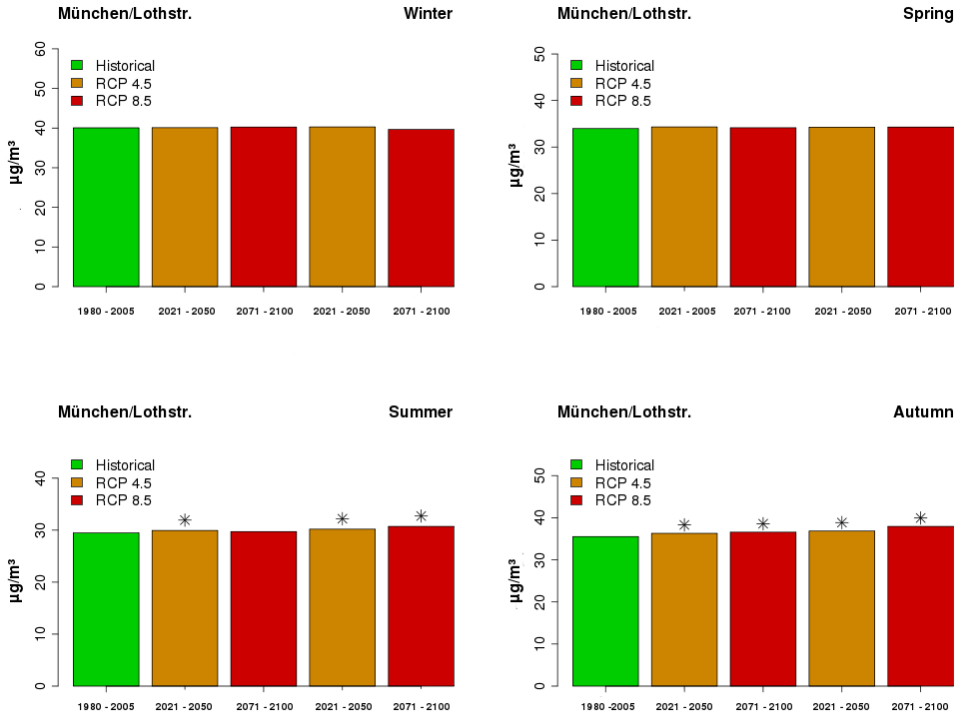


(b) München SD-PMT

Figure 9.9: Same as Figure 9.5 for station München Lothstraße (adapted from Beck and Jacobeit 2015).

Larger variations of projected $PM_{10}$ concentrations resulted from the SD-PMT model, depending on statistical and numerical ensemble runs as well as considered station. A possible reason for this could be a remaining type-internal variability of circulation types, which have been optimized with respect to $PM_{10}$ at each specific station and are used as predictors in the SD-PMT models (Beck and Jacobeit, 2015). Another explanation may be the fact that the RF approach in general provides quite robust model results with small variations compared to the SD techniques.

The estimated changes in particle levels in winter and summer presented in this Section are in accordance to future projected changes in frequencies of occurrence of $PM_{10}$ relevant circulation types discussed in Chapter 8. In winter for instance, an increase of synoptic situations with a western flow direction (zonal, cyclonic patterns), which are connected to comparably low particle concentrations in Bavaria due to good mixing conditions and humid air masses, has been detected. These findings coincide with results from Demuzere and van Lipzig (2010b) for example. A decrease in the occurrence frequencies of anticyclonic conditions in winter, which are linked to high pollution events through blocking synoptic conditions with a local accumulation of particles, has been revealed as well. In summer, an increase of synoptic-scale high pressure patterns is suggested to be the reason for increasing local temperatures and $PM_{10}$ concentrations. Consequently, decreasing frequencies of zonal, cyclonic conditions are assessed in summer.

## 9.3. Summary

The purpose of this Chapter was to compare several statistical downscaling approaches, which have been developed on the basis of large-scale atmospheric circulation types and local meteorological parameters as PM-predictors in the PACLIMBA project to model seasonal daily mean $PM_{10}$ concentrations ($PM_{daily}$) for the recent period 1980 to 2011. The models have been compared with respect to mainly used large-scale and local meteorological predictors, model skill in the validation as well as estimated daily and monthly particle levels from future climate change scenarios.

The downscaling approaches comprise on the one hand variants of the Synoptic Downscaling (SD) and on the other hand several regression-based models using local meteorological PM-predictors. All downscaling techniques have been performed on the basis of objective circulation type classifications, which have been optimized with respect to their synoptic skill for the target variable $PM_{10}$. The generated models have been evaluated via cross-validation on the basis of varying subintervals of the 1980-2011 period. The models have been calibrated in three different 20-year calibration periods. Then, the model skill has been assessed in 10-year validation periods by objective evaluation measures. The selection of the most suitable downscaling procedures has been done according to

the highest skill of the models in cross-validation. Selected models have been applied to data from ECHAM6 ensemble runs to derive estimates of possible future climate change related variations in $PM_{10}$ concentrations for two time periods (2021-2050, 2071-2100) and considering two different climate change scenarios (RCP4.5, RCP8.5), finally.

Temperature near the surface, temperature gradients between 1000 hPa and 925 hPa, humidity parameters (precipitation, relative humidity) as well as zonal wind components in different levels, vapour pressure, cloud coverage and mean sea level pressure turned out to be the most influential predictors in the best performing models. Variations of the importance of a predictor emerged with respect to considered season and station. In winter for instance, the temperature gradients are positively correlated to daily particle levels on a local scale. The temperature differences may be a proxy for atmospheric inversions for instance, which foster a particle accumulation near the surface. Mean, maximum and minimum temperatures are negatively correlated to $PM_{daily}$ in winter. A possible explanation for this connection could be stable high pressure systems in winter over Europe, which cause low temperatures and nearly no air mass exchange and therefore an accumulation of particles on a local scale. In summer, the temperature indices are positively correlated to $PM_{daily}$ as high temperatures can promote the formation of secondary particles.

A comparison of the model skill of selected circulation-type-based SD approaches and RF models using local meteorology as PM-predictor, which has been assessed over three validation periods for values of Mean Squared Skill Score (MSSS), revealed higher model skill for the local transfer models with respect to modelling of daily $PM_{10}$ concentrations. In general, highest model skill has been reached in winter at all stations, in all seasons and for all models. As best performing model variant, a local transfer models using RF and aggregated circulation types as additional predictors (RF-RFCT) turned out to have the highest model skill (MSSS up to 0.55). Time series of daily $PM_{10}$ values have been aggregated to $PM_{mean}$ in order to achieve a higher model skill for the SD variants.

An estimation of future climate-change-induced variations of $PM_{daily}$ and $PM_{mean}$ yielded out decreasing particle levels in winter until the end of this century in most of the models at nearly all stations. A reason for the decreasing particle concentrations might be an increase of zonal, cyclonic synoptic systems over Europe with humid weather conditions and frequent air mass exchanges. In summer, however, increasing particle loads have been predicted for most of the $PM_{10}$ stations in Bavaria. A decrease of synoptic situations with a western flow component have been modelled and large-scale atmospheric conditions fostering higher local temperature will occur more often. This might lead to stronger formation of secondary particles for example. The estimated changes in winter and summer are quite often significant between the historical period (1980-2005) and the

scenarios in two different time periods, especially for the local transfer models. No clear signal of particle variations in spring and autumn could be concluded.

# 10. Conclusions and Outlook

**Conclusions**

This thesis has investigated the stepwise optimization of objective circulation type classifications with respect to their synoptic skill for the target variable particulate matter with aerodynamic diameter < 10 $\mu$m ($PM_{10}$) at 16 long-term measurement sites in Bavaria/Germany for the period 1980-2011. Furthermore, seasonal large-scale atmospheric conditions, represented by monthly occurrence frequencies of circulation types resulting from the optimized classifications, have been linked to local $PM_{10}$ concentrations using various statistical downscaling methods. The most suitable approaches have been applied to GCM data to estimate future climate-change-induced variations of daily and monthly particle concentrations. Finally, a comparison between the performance of circulation-type based downscaling models and local transfer models as well as estimated corresponding future particle levels has been conducted. In the following, important conclusions, which result from the investigations of this thesis, are presented together with a brief outlook.

In Chapter 5, the initial characteristics of the $PM_{10}$ data set concerning data availability, basic quality aspects, long-term trends and correspondance between locations have been presented. Daily time series from 16 measurement sites in Bavarian cities with over 90 % data availability for the observational period 1980-2011 have been used for the analysis. The long-term trend of monthly mean particle concentrations, which has been assessed using a polynomial regression, revealed a decreasing trend at nearly all stations for the observational period since the late 1990ies. A s-mode Principal Component Analysis has been carried out to define regions of similar $PM_{10}$ variability in Bavaria. Principal Components (PC) have been extracted following the approach described for instance by Jacobeit (1993) or Philipp et al. (2007). It turned out that spatial adjacent stations are grouped together to PCs representing large-scale landscape units of the target region. The first of five regions (PC 1) represents southern Bavarian urban agglomerations. Station München Lothstrasse was selected as the representative one according to the maximum loading on PC 1. Measurement sites in the Danube valley are grouped into the second region (PC 2) with station Kelheim as the representative one. Region three (PC 3) encompasses stations north-west to the Franconian Jura. Station Schweinfurt was selected as the representative site for PC 3. Region four (PC 4) includes cities in the north-eastern part of Bavaria with Weiden as the representative site. The stations of region five (PC 5) are situated in the Middle Franconian urban area with Nürnberg Ziegelsteinstrasse as station with maximum loading.

As it is commonly known and has been mentioned in the literature review in Chapter 2, spatial and temporal variations in $PM_{10}$ concentrations reflect local emission rates, but are as well influenced

by the local and large-scale atmospheric conditions. It is assumed that the temporal variability of particles at Bavarian measurement sites is particularly influenced by meteorology on different scales, which in turn is dependent from climatic factors as altitude or exposition. Against this background, quantitative relationships between daily and monthly $PM_{10}$ concentrations at different Bavarian stations and the corresponding large-scale atmospheric circulation have been established.

*Objective circulation type classifications (CTCs) have been optimized with respect to their synoptic skill for the target variable $PM_{10}$* at the measurement sites in Chapter 6 as a first main contribution of this thesis. Variants of CTCs have been performed for varying spatial and temporal domains, different numbers of classes and varying combinations of three large-scale atmospheric variables in several levels with different weights. Main results from the analysis revealed highest synoptic skill of CTCs for cluster-analysis-based classification approaches, a mid-size domain (7.5° - 27.5° E and 40° - 60° N), 18 as number of classes, seasonal classifications, a weighted combination of three large-scale atmospheric input variables (mean sea level pressure, geopotential height, zonal and meridional wind components, relative and specific humidity, air temperature, relative vorticity in 1000, 850 and 500 hPa levels) and the conditioning by the target variable. In accordance to the findings in Beck et al. (2014b), no optimized classification exists which is the most suitable one in all seasons and at all stations. To this end, a set of best performing non-optimized (for comparison), optimized and optimized-conditioned classifications has been selected, for each station and each season separately, with respect to the maximum values of different quantitative evaluation measures. Furthermore, this fact has evoked the need to generate separate downscaling models for each season and station in further analysis.

South-east patterns and central high pressure fields over Europe have been found to have the highest influence on local $PM_{10}$ concentrations over all seasons and stations, as they are connected to comparably high mean particle concentrations. Zonal cyclonic conditions in contrast, which have appeared more often in winter and the transitional seasons in the observational period, are connected to western air mass flow and comparatively small mean particle concentrations.

A comparison of the analysed variants of classifications have revealed the maximum skill in winter (December, January, February). On the one hand, higher particle levels occur in winter months in Bavarian urban areas due to heating and traffic emissions. On the other hand, stable high pressure conditions can foster the accumulation of air pollutants in this season due to nearly no air mass exchange. Lower and more variable skill has been detected for summer (June, July, August) and the transitional seasons spring (March, April, May) and autumn (September, October, November). In summer, mean $PM_{10}$ concentrations are generally lower compared to results in winter and are mainly influenced by meteorological conditions on a local to regional scale in mid-latitudes. As a

consequence, the connections between synoptic systems and local particles are less pronounced.

The second main contribution of this thesis is related to the analysis of the *linkage of seasonal large-scale atmospheric conditions to local $PM_{10}$ concentrations using various statistical downscaling methods*. To this end, monthly occurrence frequencies of 18 Circulation Types (CTs), resulting from the previously selected optimized classifications, have been applied as predictors on a comprehensive selection of statistical downscaling tools for modelling seasonal daily and monthly $PM_{10}$ concentrations (predictands) at the 16 stations in Chapter 7. The downscaling techniques encompass variants of Synoptic Downscaling (SD) for modelling daily mean $PM_{10}$ concentrations ($PM_{daily}$). Furthermore, several multivariate statistical models (Multiple Linear Regression, Generalized Linear Models, Random Forests) have been applied for estimating monthly mean $PM_{10}$ concentrations ($PM_{mean}$) and monthly exceedances of a daily mean $PM_{10}$ value of 50 $\mu g/m^3$ ($PM_{50}$). All downscaling approaches have been compared in terms of model skill determined from cross-validation using different subintervals of the recent period of 1980-2011 as calibration and validation periods. The performance of the circulation-type-based downscaling models has been evaluated by different quantitative measures, e.g. coefficient of determination ($R^2$) and Mean Squared Skill Score (MSSS)Mean Squared Skill Score.

As it has been described for example by Cheng et al. (2007a), the consideration of the particle levels on the previous day could be used to explain variations of daily $PM_{10}$ concentrations. Two variants of the SD have been selected from a comprehensive set of tested SD configurations according to the highest model skill. The first selected variant included particle concentrations on the previous day (SD-PMT). The second one took the circulation type on the previous day into account by distinguishing between high and low pressure fields (SD-GWT). Results from the models in validation are in line with the findings in the aforementioned study due to comparably high model skill of the SD-PMT approach. Although low but positive skill has been detected in cross-validation for modelling $PM_{daily}$ by SD models, the results have given no point to apply the SD models in further analysis. Higher skill has been achieved by aggregating daily $PM_{10}$ time series to $PM_{mean}$. Consequently, the SD models have been used for the intended application on climate model data for estimating $PM_{mean}$ in further analysis.

From the comprehensive set of regression-based downscaling models, a few general statements can be concluded. Comparably high model skill has been detected for modelling $PM_{mean}$ compared to $PM_{50}$. A feasible reason for this fact is a smaller data basis of $PM_{50}$ time series, as these high pollution events occur quite rarely at some stations. Furthermore, a reduced capability of the circulation-type regression models to resolve extreme values can cause the lower skill (Beck et al., 2014b). Additional variations in model skill resulted between seasons and stations. The most

distinct connections between synoptic systems and local particle concentrations exist in winter as evaluation results from nearly all downscaling models revealed. In the other seasons, the model skills are less pronounced and more variable. From the comprehensive set of regression-based downscaling tools, the Random Forest models (RF-M) have turned out to be comparably robust with respect to model skill in cross-validation. To this end, the RF-M have been selected for the intended application on climate model data in this thesis.

In Beck et al. (2014b), the circulation-type-based downscaling models have been investigated on the basis of non-optimized circulation type classifications. Compared to the evaluation results presented in the study, the downscaling models developed in this thesis, which are based on optimized circulation type classifications, have revealed similar to higher model skill. Hence, an added value of the downscaling models can be concluded here. In addition, a general applicability of the downscaling models for the intended application on climate model data has been asserted in this thesis.

In Chapter 8, the *estimation of future climate-change-induced variations of local $PM_{10}$ concentrations* have been presented as third main contribution. The most suitable downscaling procedures for each station and each season resulting from previous analysis, which have been selected according to the maximum model skill in cross-validation, have been finally applied to CMIP5 climate models (ECHAM6, EC-Earth) to derive estimates of possible future climate-change-related variations in $PM_{10}$ concentrations. Model realizations from two climate change scenarios (RCP4.5, RCP8.5) in two time periods (2021-2050, 2071-2100) have been considered. Model data for the control period 1980-2011 (historical runs) have been applied as well.

It is of common knowledge that biases in GCM exist, which have to be taken into account when using the large-scale atmospheric fields of the models. Stevens et al. (2013) for example have outlined biases in ECHAM6 model occurring with respect to the representation of small-scale physical processes, e.g. clouds or convection. In their comprehensive study on "WEather Patterns, CycloneTRAcks and related precipitation EXtremes" (WETRAX) for the Alpine region, Hofstätter et al. (2015) have investigated the representation of dominant modes of variability (spatial patterns and corresponding time coefficients) of the atmospheric circulation in GCM data for a similar spatial domain used in this thesis. Results from the latter study have proven a general applicability of the ECHAM6 model for further investigations based on atmospheric circulation as performed in the following. Moreover, numerical ensembles have been used to consider uncertainties emerging from the GCM. To this end, three realizations from ECHAM6 projections based on two climate change scenarios have been applied. Model uncertainties may also evoke from the downscaling models. Hence, statistical ensembles have been used with four members assembled from three 20-year sub-periods and the whole period 1980-2011.

Results of estimated future climate-change-induced variations of monthly mean $PM_{10}$ concentrations ($PM_{mean}$) have revealed decreasing particle levels in winter until the end of the century at nearly all stations. In contrast, increasing particle levels have been estimated for summer. These changes, assessed as differences in the central tendency of time series between the historical period and the considered scenarios, have been found to be significant in some cases. Increasing zonal, cyclonic synoptic conditions in winter and decreasing ones in summer, resulting from the analysis of differences in frequencies of occurrence of circulation patterns in the future, have been identified as one possible explanation for the modelled changes in air pollution. Furthermore, increasing particle levels in summer could be explained by an increase of anticyclonic patterns.

Changes of $PM_{50}$ levels until the end of this century, obtained from the statistical downscaling models, have yielded out to be more variable and smaller compared to estimated $PM_{mean}$ levels. A general weak performance of the circulation-type-based RF-M to resolve $PM_{50}$ concentrations has been found in the analysis. This fact could be one explanation for the small and variable estimated $PM_{50}$ changes. Modelled changes of $PM_{50}$ have remained insignificant in most of the cases. Nevertheless, decreasing $PM_{50}$ levels have been determined in winter and increasing ones in summer for all stations, with variations occurring between the considered projections and time periods. Moreover, another explanation comprises the possibility of smaller variations of $PM_{50}$ in the future due to global climate change, as estimated from the downscaling models, compared to variations caused by anthropogenic emissions.

As the range of uncertainty might be underestimated by the usage of only one GCM, a comparison with model data from another AOGCM has been performed. Estimated $PM_{mean}$ levels resulting from downscaling models based on ECHAM6 and EC-Earth data have exposed only small changes. Differences between the observational period and the projections have remained mostly insignificant for EC-Earth-based estimations. Nevertheless, decreasing particle levels in winter and increasing ones in summer have been estimated for $PM_{mean}$ at some measurement sites as well. Due to limited access to realizations (only one run available) and considered large-scale atmospheric variables of EC-Earth data for the period 1980-2005, the comparison of results from ECHAM6 and EC-Earth data presented in this thesis could be expanded by using data from multiple AOGCM outputs of the CMIP5 project for more robust statements.

As a final contribution, *a comparison of two quantitative approaches for estimating future climate-change-induced variations of $PM_{10}$ in Bavaria* has been realized in Chapter 9. For that purpose, statistical downscaling models quantifying the relationships between daily $PM_{10}$ levels at different Bavarian stations (predictands) and the corresponding large-scale atmospheric circulation and lo-

cal meteorological conditions (predictors) have been compared with respect to model skill as well as estimated changes in future particle levels. In a two-step process, local transfer models have been developed in the framework of the research project "Particulate matter and climate change in Bavaria", funded by the German Research Foundation. First of all, local $PM_{10}$-relevant meteorological variables are downscaled from large-scale atmospheric fields and are applied as predictors in statistical transfer models for estimating $PM_{10}$ concentrations, afterwards. To this end, results from SD-PMT models and Random-Forest-based local transfer models, using local meteorological predictors for the estimation of $PM_{daily}$, have been assessed. Both techniques have used objective circulation type classifications that have been optimized with respect to their synoptic skill for the target variable. All downscaling approaches have been evaluated via cross-validation using different subintervals of the 1980-2011 period as calibration and validation periods, respectively.

In general, higher model skill has been determined for the local transfer models compared to SD models (SD-PMT) in cross-validation. Furthermore, estimations from circulation-type-based models have shown more variability with respect to climate models, numerical and statistical ensembles as well as downscaling approaches compared to results from local transfer models. Although objective classifications have been optimized with respect to the target variable, a relevant type-internal variability remains, which may lead to a less pronounced consistency of the SD-PMT estimations. Air temperature and zonal wind component have been detected to influence particle levels in Bavaria on a local, regional and synoptic scale in all seasons through the established quantitative relationships. Analysed changes in future $PM_{10}$ concentrations revealed similar tendencies of decreasing levels in winter and increasing ones in summer for all downscaling approaches.

**Outlook**

This thesis studies the impact of future climate-change-induced variations of $PM_{10}$ concentrations, without taking future changes in emissions as reductions or increase of particles into further account. Variations in future emission levels are just implicitly considered by the assumptions made for the RCP4.5 and RCP8.5 scenarios from the current AR5 of the IPCC in the used AOGCM. Assuming recent $PM_{10}$ concentrations at Bavarian stations from 1980 to 2011 for the downscaling models, the conducted analysis revealed for instance significantly increased particle levels in summer under changing atmospheric conditions until 2100. This fact evokes the need to further reduce $PM_{10}$ levels or at least keep existing thresholds set by the European Union to avoid an advanced air pollution and protect human health and environment, especially in the summer. Furthermore, the results of this thesis address the need to consider future climate changes with their impact on meteorological-climatological conditions on a local, regional and global scale in planning and decision processes on European air quality legislation.

As measurement techniques are refined, time series of smaller particles as $PM_{2.5}$ and ultrafine particles are nowadays available for at least a couple of years. These small particles have been found to be more critical to human health compared to $PM_{10}$ (Ostro et al., 2015). With the downscaling approaches developed in this thesis, the impact of large-scale atmospheric and local meteorological conditions on these air pollution parameters should be explored. Additionally, time series of other air pollutants like tropospherical ozone ($O_3$) or nitrogen oxides ($NO_x$) are interesting target variables for future investigations.

Urban areas are especially known to be vulnerable to climate change and high pollution levels. Such being the case, this thesis mainly focused on future variations of particle concentrations in Bavarian cities. Future work should extend the analysis on Bavarian background measurement sites, in order to quantify the influences of meteorology on the background particle levels. Additional investigations should consider changes in particle levels due to elevation. Here, the target region Bavaria is of special interest as measurement sites exist in an elevation gradient from quite low elevation at the river valleys (approx. 100 m.a.s.l.), mid-altitude measurement stations as Mount Hohenpeißenberg (1000 m.a.s.l.) in the alpine foreland up to a station on Mount Zugspitze (2960 m.a.s.l.).

The Bavarian State Ministry of the Environment and Consumer Protection recently published a report on climate and climate change in Bavaria, including potential strategies to mitigate and adapt on possible climate-change-induced consequences (StMUV, 2015). A stated goal for a clean air is the reduction of the emission of greenhouse gases. The emission reductions mainly focus on the German "Energiewende", a long-term transition from traditional energy production through burning of fossil fuel to renewable energy. Nevertheless, complementary strategies to the challenging goals should focus on the reduction of traffic and transportation emissions as well, because these are the main sources of air pollutants in Bavaria. For urban areas, Kuttler (2011b) have suggested greening, unsealing or designations of ventilation areas or a further development of public transportation as measures to adapt and mitigate on climate change and air pollution.

# Danksagung

Zuallerst geht mein herzlichster Dank an meinen Mentor und Doktorvater Prof. Dr. Jucundus Jacobeit. Lieber Herr Jacobeit, ich danke Ihnen für Ihre unermüdliche Unterstützung in der gesamten Promotionszeit, die anregenden Diskussionen, bei denen ich von Ihrem herausragenden fachlichen und methodischen Wissen profitieren konnte. Ihre Kritik und Ihr Lob haben mich stets weiter angetrieben. Ich schätze Ihr Engagement und Ihre Loyalität als Vorgesetzten, Ihren unermüdlicher Einsatz für Ihre MitarbeiterInnen. Das hat mir einen idealen Rahmen für meine Forschung in der Arbeitsgruppe Klima am Institut für Geographie der Universität Augsburg geboten.

Meinem Zweitgutachter Prof. Dr. Karl-Friedrich Wetzel möchte ich ebenfalls an dieser Stelle einen großen Dank aussprechen. Lieber Karl, ich danke Dir sehr für eine gute und unkomplizierte Zusammenarbeit sowie die Übernahme des Zweitgutachtens meiner Doktorarbeit.

Diese Doktorarbeit entstand im Rahmen der Helmholtz Research School Mechanisms and Interactions of Climate Change in Mountain Regions"(MICMoR). Dabei habe ich große Unterstützung von meinem Mentorenteam, Prof. Dr. Thomas Foken (Universität Bayreuth) und Dr. Peter Suppan (KIT IMK-IFU), erhalten. Liebe Mentoren, ich möchte mich von ganzen Herzen für anregende Thesis Advisory Commitee Meetings bedanken, bei denen ihr Euch viel Zeit für die Diskussion und den fachlichen Austausch über meine Arbeit genommen habt.

Wesentliche Teile der vorliegenden Arbeit entstanden während meiner Tätigkeit als wissenschaftliche Mitarbeiterin im Forschungsprojekt "Klimawandel und Feinstaubbelastung in Bayern"(PACLIMBA), welches durch die Deutsche Forschungsgemeinschaft gefördert wurde. Die Projektleitung hatte hierbei PD Dr. Christoph Beck inne, dem mein ganz besonderer Dank gilt. Lieber Christoph, ich möchte mich sehr herzlich bei Dir für die gute Zusammenarbeit über das Projekt hinaus bedanken. Der stete Austausch mit Dir, Deine ausgezeichnete methodische Kompetenz, Dein umfassendes Wissen und Deine große Geduld haben mir maßgeblich geholfen, so weit zu kommen.

Ein ganzer Stab an Kollegen und Freunden hat sich mit der Korrektur meiner Ausführungen befasst, bei denen ich mich hiermit in aller Form bedanken möchte: Barbara Haese, Elke Hertig, Tina Grunow, Irena Kaspar-Ott, Severin Kaspar, Benjamin Lang, Karin Romberg, Markus Homann, Bernd Chatelet.

Den lieben Kollegen am Institut für Geographie und im besonderen der Arbeitsgruppe Klima

möchte ich für rege Diskussionen und eine tolle Zusammenarbeit danken.

Ein ganz besonderer Dank ergeht weiterhin an meine Familie, die mit großer Ausdauer hinter mir standen, mich motiviert haben und immer für mich da waren. Meinem Liebsten danke ich sehr für das Durchhalten mit mir und die unermüdliche Unterstützung, vor allem in der Endphase der Arbeit.

# Literatur

Akaike, H. (1974). A new look at the statistical model identification. *IEEE Transactions on Automatic Control.*, 19/6:716–723.

Arneth, A., Unger, N., Kulmala, M., and Andreae, M. (2011). Clean the air, heat the planet? *Science*, 326:672–673.

Bahrenberg, G., Giese, E., and Nipper, J. (1999). *Statistische Methoden in der Geographie. Band 1. 4. überarbeitete Auflage.* Teubner Studienbücher der Geographie, Stuttgart, Leipzig.

Bahrenberg, G., Giese, E., and Nipper, J. (2003). *Statistische Methoden in der Geographie 2. 2. überarbeitete Auflage.* Teubner Studienbücher der Geographie, Stuttgart, Leipzig.

Barmpadimos, I., Hueglin, C., Keller, J., Henne, S., and Prevot, A. (2011). Influence of meteorology on PM10 trends and variability in Switzerland from 1991 to 2008. *Athmospheric Chemistry and Physics*, 11:1813–1835.

Bayerisches Staatsministerium für Umwelt, G. u. V. (2006). Feinstaub - Daten, Fakten, Ziele.

BayLfStaD (2014). Bayerisches Landesamt für Statistik und Datenverarbeitung: Bevölkerung: Gemeinde, Stichtage (letzten 6). Stand 2014.

Beck, C. (2000). Zirkulationsdynamische Variabilität im Bereich Nordatlantik-Europa seit 1780. *Würzburger Geographische Arbeiten*, 95:350 pp.

Beck, C. and Jacobeit, J. (2015). Abschlussbericht DFG-Projekt: Klimawandel und Feinstaubbelastung in Bayern. *DFG BE 2406/2-1*.

Beck, C., Jacobeit, J., and Jones, P. (2007). Frequency and within-type variations of large scale circulation types and their effects on low-frequency climate variability in Central Europe since 1780. *International Journal of Climatology*, 27:473–491.

Beck, C. and Philipp, A. (2010). Evaluation and comparison of circulation type classifications for the European domain. *Physics and Chemistry of the Earth*, 35:374–387.

Beck, C., Philipp, A., and Jacobeit, J. (2014a). Interannual drought index variations in Central Europe related to the large-scale atmospheric circulation - application and evaluation of statistical downscaling approaches based on circulation type classifications. *Theoretical and Applied Climatology*, pages 1–20.

Beck, C., Philipp, A., and Streicher, F. (2013). The effect of domain size on the relationship between circulation type classifications and surface climate. *International Journal of Climatology*, doi:10.1002/joc.3688.

Beck, C., Weitnauer, C., and Jacobeit, J. (2014b). Downscaling of monthly PM10 indices at different sites in Bavaria (Germany) based on circulation type classifications. *Atmospheric Pollution Research*, doi:10.5094/APR.2014.083.

Bobbia, M., Jollois, F.-V., Pggi, J.-M., and Portier, B. (2011). Quantifying local and background contributions to PM10 concentrations in haute-normandie, using random forests. *Environmetrics*, 22:758–768.

Brands, S., Herrera, S., Fernandez, J., and Gutierezz, J. (2013). How well do CMIP5 Earth System Models simulate present climate conditions in Europe and Africa? *Climate Dynamics*, 41:803–817.

Breiman, L. (2001). Random forests. *Machine Learning*, 45:5–32.

Brier, G. (1950). Verification of forecasts expressed in terms of probability. *Monthly Weather Review*, 78/1:1–3.

Brunekreef, B. and Holgate, S. (2002). Air pollution and health. *Lancet*, 360:1233–42.

Buchanan, C., Beverland, I., and Heal, M. (2002). The influence of weather-type and long-range transport in airborne particle concentrations in Edinburgh, UK. *Atmospheric Environment*, 36:5343–5354.

Carmichael, G., Sandu, A., Chai, T., Daescu, D., Constantinescu, E., and Tang, Y. (2008). Predicting air quality: Improvements through advanced methods to integrate models and measurements. *Journal of Computational Physics*, 227:3540–3571.

Chaloulakou, A., Grivas, G., and Spyrellis, N. (2003). Neural network and multiple linear regression models for PM10 prediction in athens: A comparative assessment. *Journal of the Air and Waste Managament Association*, 53:1183–1190.

Cheng, C., Campbell, M., Li, Q., Li, G., Auld, H., Day, N., Pengelly, D., Gingrich, S., and Yap, D. (2007a). A synoptic climatological approach to asses climatic impact on air quality in South-central Canada. Part I: Historical analysis. *Water Air Soil Pollution*, 182:131–148.

Cheng, C., Campbell, M., Li, Q., Li, G., Auld, H., Day, N., Pengelly, D., Gingrich, S., and Yap, D. (2007b). A synoptic climatological approach to asses climatic impact on air quality in South-central Canada. Part II: Future estimates. *Water Air Soil Pollution*, 182:117–130.

Dayan, U. and Levy, I. (2005). The influence of meteorological conditions and atmospheric circulation types on PM10 and visibility in Tel Aviv. *Journal of Applied Meteorology*, 44:606–619.

de Sá, J. M. (2007). *Applied statistics using SPSS, Statistica, Matlab and R.* Springer Berlin.

Demuzere, M., Kassomenos, P., and Philipp, A. (2010). The cost733 circulation type classification software: an example for surface ozone concentrations in Central Europe. *Theoretical and Applied Climatology*, 105/1-2:143–166.

Demuzere, M., Trigo, R., de Arellano, J. V.-G., and van Lipzig, N. (2009). The impact of weather and atmospheric circulation on $O_3$ and $PM_{10}$ levels at a rural mid-latitude site. *Atmospheric Chemistry and Physics*, 9:2695–2714.

Demuzere, M. and van Lipzig, N. (2010a). A new approach to estimate air-quality levels using a synoptic-regression approach. Part I: Present-day $O_3$ and $PM_{10}$ analysis. *Atmospheric Environment*, 44:1341–1355.

Demuzere, M. and van Lipzig, N. (2010b). A new approach to estimate air-quality levels using a synoptic-regression approach. Part II: Future $O_3$ concentrations. *Atmospheric Environment*, 44:1356–1366.

Elminir, H. (2005). Dependence of urban air pollutants on meteorology. *Science of the Total Environment*, 350:225–237.

Elminir, H. (2007). Relative influence of air pollutants and weather conditions on solar radiation - part 1: Relationship of air pollutants with weather conditions. *Meteorology and Atmospheric Physics*, 96:245–56.

Enke, W., Kreienkamp, F., and Spekat, A. (2008). STAT-IMM, a statistical approach to determine local and background contributions to PM10 levels. *Advances in Science and Research*, 2:119–126.

Enke, W. and Spekat, A. (1997). Downscaling climate model outputs into local and regional weather elements by classification and regression. *Climate Research*, 8:195–207.

E.U. (2008). Directive 2008/50/EC of the European parliament and of the council of 21 may 2008 on ambient air quality and cleaner air for Europe. *Official Journal of the European Union*, L152/1.

Fahrmeir, L., Kneib, T., and Lang, S. (2009). *Regression. Modelle, Methoden und Anwendungen.*, volume 2. Springer Berlin.

Flocas, H., Kelessis, A., Helmis, C., Petrakakis, M., Zoumakis, M., and Pappas, K. (2009). Synoptic and local scale atmospheric circulation associated with air pollution episodes in an urban Mediterranean area. *Theoretical and Applied Climatology*, 95:265–277.

Forkel, R. and Knoche, R. (2007). Nested regional climate-chemistry simulations for Central Europe. *Comptes Rendus Geoscience*, 339:734–746.

Gehrig, R. and Buchmann, B. (2003). Characterising seasonal variations and spatial distribution of ambient PM10 and PM2.5 concentrations based on long-term swiss monitoring data. *Atmospheric Environment*, 37:2571–2580.

Gietl, J. and Klemm, O. (2009). Analysis of traffic and meteorology on airborne particulate matter in Muenster, Northwest Germany. *Air Waste Management*, 59:809–818.

Giorgetta, M., Jungclaus, J., Reick, C., Legutke, S., Bader, J., Böttinger, M., Brovkin, V., Crueger, T., Esch, M., Fieg, K., Glushak, K., Gayler, V., Haal, H., Hollweg, H.-D., Ilyina, T., Kinne, S., Kornblueh, L., Matei, D., Mauritsen, T., Mikolajewicz, U., Mueller, W., Schmidt, H., Schnur, R., Segschneider, J., Six, K., Stockhause, M., Timmreck, C., Wegner, J., Widmann, H., Wieners, K.-H., Claussen, M., Marotzke, J., and Stevens, B. (2013). Climate and carbon cycle changes from 1850 to 2100 in mpi-esm simulations for the coupled model intercomparison project phase 5. *Journal of Advances in Modeling Earth Systems*, 5:572–597.

Gleckler, P., Taylor, K., and Doutriaux, C. (2008). Performance metrics for climate models. *Journal of Geophysical Reserach*, doi:10.1029/2007JD008972.

Greenpeace (2011). Cutting through the haze in China's air pollution debate. `http://www.greenpeace.org/eastasia/news/stories/climate-energy/2011/coal-air-pollution-media/`. [Online; accessed 04-09-2015].

Grömping, U. (2009). Variable importance assessment in regression: Linear regression versus random forests. *The American Statistician*, 63:4.

Hazeleger, W., Severijns, C., Semmler, T., Stefanescu, S., Yang, S., Wang, X., Wyser, K., Dutra, E., Baldasano, J., Bintanja, R., Bougeault, P., Caballero, R., Ekman, A., Christensen, J. H., van den Hurk, B., Jimenez, P., Jones, C., Kallberg, P., Koenigk, T., McGrath, R., Miranda, P., van Noije, T., Palmer, T., Parodi, J., Schmith, T., Selten, F., Storelvmo, T., Sterl, A., Tapamo, H., Vancoppenolle, M., Viterbo, P., and Willen, U. (2010). Ec-earth. a seamless earth-system prediction approach in action. *Bulletin of the American Meteorological Society*, 91:1357–1363.

Hertig, E. and Jacobeit, J. (2013). A novel approach to statistical downscaling considering nonstationarities: application to daily precipitation in the mediterranean area. *Journal of Geophysical Research: Atmospheres*, 118:520–533.

Hess, P. and Brezowsky, H. (1952). Katalog der Großwetterlagen Europas (catalog of the european large scale weather types). *Ber.Dt.Wetterd. in der US-Zone 33*.

Heyder, J. (2004). Deposition of inhaled particles in the human respiratory tract and consequences for regional targeting in respiratory drug delivery. *Proceedings of the American Thoracic Society*, 1:315–320.

Hofstätter, M., Jacobeit, J., Homann, M., Lexer, A., Chimani, B., Philipp, A., Beck, C., and Ganekind, M. (2015). Wetrax: Weather patterns, cyclonetracks and related precipitation extremes. *Manuskripte Geographica Augustana*, 19:240 p.

Holst, T., Rost, J., and Mayer, H. (2005). Analyse meteorologischer Einflussgrößen auf regionale und lokale Muster von Schwebstaub (PM10) und Stickstoffoxid-Immissionen (NO, NO2). *Meteorologisches Institut der Universität Freiburg*, page 118 p.

Hooyberghs, J., Mensink, C., Dumont, G., Fierens, F., and Brasseur, O. (2005). A neuronal network forecast for daily average PM10 concentrations in belgium. *Atmospheric Environment*, 39:3279–3289.

Huebnerova, Z. and Michalek, J. (2014). Analysis of daily average PM10 predictions by generalized linear models in Brno, Czech Republic. *Atmospheric Pollution Reserach*, doi:10.5094/APR.2014.055.

Huth, R. (2002). Statistical downscaling of daily temperature in Central Europe. *Journal of Climatology*, 15:1731–1742.

Huth, R., Beck, C., Philipp, A., Demuzere, M., Ustrnul, Z., Cahynova, M., Kysely, J., and Tveito, O. (2008). Classifications of atmospheric circulation patterns. *Annals of the New York Academy of Sciences*, 1146:105–152.

Jacob, D. and Winner, D. (2009). Effect of climate change on air quality. *Atmospheric Environment*, 43:51–63.

Jacobeit, J. (1993). Regionale Unterschiede im atmosphärischen Zirkulationsgeschehen bei globalen Klimaveränderungen (regional differences of the atmospheric circulation under conditions of global climate change). *Die Erde*, 124:63–77.

Jenkinson, A. and Collison, B. (1977). An initial climatology of gales over the north sea. *Synop Climate Branch*, Memo No.32:18.

Jolliffe, I. and Stephenson, D. (2011). *Forecast Verification: A Practitioner's Guide in Atmospheric Science. Second edition.* Wiley.

Jollois, F.-V., Poggi, J.-M., and Portier, B. (2009). Three non-linear statistical methods for analyzing PM10 pollution in rouen area. *CS-BIGS*, 3/1:1–17.

Jones, P., Hulme, M., and Briffa, K. (1993). A comparison of Lamb circulation types with an objective classification scheme. *International Journal of Climatology*, 13:655–663.

Kalnay, E., Kanamitsu, M., Kistler, R., Collins, W., Deaven, D., Gandin, L., Iredell, M., Saha, S., White, G., Woollen, J., Zhu, Y., Chelliah, M., Ebisuzaki, W., Higgins, W., Janowiak, J., Mo, K., Ropelewski, C., Wang, J., Leetmaa, A., Reynolds, R., Jenne, R., and Joseph, D. (1996). The NCEP/NCAR 40-year Reanalysis Project. *Bulletin of American Meteorological Society*, 77/3.

Keim, B., Meeker, L., and Slater, J. (2005). Manual synoptic climate classification for the East Coast of New England (USA) with an application to PM2.5 concentration. *CLIMATE RESEARCH*, 28:143–154.

Kiesewetter, G., Borken-Kleefeld, J., Schöpp, W., Heyes, C., Thunis, P., Bessagnet, B., Terrenoire, E., Fagerli, H., Nyiri, A., and Amann, M. (2015). Modelling street level PM10 concentrations across Europe: source apportionment and possible futures. *Atmospheric Chemistry and Physics,*, 15:1539–1553.

Kirchhofer, W. (1974). Classification of European 500 mb patterns. *Arbeitsbericht der Schweizerischen Meteorologischen Zentralanstalt*, 43:1–16.

Kistler, R., Kalnay, E., Collins, W., Saha, S., White, G., Woollen, J., Chelliah, M., Ebisuzaki, W., Kanamitsu, M., Kousky, V., van den Dool, H., Jenne, R., and Fiorino, M. (2001). The ncep/ncar 50-year Reanalysis: Monthly means cd-rom and documentation. *Bulletin of American Meteorological Society*, 82/2.

Klimaforschungsverbund, B. (1996). BAYFORKLIM: Klimaatlas von Bayern.

Kraus, H. (2008). *Grundlagen der Grenzschicht-Meteorologie. Einführung in die Physik der atmosphärischen Grenzschicht und in die Mikrometeorologie.* Springer Berlin.

Kruizinga, S. (1979). Objective classification of daily 500 mbar patterns. in: Preprints sixth conference on probability and statistics in atmospheric sciences, 9-12 october 1979 Banff, Alberta. *American Meteorological Society, Boston MA.*, pages 126–129.

Krämer, W. and Sonnberg, H. (1986). *The linear regression model under test.*, volume 1. Springer Heidelberg.

Kuttler, W. (2011a). Climate change in urban areas, part 1, effects. *Environmental Sciences Europe*, 23:11:1–12.

Kuttler, W. (2011b). Climate change in urban areas, part 2, measures. *Environmental Sciences Europe*, 23:21:1–15.

Landesamt für Umwelt, B. (2013). Das Lufthygienische Landesüberwachungssystem Bayern (LÜB).

Lesniok, M. and Caputa, Z. (2009). The role of atmospheric circulation in air pollution distribution in Katowice region (southern poland). *Journal of Environment and Waste Management*, 4:62–65.

Liedtke, H. and Marcinek, J. (1996). *Physische Geographie Deutschlands. 3. überarbeitete und erweiterte Auflage.* Klett-Perthes.

Litynski, J. (1969). A numerical classification of circulation patterns and weather types in Poland. *Prace Panstwowego Instytutu Hydrologiczno-Meteorologicznego*, 97:3–15.

Lund, I. (1963). Map-pattern classification by statistical methods. *Journal of Applied Meteorology*, 2:56–65.

Makra, L., Mika, J., Bartzokas, A., R.Beczi, Borsos, E., and Sümeghy, Z. (2006). An objective classification system of air mass types for Szeged, Hungary, with special interest in air pollution levels. *Meteorology and Atmospheric Physics*, 92:115–137.

Makra, L., Mika, J., Bartzokas, A., and Suemeghy, Z. (2007). Relationship between the Péczelys large-scale weather types and air pollution levels in Szeged, Southern Hungary. *Fresenius Environmental Bulletin*, 16/6:660–673.

McGregor, G. and Bamzelis, D. (1995). Synoptic typing and its application to the investigation of weather air pollution relationships, Birmingham, United Kingdom. *Theoretical and Applied Climatology*, 51:223–236.

McKendry, I. (2002). Evaluation of artificial neural networks for fine particulate pollution (PM10 and PM2.5) forecasting. *Journal of the Air and Waste Managament Association*, 52:1096–1101.

Medina, S., Plasencia, A., Ballester, F., Mücke, H., and Schwartz, J. (2004). Apheis: public health impact of PM10 in 19 European cities. *Journal of Epidemiology and Community Health*, 58:831–836.

Murphy, A. (1988). Skill scores based on the mean square error and their relationships to the correlation coeffcient. *Monthly Weather Review*, 116:2417–2424.

Murtagh, F. (1985). Multidimensional Clustering Algorithms. *Physica Verlag Würzburg*, 4 of Compstat Lectures.

Nguyen, C., Wang, Y., and Nguyen, H. (2013). Random forest classifier combined with feature selection for breast cancer diagnosis and prognostic. *Journal of Biomedical Science and Engineering*, 6:5.

Ostro, B., Hu, J., Goldberg, D., Reynolds, P., Hertz, A., Bernstein, L., and Kleeman, M. (2015). Associations of mortality with long-term exposures to fine and ultrafine particles, species and sources: Results from the california teachers study cohort. *Environmental Health Perspectives,*, 123(6).

Péczely, G. (1983). Catalogue of the macrosynoptic types for Hungary (1881-1983). *Hung. Meteorol. Serv.*, 53.

Philipp, A. (2009). Comparison of principal component and cluster analysis for classifying circulation pattern sequences for the european domain. *Theoretical and Applied Climatology*, 96:31–41.

Philipp, A., Bartholy, J., Beck, C., Erpicum, M., Esteban, P., Fettweis, X., Huth, R., James, P., Jourdain, S., Kreienkamp, F., Krennert, T., Lykoudis, S., Michalides, S., Pianko-Kluczynska, K., Post, P., Alvarez, D. R., Schiemann, R., Spekat, A., and Tymvios, F. (2010). Cost733cat - a database of weather and circulation type classifications. *Physics and Chemistry of the Earth*, 35:360–373.

Philipp, A., Beck, C., Huth, R., and Jacobeit, J. (2014). Development and comparison of circulation type classifications using cost 733 dataset and software. *International Journal of climatology*, 2014:19 p.

Philipp, A., Della-Marta, P., Jacobeit, J., Fereday, D., Jones, P., Moberg, A., and Wanner, H. (2007). Long-term variability of daily north atlantic-european pressure patterns since 1850 classified by simulated annealing clustering. *Journal of Climate*, 20:4065–4095.

Pitz, M., Schmid, O., Heinrich, J., Birmili, W., Maghun, J., Peters, R. Z. H.-E. W. A., and Cyrys, J. (2008). Seasonal and diurnal variation of PM2.5 apparent particle density in urban air in Augsburg, Germany. *Environmental Science and Technology*, 42:5087–5093.

Pope, C. and Dockery, D. (2006). Health effects of fine particulate air pollution: Lines that connect. *J. Air Waste Management Association*, 56:709–742.

Pope, C., Dockery, D., and Schwartz, J. (1995). Review of epidemiological evidence of health effects of particulate air pollution. *Inhalation Toxicology*, 7/1:1–18.

Rahmstorf, S., Foster, G., and Cazenave, A. (2012). Comparing climate projections to observations up to 2011. *Environmental Research Letters 7 044035*, doi:10.1088/1748-9326/7/4/044035.

Rückerl, R., Schneider, A., Breitner, S., Cyrys, J., and Peters, A. (2011). Health effects of particulate air pollution: A review of epidemiological evidence. *Inhalation Toxicology,*, 23(10):555–592.

Schiemann, R. and Frei, C. (2010). How to quantify the resolution of surface climate by circulation types: An example for Alpine precipitation. *Physics and Chemistry of the Earth*, 35:403–410.

Schäfer, K., Elsasser, M., Arteaga-Salas, J., Gu, J., Pitz, M., Schnelle-Kreis, J., Cyrys, J., Emeis, S., Prevot, A., and Zimmermann, R. (2014). Source apportionment and the role of meteorological conditions in the assessment of air pollution exposure due to urban emissions. *Atmospheric Chemistry and Physics Discussions*, 14:2235–2275.

Schäfer, K., Emeis, S., Hoffmann, H., and Jahn, C. (2006). Influence of mixing layer height upon air pollution in urban and sub-urban areas. *Meteorologische Zeitschrift*, 15/6:647–658.

Schönwiese, C.-D. (2003). *Klimatologie. 2. neu bearbeitete und aktualisierte Auflage.*, volume 2. Verlag Eugen Ulmer, Stuttgart.

Schönwiese, C.-D. (2013). *Praktische Statistik für Meteorologen und Geowissenschaftler.*, volume 5. Gebrüder Bornträger, Berlin, Stuttgart.

Seinfeld, J. and Pandis, S. (2012). *Atmospheric chemistry and physics: from air pollution to climate change. Second edition.* Wiley, J.

Smith, S., Stribley, F., Milligan, P., and Barratt, B. (2001). Factors influencing measurements of PM10 during 1995 - 1997 in london. *Atmospheric Environment*, 35:4651–4662.

Stadlober, E., Hormann, S., and Pfeiler, B. (2008). Quality and performance of a PM10 daily forecasting model. *Atmospheric Environment*, 42:1098–1109.

Stadlober, E., Huebnerova, Z., Michalek, J., and Kolar, M. (2012). Forecasting of daily PM10 concentrations in Brno and Graz by different regression approaches. *Austrian Journal of Statistics*, 41/4:287–310.

Stahel, W. (2008). *Statistische Datenanalyse. Eine Einführung für Naturwissenschaftler. 2. Auflage.* Springer Berlin.

Stefan, S., Necula, C., and Geogescu, F. (2010). Analysis of long-range transport of particulate matters in connection with air circulation over Central and Eastern part of Europe. *Physics and Chemistry of the Earth*, 35:523–529.

Stevens, B., Giorgetta, M., Esch, M., Mauritsen, T., Crueger, T., Rast, S., Salzmann, M., Schmidt, H., Bader, J., Block, K., Brokopf, R., Fast, I., Kinne, S., Kornblueh, L., Lohmann, U., Pincus, R., Reichler, T., and Roeckner, E. (2013). The atmospheric component of the mpi-m earth system model: Echam6. *Journal of Advances in Modeling Earth Systems*, 5:146–172.

StMUV (2015). Bayerisches Staatsministerium für Umwelt und Verbraucherschutz (stmuv): Klima-Report Bayern 2015 - Klimawandel, Auswirkungen, Anpassungs- und Forschungsaktivitäten.

Stocker, T., Qin, D., Plattner, G.-K., Tignor, M., Allen, S., Boschung, J., Nauels, A., Xia, Y., Bex, V., and Midgley, P. (2013). Climate change 2013: The physical science basis. Contribution of working group I to the fifth assessment report of the intergovernmental panel on climate change. *Cambridge University Press*, page 1535 pp.

Taylor, K., Stouffer, R., and Meehl, G. (2012). An overview of cmip5 and the experiment design. *Bulletin of the American Meteorological Society*, 93:485–498.

Thompson, D. and Wallace, J. (1999). Annular modes in the extratropical circulation. part i: Month-to-month variability. *Journal of Climate*, 13:1000–1016.

Toutenburg, H., Schomaker, M., Wissmann, M., and Heumann, C. (2006). *Arbeitsbuch zur deskriptiven und induktiven Statistik.* Springer Berlin.

Triantafyllou, A. (2001). PM10 pollution episodes as a function of synoptic climatology in a mountainous industrial area. *Environmental Pollution*, 112:491–500.

Umweltbundesamt (2005). Hintergrundpapier zum Thema Staub/Feinstaub (PM).

Umweltbundesamt (2013). Das Luftmessnetz des Umweltbundesamtes.

Umweltbundesamt (2015). Hintergrundpapier. Luftqualität 2014. Vorläufige Auswertung.

Valverde, V., Pay, M., and Baldasano, J. (2015). Circulation-type classification derived on a climatic basis to study air quality dynamics over the Iberian Peninsula. *International Journal of Climatology*, 35:2877–2897.

van Vuuren, D., Edmonds, J., Kainuma, M., Riahi, K., Thomson, A., Hibbard, K., Hurtt, G., Kram, T., Krey, V., Lamarque, J.-F., Masui, T., Meinshausen, M., Nakicenovic, N., Smith, S., and Rose, S. (2011). The representative concentration pathways: an overview. *Climatic Change*, 109:5–31.

WHO (2006). World health organization: Air quality guidelines for particulate matter, ozone, nitrogen dioxide and sulfur dioxide. global update 2005. *WHO Press, Geneva*.

Wichmann, H.-E. (2008). Schützen Umweltzonen unsere Gesundheit oder sind sie unwirksam? *Umweltmed Forsch Prax*, 13/1:7–10.

Wilby, R., Charles, S., Zorita, E., Timbal, B., Whetton, P., and Mearns, L. (2004). Guidelines for use of climate scenarios developed from statistical downscaling methods. *IPCC Task Group on Data and Scenario Support for Impacts and Climate Analysis (TGICA).*

Wilby, R. and Wigley, T. (1997). Downscaling general circulation model output: a review of methods and limitations. *Progress in Physical Geography*, 21/4:530–548.

Wilks, D. (2006). *Statistical methods in the atmospheric science. Second Edition.* Elsevier, Academic press.

Wojcik, R. (2015). Reliability of CMIP5 GCM simulations in reproducing atmospheric circulation over Europe and the North Atlantic: a statistical downscaling perspective. *International Journal of Climatology*, 35:714–732.

Wollschläger, D. (2012). *Grundlagen der Datenanalyse mit R. Eine anwendungsorientierte Einführung. 2. Auflage.* Vieweg + Teubner.

Yarnal, B. (1993). *Synoptic climatology in environmental analysis.* Belhaven Press London.

Yarnal, B., Comrie, A., Frakes, B., and Brown, D. (2001). Developments and prospects in synoptic climatology. *Internation Journal of Climatology*, 21:1923–1950.

Yuval, Broday, D., and Alpert, P. (2012). Exploring the applicability of future air quality predictions based on synoptic system forecast. *Environmental Pollution*, 166:65–74.

# A. Appendix

Table A.1: Description of 49 $PM_{10}$ measurement sites in Bavaria/Germany run by Bavarian Environmental Agency (LfU), German Weather Service (DWD) and Federal Environmental Agency (UBA).

| Name | ID | Latitude | Longitude | Altitude | Type |
|---|---|---|---|---|---|
| Ingolstadt/Rechbergstrasse | L1.1 | 11°25′43.6″ | 48°46′10″ | 374 | traffic |
| Burghausen/Marktler-Strasse | L1.2 | 12°49′45,5″ | 48°10′37,8″ | 420 | background |
| Trostberg/Schwimmbadstrasse | L1.14 | 12°32′17,4?? | 48°1′18″ | 488 | background |
| Mehring/Sportplatz | L1.15 | 12°46′53″ | 8°10′58,2″ | 415 | background |
| Andechs/Rothenfeld | L1.16 | 11°13′12,6″ | 47°58′7,5″ | 750 | background |
| Kelheim/Regensburger-Strasse | L2.1 | 11°52′45.3″ | 48°54′34.3″ | 348 | traffic |
| Landshut/Podewilsstrasse | L2.3 | 12°9′25.4″ | 48°32′23.3″ | 390 | traffic |
| Neustadt/Eining | L2.6 | 11°46′40,1″ | 48°51′11,6″ | 359 | background |
| Saal/Regensburger-Strasse | L2.9 | 11°56′55,7″ | 48°54′15,2″ | 340 | background |
| Regen/Bodenmaiser-Strasse | L2.11 | 13°7′44,2″ | 48°58′20,6″ | 545 | background |
| Passau/Stelzhamerstrasse | L2.12 | 13°25′19,3″ | 48°34′25,1″ | 300 | background |
| Regensburg/Rathaus | L3.1 | 12°6′6.7″ | 49°1′8.4″ | 335 | traffic |
| Weiden/Nikolaistrasse | L3.3 | 12°9′33.7″ | 49°40′44.2″ | 400 | background |
| Schwandorf/Wackersdorfer-Strasse | L3.4 | 12°7′41.3″ | 49°19′19″ | 380 | background |
| Tiefenbach/Altenschneeberg | L3.6 | 12°32′55,9″ | 49°26′18,5″ | 755 | background |
| Sulzbach-Rosenberg/Lohe | L3.8 | 11°47′10,8″ | 49°29′16,7″ | 393 | background |
| Bayreuth/Rathaus | L4.2 | 11°34′32.7″ | 49°56′49.5″ | 336 | traffic |
| Bamberg/Löwenbruecke | L4.3 | 10°53′15.7″ | 49°53′54″ | 231 | background |
| Arzberg/Egerstrasse | L4.5 | 12°11′19,1″ | 50°3′29,5″ | 418 | background |
| Naila/Selbitzer-Berg | L4.6 | 11°43′17,8″ | 50°19′23,7″ | 534 | background |
| Coburg/Lossaustrasse | L4.7 | 10°57′33,5″ | 50°15′38,1″ | 291 | traffic |
| Kulmbach/Konrad-Adenauer-Strasse | L4.8 | 11°26′33,3″ | 50°6′11,3″ | 303 | background |
| Nürnberg/Bahnhof | L5.1 | 11°5′18.4″ | 49°26′45.3″ | 307 | traffic |
| Nürnberg/Ziegelsteinstrasse | L5.2 | 11°6′21.1″ | 49°28′37.4″ | 320 | traffic |
| Fürth/Theresienstrasse | L5.5 | 10°59′4.9″ | 49°28′20″ | 293 | traffic |
| Ansbach/Residenzstrasse | L5.12 | 10°34′20,3″ | 49°18′17,6″ | 400 | traffic |
| Erlangen/Kraepelinstrasse | L5.14 | 10°57′48,7″ | 49°36′21,3″ | 284 | background |
| Schweinfurt/Obertor | L6.3 | 10°13′55.5″ | 50°2′54.5″ | 231 | traffic |
| Würzburg/Kardinal-Faulh.-Platz | L6.4 | 9°56′9.4″ | 49°47′40.5″ | 179 | traffic |
| Aschaffenburg/Bussardweg | L6.6 | 9°7′4,7″ | 49°59′29,5″ | 134 | background |
| Augsburg/Königsplatz | L7.1 | 10°53′42.1″ | 48°21′52.5″ | 492 | traffic |
| Kempten/Westendstrasse | L7.3 | 10°18′23,6″ | 47°43′30,5″ | 678 | background |
| Lindau/Holdereggenstrasse | L7.4 | 9°41′24,1″ | 47°33′15,8″ | 403 | traffic |
| Neu-Ulm/Gabelsbergerstrasse | L7.5 | 10°0′29,9″ | 48°23′49,5″ | 470 | background |
| Augsburg/Bourges-Platz | L7.6 | 10°53′18,1″ | 48°22′35,7″ | 477 | background |
| Augsburg/LfU | L7.8 | 10°54′11″ | 48°19′33,6″ | 495 | background |
| München/Stachus | L8.1 | 11°33′53.7″ | 48°8′41.1″ | 521 | traffic |
| München/Lothstrasse | L8.3 | 11°33′16.8″ | 48°9′16.3″ | 521 | traffic |
| München/Johanneskirchen | L8.12 | 11°38′52,9″ | 48°10′23,5″ | 513 | background |
| Augsburg/Karlstrasse | L14.1 | 10°53′48,6″ | 48°22′13,3″ | 485 | traffic |
| Bayreuth/Hohenzollernring | L14.2 | 11°34′12,3″ | 49°56′37,1″ | 337 | traffic |
| München/Prinzregentenstrasse | L14.3 | 11°35′32,2″ | 48°8′33,9″ | 510 | traffic |
| München/Landshuter-Allee | L14.4 | 11°32′11,4″ | 48°8′58,6″ | 521 | traffic |
| Würzburg/Stadtring-Süd | L14.5 | 9°56′51,6″ | 49°47′25,9″ | 198 | traffic |
| Nürnberg/Von-der-Tann-Strasse | L14.7 | 11°2′9,9″ | 49°26′25,7″ | 308 | traffic |
| Oberaudorf/Inntal-Autobahn | L14.8 | 12°10′25″ | 47°38′50,8″ | 482 | traffic |
| Schauinsland | | 47°54′40″ | 7°53′58″ | 1205 | rural background |
| Schmücke | | 50°39′ | 10°46′ | 937 | rural background |
| Hohenpeissenberg | | 47°48′ | 11°1′ | 985.5 | rural background |

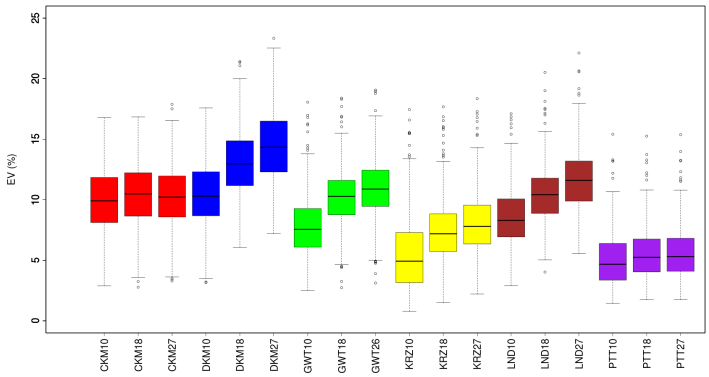


Figure A.1: Box-Whisker-Plots of Explained Variance (in %) estimated for $PM_{10}$ at 16 stations for different classification methods (k-means clusteranalysis (CKM, DKM), prototype classification (GWT), threshold-based (LND) and PCA (KRZ, PTT) as well as three number of classes (10, 18, 27). Upper/lower whiskers indicate the 1.5 interquartile range (IQR) from the upper/lower quartiles.

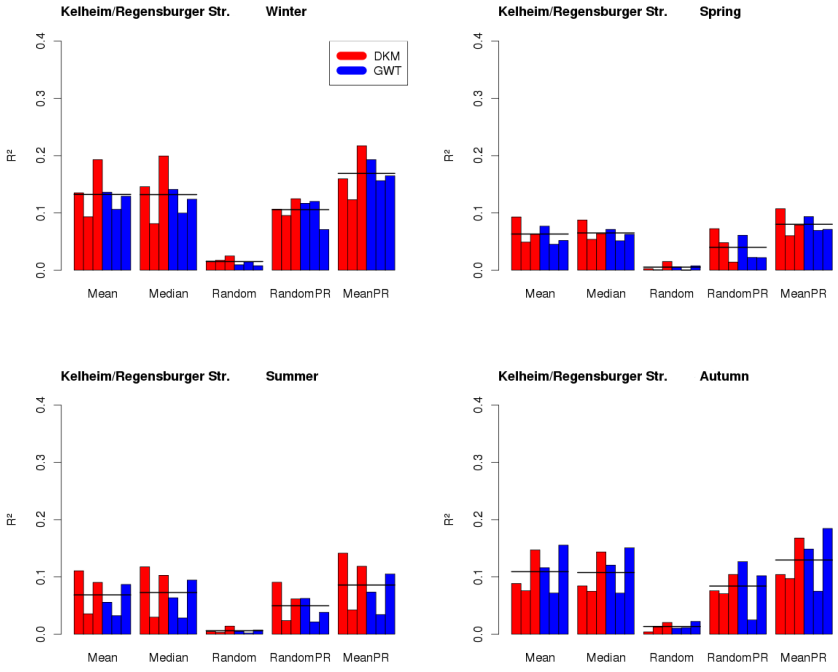


Figure A.2: Barplots indicating $R^2$ for three validation periods marked by bars. Mean, median and randomly selected $PM_{10}$ values as well as two modifications including the $PM_{10}$ concentrations on the previous day marked as random PR and meanPR (see text for further explanation) are used as Synoptic downscaling variants based on seasonal non-optimized classifications of sea level pressure classified with GWT (blue) and DKM (red) at Kelheim Regensburger Str. (L8.3). Averaged $R^2$ over three validation periods are marked as black line.

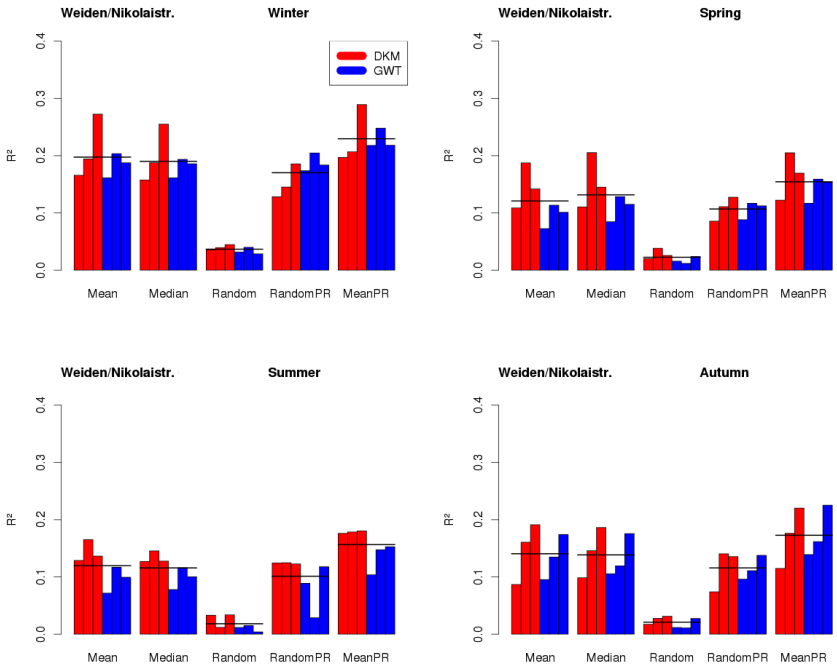


Figure A.3: Same as Figure A.2 for Weiden Nikolaistr.

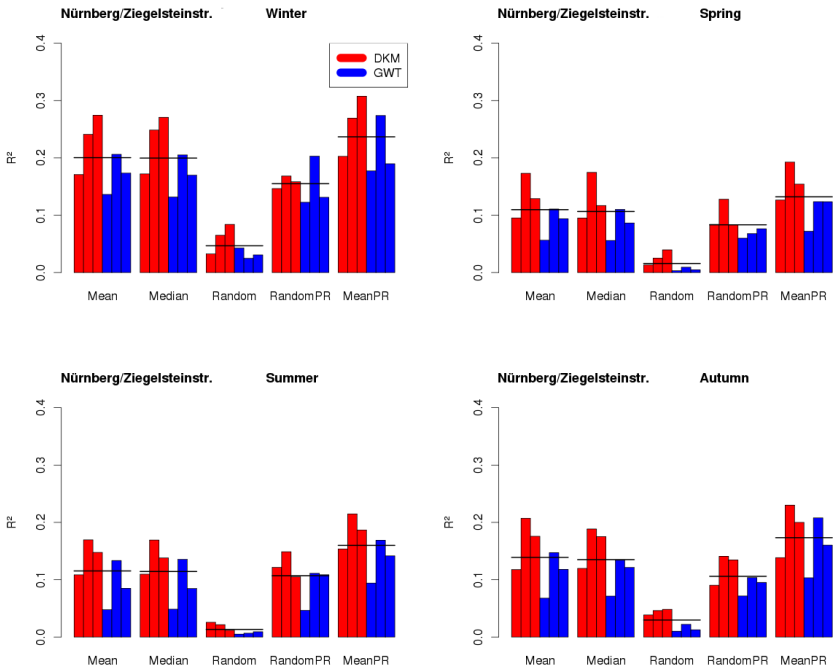


Figure A.4: Same as Figure A.2 for Nürnberg Ziegelsteinstr.

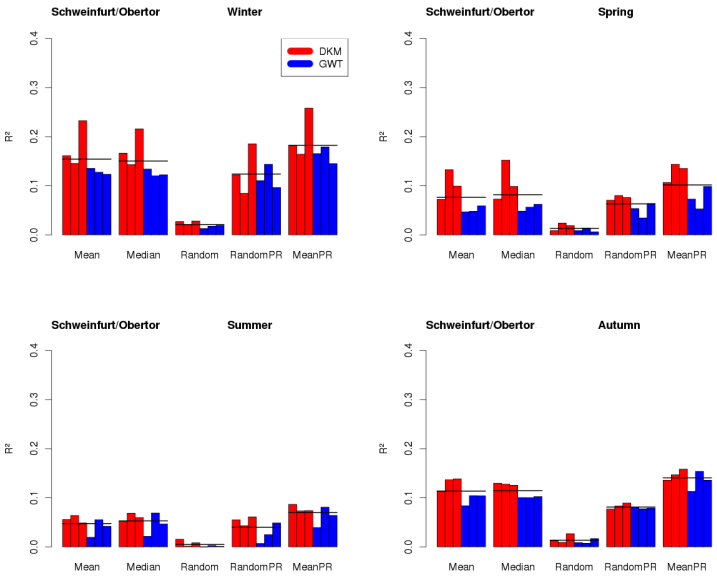


Figure A.5: Same as Figure A.2 for Schweinfurt Obertor.

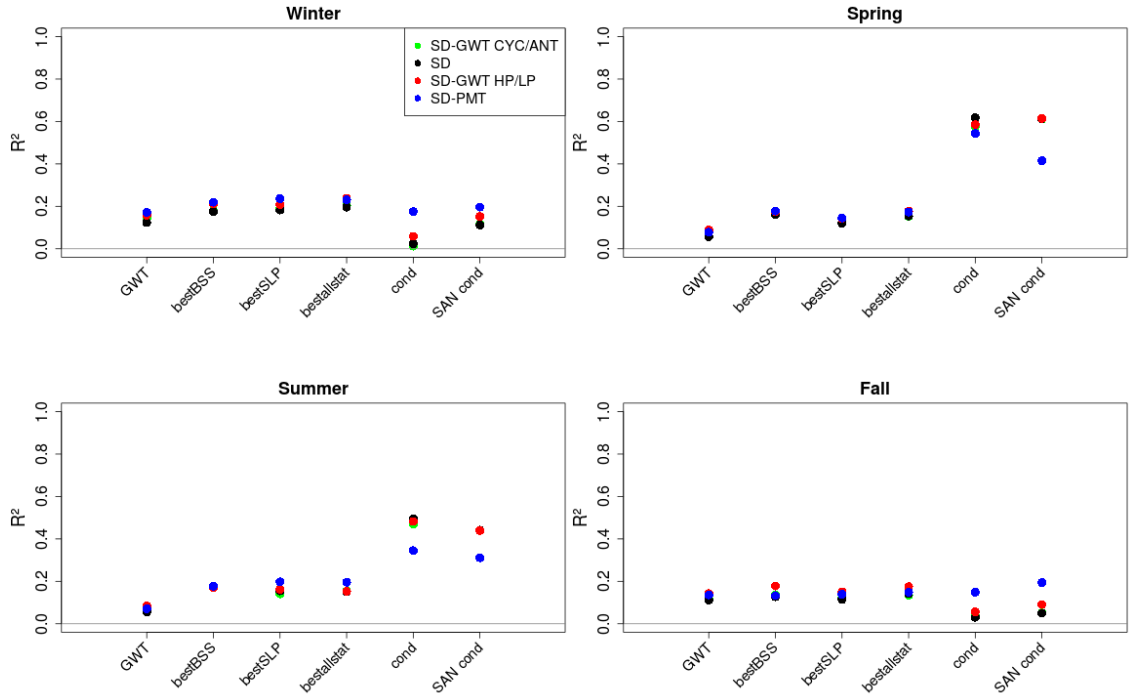


Figure A.6: Minimum values of $R^2$ from 3 validation periods between modelled and observed seasonal $PM_{daily}$ values at station Kelheim Regensburger Str. using variants of Synoptic Downscaling and representative non-optimized (GWT), optimized unconditioned (bestBSS, bestSLP, bestallstat) as well as optimized conditioned (cond., SANcond.) classifications.

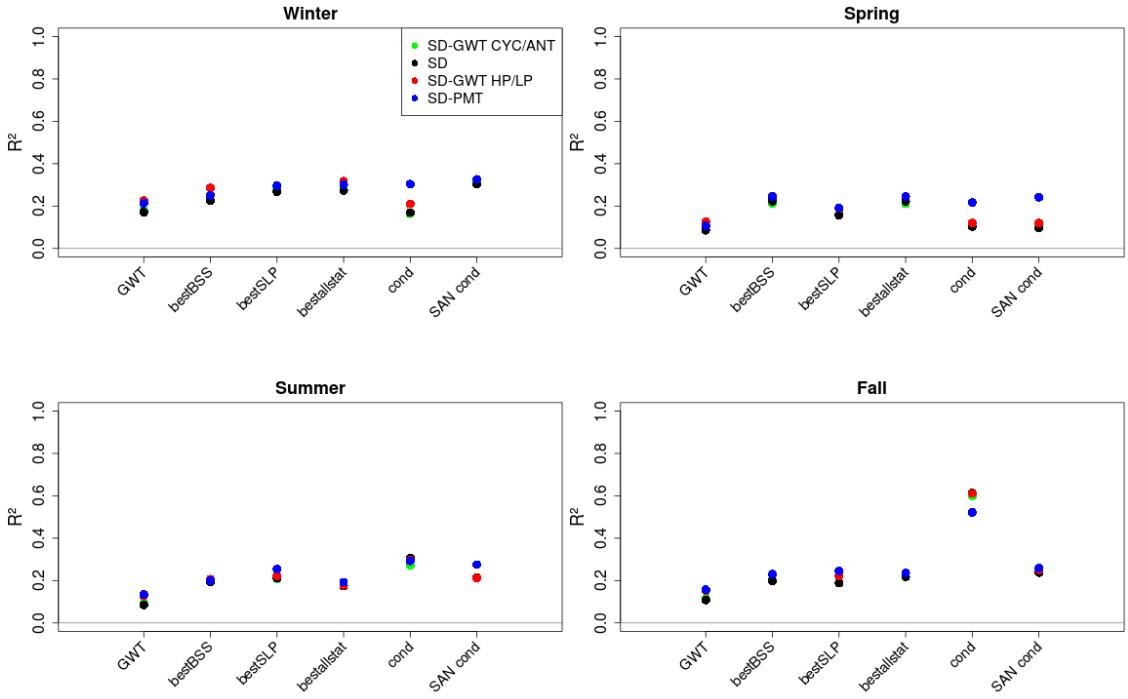


(a) Nürnberg

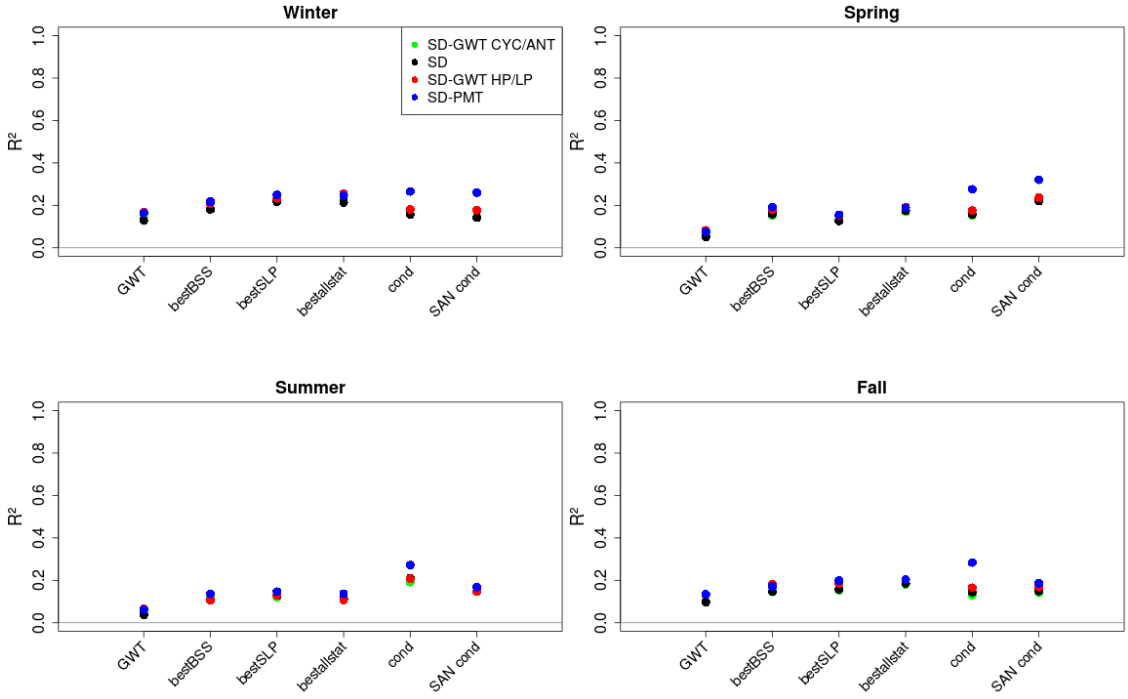


(b) Schweinfurt

Figure A.7: Same as Figure A.9 for stations Nürnberg Ziegelsteinstr. and Schweinfurt Obertor.

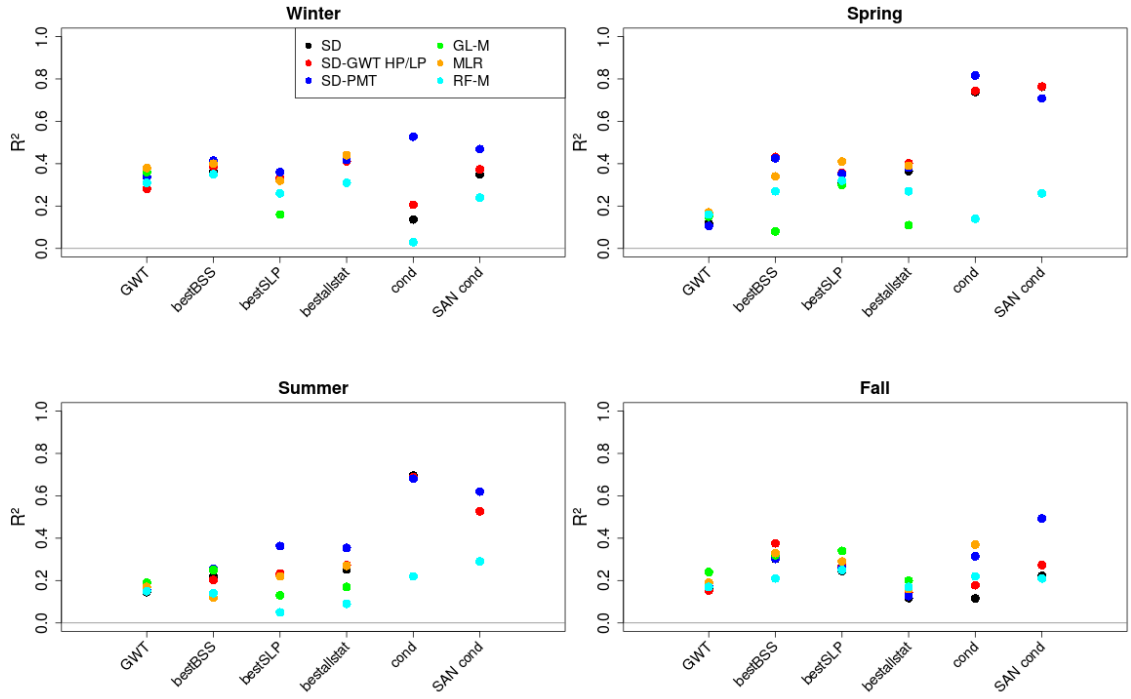


(a) Kelheim

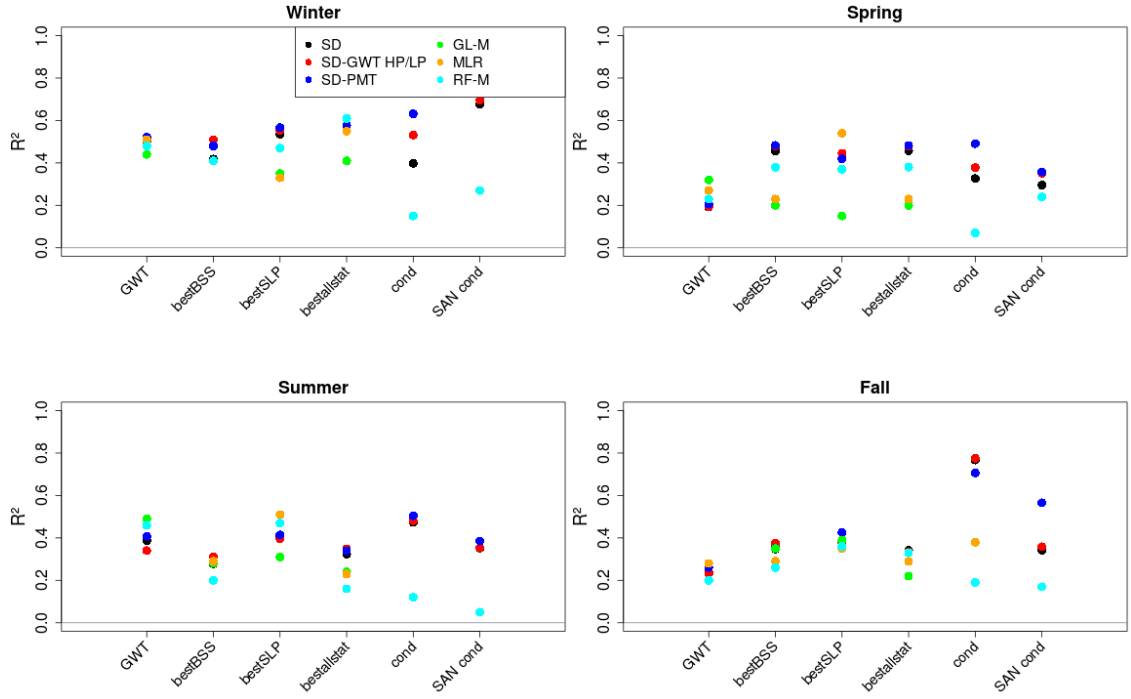


(b) Nürnberg

Figure A.8: Minimum values of $R^2$ from 3 validation periods between modelled and observed seasonal $PM_{mean}$ at station Kelheim Regensburger Str. (a) and Nürberg Ziegelsteinstr. (b) using various downscaling approaches (SD = Synoptic Downscaling with mean $PM_{10}$, SD-GWT HP/LP = SD considering high/low pressure patterns on the previous day, SD-PMT = SD considering mean $PM_{10}$ concentration on the previous day, GL-M = Generalized Linear Model, RF-M = Random Forest Model, MLR = Multiple Linear Regression) and representative non-optimized (GWT), optimized unconditioned (bestBSS, bestSLP, bestallstat) as well as optimized conditioned (cond., SANcond.) classifications.

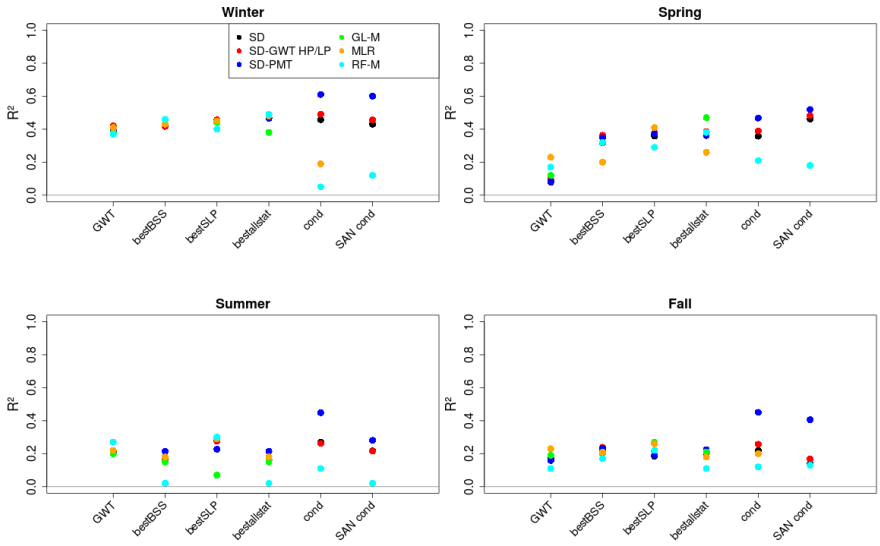


Figure A.9: Same as Figure A.8 for Schweinfurt Obertor.

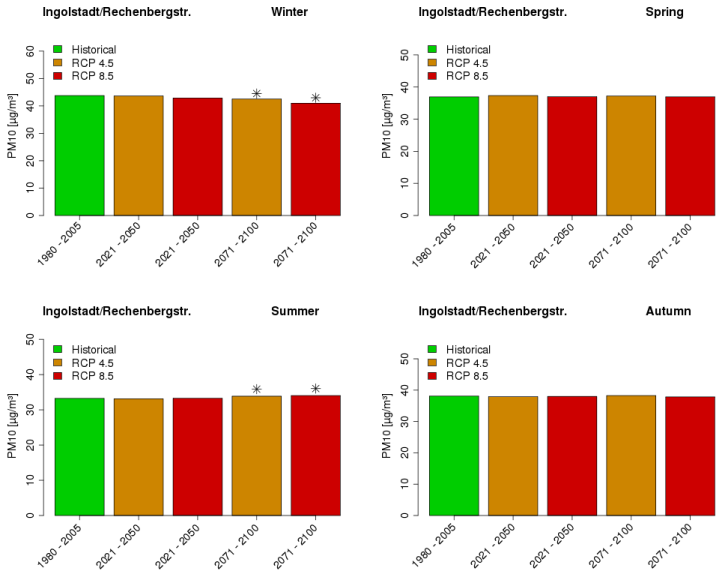


(a) Ingolstadt

Figure A.10: Modelled seasonal $PM_{mean}$ levels (in $\mu g/m^3$) at station Ingolstadt Rechenbergstr. Estimations are based on three numerical ensemble members from ECHAM6 scenarios (RCP4.5, RCP8.5) for two time periods (2021 - 2050, 2071 - 2100) using four statistical ensemble members using Synoptic Downscaling variant (SD-PMT). Stars mark statistical significance (alpha = 0.05) of differences between particular scenario and historical period.

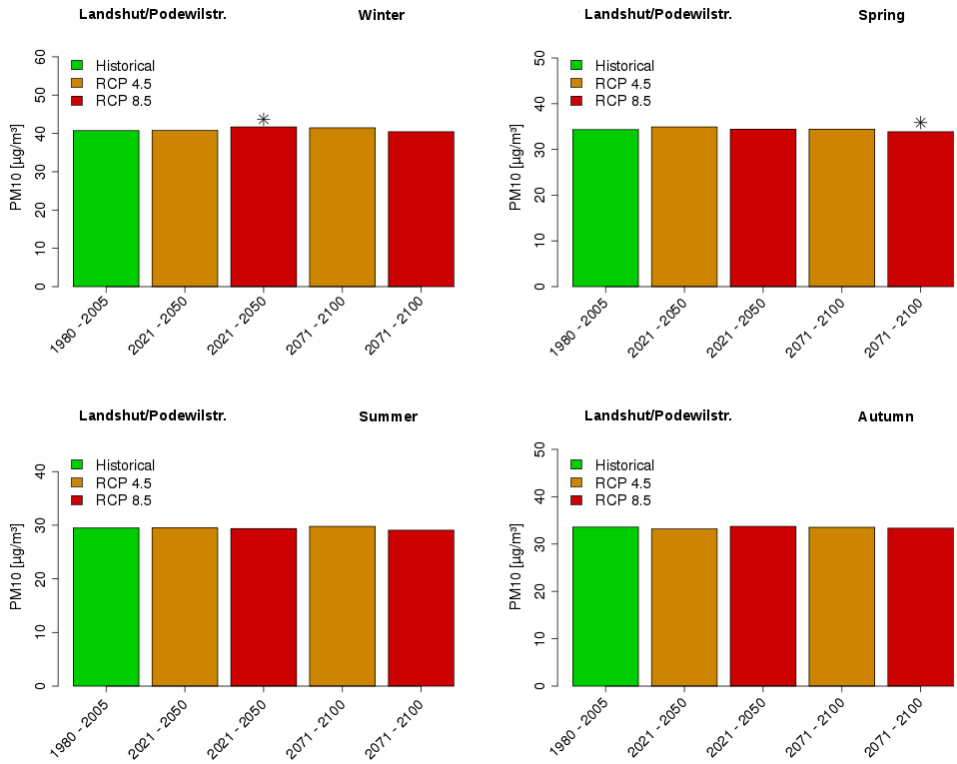


(a) Landshut

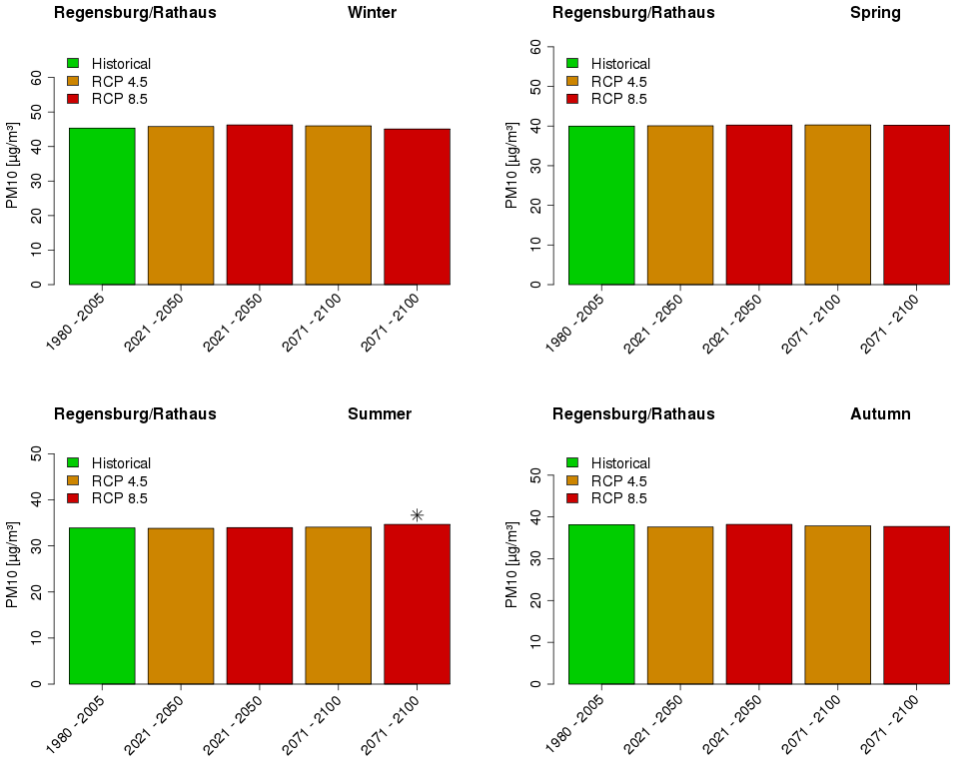


(b) Regensburg

Figure A.11: Same as Figure A.10 for stations Landshut Podewilsstr. (a) and Regensburg Rathaus (b).

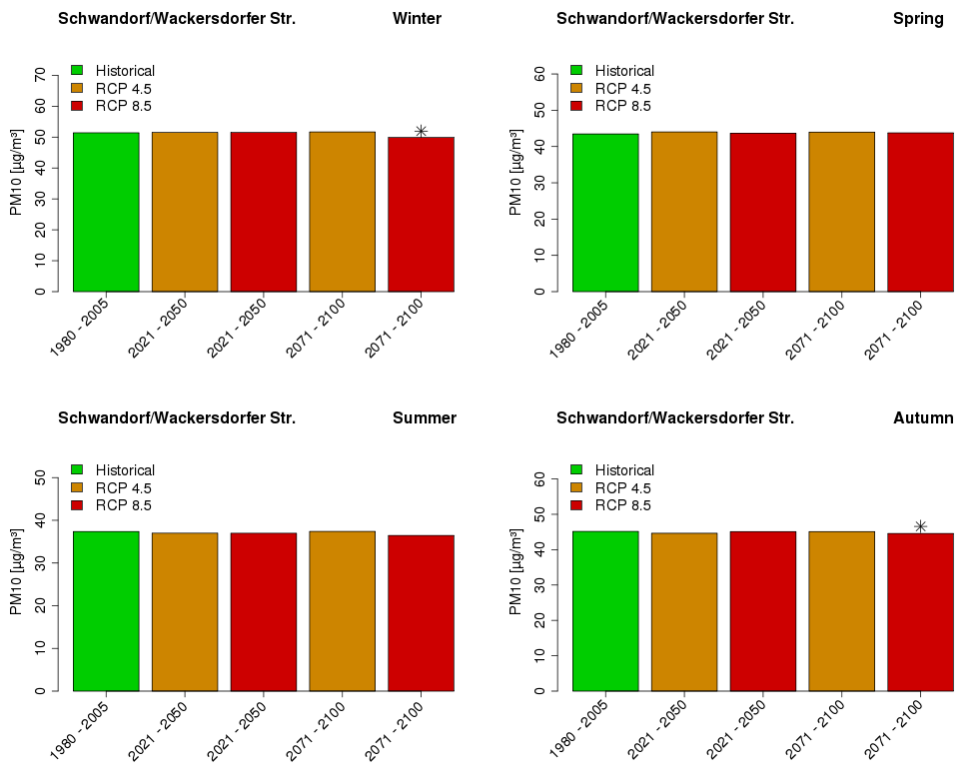


(a) Schwandorf

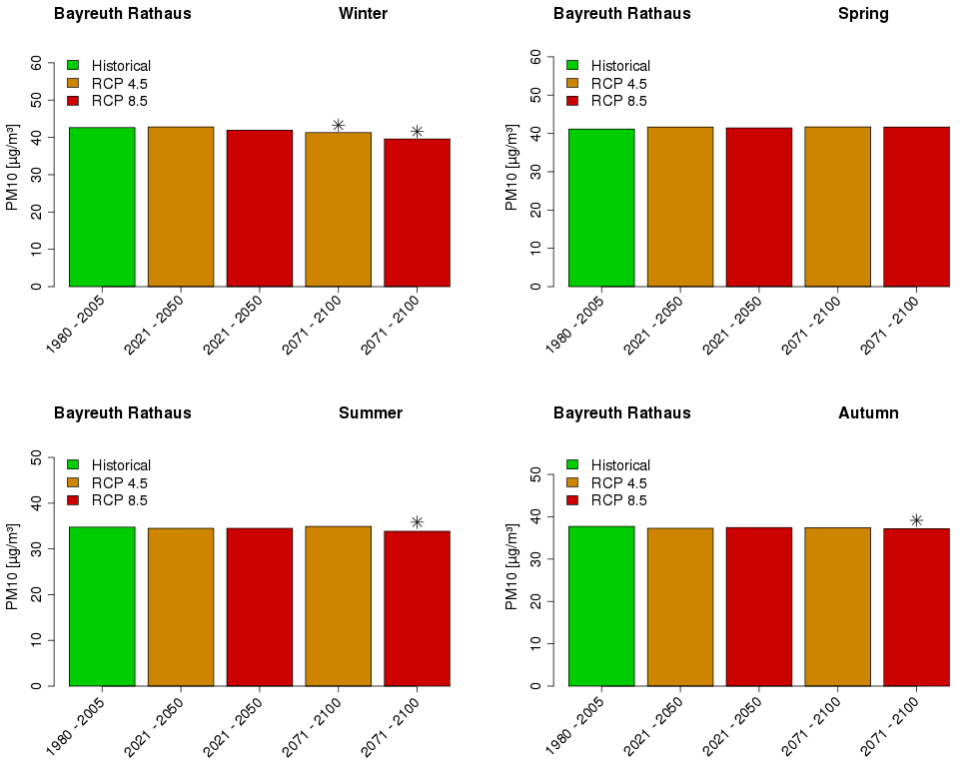


(b) Bayreuth

Figure A.12: Same as Figure A.10 for stations Schwandorf Wackersdorfer Str. (a) and Bayreuth Rathaus (b).

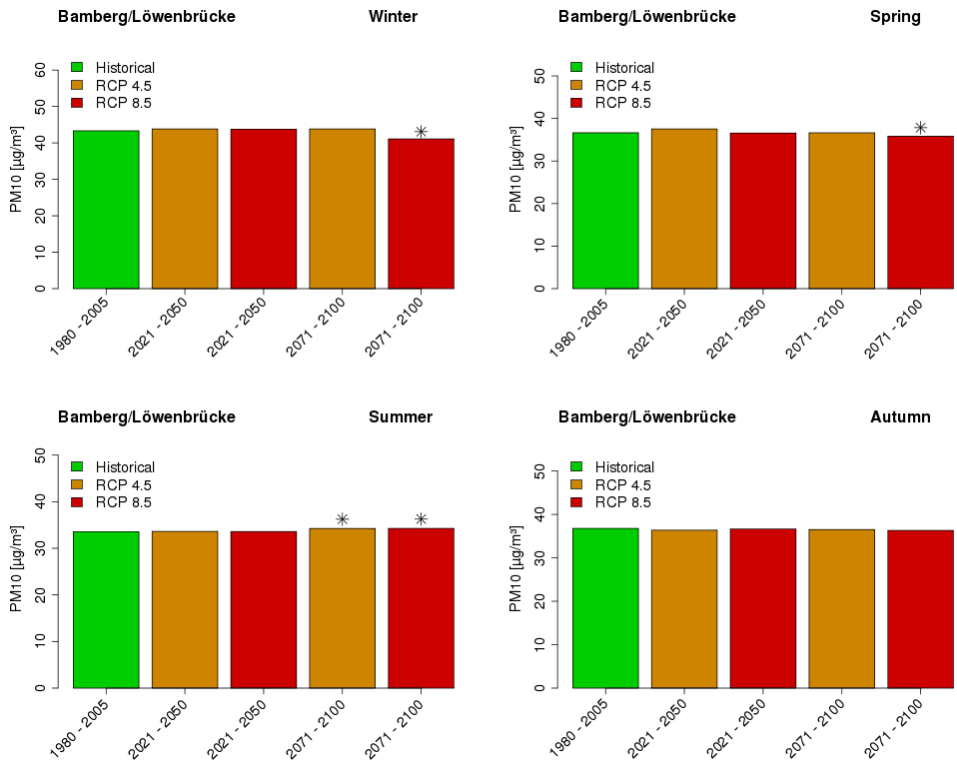


(a) Bamberg

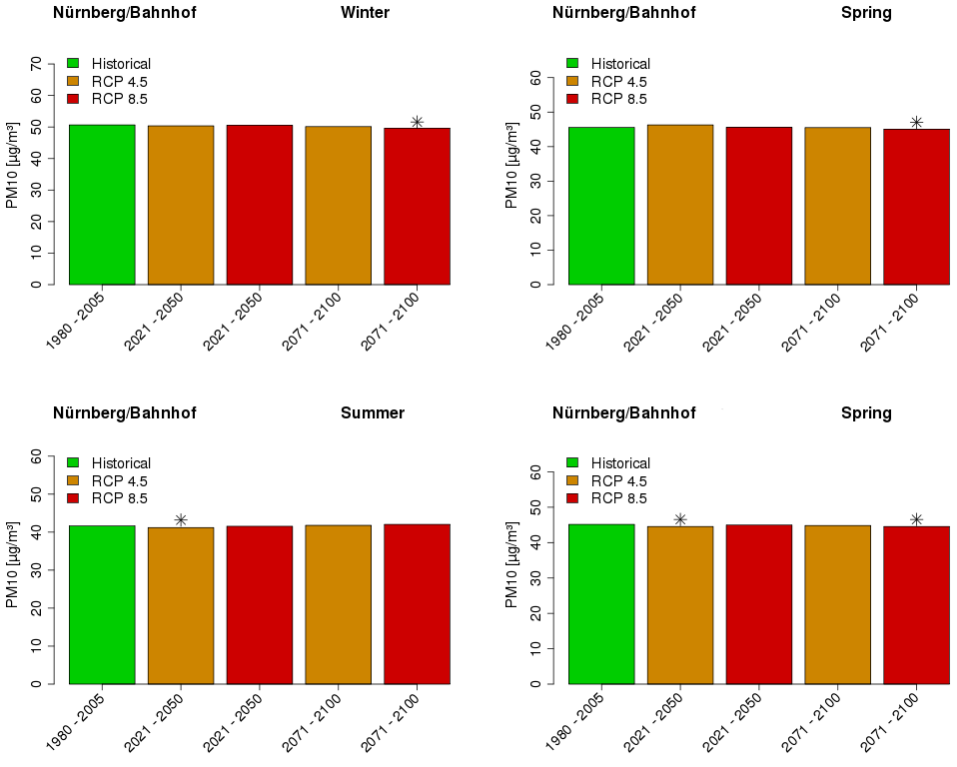


(b) Nürnberg

Figure A.13: Same as Figure A.10 for stations Bamberg Löwenbrücke (a) and Nürnberg Löwenbrücke (b).

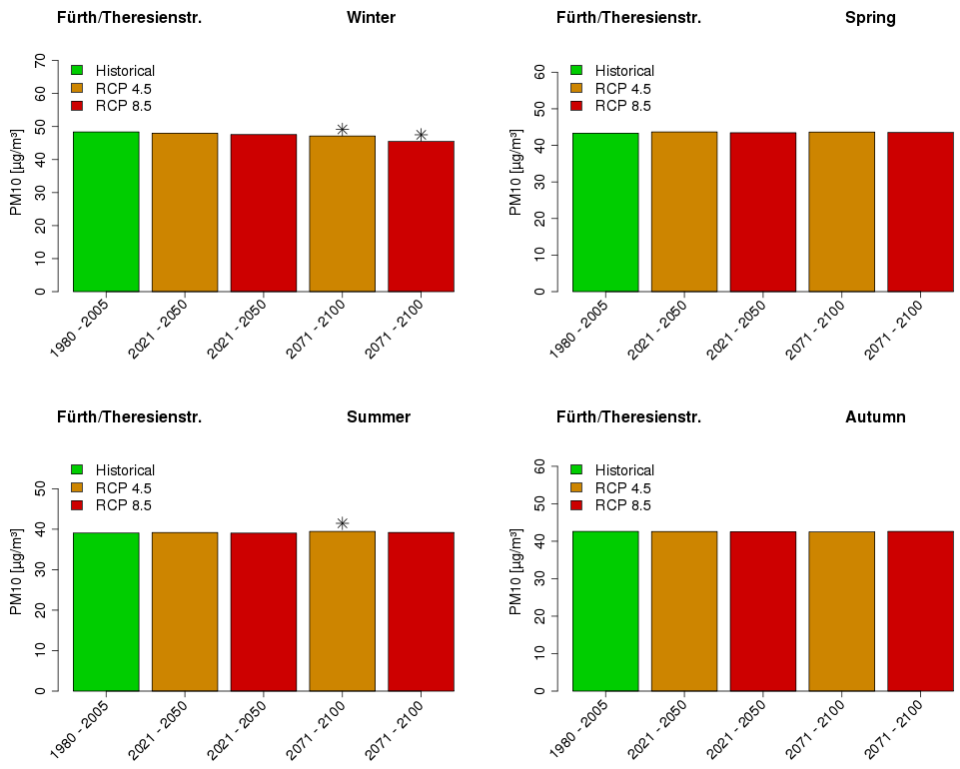


(a) Fürth

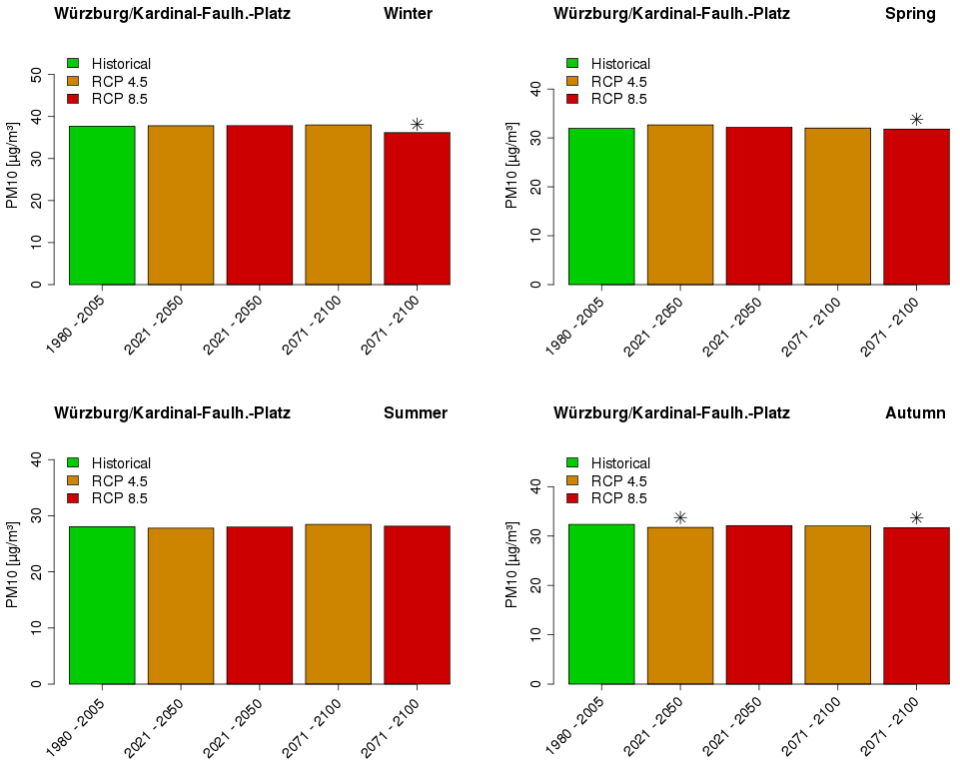


(b) Würzburg

Figure A.14: Same as Figure A.10 for stations Fürth Theresienstr. (a) and Würzburg Kardinal-Faulhaber-Platz (b).

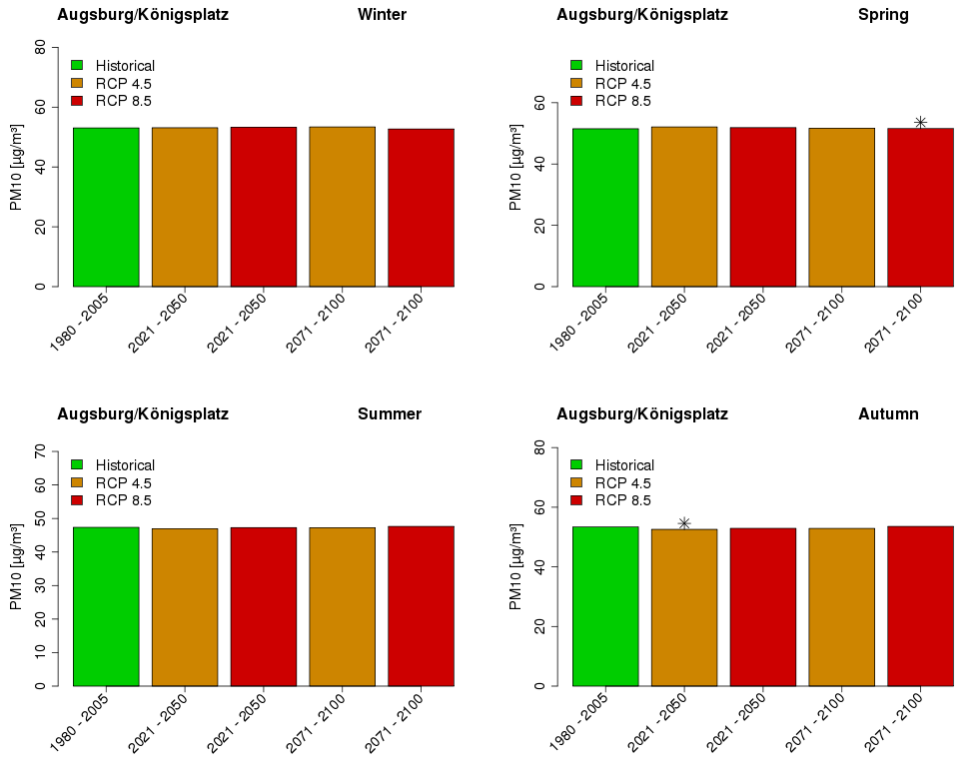


(a) Augsburg

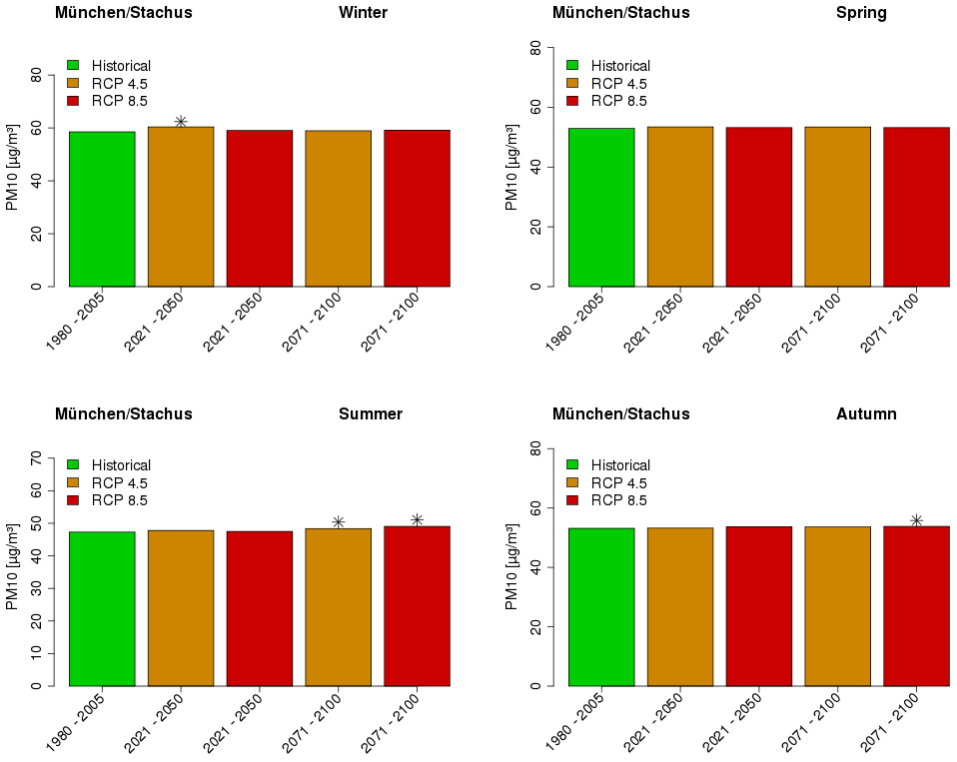


(b) München Stachus

Figure A.15: Same as Figure A.10 for stations Augsburg Königsplatz (a) and München Stachus (b).

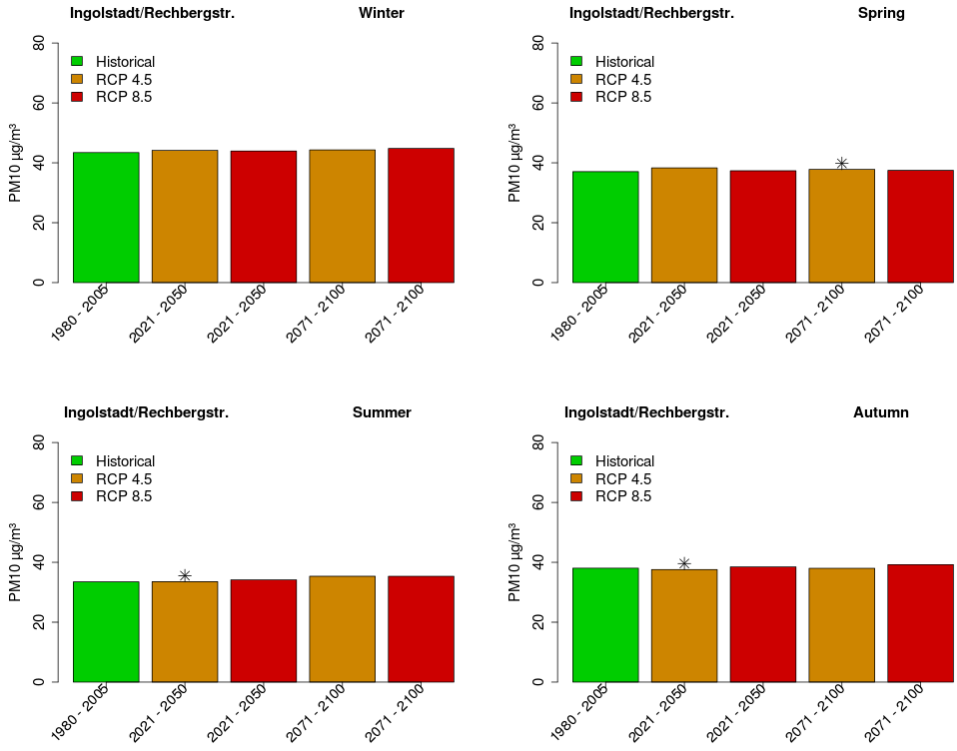


(a) Ingolstadt

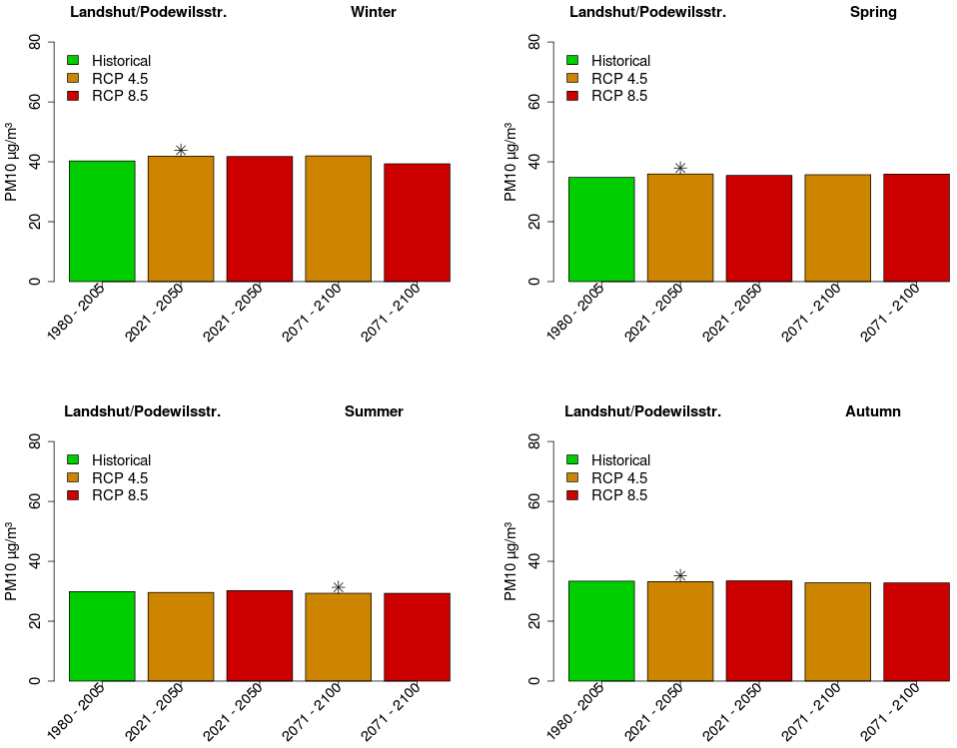


(b) Landshut

Figure A.16: Modelled seasonal $PM_{mean}$ levels (in $\mu g/m^3$) at stations Ingolstadt Rechenbergstr. (a) and Landshut Podewilsstr. (b). Estimations are based on three numerical ensemble members from ECHAM6 scenarios (RCP4.5, RCP8.5) for two time periods (2021-2050, 2071-2100) using four statistical ensemble members using Random Forest Models. Stars mark statistical significance (alpha = 0.05) of differences between particular scenario and historical period.

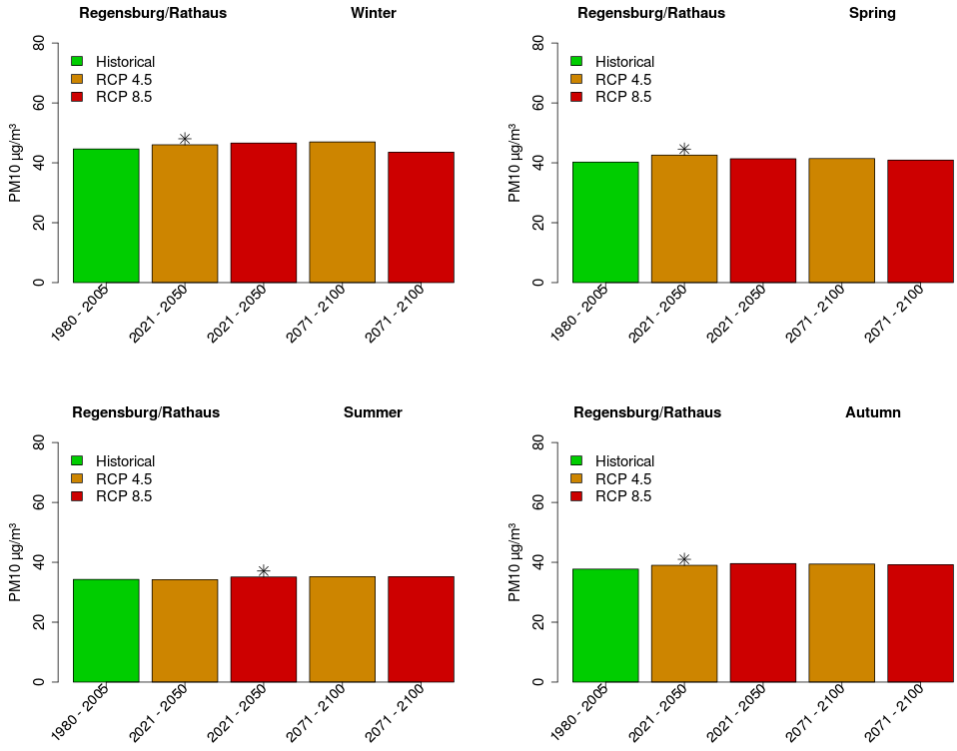


(a) Regensburg

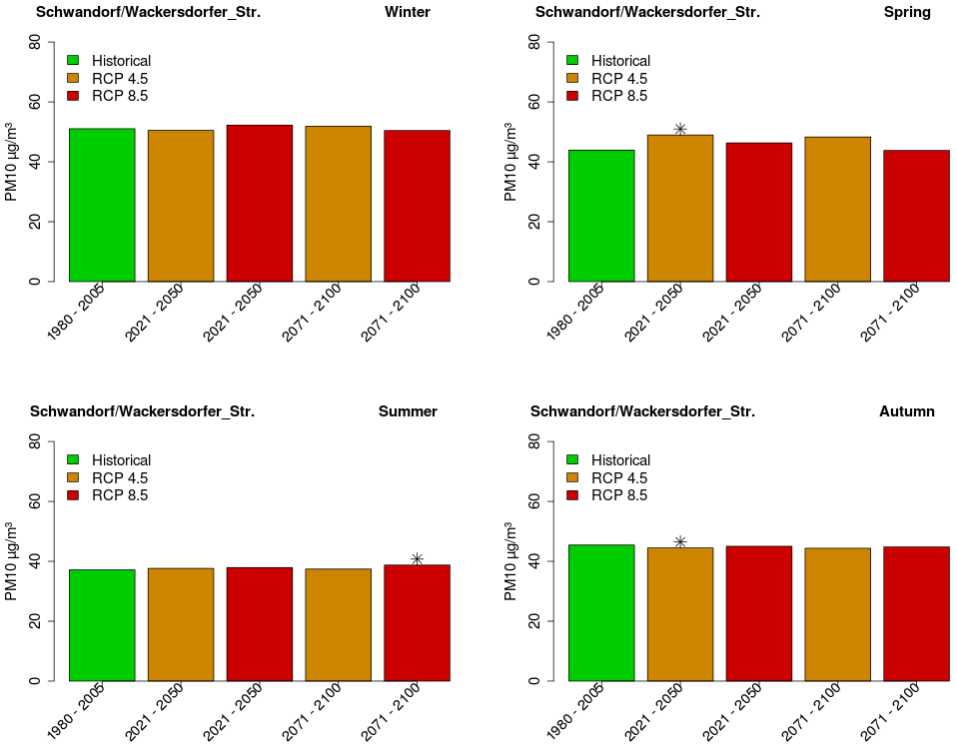


(b) Schwandorf

Figure A.17: Same as Figure A.16 for stations Regensburg Rathaus (a) and Schwandorf Wackersdorfer Str. (b).

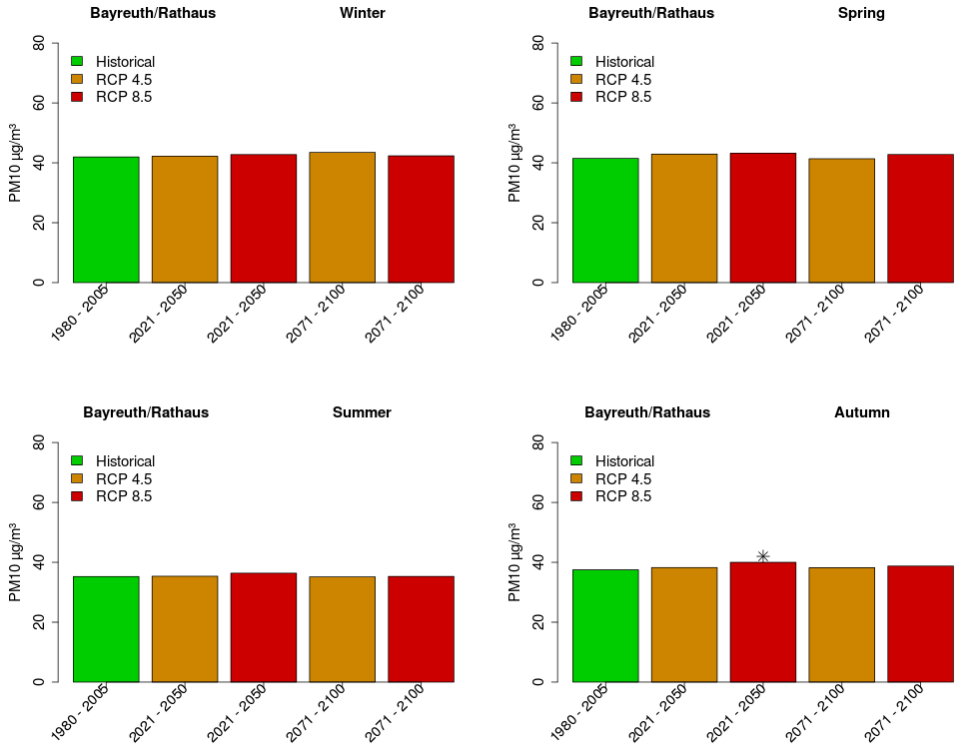


(a) Bayreuth

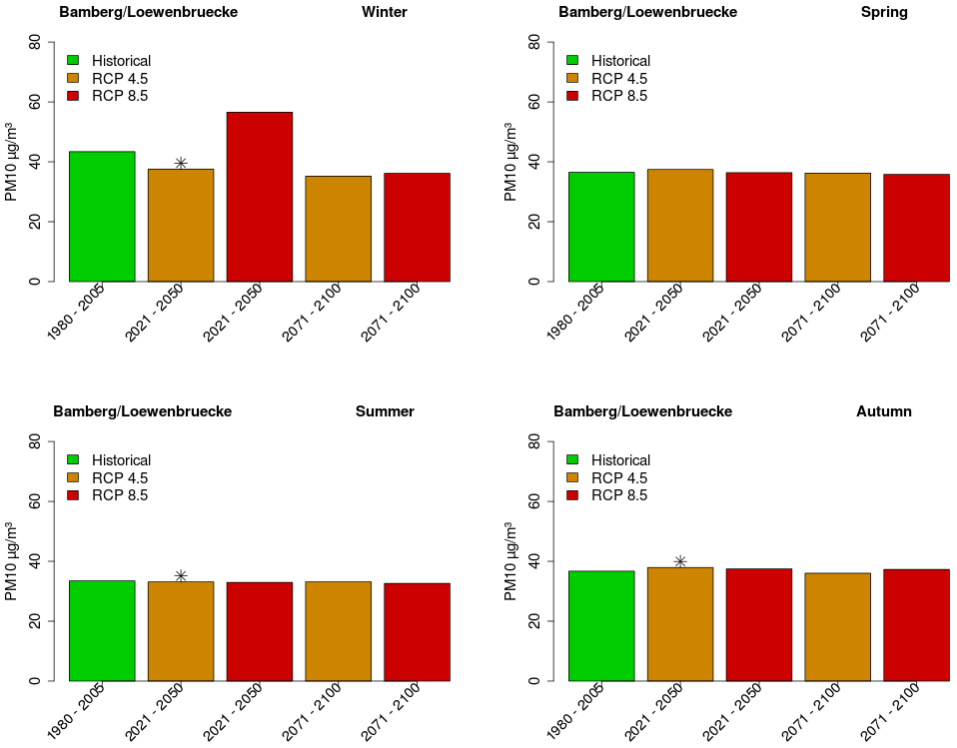


(b) Bamberg

Figure A.18: Same as Figure A.16 for stations Bayreuth Rathaus (a) and Bamberg Löwenbrücke (b).

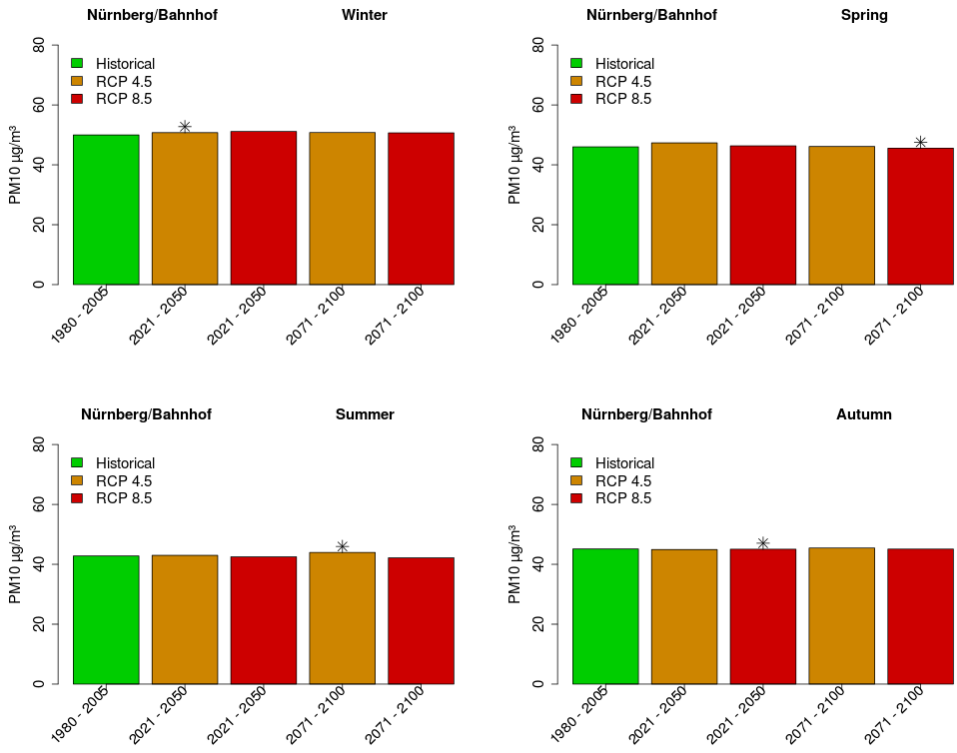


(a) Nürnberg Bahnhof

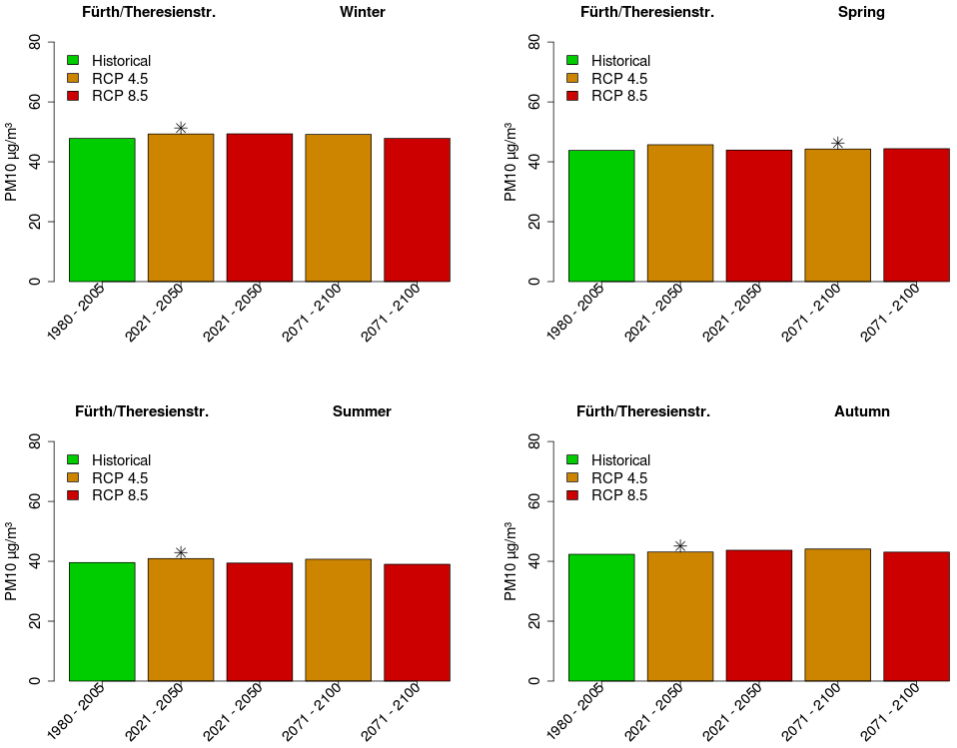


(b) Fürth

Figure A.19: Same as Figure A.16 for stations Nürnberg Bahnhof (a) and Fürth Theresienstr. (b).

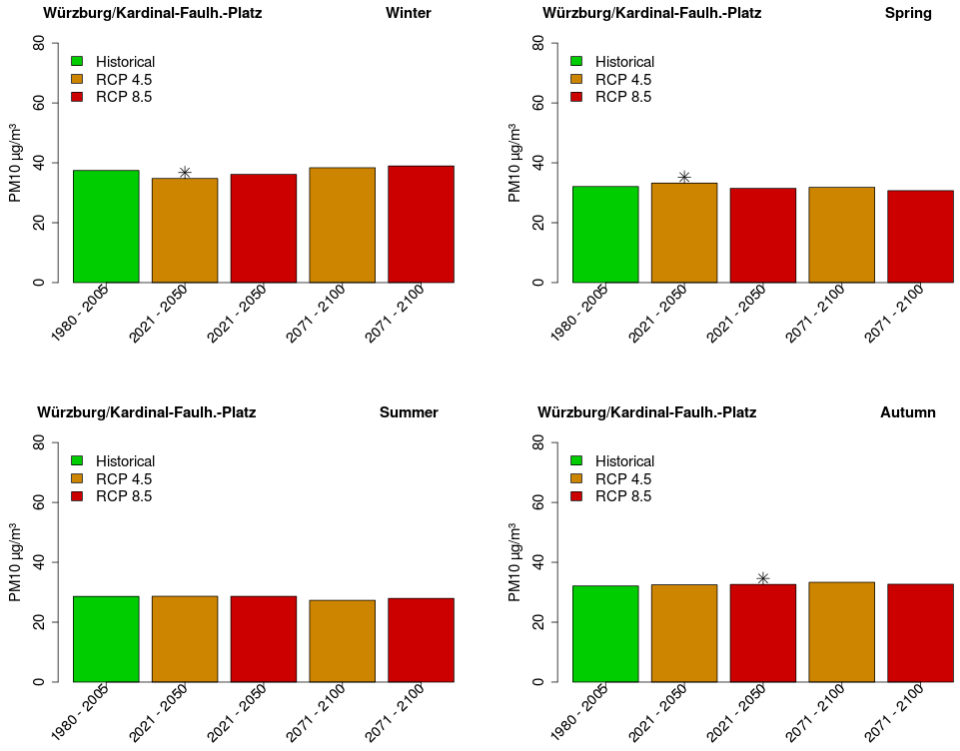


(a) Würzburg

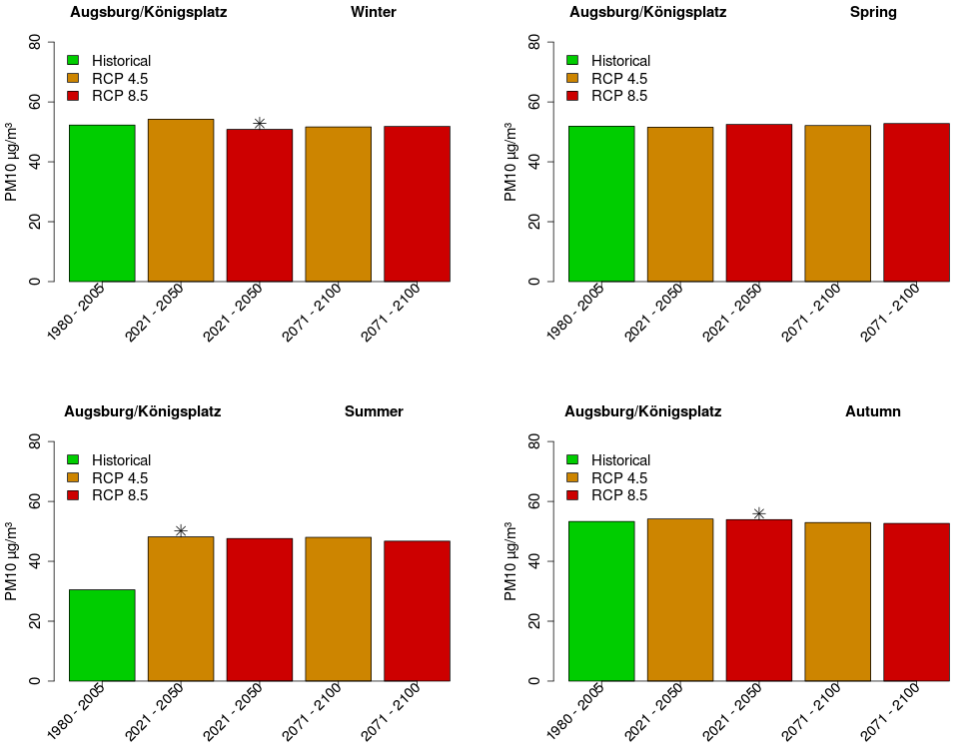


(b) Augsburg

Figure A.20: Same as Figure A.16 for stations Würzburg Kardinal-Faulhaber-Platz (a) and Augsburg Königsplatz (b).

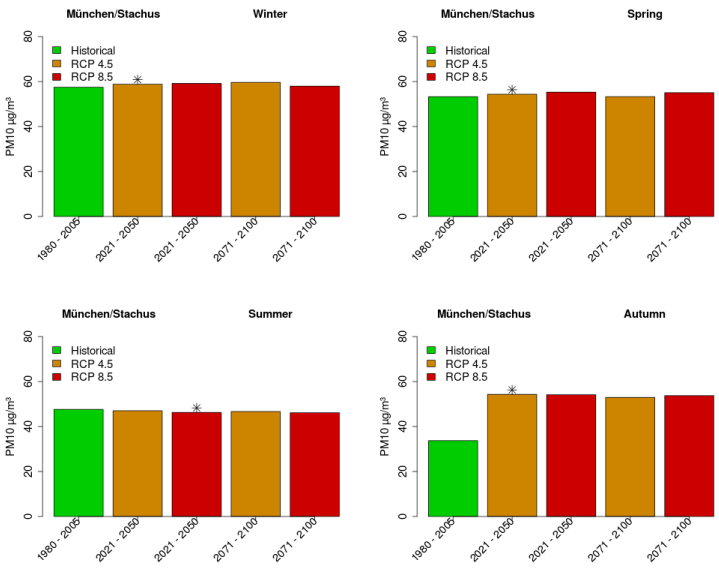


(a) München Stachus

Figure A.21: Same as Figure A.16 for station München Stachus.

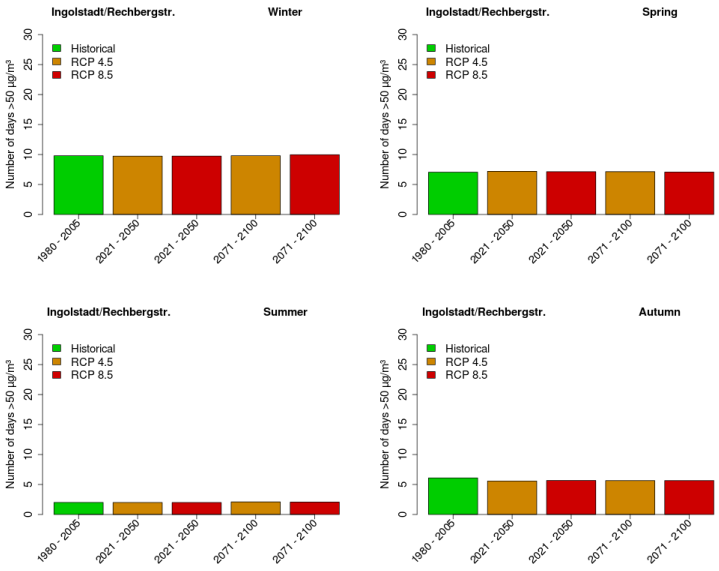


(a) Ingolstadt

Figure A.22: Modelled seasonal $PM_{50}$ levels (in $\mu g/m^3$) at station Ingolstadt Rechenbergstr. Estimations are based on three numerical ensemble members from ECHAM6 scenarios (RCP4.5, RCP8.5) for two time periods (2021-2050, 2071-2100) using four statistical ensemble members using Random Forest Models. Stars mark statistical significance (alpha = 0.05) of differences between particular scenario and historical period.

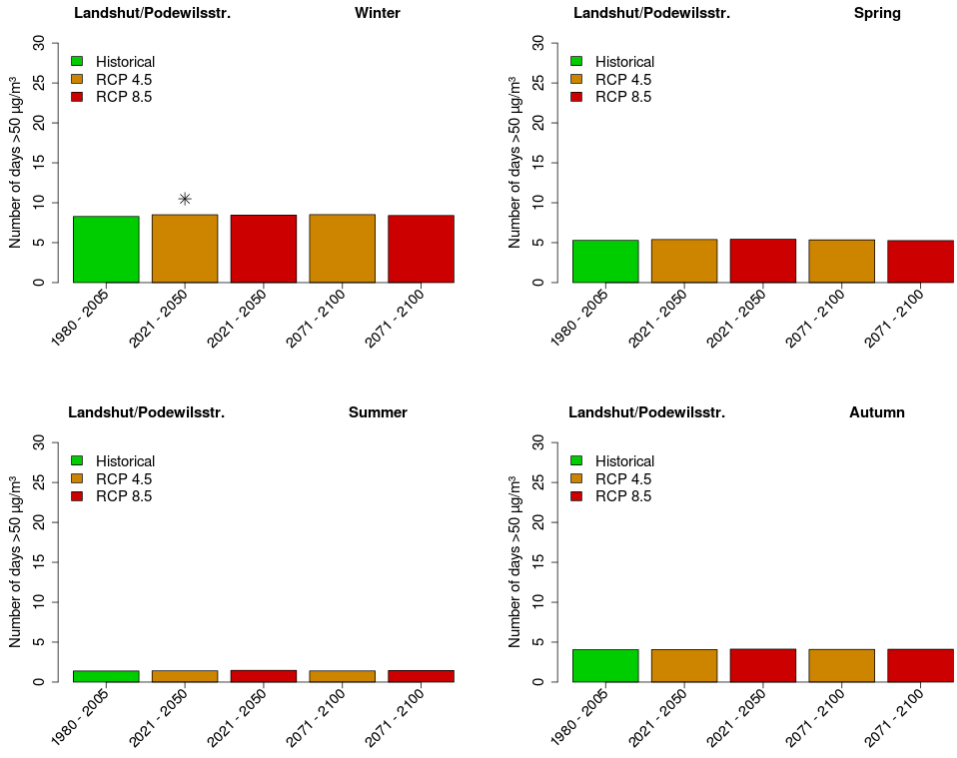


(a) Landshut

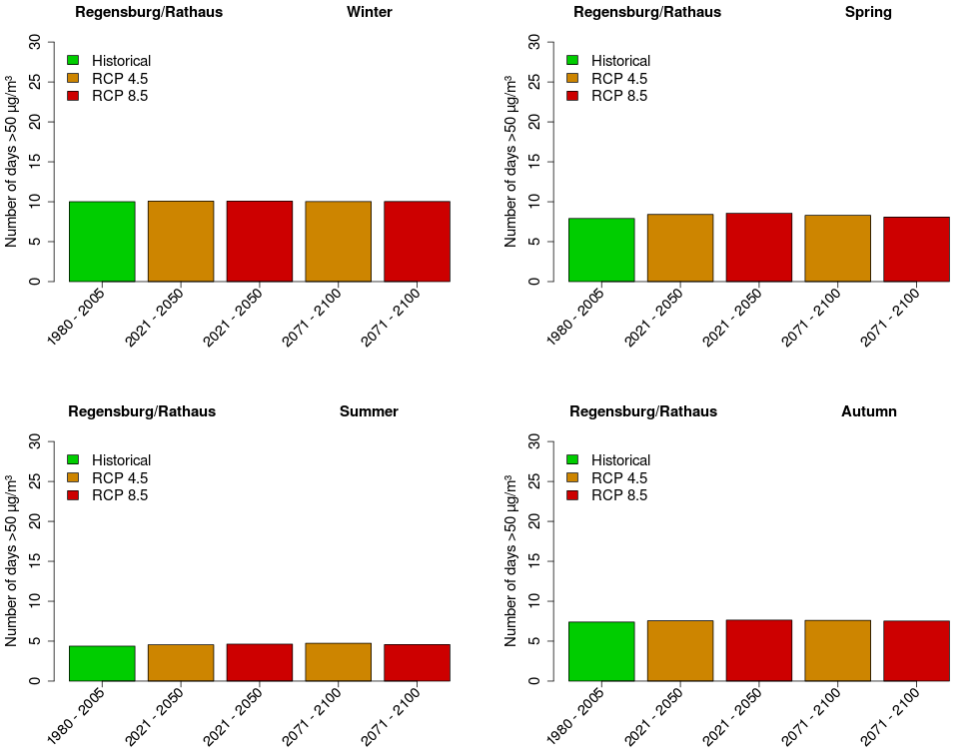


(b) Regensburg

Figure A.23: Same as Figure A.22 for stations Landshut Podewilsstr. (a) and Regensburg Rathaus (b).

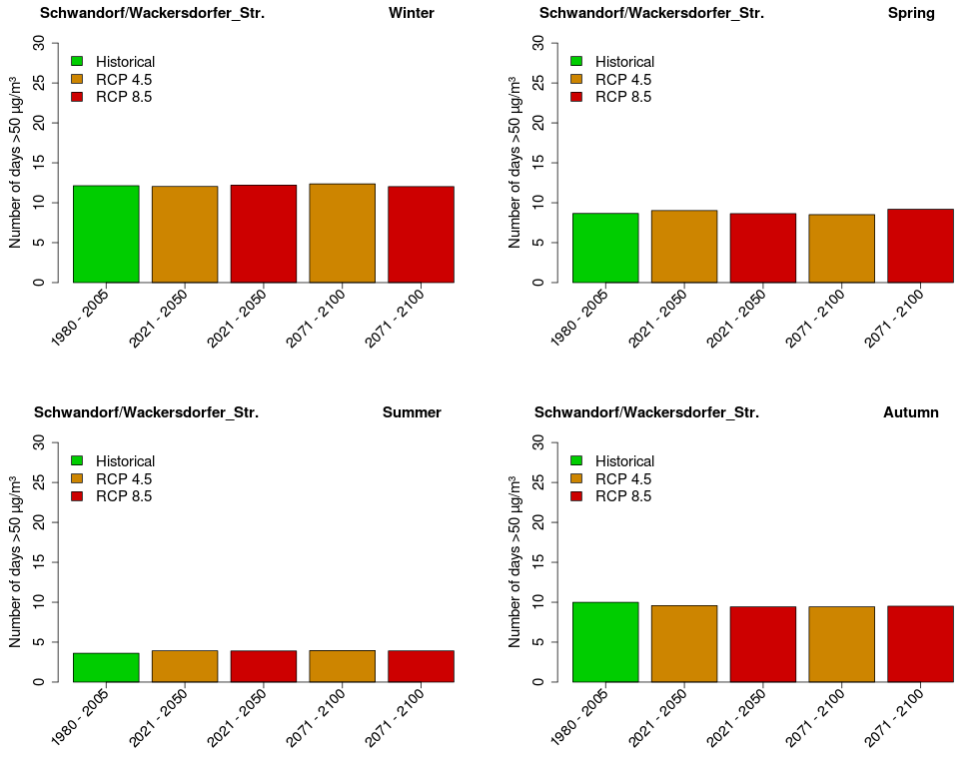


(a) Schwandorf

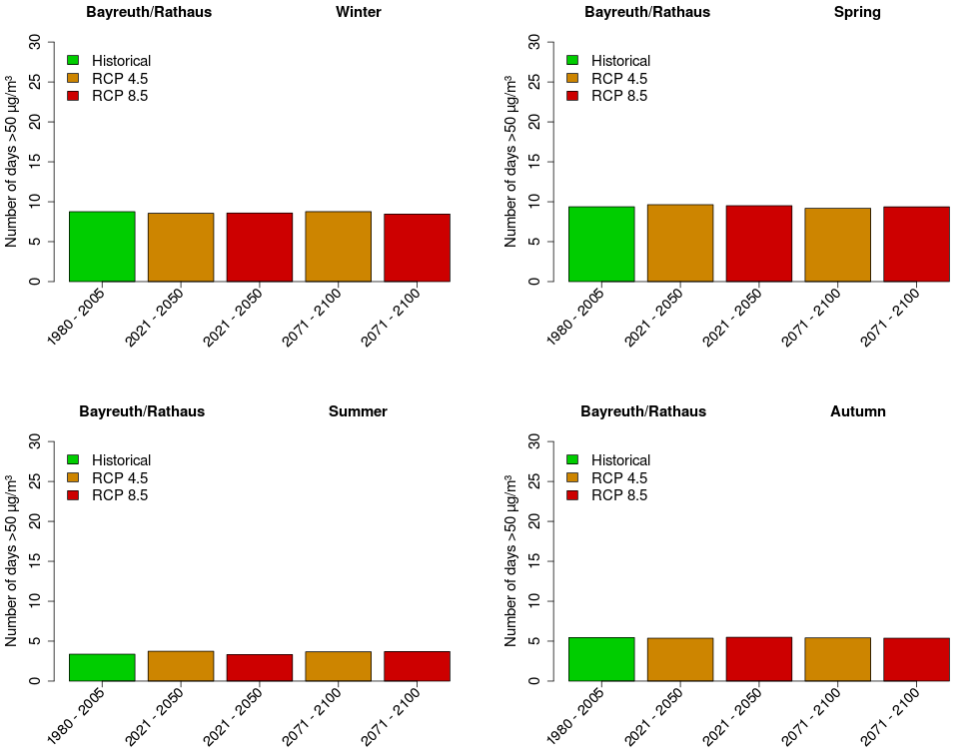


(b) Bayreuth

Figure A.24: Same as Figure A.22 for stations Schwandorf Wackersdorfer Str. (a) and Bayreuth Rathaus (b).

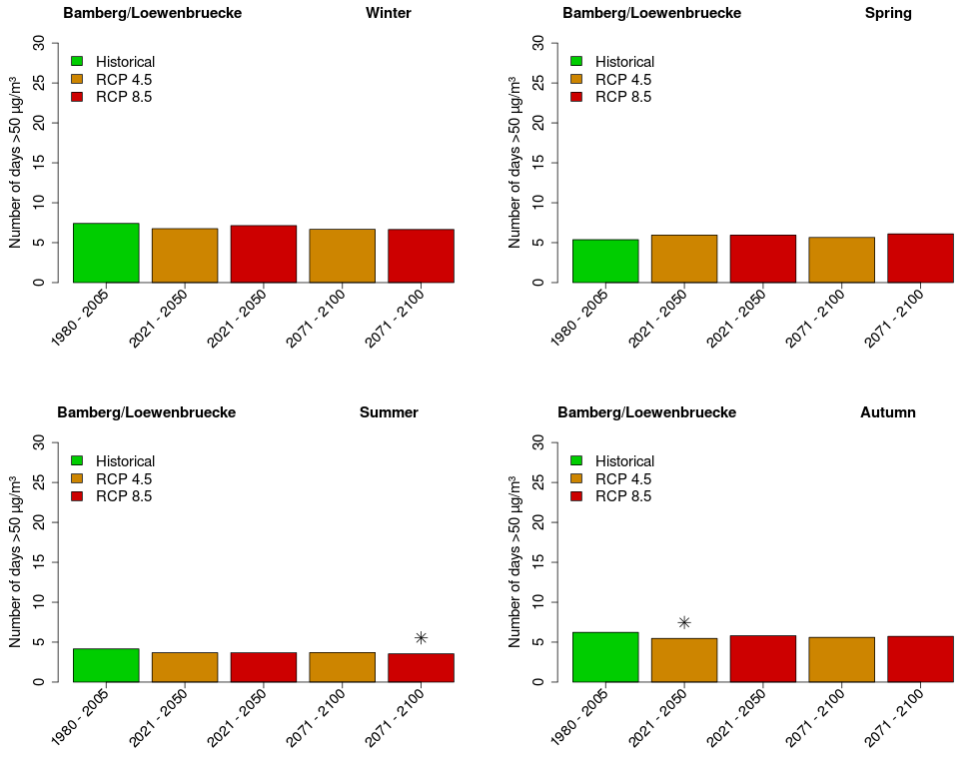


(a) Bamberg

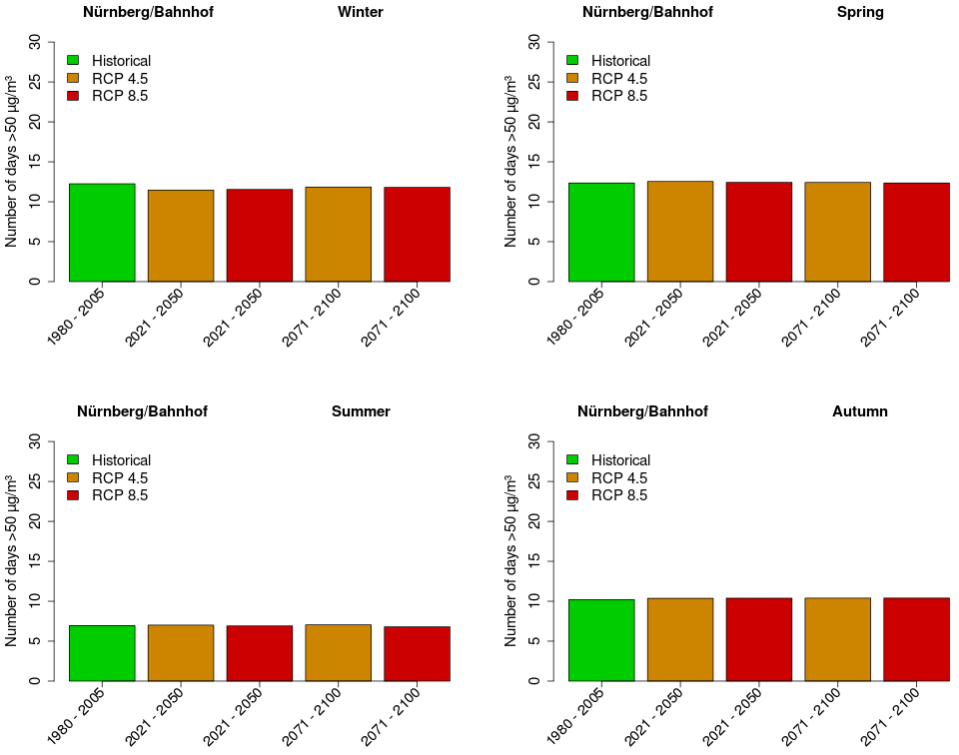


(b) Nürnberg

Figure A.25: Same as Figure A.22 for stations Bamberg Löwenbrücke (a) and Nürnberg Löwenbrücke (b).

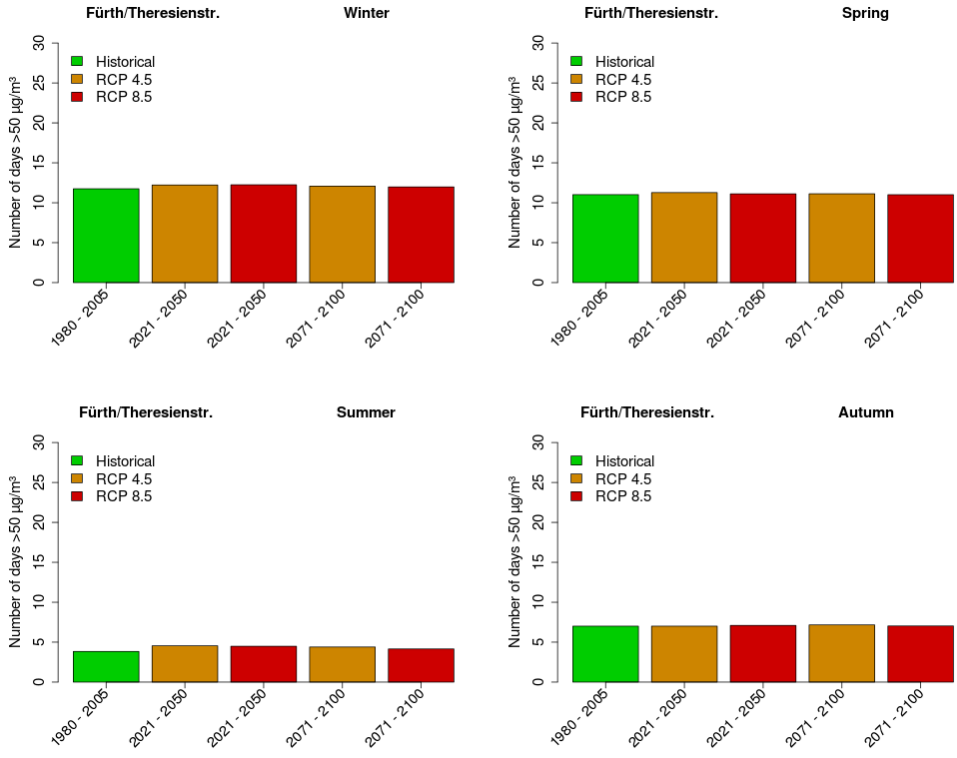


(a) Fürth

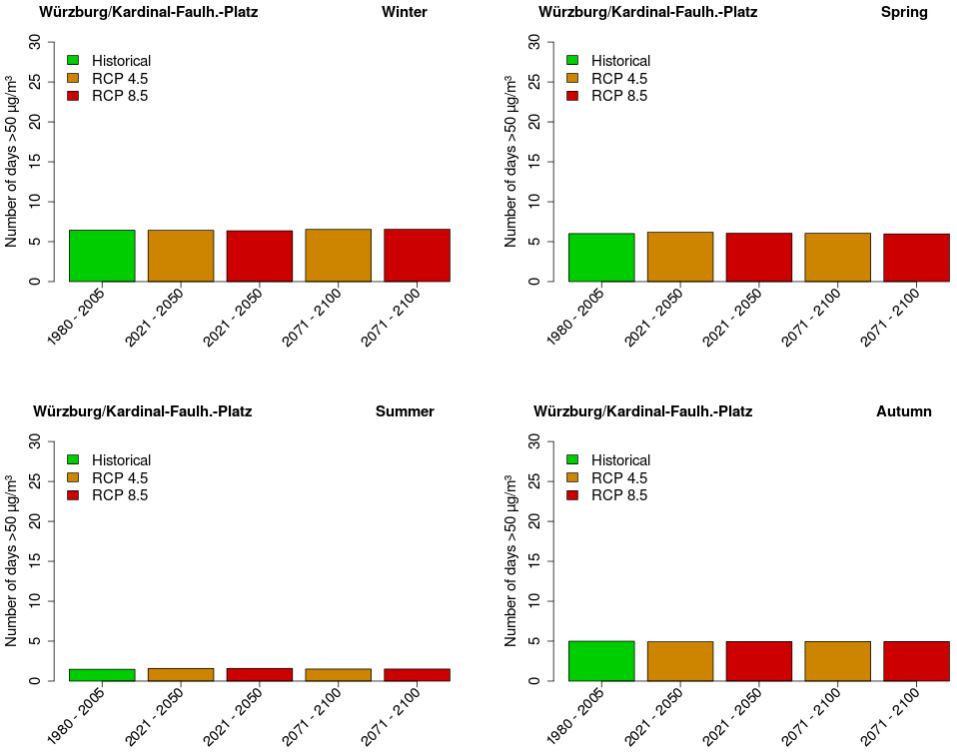


(b) Würzburg

Figure A.26: Same as Figure A.22 for stations Fürth Theresienstr. (a) and Würzburg Kardinal-Faulhaber-Platz (b).

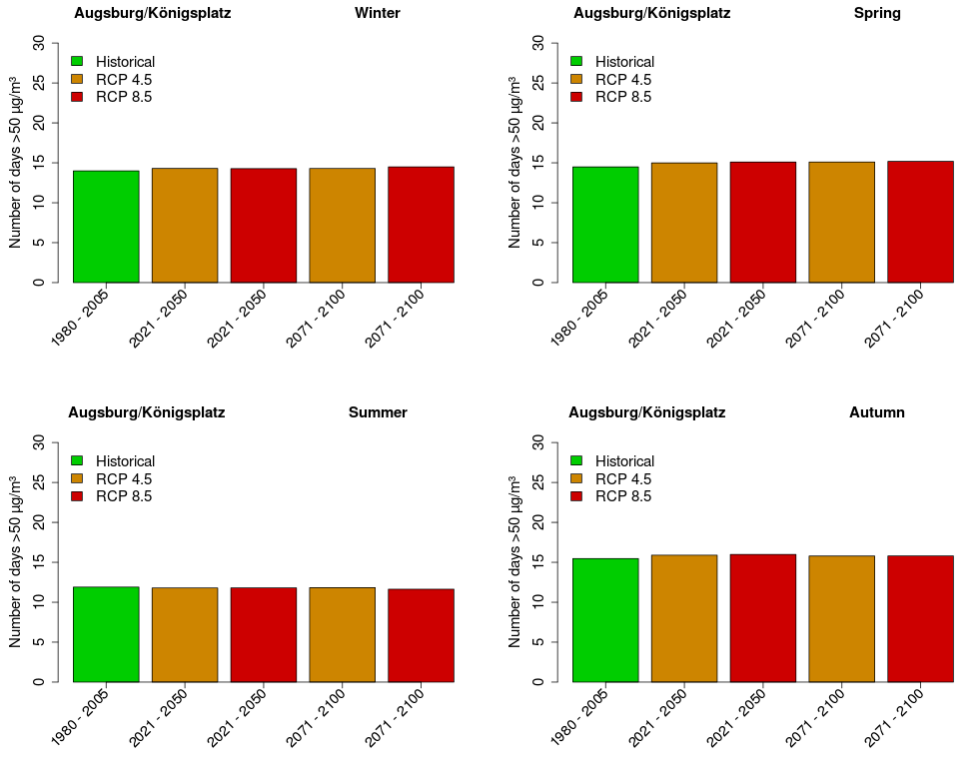


(a) Augsburg

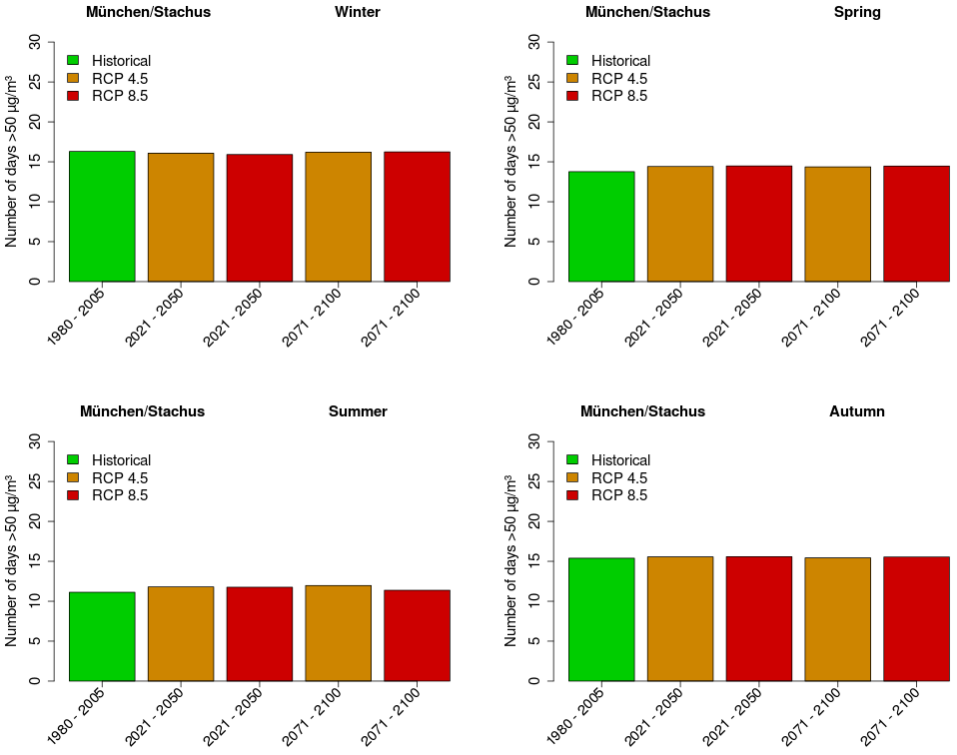


(b) München Stachus

Figure A.27: Same as Figure A.22 for stations Augsburg Königsplatz (a) and München Stachus (b).

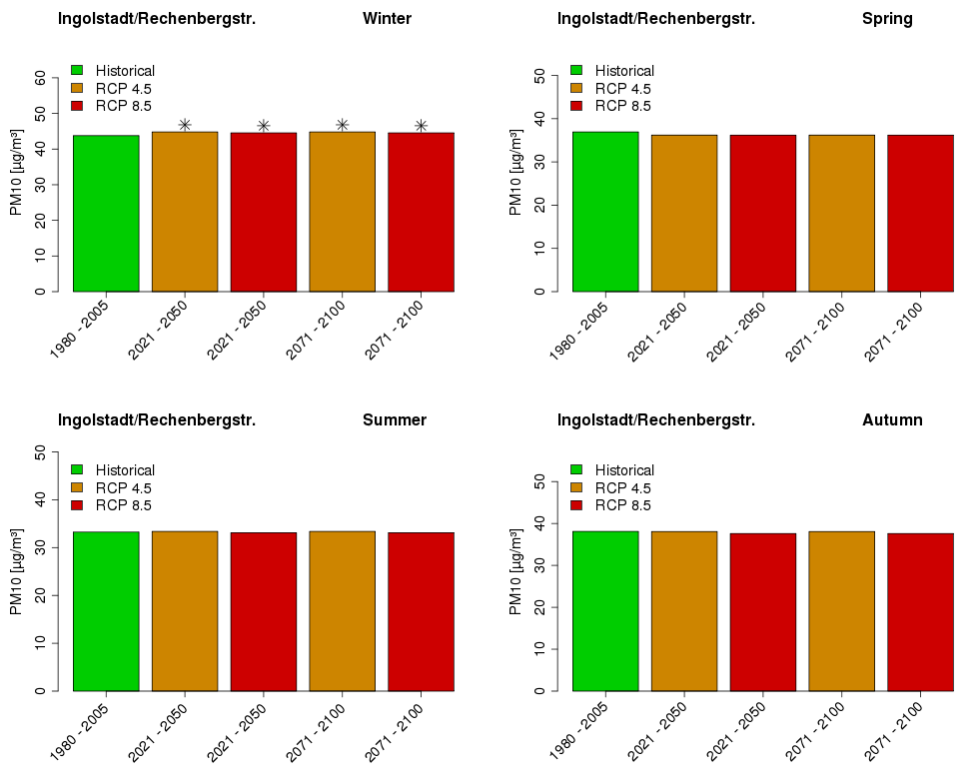


(a) Ingolstadt

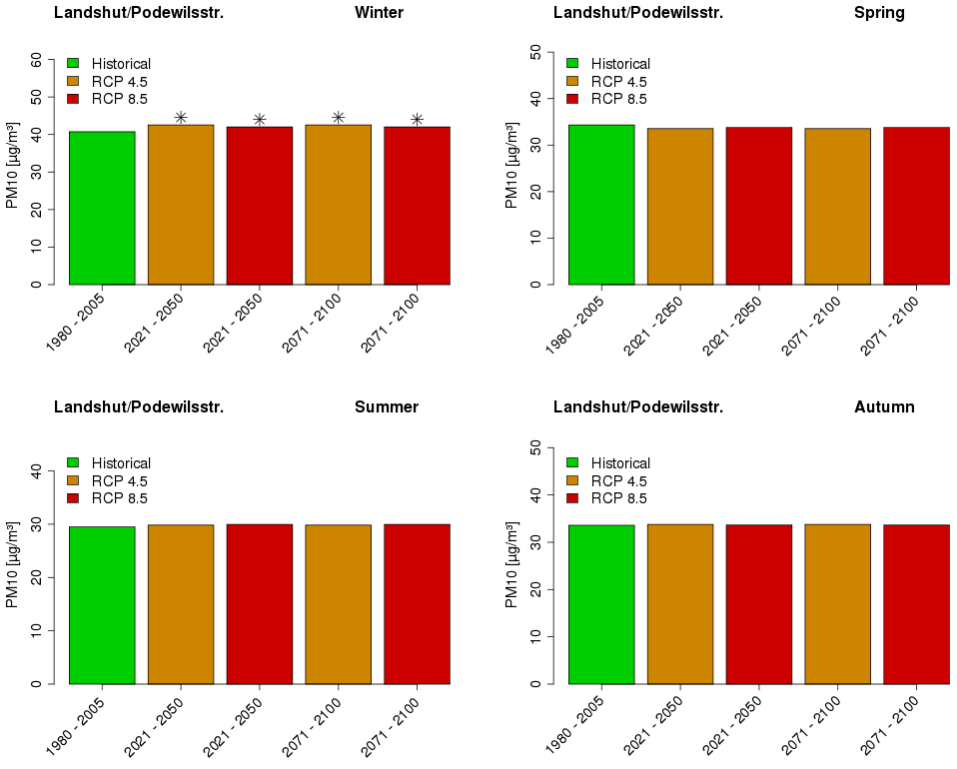


(b) Landshut

Figure A.28: Modelled seasonal $PM_{mean}$ levels (in $\mu g/m^3$) at stations Ingolstadt Rechenbergstr. (a) and Landshut Podewilstr. (b). Estimations are based on EC-Earth scenarios (RCP4.5, RCP8.5) for two time periods (2021-2050, 2071-2100) using four statistical ensemble members using Synoptic Downscaling (SD-PMT). Stars mark statistical significance (alpha = 0.05) of differences between particular scenario and historical period.

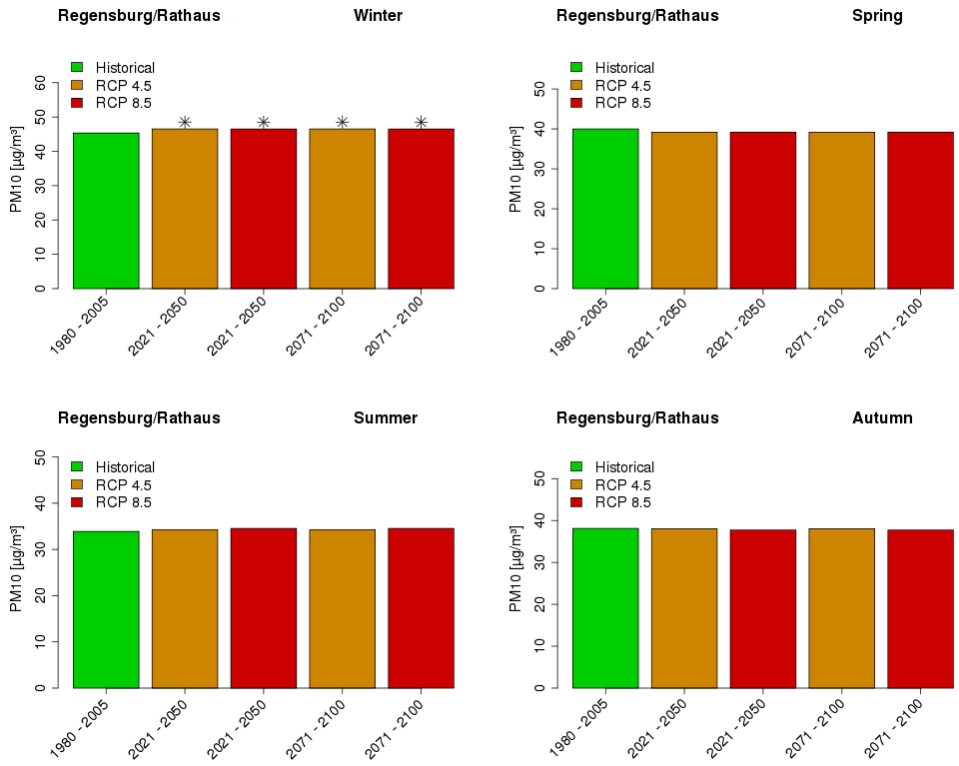


(a) Regensburg

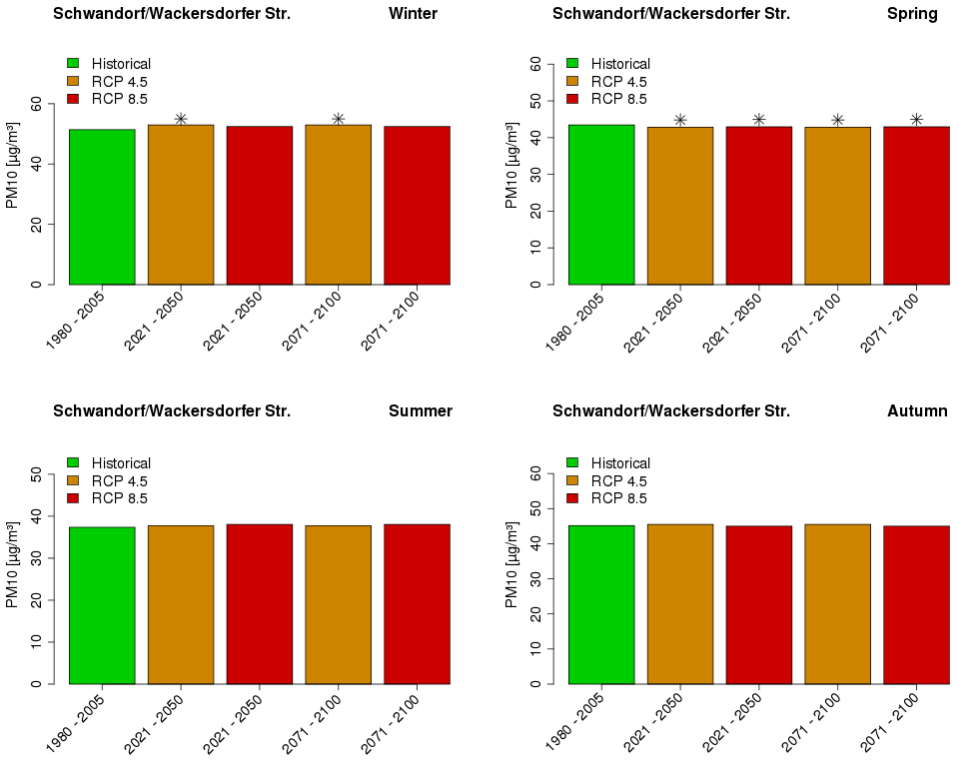


(b) Schwandorf

Figure A.29: Same as Figure A.28 for stations Regensburg Rathaus (a) and Schwandorf Wackersdorfer Str. (b).

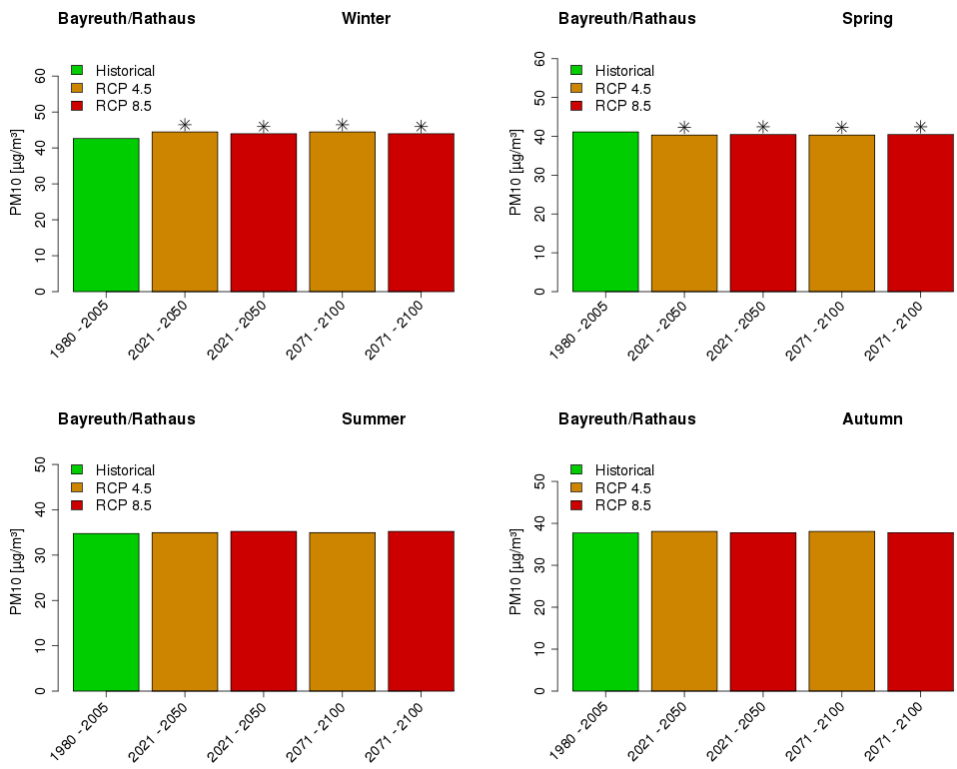


(a) Bayreuth

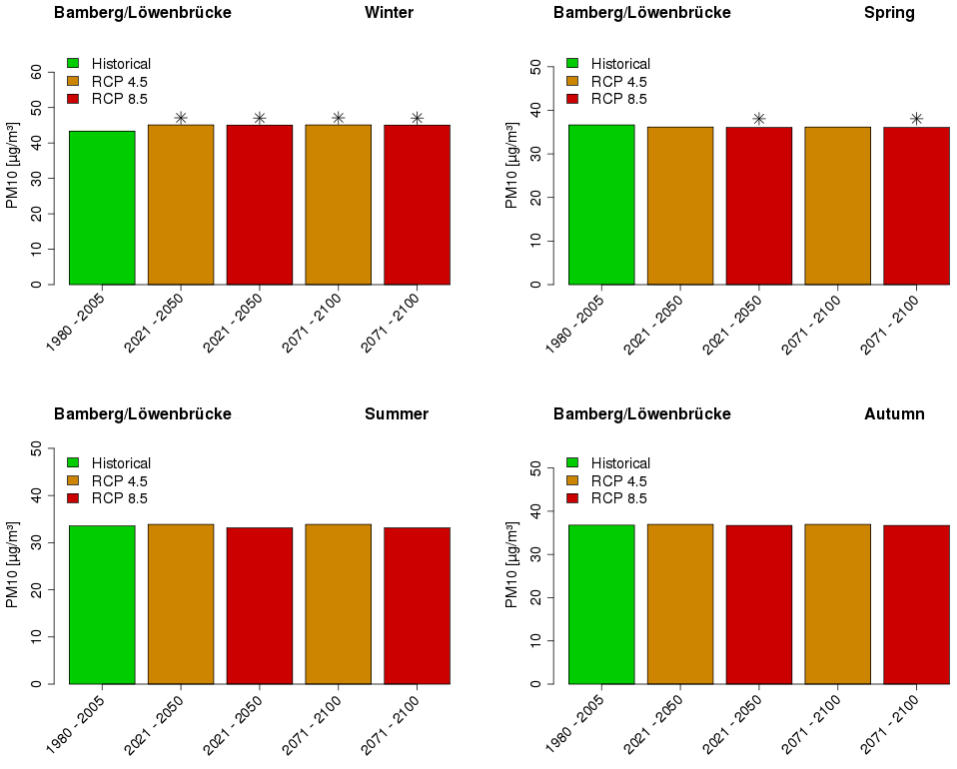


(b) Bamberg

Figure A.30: Same as Figure A.28 for stations Bayreuth Rathaus (a) and Bamberg Löwenbrücke (b).

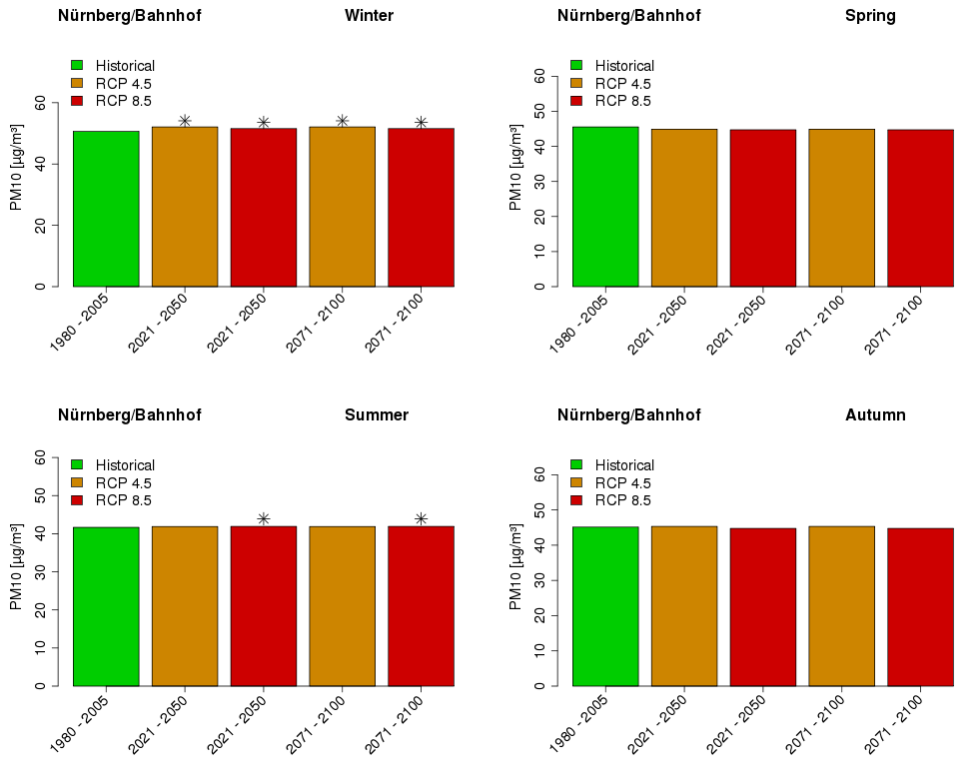


(a) Nürnberg Bahnhof

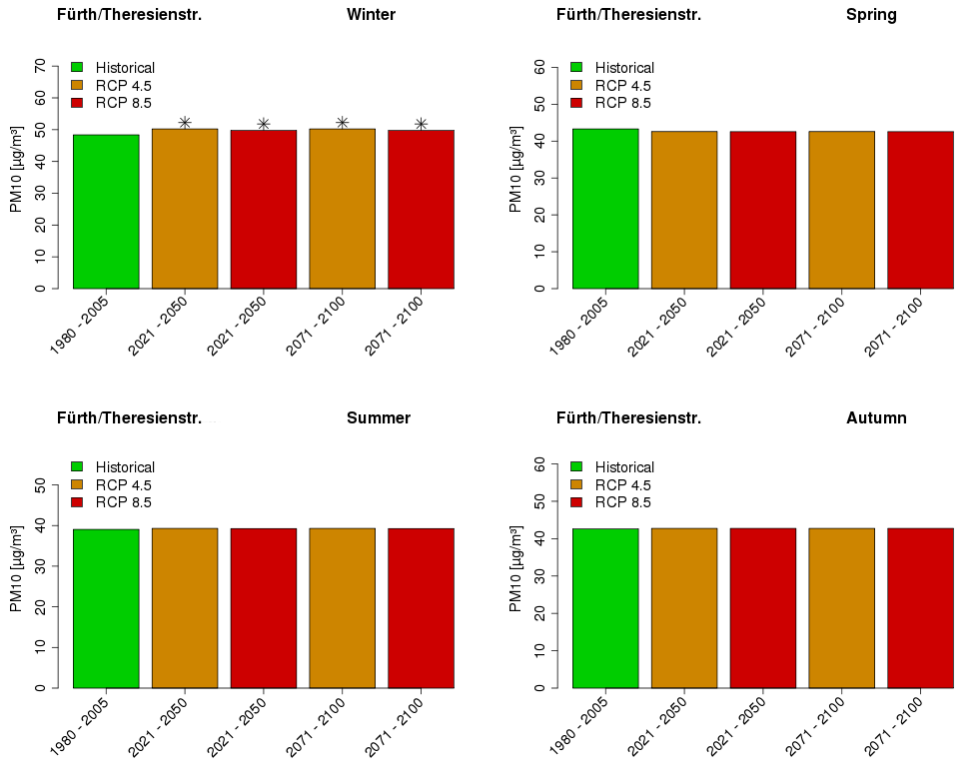


(b) Fürth

Figure A.31: Same as Figure A.28 for stations Nürnberg Bahnhof (a) and Fürth Theresienstr. (b).

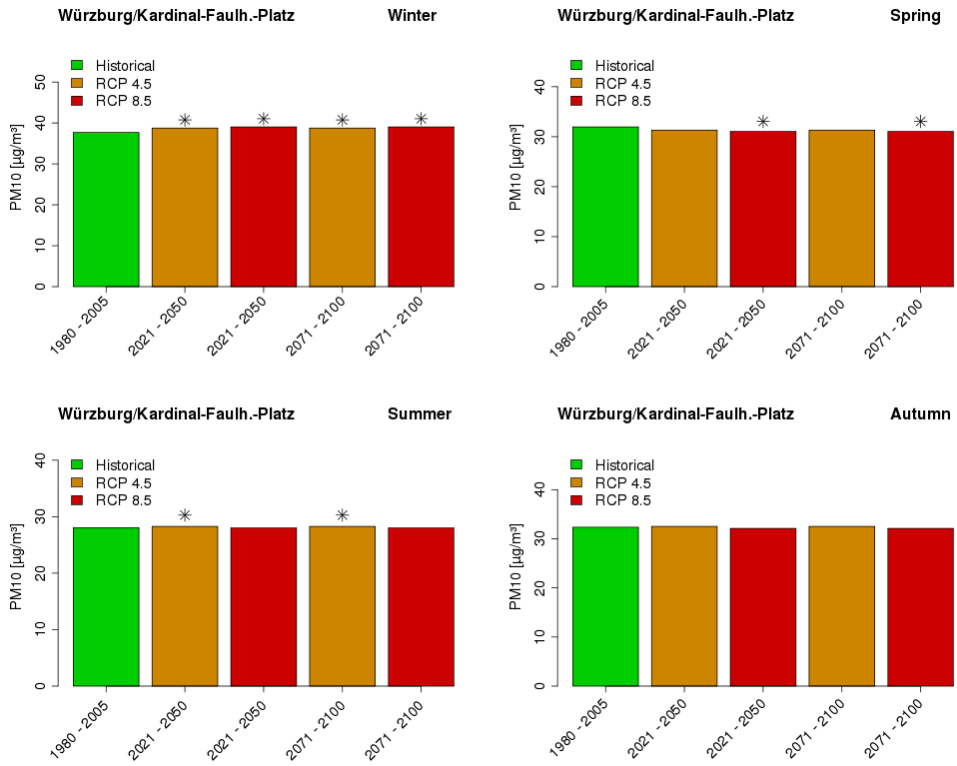


(a) Würzburg

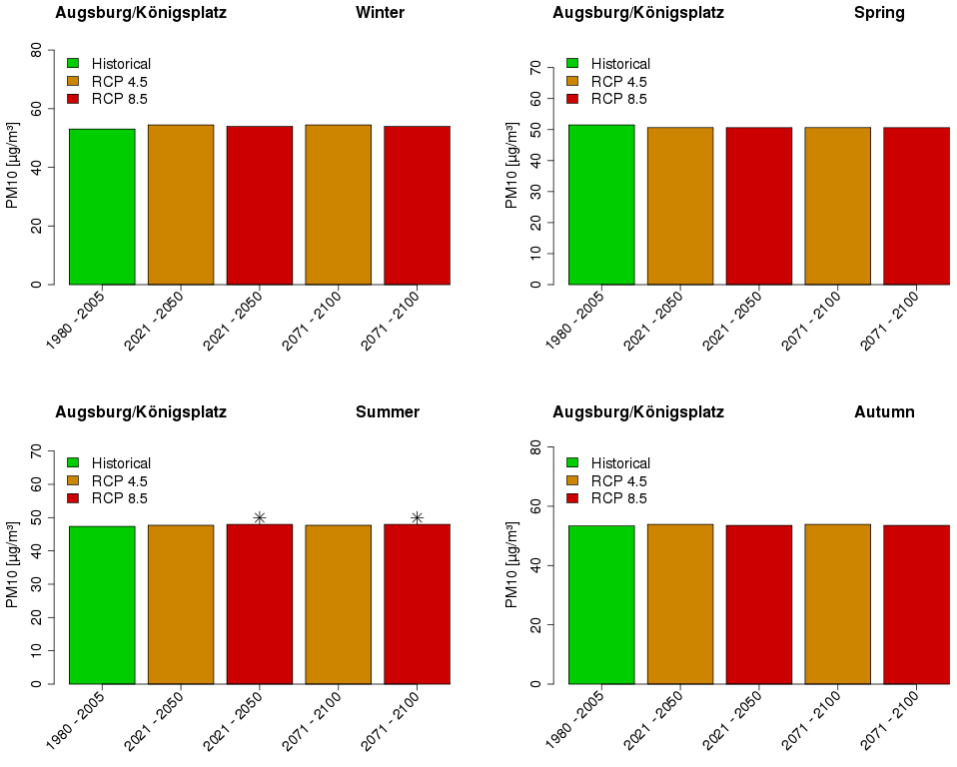


(b) Augsburg

Figure A.32: Same as Figure A.28 for stations Würzburg Kardinal-Faulhaber-Platz (a) and Augsburg Königsplatz (b).

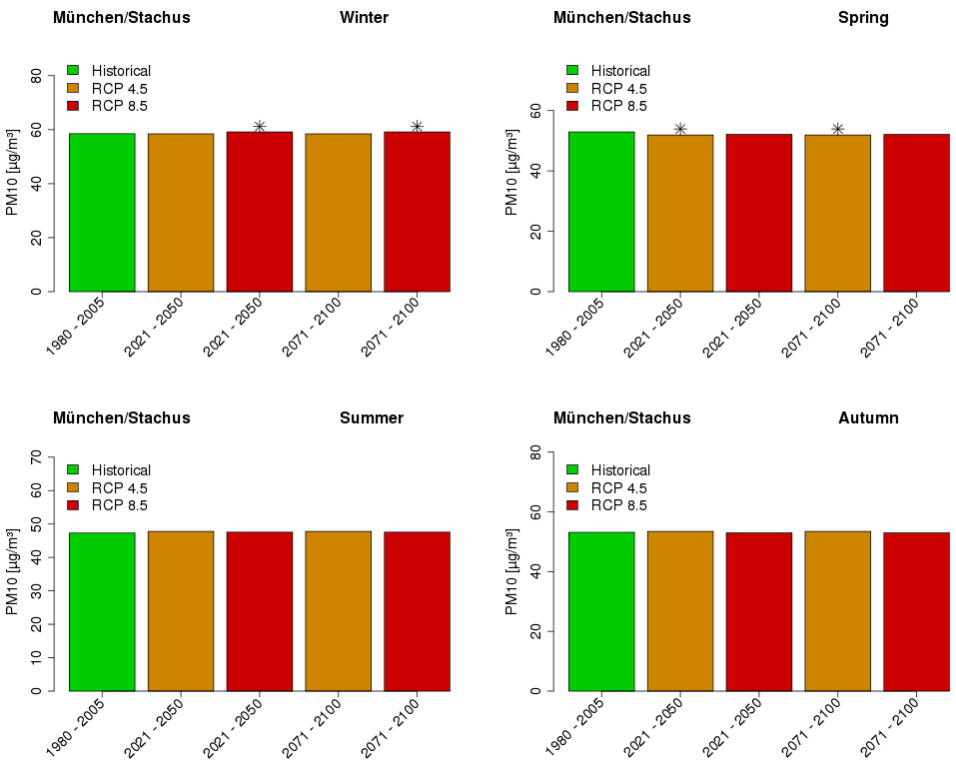


(a) München Stachus

Figure A.33: Same as Figure A.28 for station München Stachus.